UNIVERSITY OF THESSALY

SCHOOL OF ENGINEERING

DEPARTMENT OF MECHANICAL ENGINEERING

PhD Thesis

DESIGN AND DEVELOPMENT OF DIRECT GLUCOSE ALKALINE FUEL CELLS

by

ANGELIKI BROUZGOU

Chemical Engineer, National Technical University of Athens, 2007

MSc., Department of Mechanical Engineering, University of Thessaly, 2010

Submitted in partial fulfillment of the
Requirements for the
Degree of Doctor of Philosophy in the
Department of Mechanical Engineering of the
University of Thessaly
2013

Approved by the Members of PhD Examination Committee

First examiner (Supervisor)	Dr. Tsiakaras Panagiotis Professor, Department of Mechanical Engineering, University of Thessaly
Second examiner	Dr. Bebelis Symeon Associate Professor, Department of Chemical Engineering, University of Patras
Third examiner	Dr. Neophytides Stylianos Research Director Institute of Chemical Engineering and High Temperature Processes
Fourth examiner	Dr. Andritsos Nikolaos Professor, Department of Mechanical Engineering, University of Thessaly
Fifth examiner	Dr. Pelekasis Nikolaos Professor, Department of Mechanical Engineering, University of Thessaly
Sixth examiner	Dr. Stapountzis Erikos Associate Professor, Department of Mechanical Engineering, University of Thessaly
Seventh examiner	Dr. Papathanasiou Athanasios Associate Professor, Department of Mechanical Engineering, University of Thessaly

Acknowledgments

Initially, I would like to deeply thank my supervisor and Professor Tsiakaras Panagiotis who guided me into the world of research and science, who trusted me and gave me the opportunity to follow and make my dreams come true. Also, I am gratified to Professor Shuqin Song of Sun Yat-Sen University in Guangzhou, China for her invaluable support, her transition of knowledge concerning scientific issues and for her hot hospitality during my stay in China. Of course without the valuable help of Dr. Frusteri Francesco of the CNR-TAE Institute our scientific goal would have been delayed.

Moreover, my gratitude is also extended to the rest two members of my Ph.D three members committee: Prof. Symeon Bebelis and Dr. Styilanos Neophytides. As well as to the rest four members of the PhD examination committee, Prof. Andritsos Nikolaos, Prof. Pelekasis Nikolaos, Prof. Stapountzis Erikos and Prof. Papathansasiou Athanasios for their time and their useful advices.

The completion of my dissertation has been a long journey which without the invaluable support of the Laboratory's Alternative Conversion Systems Research Group I would not have managed so well. More precisely, I would like firstly to thank, Dr. Sotiria Kontou for her support and encouragement. I am also indebted to people I had the pleasure to work with, whose academic support and input and personal cheering are greatly appreciated. More precisely I would like to thank Dr. Andreas Podias, Dr. Antonios Seretis, Dr. Stratigoula Mitri, Dr. Alessandro Vinci, Mr. Giorgos Polymeros and Mr. Kiriakos Papageridis. Next, I am very grateful to Dr. Nicoletta Sachinidou and Ms Katerina Kourenta, for their linguistic interventions and advices. Moreover, to my special friends: Ms Tzorbatzoglou Fotini, Ms Despina Marou, Ms Katerina Papagianni and Mr Christos Gialamas for their love and support. PhD thesis would have not been completed without the financial support of European Union (European Social Fund– ESF) and Greek national funds through the Operational Program "Education and Lifelong Learning" of the National Strategic Reference Framework (NSRF) - Research Funding Program: Heracleitus II. Investing in knowledge society through the European Social Fund; that they have co-financed this research. Finally, I would like to give a heartfelt special thanks to my parents, Eleni and Dimitrios, as well as to my brother Frixos and my sister Maria, who supported my choices and encouraged my efforts.

DESIGN AND DEVELOPMENT OF DIRECT GLUCOSE FUEL CELLS

ANGELIKI BROUZGOU

University of Thessaly, Department of Mechanical Engineering, 2013

Supervisor: Dr. Panagiotis Tsiakaras,
Professor of Catalysis, Electrocatalysis and Fuel Cells Engineering
Department of Mechanical Engineering,
University of Thessaly

Abstract

The development of direct glucose fuel cells or glucose sensors in-vivo or in-vitro for the measurement of glucose concentration in the human blood is desirable for medical applications. An implantable, miniature, accurate and reliable sensor to monitor the glucose concentration in the body is desirable for treatment of diabetes mellitus. An implantable glucose-oxygen fuel cell has been proposed for artificial hearts using glucose and oxygen in the blood as the reactant. A practical fuel cell system has not yet been developed for this application, however. The electrocatalytic glucose sensor and glucose fuel cell are based on the catalytic glucose oxidation on an electrode surface which produces a current related to the concentration of glucose. Different electrodes have been investigated for glucose electrooxidation, e.g. platinum [1-6], gold [7-11], glassy carbon [12, 13], cobalt, rhodium and iridium [12-15], nickel and palladium [12, 13, 15], copper and silver [12, 13], phthalocyanines and porphyrins complexes of cobalt, manganese and iron [12]. Moreover, glucose oxidation has been studied in acid [16], neutral [16, 17] and alkaline [18] solutions. In literature there are

few works [3, 19] concerning the study of glucose electrooxidation on Pd-based/C electrocatalysts, in alkaline environment.

In the present Ph.D thesis, firstly literature review was conducted in order to identify the most efficient and studied electrocatalysts for direct-liquid proton exchange membrane fuel cells. In sequence, the literature review was continued including also the novel type of direct liquid anion exchange membrane fuel cells. According to the above reviews platinum was recognized as the best electrocatalyst for direct liquid-fed proton exchange membrane fuel cells, while palladium was identified as the best one for direct liquid-fed anion exchange membrane fuel cells.

The first step of design and development of fuel cells is the recognition of the most active electrocatalysts towards anode and cathode reaction. To this purpose, in the present work binary Pd-based electrocatalysts were prepared and were investigated as anode electrocatalysts for glucose electrooxidation in half direct glucose alkaline fuel cells. More precisely, Pd_xRu_y (20 wt%)/C, Pd_xRh_y (20 wt%)/C and Pd_xSn_y (20 wt%)/C are studied as anode direct glucose alkaline fuel cells' materials, while Pd_xAu_y (20 wt%)/C is investigated as glucose sensors' material. The above-mentioned electrocatalysts and the respective results are reported for first time in literature, indicating the novelty of the present PhD thesis. For the preparation of the examined electrocatalysts a modified-microwave assisted polyol method was used. The physicochemical characterization of electrocatalysts was conducted by X-ray Diffraction (XRD), Transmission Electron Microscopy (TEM), Scanning Electron Microscopy-Energy Dispersive X-RaySpectroscopy and Thermogravimetric Analysis (TG). The electrochemical characterization was carried out with the Cyclic Voltammetry (CV-half direct glucose alkaline fuel cell), Rotating Disk Electrode Technique (RDE) and Chronoamperometry techniques (CA). At room temperature Pd_3Sn_2/C and PdRh/C presented almost the same activity towards glucose electrooxidation; however the first one presented higher poisonous rate. Considering the activity (good activity) and poisonous-tolerance together (the highest among the examined electrocatalysts), $Pd_{30}Au_{70}$/C was chosen for being studied as glucose sensor. Moreover, the effect of glucose's, electrolyte's concentration and temperature were studied, extracting important kinetic parameters for glucose's electrooxidation reaction. Increasing glucose's and electrolyte's concentration, current density was

enhanced for all the examined electrocatalysts, except for Pd_xRh_y/C ones over which for electrolyte's concentration higher than 1 M KOH current density was suppressed. Finally, glucose electrooxidation reaction current density was increased increasing temperature until 40°C. For higher temperature values glucose's alkaline solution was observed to degrade forming a dark yellow caramel line smell liquid, decreasing current density values. For T>30°C, PdRh/C is suggested as anode material for glucose electrooxidation reaction, while $Pd_{30}Au_{70}/C$ as glucose sensors' material. Future outlooks are the optimization of the electrocatalysts' preparation method as well as of the PdRh/C and $Pd_{30}Au_{70}/C$ electrocatalysts and the development of a single direct glucose alkaline fuel cell.

List of publications in refereed Journals

1. L. Yan, A. Brouzgou, H. Liu, Y. Meng, M. Xiao, P. Tsiakaras and S. Song, *Glucose Electrooxidation in Alkaline Medium: Efficient and Poison-Tolerant PdAu/C Catalysts for Fuel Cell and Sensor applications* submitted to Applied Catalysis B: Environmental.
2. A. Brouzgou, S. Song and P. Tsiakaras, *Carbon-supported PdSn and Pd_3Sn_2 anodes for Glucose Electrooxidation in Alkaline Media*, submitted to Applied Catalysis B: Environmental.
3. A. Brouzgou, L. Yan, S. Song and P. Tsiakaras, *Glucose electrooxidation over Pd_xRh/C electrocatalysts in alkaline medium*, Applied Catalysis B: Environmental 147 (2014) 481-489.
4. A. Brouzgou, A. Podias and P. Tsiakaras, *PEMFCs and AEMFCs directly fed with ethanol: a current status comparative review*, Journal of Applied Electrochemistry 43 (2) (2013) 119-136.
5. Y. Wang, Ch. He, A. Brouzgou, Y. Liang, R. Fu, D. Wu, P. Tsiakaras and S. Song, *A facile soft-template synthesis of ordered mesoporous carbon/tungsten carbide composites with high surface area for methanol electrooxidation,* Journal of Power Sources 200 (2012) 8-13.
6. S. Song, Ch. He, J. Liu, Y. Wang, A. Brouzgou and P. Tsiakaras, *Two-step sequence for synthesis of efficient PtSn@Rh/C catalyst for oxidizing ethanol and intermediate products* Applied Catalysis B: Environmental 119-120 (2012) 227-233.
7. A. Brouzgou, S. Song and P. Tsiakaras, *Low and non-platinum electrocatalysts for PEMFCs: Current status, challenges and prospects*, Applied Catalysis B: Environmental 127 (2012) 371-388.

CHAPTER I

Introduction

Abstract

In this chapter, introduction information is given about the motivation and background of the present Ph.D. thesis. A review is presented of the relevant literature and the main sections of the present thesis are outlined. Glucose is a very promising fuel for fuel cells and sensors, which can be used as medical implants in human body. Among the examined electrocatalysts for glucose electrooxidation, Pt and Au are the most studied ones. However, both of them are high cost and scarce metals. On the other hand, Pd which is in abundance and at low price has been proved to exhibit in alkaline media similar or enhanced performance than Pt. Today, Pd-based electrocatalysts have not been enough studied for glucose electrooxidation reaction. The novelty of the present Ph.D. thesis is the study of Pd_x-X(=Sn, Rh, Ru, $Au)_y$/C electrocatalysts and the extraction of their kinetic parameters for glucose electrooxidation reaction. The relative results are reported for first time in literature and have led to a significant number of publications in refereed journals.

CONTENTS

CHAPTER I ..... **i**

1. Motivation and background **1**

2. PhD Thesis Chapters **5**

References…… **8**

CHAPTER II ..... **i**

1. The Fuel Cell Systems **12**

1.1. What is a Fuel Cell? 12

1.2. Historical Overview 13

1.3. Basic Elements and Materials 15

1.4. Classification of Fuel Cells 17

1.5. The Main Advantages & Disadvantages of Fuel Cells Technology 18

1.6. Fuel cells Applications 21

2. Fuels for Fuel Cells & Anode Electrocatalysts **25**

2.1. Hydrogen 25

2.2. Alcohols 28

2.3. Glucose 33

3. Alkaline fuel cells (AFCs) **35**

3.1. Historical Overview 35

3.2. AFCs Background and Principles of Operation 36

3.3. Anion (alkaline) Membrane Fuel Cells vs. Proton Exchange Membrane Fuel Cells. 40

3.4. Research Challenges and Future Perspectives 45

4. Direct Glucose Alkaline Fuel Cells (DGAFCs) **46**

4.1. Historical overview 46

4.2. Electrochemical oxidation of glucose & principle operation of abiotic direct glucose fuel cells 54

4.3. Design characteristics of DGFCs 57

4.4. Electrocatalysts for DGFCs 62
4.4.1. Pt-based electrocatalysts 63
4.4.2. Au-based electrocatalysts 71
4.4.3. Pd-based electrocatalysts 76
4.4.4. Raney-type electrocatalysts 78
4.4.5. Other electrocatalysts 81
4.5. Direct glucose fuel cells applications & future prospects 83
References 86
CHAPTER III..... i
1. Preparation Method of Electrocatalysts: modified microwave assisted polyol method. 101
2. Physicochemical Characterization 103
2.1. Transmission Electron Microscopy.....103
2.1.1. Historical background 104
2.1.2. Principles of operation 105
2.2. Scanning Electron Microscopy / Energy Dispersive X-Ray Spectroscopy (SEM/EDS) 107
2.2.1. Historical background 108
2.2.2. Principles of operation 108
2.3. X-Ray Diffraction Technique 111
2.3.1. Historical background 111
2.3.2. Principles of operation 113
2.4. Thermogravimetric analysis 115
2.4.1. Principles of operation 115
2.4.2. Instrumental apparatus 117
3. Electrochemical Methods for Catalyst Activity Evaluation 118
3.1. Introduction 118
3.2. Cyclic Voltammetry 120

3.2.1. Basic principles *120*

3.2.2. Instrumental apparatus *124*

3.2.3. Electro-kinetic analysis *126*

3.3. Chronoamperometry 129

3.4. Rotating disk electrode technique (RDE) 130

3.4.1. Basic principles *130*

3.4.2. Instrumental apparatus *131*

References… **134**

CHAPTER IV ..... **i**

1. Introduction **135**

2. Experimental **136**

2.1. Catalyst preparation 136

2.2. Physico-chemical characterization 136

2.3. Electrochemical analysis 137

3. Results and discussion **138**

3.1. Physico-chemical characterization 138

3.2. Electrochemical characterization 143

Conclusions **148**

References… **149**

CHAPTER V i

1. Introduction **151**

2. Experimental **153**

2.1. Materials 153

2.2. Catalyst preparation 153

2.3. Physicochemical Characterization 154

2.4. Electrochemical Characterization 154

3. Results & Discussion **155**

3.1. Characterization of Pd_xRh/C 155

3.2. Electrochemical Characterization 157
3.2.1. Glucose Electrooxidation 157
3.2.2. Effect of concentration of electrolyte and glucose 159
3.2.3. Effect of varying potential sweep rate 162
3.2.4. Effect of temperature 164
3.2.5. Chronoamperometric measurements 165
Conclusions 166
References… 168
CHAPTER VI 172
1. Introduction 175
2. Experimental 176
2.1. Electrocatalysts Preparation 176
2.2. Electrocatalysts Characterization 177
2.2.1. Physico-chemical Characterization 177
2.2.2. Electrochemical Characterization 177
3. Results and discussion 178
3.1. Physico-chemical Characterization 178
3.2. Electrochemical Characterization 180
3.2.1. Electrochemical active surface area (EASA) 180
3.2.2. Glucose electrooxidation reaction (GOR) 183
3.2.3. Effect of glucose's and electrolyte's concentration 184
3.2.4. Effect of the scan rate 187
3.2.5. The effect of temperature 189
3.2.6. Chronoamperometric measurements 191
Conclusions 192
References… 193
CHAPTER VII i
1. Introduction 192

2. Experimental.....193
2.1. Catalysts' preparation.....193
2.2. Physicochemical Characterization.....194
2.3. Electrochemical Characterization.....194
3. Results & Discussion.....195
3.1. Physicochemical Characterization.....195
3.2. Electrochemical Characterization.....197
***3.2.1. Glucose electrooxidation*.....197**
***3.2.2. Effect of glucose's and electrolyte's concentration*.....199**
***3.2.4. Effect of temperature*.....200**
***3.2.5. Chronoamperometric measurements*.....201**
Conclusions…… ……202
References… 203
CHAPTER VIII i
1. Introduction.....205
2. Physicochemical Evaluation.....206
3. Electrochemical Evaluation 208
References… 216
CHAPTER IX..... i
Conclusions and perspectives.....217

List of Tables

Table 2.1: Typical characteristics of fuel cell systems.....18

Table 2.2: Publications and patents related to the development of implantable abiotically catalyzed glucose fuel cells [19]. 50

Table 2.3. Pt-based electrocatalysts in DGFCs-performance characteristics.....69

Table 2.4. Au-based electrocatalysts in DGFCs-performance characteristics.....75

Table 2.5. Raney-type electrocatalysts for implantable glucose fuel cells.....80

Table 2.6. Other studied electrocatalysts for glucose oxidation reaction. 82

Table 4.1. Physico-chemical properties of the as-prepared Pd/C, Au/C and PdxAuy/C catalysts.....139

Table 5.1. Structural parameters of the as prepared catalysts.....156

Table 5.2. Electrocatalytic kinetic parameters on different electrodes in 0.5 mol L^{-1} KOH, at 25 ^{o}C, 20 mV s^{-1}. 159

Table 6.1. Structural parameters of the as-prepared catalysts. 179

Table 6.2. Electrocatalytic kinetic parameters on different electrodes in 0.5 M KOH, .182

Table 6.3. Cyclic voltammetry parameters on different electrodes in 0.5 M KOH + 0.5 glucose, at 25 ^{o}C, 20 mV s^{-1}. 184

Table 7.1. Structural parameters of the Pd_xRu_y/C electrocatalysts.....196

Table 7.2. Electrocatalytic kinetic parameters on different electrodes in 0.5 M KOH, at room temperature, 20 mV s^{-1}. 198

Table 8.1. Physico-chemical properties of the as-prepared electrocatalysts. 207

Table 8.2. Electrochemical active surface area calculated from cyclic voltammetry measurement in 0.5 M KOH, 20 mV s^{-1}. 208

Table 8.3. Forward and backward anodic peak current density. 211

Table 8.4. Kinetic parameters derive from Tafel equation. 212

List of Figures

Figure 2.1. Schematic design of a proton exchange membrane fuel cell using hydrogen as fuel. 13

Figure 2.2. Historical review of fuel cells [5]. 14

Figure 2.3. Typical planar flat-stack configuration. 17

Figure 2.4. Example of polarisation curve of a fuel cell [7]. 20

Figure 2.5: H_2-PEMFC operation results: Maximum Power Density (mW cm^{-2}) dependency on total (anode + cathode) Pt loading (µg cm^{-2}). In the brackets the reference number is reported. 27

Figure 2.6: Direct Methanol Fuel Cell operation results: Maximum DMFCs power density dependency on total (anode + cathode) platinum loading (µg cm^{-2}). In the brackets the reference number is reported. 30

Figure 2.7: Direct Ethanol Fuel Cell operation results: Maximum DEFCs power density dependency on total (anode + cathode) platinum loading (µg cm^{-2}). In the brackets the reference number is reported. 32

Figure 2.8. Operation principle of H_2-alkaline fuel cell. 37

Figure 2.9: DEFC operational results: maximum DEFCs power density (mW cm^{-2}) at 60 °C of Pt-based and Pt-free electrocatalysts in acidic and alkaline environment dependency on platinum or palladium loading (µg cm^{-2}); (Troom: room temperature; T_{40}: 40 °C; T_{80}: 80 °C; T_{100}: 100 °C; T_{145}: 145 °C; open triangle Pt-containing PEM-DEFC, filled triangle Pt-containing AEM-DEFC, open square 44

Figure 2.10: General electrode reactions of an abiotically catalyzed glucose–oxygen fuel. 55

Figure 2.11: Tentative oxidation pathways and intermediate reaction products of glucose oxidation [153]. 56

Figure 2.12: Two-chamber glucose fuel cell according to Ref. [27] with identical platinum reprinted from [19]). 57

Figure 2.13: Glucose fuel cell with hydrophobic cathode membrane (schematic outline) (reprinted from [19]).....58

Figure 2.14: Fuel cell design with oxygen-selective cathode catalyst and special electrode (reprinted from [19]). 59

Figure 2.15: Glucose fuel cell with selective electrode catalysts (schematic outline) according [71] (reprinted from [19]). 60

Figure 2.16: Simplified schematics of flow-through type fuel cells intended for blood (reprinted from [19]). 60

Figure 2.17: Simplified schematics of immersible fuel cells intended for tissue implantation: (A) fuel cell with hydrophobic cathode membrane, (B) fuel cell with oxygen-selective cathode catalyst (reprinted from [19]).....61

Figure 3.1. Pulse microwave assisted polyol process.....103

Figure 3.2. Interactions between electrons and material [6].....104

Figure 3.3. Schematic diagram of inner atomic electron shells.....109

Figure 3.4. EDS spectrum, showing K peaks of Na, Al and Si.....111

Figure 3.5. (a) A typical TGA of single walled carbon nanotubes, (b) Graph illustrating the ambiguity in determining T_{onset}. 116

Figure 3.6. Instrument of thermogravimetric analysis [11]. 118

Figure 3.7. A typical cyclic voltammogram for a reversible reaction. 121

Figure 3.8. A typical electrode reaction. 122

Figure 3.9. Fermi levels in a metal.....123

Figure 3.10. Fermi level when voltage is applied. 123

Figure 3.11. Illustration of the basic circuitry of a potentiostat [12].....124

Figure 3.12. Schematic representation of the composition of the solution phase in the vicinity of the electrode surface [13]. 125

Figure 3.13. Methodology for extracting kinetic parameters from CV measurements [14]. 129

Figure 3.14. Rotating disk electrode equipment. Reprinted from Ref. [15]. 131

Figure 3.15. Scheme of the flow on working electrode surface. Reprinted from Ref. [15]. 132

Figure 3.16. Linear sweep voltammetric measurement with RDE. Reprinted from Ref. [15]. 133

Figure 4.1. XRD patterns for Pd/C and Au/C (A) and PdxAuy/C binary catalysts (B) and their corresponding detailed Pd or Au (220) peaks scanned at 1^{o}C min^{-1} (C). 138

Figure 4.2. TEM images of Pd/C (A), Au/C (B), Pd70Au30/C (C) and Pd30Au70/C (D) and their corresponding particle size distribution (A', B', C' and D'). 140

Figure 4.3. Thermogravimetric curves of Pd/C, Au/C and PdxAuy/C samples. 141

Figure 4.4. SEM-EDS of the as prepared PdxAuy/C binary catalysts. The number in SEM is randomly and automatically given by the SEM instrument. 142

Figure 4.5.Cyclic voltammetric curves of Pd/C (A) and Au/C (B) in 0.1 mol L^{-1} NaOH aqueous solution in the absence or presence of 20 mmol L^{-1} glucose at 50 mV s^{-1} and at 36.5^{o}C. 143

Figure 4.6. Comparative results of glucose electrooxidation at Pd/C and Au/C. Electrolyte: 0.1 mol L^{-1} NaOH+ 20 mmol L^{-1} glucose; Scan rate: 50 mV s^{-1}, Temperature: 36.5^{o}C. 145

Figure 4.7. Cyclic voltammetric curves of Pd/C, Au/C and Pd_xAu_y/C mono and binary catalysts in 0.1 mol L^{-1} NaOH aqueous solution in the absence (A) or presence of 20 mmol L^{-1} glucose (B) at 50 mV s^{-1} and at 36.5^{o}C. 145

Figure 4.8. Cyclic voltammograms for $Pd_{30}Au_{70}$/C catalyst in 0.1 mol L$_{-1}$ NaOH aqueous solution containing different concentrations of glucose at 50 mV s^{-1} and at 36.5^{o}C. Inset: current density vs. higher glucose concentration. 146

Figure 4.9. Current-time record of $Pd_{30}Au_{70}$/C catalyst fixed onto rotating disk electrode (1600 rpm) by successively injection 1 mM glucose into 0.1 M NaOH solution at a regular interval time of 60 s. Applied potential: -0.2 V. Inset: the relationship between the current density and the added glucose solution. 147

Figure 5.1. XRD results of the as-prepared carbon supported Pd_xRh/C electrocatalysts. 155

Figure 5.2. TEM images of (A) PdRh/C, (B) Pd_2Rh/C, (C) Pd_3Rh/C and (D) Pd/C..156

Figure 5.3. Cyclic voltammograms of the PdxRh/C electrocatalysts in: (A) 0.5 mol L^{-1} KOH solution and (B) 0.5 mol L^{-1} KOH containing 0.5 mol L^{-1} glucose (scan rate: 20 mV s^{-1}, room temperature). 158

Figure 5.4. Cyclic voltammograms of the PdRh/C electrocatalyst in: (A) 0.1, (B) 0.3, (C) 0.5 and (D) 1 mol L^{-1} KOH containing y (=0.02, 0.05, 0.2, and 0.5 mol L^{-1}) glucose (scan rate: 20 mV s^{-1}, room temperature). Fig. 5.4 (E): Peak current desnsity in terms of KOH's and glucose's concentration. 160

Figure 5.5. (A) Cyclic voltammograms of PdRh/C electrocatalyst in 0.5 mol L^{-1} KOH containing (=0.02, 0.05, 0.2, and 0.5 mol L^{-1}) glucose (scan rate: 5 mV s^{-1}, room temperature), (B) Tafel plots derived from Fig. 5.5 (A). 161

Figure 5.6. (A) Cyclic voltammograms of the PdRh/C electrocatalyst in 0.5 mol L^{-1} KOH containing 0.5 mol L^{-1} glucose at different scan rates in room temperature, (B) Anodic peak current density vs. square root of scan rate, extracted from Fig.5.6 (A), (C)Peak potential vs. ln(v) extracted from Fig. 5.6 (A).....163

Figure 5.7. (A) Cyclic voltammograms of PdRh/C at different temperature values (T=25, 36.5, 48 and 60^oC), in 0.5 mol L^{-1} KOH containing 0.5 mol L^{-1} glucose, 5 mV s^{-1}, (B) Arrhenius plots for the Pd_xRh/C and Pd/C electrocatalysts derived from cyclic voltammograms at 5 mV s^{-1}. 164

Figure 5.8. Chronoamperometric curves at -0.13 V (vs. Hg/HgO) for 1300 sec, in a 0.5 mol L^{-1} KOH with 0.5 mol L^{-1} glucose solution.....166

Figure 6.1. XRD results of the as-prepared carbon supported Pd/C and PdxSny/C electrocatalysts. 179

Figure 6.2. TEM images of Pd_3Sn_2/C (A), PdSn/C (B) and Pd/C (C).....180

Figure 6.3. Cyclic voltammogram for Pd/C, PdSn/C and Pd_3Sn_2/C in 0.5 M KOH at 25 ^oC, 20 mV s^{-1}. 181

Figure 6.4. Cyclic voltammogram for Pd/C, PdSn/C and Pd3Sn2/C in 0.5 M KOH + 0.5 M Glucose at 25 ^{o}C, 20 mV s^{-1}. 183

Figure 6.5. Cyclic voltammograms of the Pd_3Sn_2/C electrocatalyst in: (A) 0.1, (B) 0.3, (C) 0.5 (D) 1 and 2 M KOH containing y (=0.02, 0.05, 0.2, and 0.5 M) glucose (scan rate: 20 mV s^{-1}, room temperature). Fig. 6.5 (F): Peak current density dependence of glucose's concentration. 185

Figure 6.6. Cyclic voltammograms of Pd_3Sn_2/C electrocatalyst in 0.5 mol L^{-1} KOH containing (=0.02, 0.05, 0.2, and 0.5 mol L^{-1}) glucose (scan rate: 5 mV s^{-1}, room temperature). Inset: Tafel plots. 186

Figure 6.7. (A) Cyclic voltammograms of the Pd_3Sn_2/C electrocatalyst in 0.5 M KOH containing 0.5 M glucose at different scan rates in room temperature. Inset: Dependence of anodic peak current during the forward sweep on the square roots of potential sweep rate, (B) E_p *vs.* ln(v). 188

Figure 6.8. Cyclic voltammograms at different temperature values (T=25, 30, 36.5 and 40^{o}C), in 0.5 mol L^{-1} KOH containing 0.5 mol L^{-1} glucose, 5 mV s^{-1} of: Pd_3Sn_2/C, PdSn/C and Pd/C . Arrhenius plots (second graph). 191

Figure 6.9. Chronoamperometric curves at -0.13 V (vs. Hg/HgO) for 1300 sec, in a 0.5 mol L^{-1} KOH with 0.5 mol L^{-1} glucose solution. 192

Figure 7.1. XRD patterns of (a) $PdRu_3$/C, (b) $PdRu_2$/C, (c) PdRu/C, (d) Pd_2Ru/C and (e) Pd_3Ru/C. 195

Figure 7.2. TEM images of the: PdRu/C (A), PdRu2/C (B), PdRu3/C (C), Pd2Ru/C (D) and Pd3Ru/C (E). 196

Figure 7.3. Cyclic voltammograms of the Pd_xRu_y/C electrocatalysts in 0.5 M KOH solution, 20 mV s^{-1}, room temperature. 197

Figure 7.4. Cyclic voltammograms of the Pd_xRu_y/C electrocatalysts in 0.5 M KOH containing 0.5 M glucose, 20 mV s^{-1}, room temperature. 198

Figure 7.5. Cyclic voltammograms of the Pd_2Ru/C electrocatalyst in: (A) 0.1, (B) 0.3, (C) 0.5 (D) 1 and (E) 2 M KOH containing y (=0.02, 0.05, 0.2, and 0.5 M) glucose (20 mV s^{-1}, room temperature). 199

Figure 7.6. (A, B, C, D & E) Cyclic voltammograms of Pd_xRu_y/C at different temperature values (T=25, 30, 36.5 and 40^oC), in 0.5 mol L^{-1} KOH containing 0.5 mol L^{-1} glucose, 5 mV s^{-1}, (F) Arrhenius plots for the Pd_xRu_y/C electrocatalysts derived from cyclic voltammograms at 5 mV s^{-1}. 200

Figure 7.7. Chronoamperometric curves at -0.13 V (vs. Hg/HgO) for 1300 sec, in a 0.5 mol L^{-1} KOH with 0.5 mol L^{-1} glucose solution. 202

Figure 8.1. XRD patterns (only the Pd planes are indicated). 207

Figure 8.2. Comparison of cyclic voltammetry results of the best Pd-binary electrocatalysts, in 0.5 M KOH with 0.5 M glucose, 20 mV s^{-1}, room temperature, (*$Pd_{30}Au_{70}/C$: 20 mmol L^{-1}, 36.5^oC, 50mV s^{-1}). 209

Figure 8.3. Peak current density *vs.* metal loading. In all cases Pd+M loading equals to 72 µgcm^{-2}. 210

Figure 8.4. *E*lectrochemical active surface area and lattice parameter dependency on peak current density 211

Figure 8.5. Comparison of electrocatalytic activity (peak current density) of the examined electrocatalysts at different temperature values: 0.5 M KOH, 0.5 M glucose, 5 mV s^{-1}, room temperature. 212

Figure 8.6. Arrhenius plots. 213

Figure 8.7. Comparison of examined electrocatalysts at different glucose's and electrolyte's concentration, 20 mV s^{-1}, room temperature (A-E), comparison of electrocatalysts at 0.5 M glucose. 214

Figure 8.8. Comparison of chronoamperometric measurements of the examined electrocatalysts, ,in 0.5 M KOH with 0.5 M glucose, 5 mV s^{-1}, room temperature. 215

1. Motivation and background

Glucose is the most abundant carbohydrate in nature easily produced by photosynthesis in plants such as sugar cane or corn and by a large amount of waste biomass generated by agricultural activities [20, 21]. The theoretical energy of glucose is 4430 Wh kg^{-1} and its complete oxidation (in alkaline media) to carbon dioxide can produce 24 electrons for each glucose molecule through the following chemical reactions:

Anode reaction: $C_6H_{12}O_6 + 24OH^- \rightarrow 6CO_2 + 18H_2O + 24e^-$ (1)

Cathode reaction: $6O_2 + 12H_2O + 24e^- \rightarrow 24OH^-$ (2)

Overall reaction: $C_6H_{12}O_6 + 6O_2 \rightarrow 6CO_2 + 6H_2O$ (3)

A potential approach to obtain energy from glucose is to be used as fuel of a fuel cell, where glucose can be directly oxidized generating electricity, similarly to direct methanol (DMFCs) [22, 23] and direct ethanol fuel cells (DEFCs) [24, 25].

The electrooxidation of glucose has mainly two purposes: i) in vivo applications (as human implantable devices that will power microelectromechanical (MEMS) devices [26, 27] and ii) the development of glucose electrochemical sensors for diabetes check. Glucose could be virtually withdrawn without limit from the flow of blood providing a long-term or even permanent power supply for such devices as pacemakers, glucose sensors for diabetics or small valves for bladder control. Towards this direction, initially many attempts have been focused mainly on the development of enzymatic and microbial glucose fuel cells. More precisely, in the past few decades most researches had been turned to the immobilization methods for enzymatic catalysts in an effort to increase the lifetime of enzymes and therefore of glucose fuel cells [28-34]. Enzymatic catalysts for glucose/O_2 fuel cells have excellent selectivity and can produce power densities of several mW cm^{-2}. However, they have very short lifetime, typically less than thirty days, due to the fragile nature of the enzymes and poor immobilization techniques. This makes them generally unsuitable for long-term implantable applications despite having been successfully tested in-vivo. Desirable electrocatalysts, in terms of high current, low overpotential for glucose oxidation and

good poison tolerance, is the solution to achieve fast response for glucose detection and high performance for direct glucose fuel cells.

At present, Pt [35], Au [36], Pd [37-39] and their based binary or ternary catalysts such as Pt-Pd [40], PtBi [29], PtRu [29], PtPb [41], PtAu [17, 40], Au-Ag [42], PtAuPd [43] *etc*, and multi-wall carbon nanotubes [44] have been found to exhibit good electrocatalytic activity towards glucose oxidation. Among them, Pt is the first and most widely investigated material for glucose electrooxidation.

However, it is not a very suitable catalyst due to its high chemisorbability and its poor selectivity of different substances presented in physiological solutions [12]. A number of investigations have also been devoted to Au, after it was found to be more active and poison tolerant than Pt towards the reaction of glucose electrooxidation in neutral and alkaline solutions [45]. However, the potential for glucose oxidation on Au is still too high for glucose detection [46]. Alloyed electrocatalysts are often adopted to obtain better performance than pure metals, through exploiting the specific properties of each component. It has been recognized that the activity of Pt to glucose electrooxidation in alkaline media can be enhanced by alloying Pd, Au, Bi, Ru *etc.* [40, 47]. However, novel efficient and stable electrocatalysts are still urgently needed. Concerning glucose's electrooxidation reaction mechanism over Pt, Au and Pd there is limited information.

In the hydrogen adsorption potential region on Pt, the hydrogen on the C_1 atom (on the hemiacetal group of the cyclic glucose) is first oxidized [13, 48, 49], ii) in the platinum double layer potential region, glucose is oxidized to a strongly adsorbed intermediate such as gluconolactone, gluconic acid, CO or "reduced CO_2" [50, 51]. Rao and Drake [52] discovered that the main product of electrooxidation of glucose was gluconic acid. Ernst *et al.* [36] using mass spectrometry found that the primary product of electrolysis of glucose was gluconolactone. The hydrolysis of gluconolactone leads to a stable product (gluconic acid). Yager *et al.* [53] using in-situ FTIR to study the electrooxidation of glucose found that the major adsorbate causing the surface poisoning is linear CO. Gluconolactone and gluconic acid were also found in the platinum double layer region. iii) In the platinum oxide formation region, a

reaction between glucose and the Pt-OH layer was assumed to occur and the poisoning species of the lactone type or "reduced CO_2" are decomposed through further oxidation in this region [51]. Vielstich *et al.* [51] have examined the reaction products by differential electrochemical mass spectroscopy (DEMS). If the scanning potential does not reach the platinum oxide region the oxidation current of glucose will be completely suppressed by the species produced during the glucose oxidation after several scans. If the scanning potential does reach the platinum oxide region, however, the voltammetry of glucose electrooxidation for the anodic scan will be constant after several scans. Thus, glucose electrooxidation on platinum electrodes has two different mechanisms depending on whether the electrode surface is oxide covered or not.

Platinum is not a suitable electrode for sensor application in the blood and physiological condition due to self-poisoning in glucose oxidation and chemisorption of chloride ion and other blood components on it [36]. Moreover it lacks sufficient specificity as to which of various organic substances are oxidized and it is very susceptible to poisoning by many trace agents presenting lack of long term stability [54]. The catalytic activity of platinum electrode is lost by the accumulation of chemisorbed intermediates from the glucose oxidation. A possible solution to this problem of surface poisoning by an adsorbed intermediate involves the use of underpotential deposition (UPD) method of metals onto the support. Adzic *et al.* [55] have reported that adatoms such as lead, thallium, bismuth, tin, cadmium, mercury, copper and silver on electrodes such as platinum, rhodium, iridium and palladium can enhance the rate of oxidation of some organic molecules by several orders of magnitude. Adatoms of Pb, Tl and Bi caused a great enhancement of the catalytic activity of Pt for oxidation of glucose in acid, neutral and alkaline solutions [50, 56, 57]. Sn [12], Cu and Ag [58] adatoms on Pt showed no effect for this reaction in acid solution, but it was not clear what the coverage was. In other studies with UPD layer, the catalytic activity is often strongly dependent on coverage of the UPD layer and decreases rapidly as the coverage approaches unity.

Gold showed larger currents than platinum electrodes for glucose oxidation in neutral and alkaline solutions [12]. A layer of gold oxide formed on the surface of a

gold electrode was found to cause a great effect on glucose oxidation [12]. Makovos and Liu [59] have investigated the reaction at the potentials of oxide formation on Au. The products of glucose electrooxidation on Au in neutral phosphate buffer solution were investigated by Vielstich *et al.* [51]. No CO or CO_2 was found for the oxidation of glucose on Au in the double layer region. This is different from Pt electrode for this reaction in the double layer region. It indicates that the mechanism of glucose oxidation is different between Au and Pt in the double layer region. Gold has been shown to be a poor electrocatalyst for glucose oxidation in acid solution except in the region of oxide formation [12]. This conclusion was based on data obtained with sulfuric acid solutions. Anions with strongly specific adsorption of bisulfate and sulfate anions could cause such an effect. It has been shown that Au has a sizeable activity for glucose electrooxidation but only in acids with weakly adsorbing anions.

Many others electrodes, besides Pt and Au, have also been investigated for this reaction, but most of them in acid solution. The onset potential of glucose oxidation in acid solution on the iridium electrode was approximately 0.56 V more negative than the platinum electrode for this reaction [13]. The peak current of glucose electrooxidation for electrodes (e.g. iridium, rhodium, copper, glassy carbon, platinum-ruthenium, platinum-rhodium and platinum-gold alloys, pthalocyanines and porphyrins complexes of cobalt, manganese and iron adsorbed on graphite) was smaller than platinum electrode for this reaction in acid or neutral solutions [12-15]. However, iridium, rhodium and macrocycles modified electrodes showed a poor reproducibility in neutral solutions [12]. No current was found for cobalt, nickel, silver and cobalt porphyrin electrodes for glucose oxidation in neutral buffer solutions and the palladium electrode for this reaction in acid solution [12, 13]. Chloride ions are strongly adsorbed on platinum electrodes as it was above mentioned. Moreover, platinum is an extremely non-selective electrocatalyst and decreases its catalytic activity with time. Improvements of catalytic activity for glucose oxidation by foreign metal adatoms such Pb, Bi and Tl on Pt are not suitable for in vivo application because of the difficulty of maintaining upd layer at proper coverage in biological systems.

Gold, as it has already been referred, is a more active electrocatalyst than platinum for glucose electrooxidation in neutral buffer and alkaline media. It is not

easy to be poisoned by some intermediates and/or products. Additionally, palladium has been known to exhibit superior activity for electrooxidation of alcohols and polyalcohols in alkaline solutions [60] and its abundance on the earth is at least 50 times more than that of Pt's. The combination of Pd and Au has shown good catalytic activity to glucose selective electrooxidation [61]. Therefore, gold and palladium appear to be good candidates for glucose sensors and direct alkaline glucose fuel cells.

In literature up to date there is no study over binary Pd-based electrocatalysts for glucose electrooxidation. The Ph.D thesis research involves the study and comparison of Pd_xRu_y/C, Pd_xRh_y/C, Pd_xSn_y/C and Pd_xAu_y/C (prepared via a modified microwave-assisted polyol method) as anodes electrocatalysts for glucose electrooxidation and as glucose sensor. Factors such as temperature, glucose's and electrolyte's concentration which affect the electrocatalysts' activity are also studied. Kinetic parameters are obtained via the electrochemical measurements.

2. PhD Thesis Chapters

The rest PhD thesis is classified into eight more Chapters. More precisely:

In Chapter II: The aim of Chapter II is a quick introduction at the basic elements of fuel cells, a quick view in their historical background and their applications. Then a brief discussion is done about the fuels used in fuel cells and about alkaline fuel cells. In sequence a brief historical overview of direct glucose fuel cells and the state-of-the-art of electrocatalysts that have been studied as anodes are also discussed.

In Chapter III: The experimental techniques and their main principles that were used for the physicochemical and electrochemical characterization of the studied electrocatalysts are described.

In Chapter IV: Carbon supported Pd_xAu_y binary electrocatalysts investigated for glucose electrooxidation and detection prepared by a modified pulse microwave-assisted polyol method. The physico-chemical properties were obtained by X-ray diffraction (XRD), transmission electron microscopy (TEM), scanning electron microscopy (SEM-EDS) and thermogravimetric analysis (TG). The electrochemical activity was investigated

by the aid of cyclic voltammetry and chronoamperometry. Via the Rotating disk electrode (RDE) technique $Pd_{30}Au_{70}/C$ electrocatalyst is tested also as glucose sensor.

In Chapter V: Carbon Vulcan XC-72R supported Pd_xRh (x=1, 2, 3) nanoparticles have been prepared by a modified pulse microwave assisted polyol method and have been studied for glucose electrooxidation in alkaline media. The Pd_xRh/C electrocatalysts have been characterized by X-ray diffraction (XRD), Transmission Electron Microscopy (TEM), Cyclic Voltammetry (CV) and Chronoamperometric measurements (CA).

In Chapter VI: PdSn (20 wt%) and Pd_3Sn_2 (20 wt%) nanoparticles supported on Vulcan XC-72 were prepared by a modified microwave-assisted polyol method and studied for glucose electrooxidation in alkaline media. The electro-catalysts were characterized by X-Ray Diffraction (XRD), Transmitting Electron Microscope (TEM), Cyclic Voltammetry (CV) and Chronoamperometry (CA).

In Chapter VII: (20 wt%) Pd_xRu_y/C (x:y=1:2, 1:3, 2:1 and 3:1) electrocatalysts were prepared by a modified pulse microwave assisted polyol method and studied for glucose electrooxidation in alkaline media. The physicochemical characterization of electrocatalysts was conducted by X-ray diffraction (XRD) and Transmission Electron Microscopy (TEM), while the electrochemical characterization with Cyclic Voltammetry (CV) and Chronoamperometry techniques (CA).

In Chapter VIII: The physicochemical and electrochemical results of the as-examined electrocatalysts (Pd_xSn_y/C, Pd_xRh_y/C, Pd_xAu_y/C and Pd/C) are compared. The comparison is necessary in order to identify the most efficient electrocatalysts towards glucose electrooxidation and it will be helpful for future anode materials selection for the electrooxidation of glucose at low temperature working alkaline fuel cells. Since, Pd_xRu_y/C has poor electrocatalytic activity, is excluded from the comparison.

In Chapter IX: The Conclusions and future perspectives are summarized in Chapter IX. Pd-based electrocatalysts are preferred in alkaline media as they present much better activity and they are more stable than Pt-based ones. A modified microwave assisted polyol method was chosen for the preparation of electrocatalysts, because the following remarkable advantages: i) rapid volumetric heating, ii) higher reaction rate and selectivity, iii) shorter reaction time and iv) higher yield of the product compared

to the convention heating methods. The mean particle size of the as-prepared electrocatalysts was almost 10 nm, indicating that further optimization of the method is necessary. PdRh/C is suggested as anode electrocatalyst in fuel cells, while $Pd_{30}Au_{70}$/C as material for glucose sensors as it presents the highest poison-tolerance and good activity. The development of a single direct glucose alkaline fuel cell is a future outlook.

References

[1] Q. Shen, L. Jiang, H. Zhang, Q. Min, W. Hou, J.-J. Zhu, Journal of Physical Chemistry C 112 (2008) 16385-16392.

[2] N. Fujiwara, S.-i. Yamazaki, Z. Siroma, T. Ioroi, H. Senoh, K. Yasuda, Electrochemistry Communications 11 (2009) 390-392.

[3] J.P. Spets, Y. Kiros, M.A. Kuosa, J. Rantanen, M.J. Lampinen, K. Saari, Electrochimica Acta 55 (2010) 7706-7709.

[4] D. Basu, S. Basu, Electrochimica Acta 55 (2010) 5775-5779.

[5] X. Yan, X. Ge, S. Cui, Nanoscale Research Letters 6 (2011) 313.

[6] D. Basu, S. Basu, International Journal of Hydrogen Energy 36 (2011) 14923-14929.

[7] W. Huang, M. Wang, J. Zheng, Z. Li, Journal of Physical Chemistry C 113 (2009) 1800-1805.

[8] H. Yin, C. Zhou, C. Xu, P. Liu, X. Xu, Y. Ding, Journal of Physical Chemistry C 112 (2008) 9673-9678.

[9] Z. Liu, L. Huang, L. Zhang, H. Ma, Y. Ding, Electrochimica Acta 54 (2009) 7286-7293.

[10] C. Jin, I. Taniguchi, Materials Letters 61 (2007) 2365-2367.

[11] F.M. Cuevas-Muñiz, M. Guerra-Balcázar, F. Castaneda, J. Ledesma-García, L.G. Arriaga, Journal of Power Sources 196 (2011) 5853-5857.

[12] Y.B. Vassilyev, O.A. Khazova, N.N. Nikolaeva, Journal of Electroanalytical Chemistry 196 (1985) 127-144.

[13] Y.B. Vassilyev, O.A. Khazova, N.N. Nikolaeva, Journal of Electroanalytical Chemistry 196 (1985) 105-125.

[14] A.J. Appleby, C. Van Drunen, Journal of the Electrochemical Society 118 (1971) 95-97.

[15] N. Xonoglou, I. Moumtzis, G. Kokkinidis, Journal of Electroanalytical Chemistry and Interfacial Electrochemistry 237 (1987) 93-104.

[16] K.B. Kokoh, J.M. Léger, B. Beden, C. Lamy, Electrochimica Acta 37 (1992) 1333-1342.

[17] A. Habrioux, E. Sibert, K. Servat, W. Vogel, K.B. Kokoh, N. Alonso-Vante, The Journal of Physical Chemistry B 111 (2007) 10329-10333.

[18] S.M. El-Refaei, M.I. Awad, B.E. El-Anadouli, M.M. Saleh, Electrochimica Acta 92 (2013) 460-467.

[19] A. Ahmadalinezhad, S. Chatterjee, A. Chen, Electrochimica Acta In press corrected proof (2013).

[20] J.P.H. Van Wyk, Trends in Biotechnology 19 (2001) 172-177.

[21] K.C. Swades, R.L. Derek, Nature Biotechnology 21 (2003) 1229-1232.

[22] S. Song, W. Zhou, Z. Liang, R. Cai, G. Sun, Q. Xin, V. Stergiopoulos, P. Tsiakaras, Applied Catalysis B 55 (2005) 65-72.

[23] C. Feng, T. Takeuchi, M.A. Abdelkareem, T. Tsujiguchi, N. Nakagawa, Journal of Power Sources 242 (2013) 57-64.

[24] Y. Wang, S. Song, G. Andreadis, H. Liu, P. Tsiakaras, Journal of Power Sources 196 (2011) 4980-4986.

[25] G. Andreadis, V. Stergiopoulos, S. Song, P. Tsiakaras, Applied Catalysis B 100 (2010) 157-164.

[26] S. Kerzenmacher, M. Schroeder, R. Brämer, R. Zengerle, F. Von Stetten, Journal of Power Sources 195 (2010) 6516-6523.

[27] S. Kerzenmacher, U. Kräling, M. Schroeder, R. Brämer, R. Zengerle, F. Von Stetten, Journal of Power Sources 195 (2010) 6524-6531.

[28] S.C. Barton, H.-H. Kim, G. Binyamin, Y. Zhang, A. Heller, Journal of the American Chemical Society 123 (2001) 5802-5803.

[29] S.C. Barton, J. Gallaway, P. Atanassov, Chemical Reviews 104 (2004) 4867-4886.

[30] H.-H. Kim, Y. Zhang, A. Heller, Analytical Chemistry 76 (2004) 2411-2414.

[31] S. Shleev, J. Tkac, A. Christenson, T. Ruzgas, A.I. Yaropolov, J.W. Whittaker, L. Gorton, Biosensors and Bioelectronics 20 (2005) 2517-2554.

[32] R.A. Bullen, T.C. Arnot, J.B. Lakeman, F.C. Walsh, Biosensors and Bioelectronics 21 (2006) 2015-2045.

[33] C. Kang, H. Shin, A. Heller, Bioelectrochemistry 68 (2006) 22-26.

[34] F. Gao, Y. Yan, L. Su, L. Wang, L. Mao, Electrochemistry Communications 9 (2007) 989-996.

[35] S. Lee, H.J. Kim, S.M. Choi, M.H. Seo, W.B. Kim, Applied Catalysis A 429-430 (2012) 39-47.

[36] J.R. Rao, G.J. Richter, F. Von Sturm, E. Weidlich, Bioelectrochemistry and Bioenergetics 3 (1976) 139-150.

[37] Q. Wang, X. Cui, J. Chen, X. Zheng, C. Liu, T. Xue, H. Wang, Z. Jin, L. Qiao, W. Zheng, RSC Advances 2 (2012) 6245-6249.

[38] L.-M. Lu, H.-B. Li, F. Qu, X.-B. Zhang, G.-L. Shen, R.-Q. Yu, Biosensors and Bioelectronics 26 (2011) 3500-3504.

[39] C. Zhu, S. Guo, S. Dong, Journal of Materials Chemistry 22 (2012) 14851-14855.

[40] C. Zhu, S. Guo, S. Dong, Advanced Materials 24 (2012) 2326-2331.

[41] C. Hui-Fang, Y. Jian-Shan, L. Xiao, Z. Wei-De, S. Fwu-Shan, Nanotechnology 17 (2006) 2334.

[42] Z. Liu, L. Huang, L. Zhang, H. Ma, Y. Ding, Electrochimica Acta 54 (2009) 7286-7293.

[43] D. Basu, S. Basu, International Journal of Hydrogen Energy 37 (2012) 4678-4684.

[44] J.-S. Ye, Y. Wen, W. De Zhang, L. Ming Gan, G.Q. Xu, F.-S. Sheu, Electrochemistry Communications 6 (2004) 66-70.

[45] V.S. Bagotzky, Y.B. Vassiliev, Electrochimica Acta 11 (1966) 1439-1461.

[46] S.B. Aoun, G.S. Bang, T. Koga, Y. Nonaka, T. Sotomura, I. Taniguchi, Electrochem. Commun. 4 (2003) 317-320.

[47] Y. Yamauchi, A. Tonegawa, M. Komatsu, H. Wang, L. Wang, Y. Nemoto, N. Suzuki, K. Kuroda, Journal of the American Chemical Society 134 (2012) 5100-5109.

[48] M.F.L. de Mele, H.A. Videla, A.J. Arvía, Journal of the Electrochemical Society 129 (1982) 2207-2213.

[49] M.F.L. de Mele, H.A. Videla, A.J. Arvía, Bioelectrochemistry and Bioenergetics 9 (1982) 469-487.

[50] E. Skou, Electrochimica Acta 22 (1977) 313-318.

[51] A.E. Bolzan, T. Iwasita, W. Vielstich, Journal of the Electrochemical Society 134 (1987) 3052-3058.

[52] M.L.B. Rao, R.F. Drake, Journal of the Electrochemical Society 116 (1969) 334-337.

[53] I.T. Bae, E. Yeager, X. Xing, C.C. Liu, Journal of Electroanalytical Chemistry 309 (1991) 131-145.

[54] M.F.L. de Mele, H.A. Videla, A.J. Arvía, Journal of Electroanalytical Chemistry and Interfacial Electrochemistry 141 (1982) 469-487.

[55] R.R. Adzic, Advances in Electrochemistry and Electrochemical Engineering, New York, 1984.

[56] G. Kokkindis, J.M. Leger, C. Lamy, Journal of Electroanalytical Chemistry and Interfacial Electrochemistry 242 (1988) 221-242.

[57] N. Xonoglou, G. Kokkinidis, Bioelectrochemistry and Bioenergetics 12 (1984) 485-498.

[58] M. Sakamoto, K. Takamura, Bioelectrochemistry and Bioenergetics 9 (1982) 571-582.

[59] E.B. Makovos, C.C. Liu, Bioelectrochemistry and Bioenergetics 15 (1986) 157-165.

[60] C. Bianchini, P.K. Shen, Chemical Reviews 109 (2009) 4183-4206.

[61] S. Hermans, A. Deffernez, M. Devillers, Applied Catalysis A: General 395 (2011) 19-27.

CHAPTER II

Theoretical Background*

Abstract

The aim of Chapter II is to provide a quick introduction to the basic elements of fuel cells, and a quick view to their historical background and their applications. Then a brief discussion is done about the fuels used in fuel cells and about alkaline fuel cells. Alkaline (anion) fuel cells are proved to exhibit higher power density than proton exchange membrane fuel cells. Among fuels, hydrogen, methanol and ethanol, that can be used in alkaline and proton exchange membrane fuel cells glucose is considered to be a fuel with perspectives for the development of direct glucose fuel cells. A direct glucose fuel cell can be applied mainly as an implantable device in human body or as device for electricity and heat production in sugar industry. In sequence a brief historical overview of direct glucose fuel cells and the state-of-the-art of electrocatalysts that have been studied as anodes are also discussed. According to literature, Pt- and Au-based electrocatalysts are the most studied ones. However, a new type - of Raney based electrocatalysts - seems to present better activity and stability at *in-vivo* direct glucose fuel cell operation in human body. Finally, the future prospects of direct glucose fuel cells are also discussed.

*A. Brouzgou, S. Song, P. Tsiakaras, ***Low and non-platinum electrocatalysts for PEMFCs: Current status, challenges and prospects,*** Appl. Catal. B: Environ. 127 (2012) 371-388.

A. Brouzgou, A. Podias, P. Tsiakaras, ***PEMFCs and AEMFCs directly fed with ethanol: A current status comparative review,*** J. Appl. Electrochem. 43 (2) (2013) 119-136.

CONTENTS

CHAPTER II ..... **i**

1. The Fuel Cell Systems **12**

1.1. What is a Fuel Cell? 12

1.2. Historical Overview 13

1.3. Basic Elements and Materials 15

1.4. Classification of Fuel Cells 17

1.5. The Main Advantages & Disadvantages of Fuel Cells Technology 18

1.6. Fuel cells Applications 21

2. Fuels for Fuel Cells & Anode Electrocatalysts **25**

2.1. Hydrogen 25

2.2. Alcohols 28

2.3. Glucose 33

3. Alkaline fuel cells (AFCs) **35**

3.1. Historical Overview 35

3.2. AFCs Background and Principles of Operation 36

3.3. Anion (alkaline) Membrane Fuel Cells vs. Proton Exchange Membrane Fuel Cells 40

3.4. Research Challenges and Future Perspectives 45

4. Direct Glucose Alkaline Fuel Cells (DGAFCs) **46**

4.1. Historical overview 46

4.2. Electrochemical oxidation of glucose & principle operation of abiotic direct glucose fuel cells 54

4.3. Design characteristics of DGFCs 57

4.4. Electrocatalysts for DGFCs 62

4.4.1. Pt-based electrocatalysts 63

4.4.2. Au-based electrocatalysts *71*

4.4.3. Pd-based electrocatalysts *76*

4.4.4. Raney-type electrocatalysts *78*

4.4.5. Other electrocatalysts *81*

4.5. Direct glucose fuel cells applications & future prospects 83

References **86**

List of Tables

Table 2.1: Typical characteristics of fuel cell systems. 18

Table 2.2: Publications and patents related to the development of implantable abiotically catalyzed glucose fuel cells [19]. 50

Table 2.3. Pt-based electrocatalysts in DGFCs-performance characteristics. 69

Table 2.4. Au-based electrocatalysts in DGFCs-performance characteristics. 75

Table 2.5. Raney-type electrocatalysts for implantable glucose fuel cells. 80

Table 2.6. Other studied electrocatalysts for glucose oxidation reaction. 82

List of Figures

Figure 2.1. Schematic design of a proton exchange membrane fuel cell using hydrogen as fuel. 13

Figure 2.2. Historical review of fuel cells [5]. 14

Figure 2.3. Typical planar flat-stack configuration. 17

Figure 2.4. Example of polarisation curve of a fuel cell [7]. 20

Figure 2.5: H_2-PEMFC operation results: Maximum Power Density (mW cm^{-2}) dependency on total (anode + cathode) Pt loading (µg cm^{-2}). In the brackets the reference number is reported. 27

Figure 2.6: Direct Methanol Fuel Cell operation results: Maximum DMFCs power density dependency on total (anode + cathode) platinum loading (µg cm^{-2}). In the brackets the reference number is reported. 30

Figure 2.7: Direct Ethanol Fuel Cell operation results: Maximum DEFCs power density dependency on total (anode + cathode) platinum loading (µg cm^{-2}). In the brackets the reference number is reported. 32

Figure 2.8. Operation principle of H_2-alkaline fuel cell. 37

Figure 2.9: DEFC operational results: maximum DEFCs power density (mW cm^{-2}) at 60 °C of Pt-based and Pt-free electrocatalysts in acidic and alkaline environment dependency

on platinum or palladium loading (µg cm^{-2}); (Troom: room temperature; T_{40}: 40 °C; T_{80}: 80 °C; T_{100}: 100 °C; T_{145}: 145 °C; open triangle Pt-containing PEM-DEFC, filled triangle Pt-containing AEM-DEFC, open square 44

Figure 2.10: General electrode reactions of an abiotically catalyzed glucose–oxygen fuel. 55

Figure 2.11: Tentative oxidation pathways and intermediate reaction products of glucose oxidation [153]. 56

Figure 2.12: Two-chamber glucose fuel cell according to Ref. [27] with identical platinum reprinted from [19]). 57

Figure 2.13: Glucose fuel cell with hydrophobic cathode membrane (schematic outline) (reprinted from [19]). 58

Figure 2.14: Fuel cell design with oxygen-selective cathode catalyst and special electrode (reprinted from [19]). 59

Figure 2.15: Glucose fuel cell with selective electrode catalysts (schematic outline) according [71] (reprinted from [19]). 60

Figure 2.16: Simplified schematics of flow-through type fuel cells intended for blood (reprinted from [19]). 60

Figure 2.17: Simplified schematics of immersible fuel cells intended for tissue implantation: (A) fuel cell with hydrophobic cathode membrane, (B) fuel cell with oxygen-selective cathode catalyst (reprinted from [19]). 61

1. The Fuel Cell Systems

1.1. What is a Fuel Cell?

A fuel cell is an electrochemical device that converts directly the fuel's chemical energy to electricity. By the term "directly" it is meant that it is avoided the process where the chemical energy is converted to thermal energy and then to electrical energy. Thus, there is no heat production and consequently higher efficiency in comparison with the conventional internal combustion engines [1].

The first developed fuel cells were alkaline. The principle of operation of the hydrogen-oxygen alkaline fuel cell is simply a reversal of the process of the electrolysis of water; electrical energy is generated during the oxidation of hydrogen to water.

Principle of H_2-O_2 Fuel Cell (1969):

Hydrogen Electrode (anode): $2H_2 \rightleftarrows 4H^+ + 4e^-$ (1)

$4H^+ + 4OH^- \rightleftarrows 4H_2O$ (2)

Oxygen electrode (cathode): $O_2 + 2H_2O + 4e^- \rightleftarrows 4OH^-$ (3)

Overall reaction: $2H_2 + O_2 \rightleftarrows 2H_2O$ (4)

An oxygen molecule is adsorbed on the cathode's surface, where it picks up four electrons and combines with two of the water molecules present in the electrolyte, forming four hydroxyl ions. Two hydrogen molecules are adsorbed on the anode and are contemporaneously oxidized to hydrogen ions, which ultimately combine with the hydroxyl ions producing water, and four electrons. If the process were perfectly reversible in the thermodynamic sense, the fuel cell would generate a voltage just equal to that required for the electrolysis, l.23 V [1].

Since the fuel cell technology has been evolved and solid membranes replaced liquid-electrolytes the operation of hydrogen –oxygen fuel cell has been simplified according to the following reactions:

Principle of H_2-O_2 Fuel Cell (today):

Hydrogen Electrode (anode): $H_2 \rightleftarrows 2H^+ + 2e^-$ (5)

Oxygen electrode (cathode): $1/2O_2 + 2H^+ + 2e^- \rightleftarrows H_2O$ (6)

Overall reaction: $H_2 + 1/2\,O_2 \rightleftarrows H_2O$ (7)

Even though fuel cells and batteries have a similar electrochemical basis, there are several differences in their performance. Unlike batteries, fuel cells operate as the fuel is fed to them. The energy is produced continuously as the fuel is supplied to the anode. The products of the reactions are removed from the cell together with the exhausted fuel stream. Therefore, it is necessary to have a system that continuously supplies the fuel and the oxidant to the electrodes. The absence of recharging cycles enhances the stability of the electrolyte and the other materials in the cell, which leads to higher life times (durability) [1].

Fuel cells convert chemical energy into electricity by means of electrochemical reactions. In order to obtain a net flow of electrons, it is necessary to ensure that the oxidation and the reduction reactions take place separately. The basic elements of a fuel cell using hydrogen are shown in Figure 2.1.

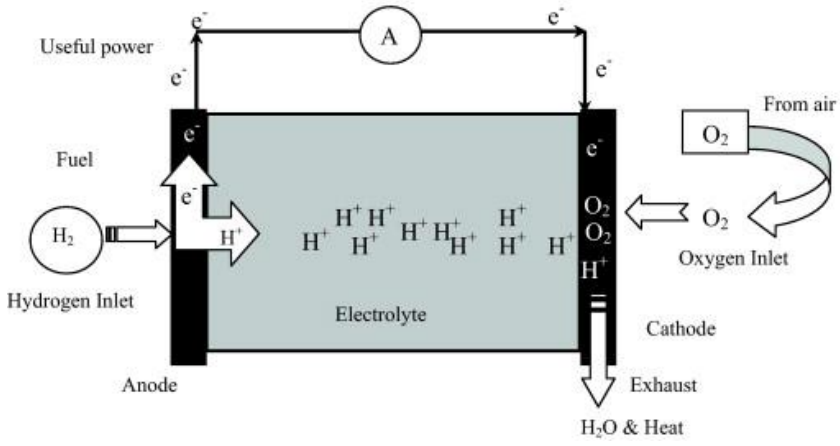

Figure 2.1. Schematic design of a proton exchange membrane fuel cell using hydrogen as fuel.

1.2. Historical Overview

In 1800 the British scientists William Nicholson and Anthony Carlisle described the process of splitting water into hydrogen and oxygen using electricity. Thus in 1838 Sir

William Robert Grove based on this idea went one step further or better went one step instead. He introduced two platinum electrodes in two separate containers containing one hydrogen and one oxygen and immersed in sulfuric acid, with continuous current flow. Then he observed that the water level was increased in both gas containers. To increase the voltage produced, Grove connected many such devices in series and created a device-the first fuel cell-he called "gas battery". Although he had observed that the fuel cell worked effectively, the interesting invention was not commercialized due: i) to difficulties in funding, ii) to the shift of the technology at that time of internal combustion engines and iii) to the widespread consumption of fossil fuels. Later William White Jacques - who accidentally gave the term fuel cells-built fuel cells such as those of Grove replacing phosphate with sulfuric acid. Considerable research in fuel cells made in Germany around 1920 that laid the groundwork for cell based on carbon and oxides. But perhaps the most important research had been done by Dr. Francis T. Bacon who developed the fuel cell known as "Bacon cell". Dr. Bacon replaced expensive platinum electrodes with nickel ones and H_2SO_4 by KOH and actually made the first **alkaline fuel cell**. Potassium hydroxide behaves just as well as the acid and is corrosive to the electrodes. Although 27 years have passed to prepare a truly working fuel cell, Bacon's contribution to the development of fuel cells and more efficient electrodes was crucial [2]. However, the serious interest in fuel cells as generators practices came into being from the 60s onwards, when fuel cells have been chosen for the U.S. space program. Fuel cells supplied with electricity spacecraft Gemini [3] and Apollo [4].

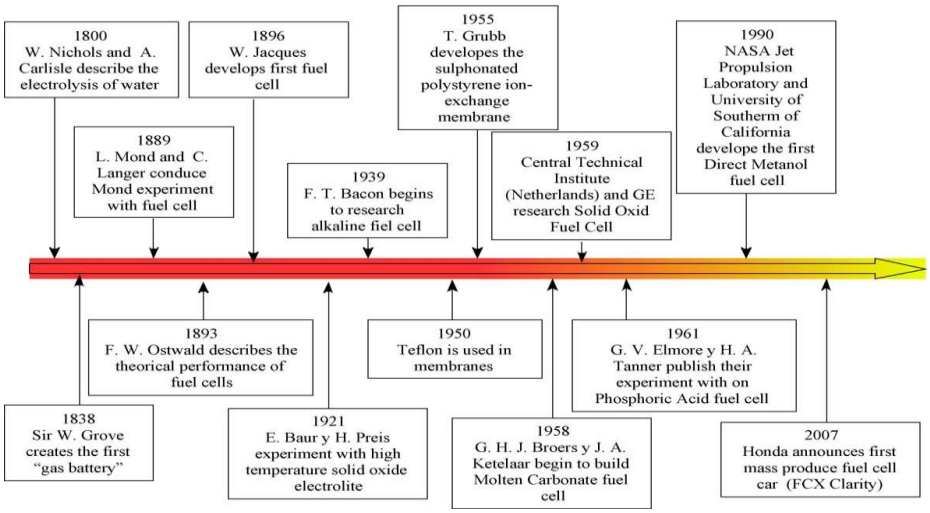

Figure 2.2. Historical review of fuel cells [5].

In Figure 2.2 an historical overview of fuel cells development from 1800 to 2007 is depicted. In the decades that followed there was rapid development in fuel cells' field. In 1970 General Motors replaced the sulfonated polystyrene with Nafion that presented excellent chemical stability which increased the lifespan of proton exchange membrane fuel cells than alkaline ones from 10.000h to 54.000h [6]. In the 1980s the company Ballard Power Systems Inc., focused on the mechanical design and development of proton exchange membrane fuel cells (PEMFCs) units for terrestrial applications. From the early 1990s until now the technology has focused on the development of fuel cells for vehicles. Today most automakers have achieved standards of cars based on fuel cell technology but which are not yet available for commercialization since the presence of stations with H_2 are necessary and the cost is still very high. Already operate H_2 stations with this first of Iceland's (2003) and others such as that of Berlin's (2005), three in Florida and much more designed to be built in California [5].

1.3. Basic Elements and Materials

Electrodes

The electrodes (Figure 2.3) are the elements at which the electrochemical reactions take place. The fuel is oxidized at the anode and the oxidant (usually oxygen from the air) is reduced at the cathode. The bases of the electrodes (bipolar plates) are usually made of porous materials (graphite) in order to achieve high area-to-volume ratios. A catalyst (usually platinum or another metallic element) is then coated on the electrodes inner surface in order to reduce the activation energy of the electrochemical reactions. Due to the high costs of the catalysts (especially those used for low temperature fuel cells) the electrodes are usually the most expensive elements of a fuel cell.

The most important functions of the electrodes are:

-To provide physical sites for the electrochemical reactions to occur.

-To transport the ionic species in order to complete the reactions (mass and charge transport).

- To separate the gas phase (H_2 and O_2) from the electrolyte.

- To evacuate the spent fuel and oxidant and the products of the reaction.

The operation of the electrodes can be seriously affected by poisoning with impurities existing in the input streams. This fact is particularly critical at the anode of H_2-fuel cells operating at low temperatures. As a result, very restrictive cleaning and reforming of the fuel are required prior to its use.

Electrolyte

The electrolyte (a solid polymer) (Figure 2.3) is the central part of the fuel cell and separates the anode from the cathode, so that the redox reactions take place at different sites of the cell. The electrolyte must therefore avoid the flow of the reactants from one side to the other of the cell. The electrolyte must also be impermeable to electrons since they must flow through an external circuit. However, in order to balance the electrochemical reactions, it must transport some ionic species from the anode to the cathode, or vice versa (H^+, OH^-, etc).

The most important functions of the electrolyte can be summarized as follows:

- To separate the anode and the cathode.
- To avoid fuel crossover from the anode to the cathode.
- To avoid electrical conduction.
- To allow the ionic species involved in the reaction to be transferred from the anode to the cathode and vice versa.

Other common elements of fuel cells are:

Gas diffusion layers (GDL)

Gas Diffusion Layers (GDLs) (Figure 2.3) are used in low temperature fuel cells to supply and distribute the fuel and air to the surface of the electrodes uniformly. They are also used to remove the exhausted reactants and the reaction products and to connect the electrodes with the current collectors. Even though GDLs are usually made of carbon cloth or carbon paper, they can be modified with Teflon sheets or other hydrophobic materials to increase their hydrophobic character and avoid water saturation.

Bipolar field flow plates

One individual cell (one electrolyte sandwiched by two electrodes) provides low voltages (~1 V) (Figure 2.3). In order to increase the electrical output power, single

individual cells are connected in series or parallel configurations, in so-called fuel cells stacks. The bipolar plates are the elements used to separate adjacent fuel cell units.

The main functions of the bipolar plates are:

- To deliver the reactant gases to the electrodes.
- To remove waste heat (refrigeration).
- To conduct electrons within an internal circuit as part of the electrochemical reaction.

Bipolar plates are commonly made of graphite due to its high electrical conductivity and high resistance to corrosion. Alternatively, bipolar plates can be made of a metal to increase their conductivity and reduce their size.

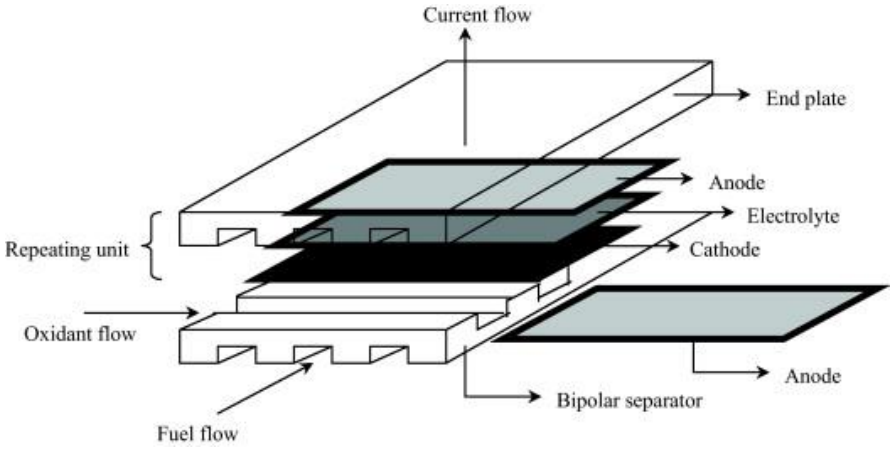

Figure 2.3. Typical planar flat-stack configuration.

1.4. Classification of Fuel Cells

According their operating temperature and the exchange ion fuel cells are classified into the following five categories:

- Alkaline fuel cells (AFCs)
- Phosphoric acid fuel cells (PAFCs)
- Solid oxide fuel cells (SOFCs)
- Molten Carbonate Fuel Cells (MCFCs)
- Proton exchange membrane fuel cells (PEMFCs).

Typical characteristics of different fuel cells systems are summarized in Tables 1.

Table 2.1: Typical characteristics of fuel cell systems.

Type of FC	Electrolyte type	Mobile ion	Operating temperature [°C]	Efficiency [%]
AFC	Polymer (alkaline environment)	OH^-	23-70	50-55
PAFC	Phosphoric acid	H^+	150-250	40-50
SOFC	Stabilized zirconia (the most common used)	O^{2-}	700-1000	45-60
MCFC	Lithium/potassium carbonate mixture	CO_3^{2-}	600-700	50-60
PEMFC	Polymer (acidic environment)	H^+	80-100	40-50

1.5. The Main Advantages & Disadvantages of Fuel Cells Technology

i) High efficiency

Since electrical power is directly obtained from the chemical reactions, the overall efficiency of the process is very high. Fuel cells do not require the existence of temperature differences or gradients to convert the energy. As a result, the performance of fuel cells is not restricted by the Carnot efficiency ($\eta_c = 1-T_L/T_H$), where T_L and T_H the low and high temperature, respectively of the reservoirs in a thermal machine).

Instead, the maximum energy or electrical work available is defined by the Gibbs energy (ΔG) of the reactants and products:

$$\eta_{rev} = \Delta G/\Delta H \quad (8)$$

where η_{rev} is the reversible efficiency and ΔH is the enthalpy change of the electrochemical reaction. The maximum efficiency of a fuel cell is around 83% when it works reversibly. This ideal value decreases when the fuel cells starts to generate electrical power. Despite this efficiency reduction, the actual performance of fuel cells, η_{rev} =40−55%) is still very high compared to thermal conversion systems.

ii) Low environmental impact

Fuel cells have very low environmental impact, particularly when compared to other devices of power conversion. The only product of the electrochemical reactions is water or CO_2 at very low concentrations. Moreover, the use of low temperatures avoids other side reactions involving pollution by products (nitrogen and sulphur oxides, etc). Another important advantage is the use of bio-alcohols. Methanol and ethanol can be used in the so-called Direct Methanol Fuel Cells or Direct Ethanol Fuel Cells (DMFCs, or DEFCs, respectively). Since alcohols can be obtained from renewable sources, this process of energy conversion is sustainable.

iii) Modularity

Individual cells can be arranged in parallel or in series in order to obtain higher electrical power. Fuel cell stacks can be designed and customized to provide different power supplies as required. Since the efficiency of the process does not vary much with the size of the pack, it is easy to use them on different scales.

iv) Non-mobile elements

Fuel cells do not have mobile parts, leading to higher durability and longer life times than other thermal engines.

Despite these advantages of fuel cells, some negative aspects must be discussed:

v) Hydrogen sources and environmental impact

Even though hydrogen is one of the most abundant elements found on Earth, hydrogen gas (H_2) is very limited in the atmosphere. The methods and sources employed for the production of H_2 usually involves the use of fossil resources (natural gas) and other non-sustainable processes. Such methods demand high economic and technological efforts. Alternative methods to produce or store hydrogen are still under research. Interest has focused on the development of devices to produce hydrogen from renewable sources, using hydrogen as an energy vector.

vi) Pre and post operations

The pre-treatment operations applied to the crude fuel (refining, reforming, cleaning, pressurizing) and post-treatment of the electrical signal obtained (DC to AC conversion) require energy and increase the cost of the overall operation. These facts are particularly critical in low temperature fuel cells.

vii) Efficiency losses: polarization

The reversible efficiency (η_{rev}) of a fuel cell is an ideal value that will never be achieved in real operations. As the fuel cell starts to generate electrical current, the voltage falls down due to a loss of efficiency. The efficiency loss in a fuel cell is called polarization.
There are three main polarization sources:

• Activation polarization, which is related to the activation energy necessary to initiate the electrochemical reactions.

• Ohmic polarization, which is the voltage loss related to the inherent electrical resistance of the physical elements between the anode and the cathode, mainly the electrolyte.

• Concentration polarization. It occurs when the current density is very high and the reactants cannot be supplied to the electrodes at the same velocity (mass transport resistance).

The actual performance of a fuel cell will be controlled by the sum of these three contributions. Polarization curves describe the actual performance of a fuel cell and relate the current density and the voltage of a cell. A typical polarization curve of a fuel cell is shown in Figure 2.4.

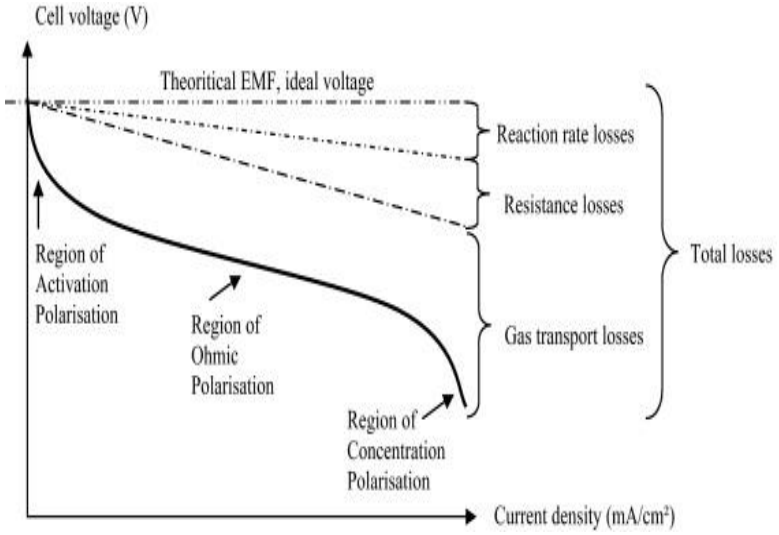

Figure 2.4. Example of polarisation curve of a fuel cell [7].

viii) High installation costs

Even though the market for fuel cells has been expanded in recent years, the technology is still not widely appreciated in the industrial sector. The costs related to their installation are still very high, and amortization times are very long. These factors tend to decrease when the applications of fuel cells diversify into different sectors.

1.6. Fuel cells Applications

Due to their flexibility and versatility, fuel cells can be used in a broad range of applications:

Space industry: Alkaline fuel cells were first used in spacecrafts in the 1960s and 1970s. They supplied not only electrical energy but also drinking water during the missions. Fuel cells were a very convenient alternative to the use of combustion engines (which would require very dense fuels) and batteries (which were too heavy). Fuel cells also fitted very well to the short times of the missions (usually less than one year) offering very reliable energy supply.

In the spacecraft launched during the Apollo program three fuel cells supplying 1.5 kW - 2.2 kW were used in a parallel configuration for over 10000 working hours in 18 missions. The fuel cells used cryogenic hydrogen and oxygen and weighed 114 kg. During the 1980s, NASA continued using 15 kW fuel cells in more than 100 missions for more than 80000 working hours.

Military applications: Different types of fuel cells are used as portable power generation plants in military missions. The high efficiencies, versatility, long operation times and silent performance make fuel cells a very useful power generation system for military purposes in terrestrial and marine operations. For example, PEMFC stacks (300 kW) have been used by the USA Navy in submarines providing a maximum speed of 145 km h^{-1}. The use of fuel cells reduces the amount of fuel used, as well as the number of auxiliary staff and equipment necessary in long-term operations.

Portable applications: The development of fuel cells has been applied in several portable electronic devices. Small fuel cells (mini-fuel cells) show longer operation times. Light prototypes of fuel cells are suitable for laptops (50 – 100 kW), mobile phones (10 W) or batteries chargers (<50 kW). The success of the performance of fuel cells in portable applications in the future will depend on the operation temperature (usually below 100ºC), fuel availability and the achievement of short starting times.

Micro power fuel cells could change the world of telecommunications, since they can be used in mobile phones or laptops with a lot more battery life. For these applications, and given the characteristics of a fuel cell, the choice is usually a Direct Methanol battery. Companies like Motorola, Toshiba, Samsung, Panasonic, Sanyo and Sony have shown that fuel cells can power telecommunication equipment. For example, they have shown that mobile phones can be run for twice as long as compared to the one that uses a lithium battery with an equivalent size and it needs only 10 min to recharge. As far as laptops are concerned, it has been shown that laptops with fuel cells may be working up to 5 h without refueling. Other applications for micro fuel cells include pagers, video-rewriters, hearing aids, smoke detectors, security alarms or reviewers counter. In these cases, fuel cells are powered by methanol [5].

Transport: Legislation surrounding environmental issues concerning the transport sector is becoming stricter, as a result of the impact of global warning. The use of fuel cells can reduce the CO_2 produced by internal combustion engines by up to 70%. However, fuel cells would not only address the environmental issues but also satisfy the features related to the starting times, fuel economy and power supply [5].

PEMFC are probably the most suitable fuel cells for vehicular applications. They work at low temperatures (around 80ºC) showing efficiency near 60% and high power densities. The use of solid electrolytes at low temperatures avoids corrosion problems. However, to date the use of PEMFC is restricted to the use of very pure hydrogen and use of platinum as electrocatalyst which is very expensive. Different vehicle companies have developed prototypes of cars and buses using hydrogen and methanol fuel cells. PEMFC using hydrogen has been also proved successful in aerospace applications [5].

Today most vehicle manufacturers use fuel cell vehicles for research, development or testing. Moreover, in 2007, the vehicle manufacturer Honda presented the model FCX Clarity at Los Angeles automobile saloon. This model is available for the consumer since the summer of 2008. This is the first fuel cell vehicle platform-exclusive in the world manufactured in series. Some fuel cell vehicles manufacturers are: Daimler-Chrysler (2008), Fiat Panda (2007), Ford Hyseries Edge (2007), GM Provoq (2008), Honda FCX Clarity (2008), Hyundai I-Blue (2007), Morgan LIFE Car (2008), Peugeot H_2 Origin (2008), Renault Scenic (2008) FCV H_2, e.t.c [5]. Regarding buses with fuel cells, in the last 7 years, a number of fuel cell buses have been in operation worldwide. These vehicles are highly efficient even if the hydrogen is produced from fossil fuels and thus reducing CO_2 emissions which would become zero if the hydrogen is produced from renewable sources. In addition, they assist in reducing noise contamination in large cities [5].

Other vehicle using fuel cells is the motorcycle. Despite its small size, motorcycles are a major source of pollution in cities. Motorcycles with two-stroke engines produce a disproportionate amount of emission when compared to its size (almost as much as a diesel truck). Using fuel cells would reduce these emissions. Fuel cells have been started to be used in electrical conveyor machinery and forklifts. The use of fuel cells in these machines involves a reduction in the cost of logistics, since hardly any maintenance or replacement is needed. Furthermore, due to constant stops and starts, there are many failures and interruptions when using a standard engine. With fuel cells, a continuous supply of power is ensured by eliminating the problems caused by the voltage drop due to the discharge of the batteries.

Another application in the transport sector is the use of fuel cells as auxiliary power units (APUS) in long-haul trucks [5]. Regarding this issue, the Department of Energy of the United States (DOE) estimated about 1.17 billion dollars [5] the annual cost of fuel and engine maintenance for slow motion periods of a truck (parking and rest periods for drivers). During this time, the APU is supplying all electricity useful to the driver (heating, air conditioning, computer, TV, radio, refrigerator, microwave, etc.). The Department of Energy states that APUs based on using fuel cells on trucks

Mercedes-Benz Class 8 of the whole country could save about 2500 million liters of diesel and between 11 and 80 tonnes of CO_2 per year

Low power stationary applications: Fuel cells are also used to supply electricity and heat in small buildings on a small scale. Fuel cells can be found in auxiliary and emergency supply systems (<10 kW), telecommunications and remote operations (100 W–1 kW) or in applications for the construction sector (< 10 kW).

Small scale PAFCs and PEMFCs are the most common fuel cells used to provide energy in buildings. In order to increase the use of these systems in cities, natural gas networks could be used together with individual reformers to obtain pure hydrogen for fuel cells. An alternative is to use different fuels, such as low molecular weight alcohols.

High power stationary applications: Fuel cells are established in the markets of heat and electricity large scale generation. PAFCs, MCFCs and SOFCs are used in stationary power plants providing a range of power from 1 to 5 MW. These fuel cells operate at very high temperatures and do not need metal based catalysts. This fact avoids strict pre-treatment operations of the fuel and reduces the cost of the operation.

Today more than 2500 fuel cell systems have been installed worldwide in hospitals, shelters, centers for elderly care, hotels, offices and schools. In these cases, the fuel cell system is connected to the grid to provide additional electrical power to the plant [8] or as an independent system of the grid to generate electricity in remote or isolated areas [9-11]. Systems of electric power generation based on fuel cells today achieve an efficiency of 40% in the process: using some hydrocarbon as a fuel and taking as starting point the fuel and as end point electricity generation. Because the fuel cells are working quietly and do not produce environmental pollution, they can be placed near the electricity. Furthermore, in stationary applications, fuel cells are used at high temperature, so the co-generation can increase efficiency up to 85% while reducing energy consumption.

In the field of telecommunications, computers, Internet and telecommunications networks have become essential for humans. This implies the need for a fully reliable

electricity supply. Just in this field of application it has been shown that the fuel cell achieved a reliability rate of 99,999% [12].

Thus, fuel cells are starting to compete with batteries for power ranges between 1 and 5 kW in telecommunications systems located at remote places inaccessible to the electrical network. They also use fuel cells to provide power as a primary or support system for telecommunications switching nodes, transmission towers, reception or other electronic devices that can benefit from the DC power supplied by a fuel cell [13]. Other applications for stationary fuel cells are in landfills and wastewater plants [14]. The use of fuel cells reduces harmful emissions and allows the generation of power from methane gas (hydrogen-rich fuel used by certain types of fuel cells) that produces the plant. They have also been installed in the breweries of Sierra Nevada (California) and Kirin, Asahi and Sapporo (Japan), to take advantage of the methane produced in the untreated landfills.

2. Fuels for Fuel Cells & Anode Electrocatalysts

The most important factor of fuel cells' operation is the electrodes and more precisely the type of anode electrocatalyst where the electrooxidation of the fuel takes place. Electrodes for fuel cells are the most crucial component of them. The main requirement of a good electrode is the particles of the electrocatalyst to be in direct contact with an electronic conductor in order to ensure the electrons are supplied to or removed from the reaction site. Electron conductivity is usually provided by a carbon support onto which the particles are bound. Depending on the fuel the anode electrocatalyst has to oxidize hydrogen (or another gas reactant, e.g. methane) or liquid alcohol. In the following sub-sections the types of fuels and the respective research in literature for anode electrocatalysts for fuel cells are discussed.

2.1. Hydrogen

From the point of view of global warming and from that of the inevitable exhaustion of Earth's oil reserves; it has become highly desirable to develop an

alternative energy source for automobiles. Since the development of proton exchange membrane fuel cells (PEMFCs), which are fuelled by hydrogen, and oxygen (air) and produce only water, hydrogen has generally been seen to be the most promising approach.

In literature a lot of novel materials have been studied as anode and cathode electrocatalysts for (H_2-PEMFCs). However, Pt or Pt-based binary or ternary catalysts are still the well-known and commonly-adopted materials providing the highest activity for electrode reactions and lifetime stability. Nevertheless, the total Pt reserves in the world will be depleted if each vehicle, which is powered by a 75 kW fuel cell stack, needs approximately 75 g of Pt (~1 mg Pt per Watt) [15]. More precisely, one and a half billion cars will require more than 110,000 tons of Pt, which is far more than the world-wide estimated Pt reserves (~28,000 tons) [16], in addition to the other applications of Pt in the area of catalysis, jewellery and so on. To the above reasons, it should also be added the high cost of Pt, which is one of the main obstacles to PEMFC's commercialization.

More precisely, Figure 2.5 [17] summarizes the results of the main investigations, appeared the last decade in the international literature, concerning both low-Pt anode and low-Pt cathode catalysts for H_2-PEMFCs. As it can be clearly seen, the results could be classified into three main regions of maximum mass specific power density (max-MSPD) values: (a) higher than $5\,mW\,\mu g^{-1}_{Pt_{total}}$, (b) between $1\text{-}5\,mW\,\mu g^{-1}_{Pt_{total}}$ and (c) lower than $1\,mW\,\mu g^{-1}_{Pt_{total}}$. In the region (a), there are few catalysts which meet the MSPD target of $>5\,mW\,\mu g^{-1}_{Pt_{total}}$.

More precisely, the reported maximum MSPD, $23.5\,mW\,\mu g^{-1}_{Pt_{total}}$ (750 mW cm^{-2}; 32 $\mu g_{Pt}\ cm^{-2}$), has been achieved by Sung *et al.* [18]. A carbon supported Pd-based PdPt catalyst with an atomic ratio 19:1 has been fabricated by the conventional sodium borohydride reduction method combined with freeze-drying. As cathode a Pt/C electrocatalyst has been used. The amount of the platinum was only 5 at. % Pt (19:1 atomic ratio of Pd:Pt) showing that Pd-based catalysts can successfully enhance the PEMFCs' performance. Antolini *et al.* [19] also examined Pd-based catalysts.

According to their results the MSPD was 6.57 mW $\mu g^{-1}_{Pt_{total}}$ (710 mW cm^{-2}). The electrocatalysts were prepared by the reduction of metal precursors with formic acid, managing a total platinum loading of 108 μg_{Pt} cm^{-1} (96:4 atomic ratio of Pd:Pt).

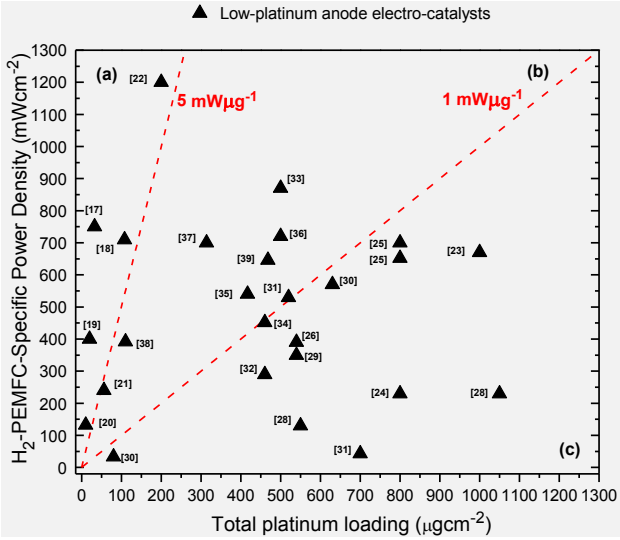

Figure 2.5: H_2-PEMFC operation results: Maximum Power Density (mW cm^{-2}) dependency on total (anode + cathode) Pt loading (μg cm^{-2}). In the brackets the reference number is reported.

Cavarroc et al. [20] manufactured ultra-low Pt content MEA (10 μg cm^{-2}) for the anode and 10 μg cm^{-2} for the cathode by magnetron co-sputtering of carbon and Pt on a uncatalyzed gas diffusion layer, which gave a power density of 400 mW cm^{-2} or 20 mW $\mu g^{-1}_{Pttotal}$. Additionally, Gruber et al. [21] also sputter-deposited Pt thin film layers onto different porous electrodes, as the platinum thin film layer presents the advantage to be active in the immediate neighborhood of the electrode with the proton-conducting membrane. The total Pt loading was only 10 μg cm^{-2} and the maximum mass specific power density almost reached 13.2 mW$\mu g^{-1}_{Pttotal}$ (132 mW cm^{-2}) (Figure 2.5, region a). The aforementioned works managed to decrease the Pt amount and simultaneously increase its utilization coefficient. To reduce Pt loading, except for the trend to alloy the Pt or to modify its support, a proper MEAs fabrication method could also be a promising way. Erlebacher et al. [22] succeeded to control very low values of Pt loading (56 μg cm^{-2} of total platinum loading) by adopting a stamping technique and then to fabricate Pt-plated nanoporous gold leaf, which is a carbon-free electrocatalyst. Despite of the very low Pt amount, they obtained 4.28 mW

$\mu g^{-1}_{Pttotal}$ (240 mW cm^{-2}). Finally, Manthiram et al. [23], fabricated a high performance MEA (1200 mW cm^{-2}, 200 μgPt cm^{-2}) by a modified thin-film method using un-catalyzed gas diffusion electrodes to support the thin film catalysts layer. The anode and the cathode catalysts were Pt supported on carbon black with a loading of 100 μg cm^{-2} for each electrode.

As it can be distinguished in Figure 2.5, a serious number of investigations have also been appeared [24-33] the last decade with fuel cell maximum mass specific power density values below 1 mW $\mu g^{-1}_{Pttotal}$ (region c, in Figure 2.5), while for some others [34-40] the values are embraced in the range between 1 -5 mW $\mu g^{-1}_{Pttotal}$ (region b, Figure 2.5). From a quick glance at the catalysts that belong to regions (b) and (c), it is deduced that in the last years one of the common approaches to succeed the Pt loading target was to adopt also novel supports, except carbon black. However, although the development of fuel cell technology appears to be progressing smoothly towards eventual commercial exploitation, a viable method for storing hydrogen on board a vehicle is still to be established [41].

2.2. Alcohols

The commercial processes for hydrogen production which are presently used include steam reforming of natural gas, partial oxidation of heavy oil residues (followed by water–gas shift (WGS) conversion) and electrolysis of water. Hydrogen is mainly used as feedstock for the chemical industry and as liquid fuel for space applications. However, recent developments in the area of fuel cells dictate that, in the near future, hydrogen will be used, to a large extent, as a secondary energy carrier for the production of electricity for mobile and small-to-medium scale stationary applications. The expected increased demand for hydrogen for fuel cell applications, in combination with environmental concerns related to reducing atmospheric pollution and global greenhouse gas emissions, dictate the development of new methods for hydrogen production, especially from renewable sources, such as biomass [42].

Hydrogen can be produced in a renewable manner from lignocellulosic biomass with the use of several methods, including pyrolysis, gasification and steam

reforming. Of special interest are methods in which biomass is converted to intermediate liquid bio-fuels, such as pyrolysis oil or ethanol. The main advantage of liquid bio-fuels is their high energy density and ease of handling, and the fact that they can be used for the on-demand production of hydrogen for fuel cells, with applications in mobile and stationary grid-independent power systems [42].

Among the various processes and primary fuels that have been proposed for the production of hydrogen for such applications, steam reforming of methanol and ethanol is very attractive (e.g. eq.9):

$$C_2H_5OH+3H_2O \rightarrow 6H_2+2CO_2 \quad (9)$$

In addition to advantages related to natural availability, storage and handling safety, ethanol can be produced renewably from several biomass sources, including energy plants, waste materials from agro-industries or forestry residue materials, organic fraction of municipal solid waste, etc. In contrast to other, fossil-fuel-based, systems which have been proposed for the same application, namely methanol and gasoline, the bioethanol-to-hydrogen system has the significant advantage of being nearly CO_2 neutral, since the produced carbon dioxide is consumed for biomass growth, thus offering a nearly closed carbon loop.

In the following lines the state-of-the-art electrocatalysts for direct methanol and direct ethanol fuel cells are discussed. According to the literature, a number of Pt alloys [43, 44], with Pt-Ru [45] to be the best, exhibit an enhanced electrocatalytic activity for MOR by removing CO-like intermediates through bi-functional mechanism at lower potential values. The up-to-date low Pt anode and cathode DMFCs' electrocatalysts and for the sake of comparison some examples of the best reported electrocatalysts with high total Pt loading are depicted in Figure 2.6 [17].

The results can be classified in three regions: region (a) which embraces the catalysts with maximum *mass specific power density* higher than $0.1\ \text{mW}\ \mu g^{-1}_{Pt_{total}}$, region (b) which includes the catalysts with maximum *mass specific power density* between

0.01 mW $\mu g^{-1}_{Pt_{total}}$ and 0.1 mW $\mu g^{-1}_{Pt_{total}}$, and region (c) with maximum *mass specific power density* lower than 0.01 mW $\mu g^{-1}_{Pt_{total}}$.

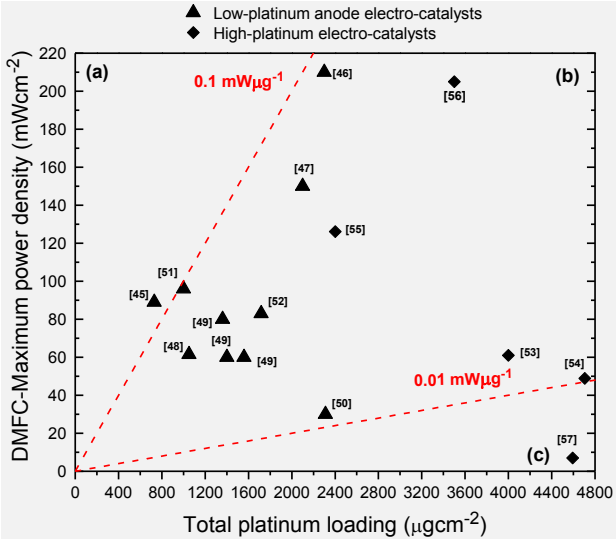

Figure 2.6: Direct Methanol Fuel Cell operation results: Maximum DMFCs power density dependency on total (anode + cathode) platinum loading (μg cm^{-2}). In the brackets the reference number is reported.

The lowest total Pt loading reported is 730 $\mu g_{Pt_{total}}$ cm^{-2} and it has been studied under DMFC conditions (region a, in Figure 2.6) by Gonzales *et al.* [46]. They prepared carbon-supported anode Pt-Sn electrocatalysts, by co-impregnation of Pt and Sn precursors with formic acid as the reducing agent. The examined electrocatalyst exhibited performance, 89 mW cm^{-2} (0.12 mW $\mu g^{-1}_{Pt_{total}}$). According to the authors [46], Pt-Sn with an appropriate atomic ratio of Pt:Sn oxidizes CO at lower potentials than pure Pt. Therefore, in this work the good DMFC performance could be attributed to the Pt-Sn alloy effect and its synergistic action on CO removal.

According to the state of the art [17], the highest fuel cell performance (210 mW cm^{-2} or 0.09 mW $\mu g^{-1}_{Pt_{total}}$) was achieved over a PtRu alloy supported on graphitic mesoporous carbon [47] and it has been attributed to the crucial role of the mesoporous carbon pore size. The second best fuel cell performance of 150 mW cm^{-2} or 150 mW cm^{-2} has been reported by Aricò *et al.* [48], over Pt-decorated (2100 $\mu g_{Pt_{total}}$ cm^{-2}) unsupported Ru electrocatalyst,. Most of the reported results in Fig.

2.5 have been obtained over anodes with total Pt loading higher than 1000 $\mu g^{-1}_{Pt_{total}}$ cm^{-2} (region b) [47-57]. Region (c) contains the results of high Pt loading anode with very low performance [58].

It is a fact that year by year the anode Pt loading is significantly reduced along with the improvement of catalyst synthesis methods, MEA fabrication techniques, and so on. Nevertheless, despite of the attempts and the improvements to lower Pt loading in order to achieve a desirable DMFC performance the total Pt loading (anode + cathode) still remains very high. More precisely, as it has been mentioned above, today the acceptable mass specific power density (MSPD) target for H_2-PEMFCs is ~5 mW $\mu g^{-1}_{Pt_{total}}$. If the same or at least the half target will be adopted from the international research community for DMFCs it is obvious that much stronger effort is necessary for their commercialization. This is due to the fact that up to now the best DMFC mass specific power density value is close to 0.12 mW $\mu g^{-1}_{Pt_{total}}$ [46] [70] (Figure 2.6).

The performance of low platinum anode or cathode catalysts for DEFCs (at ~90^0C), in terms of maximum power density dependency on total platinum loading (MEA's platinum loading) is reported in Figure 2.7. For comparison reasons, the performance of some anode and cathode catalysts with higher platinum loadings is also included. As it can be seen, the results can be distinguished in two main regions: (a) with the catalysts' presented activity between 0.05 mW $\mu g^{-1}_{Pt_{total}}$ and 0.016 mW $\mu g^{-1}_{Pt_{total}}$ [59-73], and (b) with the catalysts' presented activity is below 0.016 mW $\mu g^{-1}_{Pt_{total}}$ [74-81]. As it is shown, until today the lowest total Pt loading used for DEFCs is 573 μg cm^{-2}, in the case of PtRuIrSn/C catalyst [72], which exhibited a good maximum power density of 29 mW cm^{-2}, (0.05 mW $\mu g^{-1}_{Pt_{total}}$) and long-term stability.

The second best *maximum mass specific power density* value (0.047 mW $\mu g^{-1}_{Pt_{total}}$, or 105 mW cm^{-2}) was achieved by Sun *et al.* [61] using PtRu/C as anode and Pt/C as cathode. However, the ever highest power density (110 mW cm^{-2} or 0.028 mW $\mu g^{-1}_{Pt_{total}}$) was achieved in 1998 by Aricò *et al.* [73], at an operating temperature of 145°C. The anode was Pt-Ru (2 mg_{Pt} cm^{-2}) binary electrocatalyst and the cathode was Pt (2 mg cm^{-2}),

both supported on carbon. A high performance, 96 mW cm^{-2} or 0.017 mW $\mu g^{-1}_{Pt_{total}}$, has been obtained by Sun *et al.* [59], over double-layer anode and cathode both consisted of one layer –Pt_3Sn and a second-layer PtRu. The best fuel cell performance was observed in the case the Pt_3Sn was the first layer (close to the anode diffusion layer) and the Pt-Ru (adjacent to the Nafion) the second one.

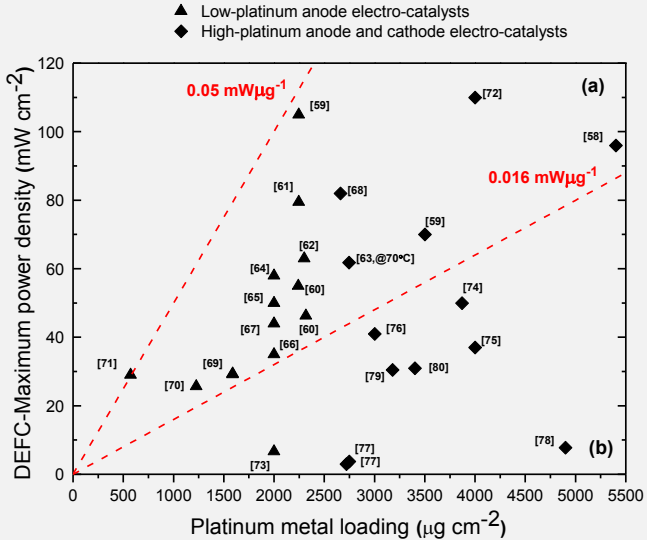

Figure 2.7: Direct Ethanol Fuel Cell operation results: Maximum DEFCs power density dependency on total (anode + cathode) platinum loading (μg cm^{-2}). In the brackets the reference number is reported.

It is worth to be noticed that as in the case of DMFCs concerning the last five years investigations, the nanomaterials [82, 83] have attracted great interest because of their unusual catalytic, mechanical, electrical and optical properties. Recently, different kinds of carbon nanomaterials such as hollow graphitic nanoparticles [84], carbon nanotubes [85] and graphitic carbon nano-fibers [84] were investigated and different fabrication methods have been adopted. These carbon materials can exhibit superior performance compared to the conventional carbon supports for EOR anode catalysts. In conclusion, compared to DMFCs, the best performance of DEFCs, in terms of max-MSPD, is three times lower.

2.3. Glucose

Glucose, with molecular formula $C_6H_{12}O_6$, is a monosaccharide. It was first isolated in 1747 from raisins by Andreas Marggraf. In the solid state, glucose does not exist as the open chain; rather it exists in two separate crystalline forms, known as α-D-glucose and β-D-glucose.

Glucose is ideal fuel to room temperature fuel cells. It is abundant, stable, non-poisonous, odourless, easy to obtain and transportable. Glucose is also water-soluble, which is an important property when dealing with low temperature fuel cells. Its solution offers many advantages over methanol; the boiling point of glucose is higher than that of methanol. Unlike methanol, it is non-volatile. If a highly active catalyst can be found, it is possible to design a room temperature glucose powered liquid fuel cell for practical applications.

Glucose has been started attracting much interest as fuel in fuel cells mostly due to its high energy content (4430 Wh kg^{-1}) and its importance as fuel in Direct Glucose Fuel Cells (DGFCs) and their applications as implantable human devices [86-88]. Electro-oxidation of glucose has been studied extensively for several decades because of the interest in the development of glucose sensors and glucose-oxygen fuel cells. The development of implantable fuel cells operable on glucose and oxygen dissolved in a patient's blood was first considered as a far-reaching trend.

However, direct glucose fuel cells' anodes have displayed low efficiency and unstable operation. Many technical problems must be solved. Glucose sensors can analyze the blood glucose concentration of a diabetic patient. Two types of such sensors are possible. One is based on oxidation of glucose by enzymes and the other is based on the direct electrochemical oxidation of glucose on electrodes. However, the first type is very unstable due to the death of enzymes. Investigations are conducted to improve glucose sensor and direct glucose fuel cells' design in order to overcome some disadvantages such as the loss of sensor activity over time and the instability of DGFCs [89]. In the 1960s, Bagotzky and Vassiyev [90] first reported the electro-

oxidation behavior of glucose in acidic medium. Then extensive studies of glucose oxidation were carried out in neutral, acidic and alkaline solutions.

Its complete oxidation to carbon dioxide can produce 24 electrons for each glucose molecule through the following chemical equations:

Anode reaction: $C_6H_{12}O_6 + 24OH^- \rightarrow 6CO_2 + 18H_2O + 24e^-$ (1)

Cathode reaction: $6O_2 + 12H_2O + 24e^- \rightarrow 24OH^-$ (2)

Overall reaction: $C_6H_{12}O_6 + 6O_2 \rightarrow 6CO_2 + 6H_2O$ (3)

However, the completion of reaction is rare and unlikely. Up-to-date only partial oxidation of glucose has been achieved and the initial step involves breaking a C-H bond producing gluconic acid. A possible mechanism of gluconic acid generation has been proposed in literature [89]. The first step of glucose electrochemical reaction involves the adsorption of glucose, followed by oxidation of the hydrogen atom bound to the carbon atom C1. The adsorbed species are further oxidized leading to the formation of gluconolactone. Hydrolysis of gluconolactone gives the gluconic acid generating only two electrons [91]. The gluconic acid yields according to the following chemical equations:

Anode reaction: $C_6H_{12}O_6 + 2OH^- \rightarrow C_6H_{12}O_7 + H_2O + 2e^-$ (4)

Cathode reaction: $0.5O_2 + H_2O + 2e^- \rightarrow 2OH^-$ (5)

Overall reaction: $C_6H_{12}O_6 + 0.5O_2 \rightarrow C_6H_{12}O_7$ (6)

Consequently, the stability of glucose is one of its advantages as fuel, but at the same time constitutes a disadvantage when it is to decompose to extract energy. Special electrocatalysts are necessary in order to obtain electricity from this renewable source. The state-of-the art glucose electrocatalysts will be discussed in the 5.4 sub-section.

According to literature direct alkaline glucose membrane fuel cells (AEM-DGFC) tend to perform superior performance than proton conducting membrane fuel cells [92]. More precisely when the electrolyte is changed from acidic to alkaline the

enhanced kinetics of the glucose oxidation (GOR) and oxygen reduction reaction (ORR) in alkaline media are observed [91, 93, 94]. Moreover, in an AEM-DGFC the direction of the electro-osmotic drag is from the cathode to the anode, which can reduce the rate of fuel crossover from the anode to cathode and thereby improve cell performance [95, 96]. In addition, the cost of AEMs is much lower than that of PEMs (typically Nafion®).

In literature many attempts [97-102] have been done to develop efficient and stable electrocatalysts for glucose electro-oxidation mostly in alkaline media. Many of them have been focused on Pt [91, 103] and Au [104, 105] or on their bi-metallic catalysts, Pt-Bi [99], Pt-Pd [106], Pt-Ru [107], Pt-Au [97, 108], Ag-Au [109-111] and tri-metallic catalysts [112], while Pd-based electrocatalysts have not been yet studied towards glucose electrooxidation.

However, Pd-based electro-catalysts have been proved [92, 113] to perform much better activity than Pt-based ones in alkaline environment due to the quicker oxidation kinetics of various alcohols. Further discussion for the up-to-date electrocatalysts for glucose electrooxidation is done in the 4.4 sub-section of the present chapter. In section 4 that follows the alkaline fuel cells in terms of historical background, principles of operation and research challenges and future perspectives are discussed.

3. Alkaline fuel cells (AFCs)

3.1. Historical Overview

The pioneer of alkaline fuel cell (AFC) research, development and demonstration is Dr. Francis T. Bacon [1]. Dr. Bacon commenced his research in this area in 1932 and had completed the construction of a 5-kW hydrogen-oxygen fuel cell power plant and its performance evaluation in 1952. One of the main reasons why Bacon chose an alkaline electrolyte was to use non-noble metal electrocatalysts. In this fuel cell the electrocatalysts were nickel for the anode and lithiated nickel oxide for the cathode

(lithium improves the electronic conductivity and the corrosion resistance of nickel oxide). In order to obtain a stable-three phase zone, he designed the electrodes for dual porosity, the larger pores on the gas side and the smaller ones on the solution side. The electrolyte in the Bacon cell was 30% KOH and the operating temperature and pressure were 200 ^{o}C and 50 atm, respectively [1].

Many research groups started to focus on AFCs for applications after 1950s, when the NASA Apollo space program started using AFC systems and this technology is still used for today's shuttle missions. By the 1970s, a car had been built, by Kordesch [114], which ran on alkaline fuel cells combined with a lead-acid battery. Despite its early success, interest in AFC technology then dropped owing to economic factors, material problems, and certain inadequacies in the operation of electrochemical device. Discoveries and major scientific advances (especially with regard to PEMFCs) in the past two decades have created renewed interest in AFCs. Some previous limiting requirements such as the use of essentially pure fuels have been overcome by using a polymer membrane as an electrolyte. Expectations are that, in some years' time, the alkaline polymer electrolyte fuel cells will be used in numerous power applications, ranging from portable power and vehicle propulsion to distributed power generation.

3.2. AFCs Background and Principles of Operation

A scheme illustrating the operating principles of an H_2 fed -AFC is depicted in Figure 2.8. In anode two hydrogen molecules are joined by four hydroxyls and form water while at the same time release water. The half-cell reactions are the following:

$$\text{Anode: } 2H_2 + 4OH^- \rightarrow 4H_2O + 4e^- \quad (8)$$

$$\text{Cathode: } O_2 + 2H_2O + 4e^- \rightarrow 4OH^- \quad (9)$$

$$\text{Overall: } 2H_2 + O_2 \rightarrow 2H_2O \quad (10)$$

Electrons which are released from the above reaction reach the cathode through an external circuit. The cathode electrons are released from the anode combine with an

oxygen molecule and two water molecules resulting in the formation of hydroxyl groups according to the eq.9:

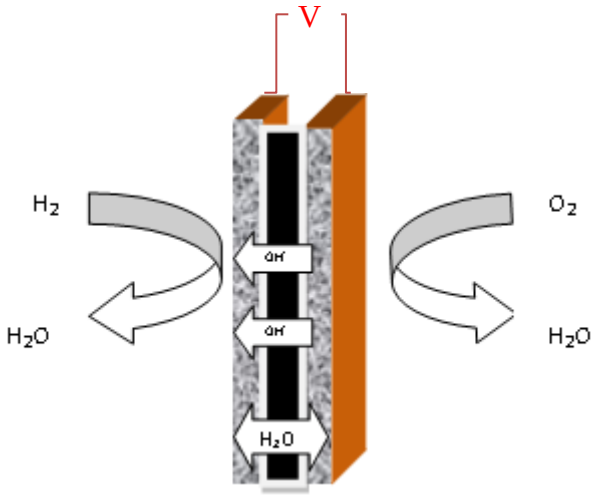

Figure 2.8. Operation principle of H_2-alkaline fuel cell.

Potassium hydroxide, which is the most conducting of all alkaline hydroxides, is most of the times the electrolyte of choice. The unique advantage of an alkaline electrolyte over an acid one for a fuel cell is that noble metal electrocatalysts are not necessary for the former. In addition, even with the non-noble metal or oxide electrocatalysts, the oxygen electrode performance (cathode) is extremely good. Alkaline fuel cells have been developed with platinum electrocatalysts as well. In recent times, it was shown that a heat-treated cobalt tetraphenyl porphyrin deposited on high-surface-area carbon exhibits the highest activity ever reported for oxygen reduction reaction. The reason for this is that anion adsorption is minimal from alkaline electrolytes. The Tafel slope for oxygen reduction from alkaline electrolytes is <60 mV/decade throughout the entire operating range. Alkaline fuel cells generally operate at around 60-80^{o}C. In some cases, the operating pressure is a few atmospheres, but most often it has been at atmospheric.

A major issue with traditional AFCs is that of electrolyte (liquid phase) and electrode degradation caused by the formation of carbonate/bicarbonate ($CO3^{2-}$/HCO^{3-}) on reaction of OH^- ions with CO_2 contamination in the oxidant gas stream [1]:

Carbonate formation: $CO_2 + 2OH^- \rightarrow CO_3^{2-} + H_2O$ (11)

Bicarbonate formation: $CO_2 + OH^- \rightarrow HCO_3^-$ (12)

The major cause of the degrading performance of AFCs is the consequent precipitation of metal carbonate crystals (most commonly Na_2CO_3 or K_2CO_3, depending on the alkaline electrolyte used) in the electrolyte-filled pores of the electrodes, blocking pores and mechanically disrupting and destroying active layers [115].

The cost of fuel cells still retards commercialization in most markets. AFCs are promising on a cost basis mainly because cheap and relatively abundant non-platinum- group metals (non-platinum group metal (PGM)) are viable catalysts, but are hindered by degradation due to formation of precipitates as above reported. Catalyst electrokinetics (for fuel oxidation and oxygen reduction) is improved in alkaline, as opposed to acidic conditions (the acid-stability criterion precludes the use of most non-PGM catalysts in PEMFCs). The replacement of the KOH (aq) electrolyte with an alkaline electrolyte membrane (AEM), to give AMFCs, retains the electrocatalytic advantages but introduces CO_2 tolerance (there being no mobile cations that could give carbonate/bicarbonate precipitates) with the additional advantage of being an all-solid-state fuel cell (as with PEMFCs – i.e., no seeping out of KOH(aq)). Additionally, thin (low electronic resistance) and easily stamped (cheap) metal mono/bipolar plates can be used, with reduced corrosion-derived problems at high pH (the cost of bipolar plates for PEMFCs can be as much as one third of the cost of the stacks themselves) [115].

A key and yet to be convincingly met requirement is, however, the development of a dispersible alkaline ionomer (sometimes termed an anionomer) to maximize ionic contact between the catalyst reaction sites and the ion-conductive membranes. Because as in the case of AFCs, water is produced at anode and consumed at cathode in AMFCs (when fuelled with hydrogen and with four electron reduction of oxygen at the cathode), which is fundamentally different to what occurs in PEMFCs containing acidic electrolytes; this can cause high overpotentials at AMFC anodes, due to suspected flooding [115].

The use of an anion exchange membrane (AEM) as a solid electrolyte including no metal cations prevents precipitation of carbonate/bicarbonate salts (the electrolyte containing the cationic groups is already a solid). The carbonation process is quick even if the AEM has been exposed to the air for only a short time. The conductivities of the AEMs in OH^- form may have been underestimated because most studies up to date have not disclosed vigorous CO_2 exclusion procedures during conductivity measurements. It has been hypothesized that OH^- ion conductivities in AEMs can be estimated by measuring the ionic conductivities of HCO_3^- from AEMs and multiplying by 3.8 [115]. This carbonation process may not to be a serious problem due to an in situ "selfpurging mechanism" because OH^- anions are continuously generated at the cathode in AMFCs.

AEMs are solid polymer electrolyte membranes that contain positive ionic groups (typically quaternary ammonium (QA) functional groups such as poly-$NMe3^+$) and mobile negatively charged anions. A widely quoted concern with AEMs is membrane stability, especially at elevated temperatures [115].

The general issues are:

1. The diffusion coefficients and mobilities of OH^- anions are less than that of H^+ in most media, and QA ionic groups are less dissociated than the typical sulfonic acid groups (pKa for sulfonic acid groups are typically -1 but for QA groups the related pKb values are around +4); there were concerns that AEMs would not possess adequate intrinsic ionic conductivities for application in fuel cells.
2. The OH^- anions are effective nucleophiles which potentially cause degradation [115]. If the AEMs contain good leaving groups (e.g., QA $-NMe3^+$ groups) then the chemical stability of the AEMs might have been inadequate for use in fuel cells, particularly at elevated temperatures.
3. Precursor anion-exchange membranes are generally submerged in aqueous NaOH/KOH solutions to exchange them to the OH^- form AEM; the AEM must have the chemical stability to withstand this process. Despite this, over a decade ago, the stabilities of various benzyltrimethylammonium-based AEMs were found to be stable at up 75^oC in NaOH(aq) at concentrations up to 6 mol dm^{-3} for several days [115]. A

major potential application of AMFCs is, however, as power sources for at or near room temperature (as for PEMFCs), which means such degradation can be minimal.

The following sub-sections consider the state of-the-art of H_2-PEMFCs, DEFCs and DMFCs of low loading anode electrocatalysts in PEMFCs and the current understanding and application of AEMs in ethanol-fuelled AMFCs. The purpose is to realize the differences between the two kinds of fuel cells and the enhanced AMFCs performance in comparison to PEMFCs.

3.3. Anion (alkaline) Membrane Fuel Cells vs. Proton Exchange Membrane Fuel Cells

The comparison of alkaline (anion) vs. proton exchange membrane fuel cells is focused on direct ethanol fuel cells due to the fact that ethanol is a difficult oxidized (see section 3.2) fuel which needs further research attention.

When focusing on portable appliances and consumer electronics equipment, where DAFCs are considered as the systems of choice, the percentage of the catalyst cost contribution on the total system cost may be significantly higher due to higher amounts of precious metals used. Thus, despite the fluctuating metal market prices, it is clear that every improvement in electrochemical kinetics will eventually be reflected in lower stack and fuel cell system cost. In this respect, the maximum *mass specific power density* (max-MSPD) with respect to several PEM- and AEM-DEFC power density data is of foremost importance. Hereafter, barriers/challenges for both technologies are listed [92].

For the proton exchange membrane

- The cost of the system, not only because a considerable amount of Pt-based catalysts at both the anode and cathode is required, but also because acid electrolyte membranes (e.g. Nafion, and Nafion-based) are expensive.
- The incomplete oxidation of EtOH to acetaldehyde and acetic acid that liberates only 2 and 4 electrons, respectively, and greatly reduces the Faradaic efficiency of the fuel cell.

- The kinetics of the EOR in acid media is slow, leading to a large activation loss.
- EtOH crossover from the anode to the cathode within the PEM that leads to a parasitic current generation (mixed potential formation).
- The use of a cathode catalyst tolerant to EtOH.
- The durability of the state-of-the-art catalyst employed (e.g. PtSn/C) has been scarcely analyzed. Thus, the chemical stability of the catalysts over longer periods of time is an issue of foremost importance that still needs to be considered and is suggested for further investigations.
- The complete oxidation of EtOH to CO_2 remains a challenging issue (the most important one). Nowadays, Pd-based catalysts show appreciable performance toward the EOR in alkaline media. However, EOR is incomplete and EtOH is selectively oxidized to acetate.
- The activity and durability of the Pd catalyst. The activity and durability of the Pd catalyst for the EOR in alkaline media needs to be further enhanced, and the design of multi-metallic electro-catalysts is essential.
- A challenging issue in the cathode catalyst material is how to enhance the catalytic activity of non-Pt catalysts, making them comparable to that of Pt. For example, so far, Ag-based cathode catalysts for the oxygen reduction reaction (ORR) in alkaline media have a larger particle size than Pt-based catalysts do. Hence, a target in the cathode electrode is to develop new synthesis methods that can lead to high electrochemical surface area Ag-based catalysts.
- A significant improvement is needed to upgrade the OH^- conductivity, chemical, mechanical and thermal stability of the existing AEMs. The OH^- conductivity can be improved by increasing the amount of charged groups in the membrane; however, there is a trade-off with the mechanical properties. A loss of the mechanical properties by promoting excessive water uptake is the result of increasing the concentration of the charged groups. The thinness of the AEM is an important requirement related to mechanical stability; to keep good mechanical stability when immersed in water, an AEM as thin as ~50 μm is necessary. AEM suffers also of a poor chemical stability in alkaline media, stemming from the

hydroxide attack on the cationic group. The result of this degradation is an important loss in the number of anionic exchange groups, and a decrease of the ionic conductivity.

- Like the AEM, both the ionic conductivity and the thermal and chemical stability of the nowadays ionomers present within the catalyst layers are still low. Hence, significant work is needed to enhance the ionic conductivity and stability of ionomers. Recently, Mamlouk et al. [116, 117] , studied the effect of ionomer content and the effect of catalyst layer thickness without ionomer on cell performance.

Water transport management is a key issue for both PEM- and AEM-DEFCs. The appropriate management of this process is necessary so as to avoid either cathode flooding (high water crossover) or a high cathode activation loss (too low water crossover). EtOH transport management is another key issue for both PEM- and AEM-DEFCs. Note that in AEM-DEFCs, as the cathode catalyst (non-Pt) is generally tolerant to EtOH oxidation, the mixed potential problem as a result of fuel crossover is not as serious as in PEM-DEFCs.

Furthermore, the effect of the EtOH crossover in AEM-DEFCs is suppressed; the EtOH crossover within the membrane takes place in the opposite way to the OH^- transport, thereby diminishing that detrimental process. EtOH crossover adversely affects fuel efficiency (i.e. energy density), due to the wasteful oxidation on the cathode side leading to a mixed potential formation [32, 33]. This mixed potential on the cathode causes a decrease in DEFC voltage, and eventually results in decreased fuel efficiency, thereby lowering the energy density of the system. Low EtOH flow rates and low concentrations enable very high fuel efficiencies. However, mass transport limitations prevent the attainment of useful power densities under those conditions that enable high fuel efficiencies [118].

Moreover, the electro-oxidation reaction of EtOH in acid PEM-based DEFCs evolves through multiple steps resulting in the production of mainly acetic acid and acetaldehyde [119]. On the other hand, the EtOH electro-oxidation in alkaline AEM-based DEFCs evolves through a simpler path producing less acetic acid in the form of ions (CH_3COO^-) and favoring the formation of acetate [120]. This results in fuel

utilization much higher than the one achieved in the PEM-based DEFCs, better cell performances, and a higher energy density [92].

An important drawback however, of the AEM-based DEFC, is the formation of a pH gradient with time (more alkaline at the cathode, more acidic at the anode) that will cause the occurrence of an electromotive force in opposition to the electromotive force of the reaction itself [121, 122]. In case of a high pH gradient, this will strongly deteriorate the polarisation performance. Wang et al. [121] discussed in their study this thermodynamic disadvantage for an AEM-based DMFC. As reported, the significant reduction of activation overpotential in alkaline media can compensate for the voltage loss due to the thermodynamic effects associated to the pH gradient. Furthermore, Aricò et al. [122] mentioned in their work that recirculation of the liquid electrolyte through the device not only enhances conductivity but significantly reduces the pH gradient. Nevertheless, PEM- and AEM-DEFCs are attracting increasing interest, as electrochemical energy converters for portable appliances; as a result there exist a blossoming research activity focused on PEM- and AEM-DEFCs [92].

Single cell polarization performance data for PEM- and AEM-DEFCs were collected and depicted in Figure 2.9. It presents the dependency of the maximum (peak) *power density per square centimeter of geometric area* (or maximum *area-specific power density*, max-ASPD) on total metal loading (MEA's metal loading); here metal can be either Pt, and Pt-based catalysts for PEM-DEFCs, or Pt-based, Pd-based catalysts for AEM-DEFCs. Lines of constant maximum *mass specific power density* (max-MSPD) can be drawn.

If we look now at the lines of constant maximum *mass specific power density* (max-MSPD) in Figure 2.9, the following observations can be drawn:
(a) Three regions are distinguished: (I) with max-MSPD values between $0.2\ \text{mW}\ \mu\text{g}^{-1}_{\text{Pt or Pd}}$ and $0.1\ \text{mW}\ \mu\text{g}^{-1}_{\text{Pt or Pd}}$, (II) with max-MSPD values between $0.1\ \text{mW}\ \mu\text{g}^{-1}_{\text{Pt or Pd}}$ and $0.05\ \text{mW}\ \mu\text{g}^{-1}_{\text{Pt or Pd}}$ and (III) with max-MSPD values lower than $0.05\ \text{mW}\ \mu\text{g}^{-1}_{\text{Pt or Pd}}$. Each line has been drawn at the maximum MSPD of each catalyst's category that is reported in

Figure 2.9 (Pt-containing AEM, Pd-containing PEM-DEFC, Pd-containing AEM-DEFC, Pt-Pd containing alkaline acid DEFC).

(b) The best performing PEM-DEFC with low Pt-based electro-catalysts is the one reported Fatih *et al.* [72] with a max-MSPD of ca. 0.05 mW $\mu g^{-1}_{Pt\ or\ Pd}$.

(c) An AEM-based DEFC, also with low Pt-based electro-catalysts, achieved a similar max-MSPD (0.04 mW $\mu g^{-1}_{Pt_{total}}$), representing the best performing AEM-based low-Pt DEFC, operating at room temperature, reported in the literature [123]. All other Pt-based PEM s [59, 61, 69, 74, 75, 77, 79-81, 124-138] and AEM-DEFC studies [139-141] found in the open literature, reported lower max MSPD values, as it can be also seen from Figure 2.9.

(d) Pd-based AEM-DEFCs exhibited a power output per unit mass of Pd as high as 0.16 mW $\mu g^{-1}_{Pd\ total}$ [142], whereas all other Pd-based AEM-DEFC studies [143-145] found in the open literature, reported lower max MSPD values.

(e) AA-DEFCs exhibited a power output per unit mass of metal as high as 0.2 mW $\mu g^{-1}_{Pd\ total}$ [146], whereas all other AA-DEFC studies [147, 148] found in the open literature, reported lower max MSPD values.

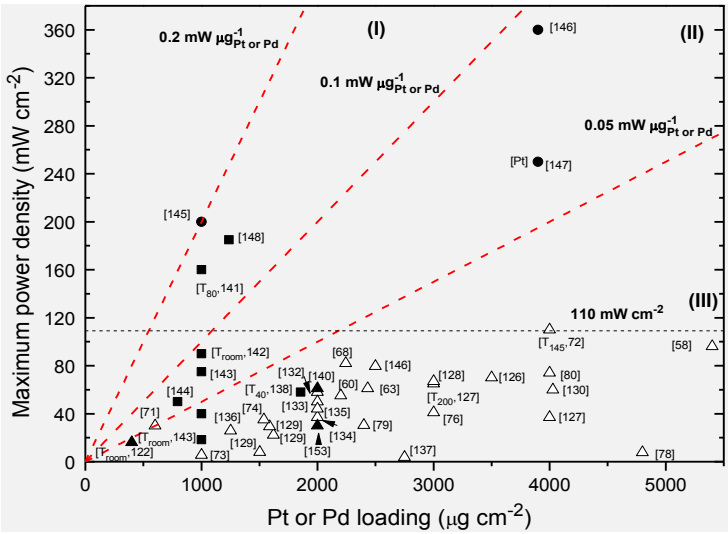

Figure 2.9: DEFC operational results: maximum DEFCs power density (mW cm^{-2}) at 60 °C of Pt-based and Pt-free electrocatalysts in acidic and alkaline environment dependency on platinum or palladium loading (µg cm^{-2}); (Troom: room temperature; T_{40}: 40 °C; T_{80}: 80 °C; T_{100}: 100 °C; T_{145}: 145 °C; open triangle Pt-containing PEM-DEFC, filled triangle Pt-containing AEM-DEFC, open square Pd-containing PEM-DEFC, filled square Pd-containing AEM-DEFC, open circle Pd or Pt-containing alkaline-acid DEFC.

According to Figure 2.9, the AEM-DEFCs, in most of the cases present not only higher activity than PEM-DEFCs mainly due to the lower ethanol's crossover effect, but also provide the possibility of using non-Pt cheap electrocatalysts. Moreover, the most interesting thing about the AEM-DEFCs is that they operate at lower temperature values (60°C) than the one's of PEM-DEFCs' (80°C). Finally, a new interesting approach is the development of alkaline-acid fuel cells. Those also exhibit very high and comparable polarization performance to Pt-based PEM-DEFCs and Pd-based AEM-DEFCs. Moreover, it has been demonstrated that with a Pd-based electrocatalyst, the peak power density of an AEM-DEFC can be as high as 185 mW cm^2 at 60^oC [149]. However, they are still questioned since the number of works in the literature is very limited and much further investigation is necessary.

3.4. Research Challenges and Future Perspectives

The following research challenges must be overcome in order AEMs be applied successfully in pre-commercial stage [115]:

1. AEMs must be created with higher conductivities, to ensure good fuel cell performances at high current densities. It should be noted, however, for example, that with application of an alkaline DMFC as a power source for portable devices, an overriding priority is maximizing the energy density of the fuel and fuel efficiency (cell voltage). These DMFCs will be operated at low-to-medium current densities (higher efficiencies), where electrodes overpotential is the dominant cause of voltage losses.
2. It is essential that a solubilized form of an alkaline anion-exchange polymer should be developed to improve the interface between the electrodes and the AEM electrolyte. Success in this effort will decrease MEA resistances. A water-based soluble form which can be rendered water insoluble when cast would be preferred, as there are safety concerns (primarily with industrial scale production) about using organic solvents near finely dispersed (pyrophoric) metal catalysts (unsupported or supported on carbon).
3. If AEMs are to be applied to fuel cells for other applications (such as automotive power etc.), more temperature stable AEMs must be developed. Operation of alkaline-membrane-based fuel cells at elevated temperature would reduce thermodynamic voltage losses due to pH differences across the AEM and would also improve the

electrokinetics. Successful, stable over long term, and being operational at elevated temperatures, all would allow application in fuel cells for the automotive mass market.
4. If AEMs are shown to be stable in fuel cells over thousands of hours, an in-depth investigation into effective and cheaper non-noble metal catalysts (e.g., Ni, Ag etc.) is indicated. There would also be a greater chance of finding methanol tolerant catalysts for use as cathodes.
5. Finally, removal of fluorine from the polymer systems would be of interest to enhance the environmental credentials of the technology (facilitating easier disposal) and reduced costs. The substitution of fully fluorinated FEP with non-fluorinated LDPE is feasible. While oxidative radical degradation is a problem at the cathode and anode (via oxygen diffusion through the membrane) using non-fluorinated PEMs. It has been shown using electron paramagnetic resonance (EPR) that such degradation is prevented in highly alkaline (pH > 11.7) conditions pertinent to AEMs.

4. Direct Glucose Alkaline Fuel Cells (DGAFCs)

4.1. Historical overview

Although today batteries are considered to be the first choice in supplying power to electronic medical implants, there are numerous efforts to develop alternative power-supply systems that are capable of operating independently over prolonged periods of time, without the need of external recharging or refuelling [150-152]. Among them are fuel cell systems, which convert endogenous substances and oxygen into electricity by means of electrochemical reaction. Unlike batteries, these systems are constantly replenished with fresh reactants from the body fluids, and are therefore theoretically capable of operating indefinitely, as long as there is a constant supply of reactants. Its ubiquitous availability in body fluids makes glucose the most considered fuel for implantable direct glucose fuel cell systems [153].

In general, glucose-consuming fuel cells can be divided into three main types according to the type of catalyst that is used to enable the electrode reactions: enzymatic, microbial, and abiotic.

i) *Enzymatic fuel cells* employ enzymes such as glucose oxidase and laccase in their isolated forms.

ii) *Microbial fuel cells* the enzymatic system of a whole, electroactive micro-organism is used.

iii) *Abiotically catalyzed fuel cells* make use of non-biological, abiotic catalysts, e.g., or activated carbon [153].

Over the last four decades there has been applied research activity both in the development of enzymatic and microbial fuel cells. Whereas implantable *enzymatic glucose fuel cells* are currently under development. The limited stability of enzymes renders their application in a long-term implantable fuel cell power supply. Power-supply systems based on microbial fuel cells are not seriously considered for implantation, due to the infective nature of most known micro-organisms and the associated risks therewith [153].

In past reviews, only minor attention has been given to abiotically catalyzed glucose fuel cells, although these systems were already developed as implant power supplies in the late-1960s, and their feasibility to power cardiac pacemakers has been demonstrated *in vitro* as well as in animal trials. Abiotically catalyzed fuel cells employ mainly noble metal catalysts and are therefore considered to be advantageous regarding their sterilizability, long-term stability, and biocompatibility. However, following the introduction of the lithium iodine battery in 1972 and the subsequent improvement of pacemaker battery lifetime no further development of abiotically catalyzed glucose fuel cells has been reported. Instead the research has been refocused towards the application of the concept for glucose sensor technology [153].

The current interest in autonomous, self-sufficient MEMS (micro-electro-mechanical systems) implants has revived the research in long-term stable, implantable glucose fuel cells based on abiotic catalysts. The following lines review the development of abiotically catalyzed glucose fuel cells for implantable devices since the early beginnings in the 1960s. Not considered are non-medical applications of abiotically catalyzed glucose fuel cells, for instance as sensor power supply as above mentioned, running on tree sap, since their operation conditions differ greatly

from physiological environments and the design is not constricted by the vigorous demands on implantable systems in terms of patient safety and system size.

The concept of abiotically catalyzed glucose fuel cells appeared for the first time in a publication by Bockris [154], who investigated the anodic oxidation of cellulose and lower carbohydrates with respect to its applicability in fuel cells. In 1966, a patent was issued to Union Carbide for a method of using solid organic fuels in a fuel cell, where the performance of a fuel cell oxidizing glucose in alkaline solution was reported.

It was not until 1967 that the first abiotically catalyzed glucose fuel cell intended to operate on glucose from body fluids was presented by Warner and Robinson [154]. Their prototype employed an air-breathing cathode and it was suggested as a future power supply for medical implants. They demonstrated fuel cell performance in unbuffered 10% (0.56 mol L^{-1}) glucose solution over a period of 240 h, reaching a plateau performance of 165 µW cm^{-2} within the initial 24 h of operation [154]. First experiments with pleural fluid and plant saps resulted in a lower and more rapidly decreasing cell performance, which has been attributed to the blocking of the electrode by adsorbed proteins. In 1968, Wolfson *et al.* [155] presented a similar device for pacemaker power supply under the name "Bioautofuel Cell". Their prototype was a *two chamber* fuel cell consisting of two identical platinized fuel cell electrodes immersed in separate beakers. They used phosphate and bicarbonate buffer systems, and an ionic connection between the beakers established by a saturated KCl-agar bridge. The anode compartment contained 5.0×10^{-3} mol L^{-1} glucose and was purged with nitrogen to remove dissolved oxygen from the solution. Although their two chamber prototype was clearly not suitable for operation in a physiological environment where glucose and oxygen were present in the same solution, they carried out a number of experiments regarding the effect of varying glucose concentrations, electrolyte solution buffer capacity, and pH. The detrimental effect of fuel in the cathode or oxygen in the anode compartment was also demonstrated. The reported fuel cell performance amounted to 3.5 µW cm^{-2}, and the fuel cell's capability of powering a transistor blocking oscillator circuit over a period of 18 days could be demonstrated.

In the following years several academic and corporate activities related to implantable glucose fuel cells have been reported. Scientists of the Monsanto Research Corporation developed catalyst materials for glucose oxidation. At Union Carbide [156] the performance of oxygen reduction catalysts in physiological solution were investigated. Other companies involved were the German Robert Bosch GmbH, who was granted a patent on the application of organo-chemical redox systems for the anodic oxidation of amino acids in an implantable fuel cell and the US-based Leesona Moos Corporation [157], where electrocatalysts for hydrocarbon oxidation and oxygen reduction from the gold–palladium series were developed.

A major development effort was sponsored by the Artificial Heart Program of the United States National Heart and Lung Institute [158], since it was expected that implantable glucose fuel cells could generate electricity in the range of several watts and therefore supply an artificial heart. However, in a theoretical study, the feasibility of extracting enough oxygen from the blood to operate a 12.5 μW implantable fuel cell system was evaluated as only marginally feasible, depending on the effective diffusion coefficient of oxygen in the blood. From a similar study a marginal feasibility of obtaining 4.5 μW from an implantable system based on the reaction of glucose to gluconic acid was concluded. However, the construction of corresponding prototypes has not been reported.

The first truly implantable fuel cell prototypes, intended for the use with cardiac pacemakers, were developed at the American Hospital Supply Corporation and the Michael Reese Hospital in 1970. Reports of implantable prototypes developed at Siemens [159] and also Tyco followed in 1972 .

For almost 30 years no further work on implantable abiotically catalyzed glucose fuel cells had been published, until in 2005 the concept was picked up again in the context of low power medical MEMS implants. The relevant publications and patents related to implantable abiotically catalyzed glucose fuel cells are summarized in Table 2.2.

Table 2.2: Publications and patents related to the development of implantable abiotically catalyzed glucose fuel cells [19].

Year, Reference	Affiliation	Comment
1964, Bockris et al. [154]	University of Pennsylvania, Philadelphia (PA).	Anodic oxidation of glucose and other carbohydrates in alkaline/acidic solution.
1966, Kordesch and Koehler [160]	Union Carbide Corporation, New York (NY).	US Patent: method of using glucose and other solid organic fuels in a fuel cell.
1967,Warner and Robinson [161]	Emory University, Atlanta (GA).	Glucose fuel cell prototype operating on 10 wt% glucose solution and atmospheric oxygen, intended as a power supply of medical implants; use of pleural fluid and plant saps as fuel source.
1968,Wolfson et al. [155]	University of Pennsylvania, Philadelphia (PA).	Glucose fuel cell as power source for cardiac pacemakers. Investigation of cell performance under physiological and varying pH and glucose concentration.
1969, Colton and Drake [162]	Monsanto Research Corporation, Everett (MA).	Feasibility study for an implantable glucose fuel cell, e.g., as a power supply for the artificial heart.
1969, Rao and Drake [163]	Monsanto Research Corporation, Everett (MA).	Studies into the electrooxidation of glucose; electrode poisoning effect of gluconic acid.
1969, Yao et al. [164]	Michael Reese Hospital and Medical Center, and the Institute of Gas Technology, both Chicago (IL).	Investigation of the anodic oxidation of glucose, gluconic acid, glucosamine, and related compounds at neutral pH in a two compartment fuel cell.
1969, Arzoumanidis and O'Connell [157]	Monsanto Research Corporation, Everett (MA).	Anodic oxidation of glucose in phosphate buffer saline with electrodes catalyzed by 4,4',4'',4'''-tetrasulfophthalocyanine-molybdenum dioxide salts.

Table 2.2-continue: Publications and patents related to the development of implantable abiotically catalyzed glucose fuel cells [19].

Year, Reference	Affiliation	Comment
1970, Kozawa et al. [165]	Union Carbide Corporation, Cleveland.	Evaluation of various oxygen reduction catalysts (various noble metals and ferric phathalocyanine) in neutral solution, also containing additons of blood.
1970, Kozawa et al. [166]	Union Carbide Corporation, Cleveland (OH).	Oxygen and hydrogen peroxide reduction on ferric phthalocyanine-catalyzed graphite.
1970, Drake et al. [158]	American Hospital Supply Corporation, Everett (MA), and the University of Vermont, Burlington .	*In vitro* and *in vivo* studies on a tissue implantable glucose fuel cell with permselective membranes.
1970, Wolfson et al. [167]	Michael Reese Hospital and Medical Center, Chicago (IL).	*In vitro* studies on an implantable glucose fuel cell with permselective membranes in neutral solution also containing additions of plasma.
1971, Appleby [168]	Illinois Institute of Technology.	Feasibility study for an implantable glucose fuel cell to power an artificial heart.
1972, Malachesky et al. [159]	Tyco Laboratories,Waltham (MA).	Parametric *in vitro* and *in vivo* studies on glucose fuel cells designed as an artificial heart power source. Demonstrated gluconic acid as fuel with similar performance; a marked decay of anode performance has been observed *in vivo.*
1972, Schumann et al. [169]	Robert Bosch GmbH, Stuttgart (Germany).	German patent: anodic oxidation of amino acids in an implantable fuel cell via the application of organo-chemical redox systems.
1972, Wolfson and Yao [170]	University of Pittsburgh, and Montefiore Hospital, both Pittsburgh (PA).	Investigation of the effect of creatinine, alanine, urea, uric acid, ammonium chloride, and plasma components on the performance of an implantable fuel cell.
1972, Rao et al. [171]	Siemens AG, Erlangen (Germany).	First report on a glucose fuel cell with a special electrode arrangement and activated carbon cathode, presented at the Third International Conference on Medical Physics.

Table 2.2 continue: Publications and patents related to the development of implantable abiotically catalyzed glucose fuel cells **[19].**

Year, Reference	Affiliation	Comment
1973, Giner et al. [172]	Tyco laboratories, Waltham (MA).	Overview on the Tyco work on implantable glucose fuel cells.
1973, Fishman and Henry [173]	Montefiore Hospital and Medical Center, Bronx (NY).	Meeting abstract of the Electrochemical Society Meeting 1973: report on electrodeposited selective catalysts for glucose oxidation and oxygen reduction in an implantable fuel cell.
1973, Henry and Fishman [173]	Montefiore Hospital and Medical Center, Bronx (NY).	Meeting abstract of the Electrochemical Society Meeting 1973: investigation of the transient behavior of the rest potential of an electrodeposited platinum black electrode in aerated glucose saline solution and the effect of lead acetate addition to the plating bath.
1973, Henry and Fishman [173]	Montefiore Hospital and Medical Center, Bronx (NY).	Meeting abstract of the Electrochemical Society Meeting 1973: *in vivo* studies with an implantable glucose fuel cell comprising selective Au–Pd electrodes and semipermeable membranes; pulsed cell operation over 5 h without rastic decay.
1973, Rao et al. [174]	Siemens AG, Erlangen (Germany).	*In vitro* studies with an implantable glucose fuel cell: concept of a special electrode arrangement in combination with selective oxygen reduction catalysts; fabrication of electrodes and membranes from PVA–PAA hydrogel and results of an 1100 h long-term test.
1974, Ng et al. [175]	Institute of Gas Technology, Chicago (IL).	US Patent: air breathing implantable glucose fuel cell intended as power supply for the artificial heart.
1974, Wan and Tseung [176]	Royal College of Surgeons of England, and The City University, London.	*In vitro* and *in vivo* studies on an implantable fuel cell with selective electrodes; addition of lead acetate to platinum plating solution.

Table 2.2 continue: Publications and patents related to the development of implantable abiotically catalyzed glucose fuel cells **[19].**

Year, Reference	Affiliation	Comment
1974, Rao et al. [177]	Siemens AG, Erlangen (Germany).	*In vitro* studies with an implantable glucose fuel cell.
1974, Rao and Richter [178]	Siemens AG, Erlangen (Germany).	Overview article on implantable bioelectrochemical power sources; 200 h *in vitro* results from an implantable glucose fuel cell.
1975, Affrossman et al. [179]	University of Strathclyde, Glasgow (Scotland).	Application of lactic acid, glucose, and glucosamine as fuel in an implantable fuel cell; effect of differently charges membranes on fuel permeability.
1975, Rao and Richter [180]	Siemens AG, Erlangen (Germany).	US Patent: implantable glucose fuel cell with special electrode arrangement and selective oxygen reduction catalyst.
1976, Sharrock et al. [181]	University of Strathclyde, Gasgow (Scotland).	Implantable fuel cell-based sensor for creatinine, uric acid, and lactic acid, employing an activated carbon anode.
1976, Gebhardt et al. [154]	Siemens AG, Erlangen (Germany).	Raney-type electrocatalyst for glucose oxidation in an implantable glucose fuel cell prepared from platinum and ferrous metals.
1976,Weidlich et al. [182]	Siemens AG, Erlangen (Germany).	*In vivo* experiments with an implantable glucose fuel cell over a period of 5 months.
1976, von Sturm and Richter [183]	Siemens AG, Munich (Germany).	US Patent: integration of a glucose fuel cell as external coating on a cardiac pacemaker.
1976, Rao et al. [184]	Siemens AG, Erlangen (Germany).	Summary of the Siemens activities in the field: materials and design, *in vitro* experiments over a period of 600 days, Raney-type electrocatalysts, and the effect of amino acid mixtures on anode performance.
1978, Richter et al. [185]	Siemens AG, Berlin and Munich (Germany).	US Patent: fabrication of Raney-type platinum electrodes for implantable glucose fuel cells.
1978, Rao et al. [186]	Siemens AG, Erlangen (Germany).	Influence of amino acids on the glucose oxidation on platinum, platinum black and Raney-platinum electrodes in neutral media.

Table 2.2 continue: Publications and patents related to the development of implantable abiotically catalyzed glucose fuel cells **[19].**

Year, Reference	Affiliation	Comment
1981, Giner et al. [187]	Giner Inc.,Waltham (MA).	Influence of amino acids on the glucose oxidation on platinized platinum electrodes in Krebs–Ringer solution, focus on the development of an implantable glucose sensor.
1983, Rao [188]	Siemens AG, Erlangen (Germany).	Summary of the Siemens activities in the field: materials and design, *in vitro* and *in vivo* experiments over a period of 600 and 150 days, respectively; Raney-type electrocatalysts and the oxidation of gluconic and glucaric acid on those.
2005,Woias et al. [189]	University of Freiburg (Germany).	Energy harvesting concepts for autonomous microsystems, among them abiotically catalyzed glucose fuel cells.
2006, von Stetten et al. [190]	University of Freiburg (Germany).	Fabrication and characterization of a prototype based on the Siemens concept.
2007, Kerzenmacher et al. [191]	University of Freiburg (Germany).	Fabrication and characterization of a surface-mountable abiotically catalyzed glucose fuel cell.

4.2. Electrochemical oxidation of glucose & principle operation of abiotic direct glucose fuel cells

Compared with other small organic molecules, glucose can theoretically be completely oxidized to CO_2 and H_2O, releasing 24 electrons per glucose molecule, although the transfer of 24 electrons has not yet been achieved. The Direct Glucose Fuel Cells (DGFCs) should thus be very promising high-energy power sources. Furthermore, considering that glucose can be produced in as very highly efficient manner during photosynthesis in nature, the entire-process is carbon-neutral, which clearly offers environmental benefits. Theoretically, glucose can be completely oxidized to carbon dioxide and water, releasing 24 electrons per molecule glucose.

The corresponding fuel cell reaction and the theoretical cell voltage U^0 would then be given as:

Anode:	$C_6H_{12}O_6 + 24\ OH^- \rightarrow 6CO_2 + 18\ H_2O + 24e^-$	(13)
Cathode:	$6O_2 + 12H_2O + 24e^- \rightarrow 24\ OH^-$	(14)
Overall:	$C_6H_{12}O_6 + 6O_2 \rightarrow 6CO_2 + 18\ H_2O$	(15)

,ΔG^0 =-2.870 x 10^6 J mol^{-1}, U^0=1.24 V.

In practice, the transfer of 24 electrons per molecule glucose has not yet been achieved. In their early study on glucose electro-oxidation in neutralmedia (0.5 mol L^{-1} glucose in 1mol L^{-1} phosphate buffer at pH 7.4, 0.5 mol L^{-1} NaCl) employing platinized platinum electrodes, Rao and Drake [192] reported gluconic acid to be the only reaction product that could be identified by thin layer chromatography. In a later mass spectroscopic study of glucose oxidation products (0.1 mol L^{-1} glucose, in chloride free $NaHCO_3$ buffer at pH 7.4). Ernst et al. [193] identified glucono lactone as the product of glucose oxidation in the potential range of 300–400mV vs. RHE (reversible hydrogen electrode), which itself undergoes hydrolysis to form gluconic acid, a non-toxic metabolite [194].

The oxidation of glucose to gluconic acid only yields two electrons per molecule glucose and the corresponding electrode reactions are thus given as:

Anode:

Cathode:

Overall: $C_6H_{12}O_6 + 1/2O_2 \rightarrow C_6H_{12}O_7$

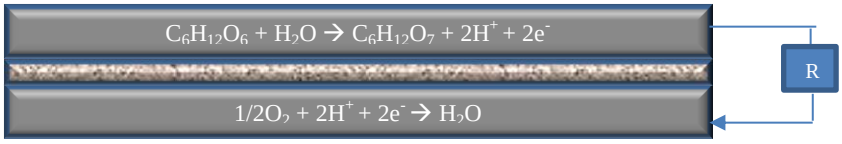

Figure 2.10: General electrode reactions of an abiotically catalyzed glucose–oxygen fuel.

In that case ΔG=-2.51 x10^5 J mol^{-1}, U^0=1.3V.

Several research groups demonstrated that gluconic acid can be oxidized in a similar way as glucose, although at lower reaction rate [164, 195]. Apart from gluconic acid as the main reaction product Kokoh *et al.* [196] detected glucuronic, oxalic, glyoxylic, and tartaric acids as well as traces of glycolic and formic acid by means of HPLC (high

pressure liquid chromatography) analysis. They used unmodified platinum electrodes and the oxidation was carried out by a continuous triple pulse electrolysis program with the oxidation potential set to 0.62V vs. RHE (50.6×10^{-3} mol L^{-1} glucose in KH_2PO_4/NaOH buffer at pH 7.3). This is in agreement with the findings of Lerner and Gebhardt [197] who estimated the number of electrons transferred per glucose molecule. On platinized platinum electrodes (potential range: −200 to 0mV vs. a saturated calomel electrode, SCE) between 4 and 20 electrons are transferred, and for a Raney-type platinum catalyst (at 400mV vs. RHE) the mean number of electrons was estimated to be 17, from measuring the gradual depletion of 0.1% (5.6×10^{-3} mol L^{-1}) glucose in phosphate buffer over a period of 800 h [195].

The different findings concerning the reaction products might be due to analytical limitations and the fact that not only the catalyst material but also the pH and the ionic strength of the electrolyte influence the reaction mechanism of glucose electro-oxidation [198]. A detailed description on the mechanisms of glucose electro-oxidation in different media and at different pH can be found in the works of Demele and Vassilyev [199-202].

An overview about the tentative oxidation pathways and intermediate reaction products of glucose oxidation is given in Figure 2.11.

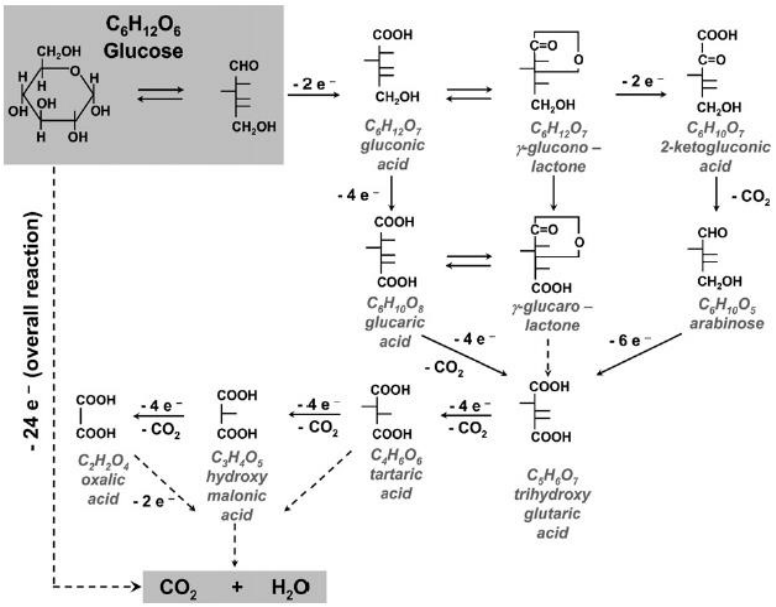

Figure 2.11: Tentative oxidation pathways and intermediate reaction products of glucose oxidation [153].

4.3. Design characteristics of DGFCs

Taking into consideration that the application of a DGFC will be in a human body the site of implantation becomes important when reactant availability, implantation procedure, and patient safety are considered.

The availability of glucose and oxygen in body fluids only as a mixture is an important constraint in the design of implantable glucose fuel cells. Since most known noble metal catalysts are active towards glucose oxidation and oxygen reduction, the simultaneous presence of glucose and oxygen at both electrodes would lead to an electrochemical short-circuit. Anode and cathode would assume a similar potential and no electricity could be generated.

Initially, glucose fuel cells have therefore been constructed as *two-chamber cells* where anode and cathode are placed in separate compartments, connected by an ion bridge (Figure 2.12).

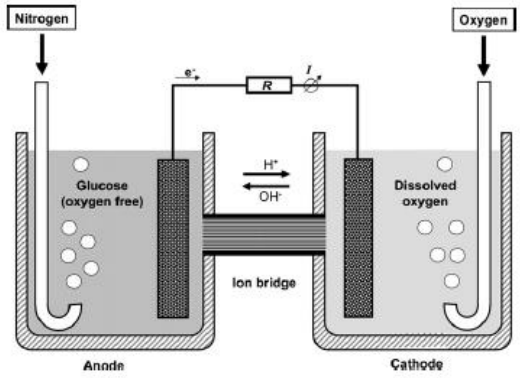

Figure 2.12: Two-chamber glucose fuel cell according to Ref. [27] with identical platinum reprinted from [19]).

The reactants glucose and oxygen were separately added to the individual compartments for anode and cathode, respectively.
To enable fuel cell operation in a physiological solution containing both glucose and oxygen the following three reaction separation concepts are reported.

In the first concept a phase separation of oxygen from body fluid is achieved at the cathode. A *hydrophobic cathode membrane* allows only for the diffusion of gaseous

oxygen but hinders glucose from reaching the cathode [162]. The embodiment of this concept is illustrated in Figure 2.13.

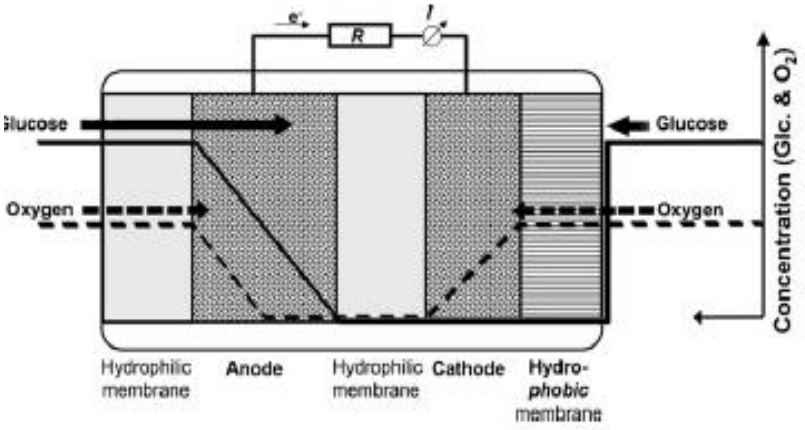

Figure 2.13: Glucose fuel cell with hydrophobic cathode membrane (schematic outline) (reprinted from [19]).

Between cathode and anode a hydrophilic ion conducting separator membrane is placed for electrical insulation. The outer part of the anode serves as sacrificial layer, where oxygen can directly react with glucose on the surface of a noble metal catalyst. This reduces the oxygen concentration in the interior of the anode, where glucose then is electrooxidized under predominantly anoxic conditions and at a potential more negative than the cathode potential.

The degree of reactant separation is dependent on the concentration of oxygen: at lower oxygen concentrations the reactant separation becomes more effective and the anode assumes a more negative potential. However, the resulting increase in fuel cell performance is countered by the reduced cathode performance at lower oxygen concentrations [159]. Since some glucose is consumed by the direct reaction with oxygen a surplus of glucose over oxygen is a prerequisite for this embodiment. This is usually the case in body fluids where the glucose concentration amounts to approximately 5×10^{-3} mol L^{-1}, compared to less than 0.2×10^{-3} mol L^{-1} of oxygen. The advantage of the concept is that platinum and other highly active noble metals can be used as catalysts for both the anode and the cathode reaction [158, 167].

In the second reactant separation concept an *oxygen-selective cathode catalyst* is used, that is inactive towards glucose oxidation. By arranging the anode sandwiched between

the cathode and an impermeable surface (or alternatively between two cathodes) the interior of the fuel cell is depleted from oxygen, and the anodic glucose oxidation takes place under predominantly anoxic conditions. A hydrophilic separator membrane electrically insulates anode and cathode while at the same time allowing for the diffusion of glucose and ions. As *oxygen-selective* cathode catalysts activated carbon and silver have been employed. Since body fluid access is required only at the cathode the fuel cell could be constructed as a thin layer directly on the implant surface, as depicted in Figure 2.14 [183].

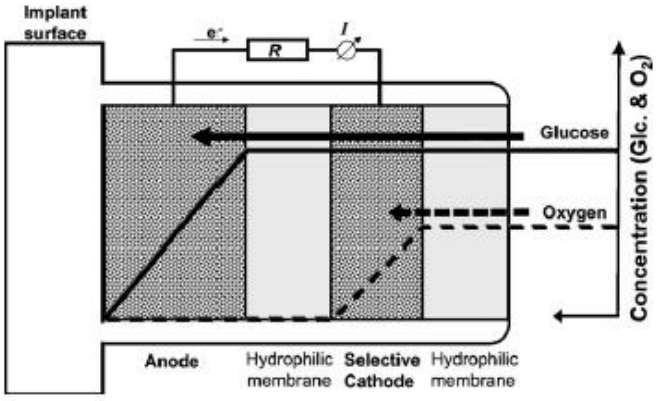

Figure 2.14: Fuel cell design with oxygen-selective cathode catalyst and special electrode (reprinted from [19]).

Also with this concept the degree of reactant separation is dependent on oxygen concentration. At higher oxygen partial pressures not all of the oxygen can be depleted at the cathode and the resulting presence of oxygen at the non-selective anode leads to the formation of a more positive anode potential. This results in a decrease of both, cell voltage and power output [203].

With the third concept the need for reactant separation is circumvented by employing *selective electrocatalysts*, that either catalyze glucose oxidation or oxygen reduction. This allows for the construction of a glucose fuel cell from two electrodes exposed to the same solution, as depicted in Figure 2.15.

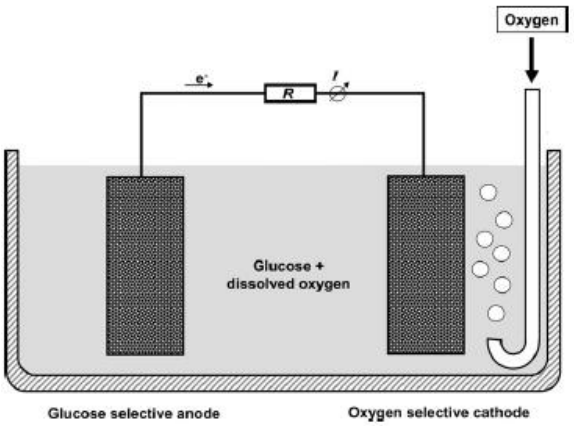

Figure 2.15: Glucose fuel cell with selective electrode catalysts (schematic outline) according [71] (reprinted from [19]).

Whereas *oxygen-selective* abiotic catalysts are available (e.g., silver, ferric phthalocyanine, and activated carbon), the information on abiotic catalysts selective towards glucose oxidation is scarce. A fuel cell of this type has been constructed from a pair of *selective* platinum-based electrodes. Unfortunately the experimental methods and results are not clearly reported. Also, the authors did not elaborate on the origin of the observed selectivity in their electrodes [204].

Theoretically, an implantable fuel cell can either be directly in contact with the blood stream or implanted in tissue. For *blood stream* implantation fuel cells of the *flow-through type* have been developed, as depicted in [159, 172, 183].

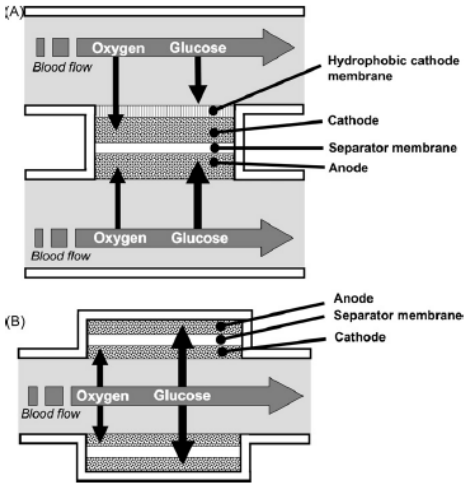

Figure 2.16: Simplified schematics of flow-through type fuel cells intended for blood (reprinted from [19]).

The blood flow promises a steady reactant supply that is not limited by diffusion from blood vessels into the surrounding tissue. However, a blood stream implantable device has to be designed in a way that blood flow is not impaired, and that no areas of reduced flow velocity are formed, which would increase the risk of thrombi formation [183]. The employed materials have to be compatible with blood, especially with respect to coagulation [205]. The concept suffers from complications arising when having to surgically introduce the device into a major blood vessel. Implantation in the blood stream has therefore been considered mainly in early studies, where the increased reactant supply posed a major factor to reach the final aim of powering an artificial heart [162].

In contrast, the reactant supply of *immersible* fuel cells developed for *tissue implantation* [158, 167, 203] relies solely on diffusion. While the surrounding tissue poses an additional mass transfer resistance, the risk of thrombi formation and blood coagulation is minimized.

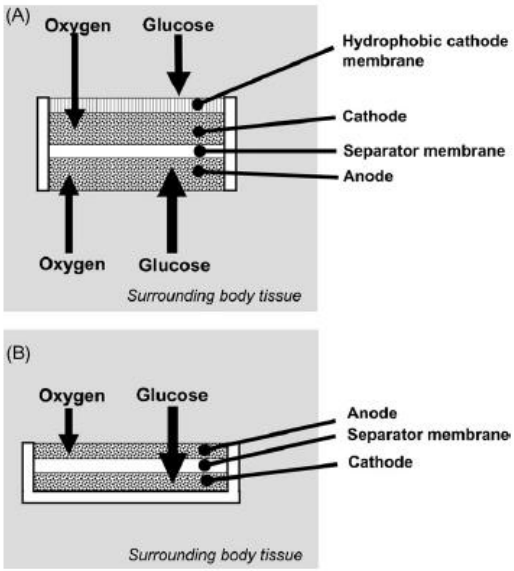

Figure 2.17: Simplified schematics of immersible fuel cells intended for tissue implantation: (A) fuel cell with hydrophobic cathode membrane, (B) fuel cell with oxygen-selective cathode catalyst (reprinted from [19]).

The fuel cell can be implanted in a similar way as the pacemaker device, enabling fuel cell integration directly on the exterior surface of the pacemaker [155]. This would facilitate implantation procedures and eliminate the risk of lead failure, which was a

common reason for pacemaker break down at that time [206]. A third embodiment where the fuel cell cathode is of the *air breathing type* and only the anode is in contact with the body fluids was disclosed in a patent assigned to the Institute of Gas Technology [180]. The concept promises an increased performance due to the considerably higher oxygen partial pressure, but the device is fairly complicated and demands a mechanical pumping mechanism to ensure a constant supply of oxygen through a percutaneous airway.

4.4. Electrocatalysts for DGFCs

The oxidation of glucose on abiotic electrode-catalysts was reported first by Bagotzy *et al.* [154]. The electrooxidation of glucose in alkaline solutions at high temperatures was investigated by Bockris *et al.* [30]. Investigating the electrooxidation of glucose in neutral phosphate buffer solutions, Rao and Drake [163] discovered that the main product of electrooxidation was gluconic acid, which was adsorbed on the platinum electrode surface, thereby inhibiting glucose oxidation. The authors suppose that gluconic acid is not susceptible to oxidation. However, other studies [164, 201] showed that the anodic behaviour of gluconic acid and glucose on a platinum electrode is exactly the same in all regions, except for the region of high anodic potentials. Yao et al. [164] consider the slow steps of electrooxidation of glucose and gluconic acid to be the same.

Platinum [207], silver [208], gold [209], copper [210], nickel [211], iron and cobalt [212], were commonly used as electro-catalytic materials for glucose oxidation. The experimental results showed that glucose electrooxidation depends strongly on the electrode materials. Platinum has good activity towards glucose oxidation in acidic medium while gold has better oxidation rate in neutral and alkaline medium. Unfortunately, pure metals lose their activity with time due to electrode poisoning. The major poison on Pt, according to a number of reports based on spectroscopic and electrochemical measurements, is adsorbed CO [213]. The catalytic activity of the platinum electrode also depends on the nature of the electrode surface, for example, the involvement of adsorbed reactive oxygen containing species (OH ads). This is

believed to be involved in the oxidation of both poison and reactive organic intermediates [89].

In the following sub-sections the state of-the-art of Pt-based, Au-, Pd- and Raney based electrocatalysts are referred and discussed. Moreover, some other non-precious electrocatalysts that have been examined for glucose electrooxidation electrocatalysts are also referred.

4.4.1. Pt-based electrocatalysts

The electrocatalytic oxidation of glucose at platinum electrodes has been widely studied, mainly with a medical aim (searches for a glucose sensor sensitive enough for rapid quantitative determinations of diabetes). Most of the studies were thus done in physiological buffered media [214]. Studies of Pt single-crystal electrodes have shown that this reaction depends strongly on the crystallographic orientation of the electrode surface [215].

The first step in glucose oxidation is the glucose adsorption [216, 217] according to the following equation that *happens in hydrogen adsorption region*:

(16)

Parallel to reaction (16) in the same potential region the catalytic decomposition of glucose into hydrogen and gluconolactone (gluconic acid) is possible.

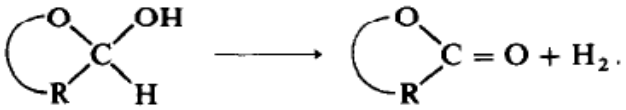

(17)

On the other hand, the linear and the bridge CO were found to be the major adsorbates responsible for the platinum electrode poisoning during the catalytic decomposition of glucose.

Bolzan *et al.* [218] postulated that during the oxidation of glucose on platinum in neutral solution, several reactions can take place simultaneously in the hydrogen

adsorption region: i) oxidation of glucose to gluconate, ii) adsorption of reduced CO_2 and iii) adsorption of organic fragments from the rest of the hydrocarbon chain. Mass spectroscopy showed that the strongly adsorbed intermediates formed in the hydrogen region are oxidized in the double layer region:

Ernst *et al.* [219] found that the glucanolactone is the only reaction product that is formed by the anodic process in the hydrogen as well as the double layer region.
According to their main findings:
(a) Varying the potential limit showed that adsorbed hydrogen does not play a role in the poisoning of the surface. The first peak that is usually appeared at potentials lower than 0.6 V, becomes more important when the lower potential limit decreases.
(b) Investigations at different sweep rates showed that the overall kinetics is controlled both by adsorption and diffusion, depending on the sweep rate and on the concentration of the glucose.
(c) When varying the concentration of glucose, the reaction orders obtained showed that, as a first approximation, the rate-determining step depends on the initial concentration of polyol. In fact the results were more difficult to be explained because of the complexity of the electrooxidation process involving adsorption steps.
(e) The evidence for the participation of adsorbed OH^- in the oxidation of glucose is indicated by the determination of reaction order with respect to the concentration. The value obtained was close to it, gluconolactone was identified as one of the main products produced during the prolonged electrolysis of glucose on palladium electrode in alkaline medium by FT-IR spectrometer.

At potentials greater than 0.6 V and up to the anodic limit the adsorbed dehydrogenated intermediated formed by the first step of reaction leads by oxidation to a δ-gluconolactone structure, i.e. no breaking of the C-O-C bond is observed on the surface.

$$\text{Pt-R-CH-OH}_{ads} \rightarrow \text{Pt-R-C=O}_{ads} + H^+ + e- \quad (18)$$

, where Pt-R-C=O_{ads} is δ-gluconolactone structure.
Desorption of lactone occurs slowly leading to gluconate by hydrolysis.

$$\text{Pt-R-C=O}_{ads} \rightarrow \text{Pt-R-C=O} \quad (19)$$

$$\text{Pt-R-C=O} + OH^- \rightarrow \text{R-COO}^- \quad (20)$$

During the negative potential sweep the surface lactone production remains the dominant process on the oxidised surface. When the potential is cathodic enough to reduce the surface, reactive OH^- are released in the immediate vicinity of the surface by reaction. Breaking of the C-O-C bond occurs, the oxidation process (being responsible for the peak seen during the backward sweep of the voltammogram) leads to weakly bonded -gluconate. Weakly bonded gluconate desorbs into solution. In the hydrogen region, the same processes occur as in the first step of glucose oxidation, except that reactive OH- are produced by reduction of water.

Uniform three-dimensional (3D) dendritic Pt nanostructures (DPNs), were synthesized and examined for glucose electrooxidation at room temperature by Shen *et al.* [103]. The DPNs showed improved electrocatalytic activity toward glucose oxidation with respect to the monodisperse Pt nanoparticles. This improvement was attributed to the porosity structure and their greatly enhanced effective surface area. According to the authors monodisperse Pt nanoparticles can be potentially useful in electrocatalytic applications such as in fuel cells or biosensors.

A fuel cell with a cation exchange membrane (CEM), which is often used for conventional polymer electrolyte fuel cells, showed an open circuit voltage (OCV) of 0.86 V and a maximum power density (P_{max}) of 1.5 mW cm^{-2} with 0.5 M D-glucose and humidified O_2 at room temperature. The performance significantly increased to show an OCV of 0.97 V and P_{max} of 20 mW cm^{-2} with 0.5 M D-glucose in 0.5 M KOH solution when the electrolyte membrane was changed from a cation to anion exchange membrane (AEM) [91]. The anode and cathode electrocatalysts were Pt and Pt-Ru unsupported, respectively.

In a direct liquid-fed fuel cell, the membrane can be either an acid type (e.g., Nafion) or an alkaline type. It has recently been demonstrated that when the electrolyte is changed from acidic to alkaline, i.e., an anion-exchange membrane (AEM), the performance is substantially improved [92]. This behaviour can be attributed mainly to the enhanced kinetics of the glucose oxidation reaction (GOR) and oxygen reduction reaction (ORR) in alkaline media compared with those in acid media [93]. Moreover, in an AEM-DGFC the direction of the electro-osmotic drag is

from the cathode to the anode, which can reduce the rate of fuel crossover from the anode to cathode and thereby to improve fuel cell performance [95, 96]. In addition, the cost of AEMs is much lower than that of PEMs (typically Nafion®).

Abplett *et al.* [220] demonstrated a miniature fuel cell operating on glucose solutions (acid environment) for the anode, which was made of $PtRuO_2$-unsupported, and operating under oxygen for the cathode, which was made of Pt-unsupported. The operation of the fuel cell demonstrated a strong negative dependence of the current on polarization at moderate to high polarizations, which manifested as a loss of current at high polarizations. This loss became more pronounced with higher fuel concentrations. The authors suggested that this loss may be due not to a loss of electron transfer efficiency at the anode but is instead due to the binding of gluconolactone to Pt reaction sites on the anode, leading to a blockage of these sites for further reaction and suppressing currents at high polarization. Despite the acid environment the P_{max} (1.67 mW cm^{-2}), as it is observed in Table 2.3, is higher than in some cases in alkaline environment. However, in literature it has been observed that, in alkaline environments, the rate of electro-oxidation of glucose is higher than that in acidic and neutral media [217, 221-223]. Moreover, since human blood and body fluids are neutral, it is more useful to investigate glucose oxidation in neutral environment.

A simple batch direct glucose fuel cell with PtRu/C as anode and activated charcoal as cathode was constructed and operated to study the effect of different temperature and concentration of glucose and KOH by Basu *et al.* [107]. The anode was completely submerged in the fuel-electrolyte solution while the cathode was just touching the solution. The other side of the cathode was open to air. The distance between the anode and the cathode was kept at 8mm. An open-circuit voltage (OCV) of 0.91 V was obtained using 0.3M glucose in 1M KOH solution. OCV increased with the increase in glucose concentration. The maximum peak power density of 1.38 mW cm^{-2} was obtained using 0.2M glucose in 1M KOH at 30 ^{o}C and it decreased with further increase in glucose concentration and temperature. The DGFC was continuously operated for 260 h at constant load of 500 Ω producing final constant voltage of 0.21 V.

It is pointed out that when operated at optimal conditions (e.g. in alkaline media) abiotic glucose fuel cells have been shown to exhibit power densities of up to 20 mW cm^{-2} (Table 2.3). This is different for fuel cells intended for implantation: Here reactant concentrations, pH, and temperature are predefined by the physiological environment For instance, when implanted into muscle tissue (e.g. near or with a pacemaker), such a fuel cell has to operate at nearly neutral pH, 37 °C, and limited availability of glucose (3 – 5 mmol l^{-1}) and oxygen (~ 7 % oxygen saturation). Under such conditions abiotic glucose fuel cells show power densities of only a few µW cm^{-2}. However, this would be sufficient to power a cardiac pacemaker (5-10 µW) by having a glucose fuel cell installed as a thin layer coating on its capsule surface (15-20 cm^2). In the future, such fuel cells may also be used to supply implanted low-power sensor systems for the monitoring of clinically relevant parameters such as glucose or oxygen concentration, blood pressure or temperature.

A different direct glucose fuel cell exposed to an externally generated electromagnetic field between electrodes to cause both the splitting of the fuel molecule into smaller units (i.e. electrochemical reforming) and an increase in the activity of catalyst materials on the fuel before electrochemical oxidation was developed by Spets *et al.* [224]. The anode was made of bimetallic PtPd/C electrocatalyst and the cathode CoTTP (cobalt porphyrin complex) and $MnCo_2O_4$. In this kind of fuel cell membrane was concerned as resistance and so it was not used. Despite the fact that it would be expected the magnetic field to enhance catalytic activity, as it is deduce from Table 2.3 (A) the exhibiting power density (0.0055 mW cm^{-2}) is not higher than the other direct glucose fuel cell.

In literature there are not a lot of works that examine electrocatalysts on different supports than carbon. Ryu *et al.* [225] demonstrated a hybrid process that deposits Pt thin film on the nanoparticle formed CNT in order to further increase the catalyst surface area. They also introduced a new method for nanoparticle formation using intense pulsed light (IPL). The intense light heats the Pt on CNT instantly, which causes the surface diffusion of Pt atoms and form nano-islands. From the measured I–V curves, maximum power densities were calculated to be 0.178 µW cm^{-2} and 0.768

μW cm^{-2} for 10 min Pt sputtered CNT mat electrode, and 3min/IPL/7 min Pt sputtered CNT mat electrode, respectively. However, in comparison with the rest referred electrocatalysts in Table 2.3 (A), the as-mentioned electrocatalysts' performance is low.

Sun *et al.* [226] shown that a combinatorial method originally developed for the discovery of fuel cell electrocatalysts can also be used effectively in the search for better glucose sensor materials. Moreover, they proved that a broad range of binary, ternary, and higher Pt-Pb alloy compositions resist poisoning in glucose solutions and allow glucose to be sensed amperometrically at potentials negative of the oxidation of common interfering agents. Cui *et al.* [93] studied extensively the glucose oxidation on carbon nanotube electrodes electrodeposited with Pt–Pb alloy nanoparticles. The enhanced glucose oxidation was ascribed to the advantage of high surface area and good electrocatalytic activity of carbon nanotubes and Pt–Pb alloy nanoparticles.

On the other hand Balcázar *et al.* [227] evaluated PtAg/C as cathode in direct glucose fuel cell using Au/C as anode. The PtAg/C had better catalytic activity than Pt/C towards oxygen reduction in alkaline environment and in presence of glucose. PtAg-based material could be an excellent candidate for use in alkaline fuel cells, bio-fuel cells and microfluidic fuel cells that use glucose as fuel, exhibiting 0.63 mW cm^{-2}.

In Table 2.3 (B) are listed the works that concern the fabrication of direct glucose fuel cells with the aim of implementation. The current interest in autonomous, self-sufficient MEMS (micro-electro-mechanical systems) implants has revived the research in long-term stable, implantable glucose fuel cells based on abiotic catalysts. The availability of fuel cell reactants, oxygen and glucose, only as a mixture in the physiologic environment, has traditionally posed a design challenge: Net current production requires oxidation and reduction to occur separately and selectively at the anode and cathode, respectively, to prevent electrochemical short circuits.

Table 2.3. Pt-based electrocatalysts in DGFCs-performance characteristics.

A.DIRECT GLUCOSE FUEL CELLS UNDER OPTIMAL CONDITIONS				
Electrocatalysts	**Maximum Power Density (mW cm-2)**	**Membrane**	**Experimental conditions**	**Ref.**
Anode: Pt-unsupported **Cathode:** PtRu-unsupported	20	Tokuyama Corporation	0.5 M KOH, 0.5 M glucose (4 mL min^{-1}), O_2 (100 mL min^{-1}), room temperature	[91]
Anode: $PtRuO_2$-unsupported **Cathode:** Pt-unsupported	1.67	Nafion 117	1 M glucose, (0.1 mL min^{-1}), O_2 (20 sccm), 60◦C	[220]
Anode: Pt-unsupported **Cathode:** PtRu-unsupported	1.5	Nafion 112	0.5 M glucose (4 mL min^{-1}), O_2 (100 mL min^{-1}), room temperature	[91]
Anode: PtRu/C **Cathode:** activated carbon	1.38	Membraneless	1M KOH, 0.2 M glucose, 30◦C	[107]
Anode: Au/C **Cathode:** PtAg/C	0.63	Membraneless	0.3 M KOH, 100 mM glucose (0.1 mL min^{-1}), cathode: 0.3 M KOH oxygen saturated, room temperature	[227]
Anode: PtPd/C **Cathode:** CoTTP-$MnCo_2O_4$/C	0.0055	Membraneless	2M KOH, 1M glucose, without diffusion layer, 20◦C	[224]
Anode: $Pt_{nanoislands}$/CNT **Cathode:** $Pt_{nanoislands}$/CNT	0.0008	Membraneless	0.5M glucose, PBS buffer (pH 7.4) (15 ml h^{-1}) ,cathode is open to the air, room temperature	[225]

B. IMPLANTABLE DIRECT GLUCOSE FUEL CELLS				
Electrocatalysts	**Maximum Power Density (μW cm-2)**	**Membrane**	**Experimental conditions**	**Ref.**
Anode: activated carbon with 10%Pt **Cathode:** activated carbon	20 (7 days)	Membraneless	physiological phosphate buffer, 0.1 wt% glucose, air, 37◦C	[228]
Anode: Pt_{porous} **Cathode:** Pt_{porous} /with metalized silicon wafer	5.1 (90 days operation)	Supor450-filter membrane	Six fuel cell stack, 5.0 mmol L^{-1}glucose, physiological phosphate buffer, dissolved oxygen (7% saturation), (pH=7.3), 37 ◦C	[229]

A prototype direct glucose fuel cell feeding glucose with oxygen from one side, was constructed by Stetten *et al.* [228]. The electrodes were consisted of activated carbon coating a noble metal screen that collects the electrons. The activated carbon at the glucose electrode contained an additional 10 % of platinum. The operating time of the constructed direct glucose fuel cell was 7 days at 20 μW cm^{-2}. Over the time the power output slightly decreased, presumably due to the poisoning of the platinum catalyst by oxidation products. This is the highest reported activity for implantable direct glucose fuel cells.

However, Kloke *et al.* [229] fabricated a six direct glucose fuel cells connected in parallel, with porous Pt that exhibited a power density of 5.1 μW cm^{-2} under close to physiological conditions, which is not a very high value of power density, but its operational conditions are for implantable glucose fuel cells and its stability is the highest reported in literature. During continuous operation over 90 days the fuel cell showed a mean continuous decay of about 0.8% per day, which is related to catalyst poisoning at the anode. It has been demonstrated that the porosity and structure of

the support membrane has a strong effect on the amount of glucose and oxygen that passes through the cathode.

4.4.2. Au-based electrocatalysts

Glucose oxidizes poorly on gold electrodes in acid solutions. No glucose oxidation current was observed in 0.5 M H_2SO_4, till the gold surface started to oxidize, as it was stated by Vassilyev *et al*. [230]. Moreover, being present in the solution and, most likely, adsorbed on the gold electrode surface, glucose shifts the onset of the oxidation of the surface to slightly more positive potentials.

At low concentrations of glucose, currents due to its oxidation appear only in the region of formation of the second oxy-compound ($E_{reference}$ ~ 1.43 V). However, at considerable glucose concentration values (C > 0.011 M) the oxidation current can be observed also in the region of formation of the first oxy-compound (E_r ~1.25-1.35 V). For glucose electrooxidation gold turned out to be a much worse catalyst in 0.5 M H_2SO_4, than platinum. Even the maximum oxidation current at E_r > 1.4 V appeared to be by an order of magnitude smaller than that in the case of glucose electrooxidation on platinum [230].

As far as neutral solutions are concerned, the behavior of gold and platinum as catalysts for glucose electrooxidation changes. Glucose electrooxidation on gold begins at lower positive potentials than on platinum, and electrooxidation currents at E_r <1 V are considerably larger for gold than for platinum.

On the potentiodynamic curve of glucose electrooxidation in a phosphate buffer solution with pH = 7.1, at glucose concentrations less than 0.055 M, three maxima can be discerned: E_r^1 ~ 0.66-0.7 V, E_r^2 ~0.94-0.98 V, E_r^3 ~ 1.43 V, according to Vassilyev *et al*. [230]. At glucose concentrations higher than 0.055 M the first and second maxima approach one another and almost merge into one large maximum. A sharp decrease in the current is observed after the second maximum, and at a potential at which oxide corresponding to this decrease has already formed, the current becomes very small.

The comparison of the polarization curves of glucose electrooxidation on gold in neutral solutions with the potentiodynamic curve of gold electrode oxidation in a background solution shows that glucose electrooxidation starts long before the noticeable oxidation of the gold electrode's surface begins.

A fall after the first maximum corresponds to the onset of the noticeable oxidation of the gold electrode surface. The second maximum corresponds to the potential of the second oxidation wave on the gold electrode surface, the third one to the potential of the maximum on the potentiodynamic curve of gold surface oxidation.

According to Vassilyev *et al*. [230] in alkaline solutions the current values due to oxidation of glucose on gold exceed those due to oxidation on platinum to an even greater degree.

In Scheme 1 is depicted the reaction pathway of glucose electrooxidation on gold electrode in alkaline solution:

$$Au + OH^- \rightarrow Au\text{-}OH_{ads}^{(1-\lambda)} + \lambda\, e^- \quad (21)$$

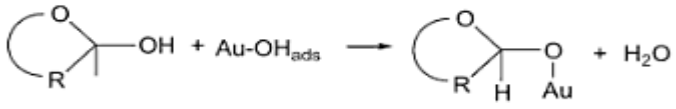

(22)

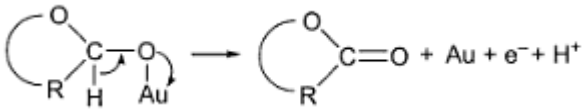

(23)

Scheme 1: Reaction pathway of glucose electrooxidation on gold electrode in alkaline solution.

The formation of catalytically active sites Au-OH_{ads} is the most important step for glucose oxidation. On the other hand, the generation of an oxide precursor in the potential region prior to gold oxide formation is an important property of Au electrodes, which plays a key role in enhancing the catalytic activity of Au in alkaline solutions.

Because of high surface area, nanoporous materials have attracted great interest for their wide applications in catalysis, sensors, fuel cells, actuators, and so on. Especially, metal electrodes with nanoporous structure on its surface possess great advantages in analysis and chemical reactions [231-233].

When the electrocatalyst is nanoporous gold (NPG) [154], due to its rough surface morphology and its availability for OH- adsorption, NPG exhibits a much better electrocatalytical activity toward glucose oxidation in neutral and alkaline solutions as compared to bulk gold) [154]. Recently, Liu *et al.* [154], found that a tiny amount of Ag components in NPG nanostructures can significantly enhance the rate for electrocatalytic oxidation of glucose. The main reason proposed was that the existence of Ag promotes the chemisorption of OH^- ions on the gold surface, thereby forming more active sites ($Au\text{-}OH_{ads}$) for glucose electrooxidation.

Moreover, Ag ad-layer onto gold single crystal surfaces acted as good catalysts towards glucose electrooxidation [234]. Moreover, if metal nanoporous films (NPFs) could be directly formed on the surface of an electrode, transfer of electronic response from the surface to the substrate would be much faster than that of an electrode coated with nanostructured material by adsorbing method.

In literature, silver modified Au-monolayer electrode was used as anode in direct glucose fuel cell having stable catalytic activity and showing high reproducibility in the glucose oxidation over a long period of time [110]. The silver modified Au electrodes also exhibited enough durability to be used in serious operations without gold film being peeled off. Open-circuit potential of 0.65 V and maximum power of 0.22 mW cm^{-2} at cell voltage of 0.32V were obtained by using air and about 1mL solution containing 0.3M sodium hydroxide and 10mMglucose.

Preparation of Pt-coated nanoporous films of gold improved the glucose oxidation 180 times compared to the polished Pt-electrode [235]. Because of their nanoporous structures, the resulting metal nanoporous films may possess higher surface area than that of the polished ones.

On the other hand Huang *et al.* [104] fabricated 3-D micro-nano hierarchical porous Au gold films. Besides the much larger current due to the higher surface area of the 3D PGF, the peaks for the redox pair (-0.15/-0.42 V) of gold oxide monolayer appear at more negative potentials (compared to smooth gold), which is a typical redox characteristic of gold nanomaterials.

A pair of broad "pre-redox peaks" is appeared between -1.1 and -0.3 V. These are related to the electrochemical transition between the gold adatoms and the incipient hydrous gold oxide (AuOHads) premonolayer. The incipient hydrous gold oxides, produced at quite low potentials, are highly reactive and may trigger and mediate the electrooxidation of some biomolecules. The multifunctional 3D PGFs exhibited excellent stability, high electrocatalytic activity toward the oxidation of glucose.

Pasta *et al.* [236] studied the electrocatalytic properties of nanostructured gold electrodes towards glucose electrooxidation and they compared the results with a commercial gold pin electrode. On nanostructured gold electrodes the observed oxidation processes shifted to lower potentials and good electrocatalytic activity. The high current density was attributed to the presence of more defective sites on the surface of gold nanoparticles.

It is well known that surface reactions usually require lower activation energy in presence of defective sites (i.e. kink atom, adatom, edge adatom, etc.); as a consequence, the nanoparticles should have an intrinsic large number of defects which are responsible for increased glucose oxidative adsorption.

Au-film electrodes prepared by electrodeposition in glucose and Au containing bath exhibited good performance as anodes in a membraneless direct glucose fuel cell [237]. The direct glucose fuel cell exhibited 0.30 mW cm^{-2} in a PBS solution containing 400mM glucose. The oxygen was fed near to the cathode which was made of 3-D porous Pt. The good fuel cell performance was attributed to the increase surface-area and crystal-facet differences from the dynamic adsorption–desorption of added glucose and its electrooxidation products on electroplating Au particles.

The activity for glucose oxidation of Au-self assembled monolayer was tested at 37 ^{o}C by Ivanov *et al.* [238]. It was observed that the surface of the gold at elevated temperatures is transformed and the modified surface exhibits high activity towards glucose oxidation.

Gold nanoparticles supported on graphene sheets electrocatalyst was investigated for glucose electrooxidation by Hu *et al.* [239]. The electrocatalyst's good

electrocatalytic activity was ascribed to the synergistic effect of graphene and Au NPs. More precisely, electrical network formed through the Au-nanoparticles direct integrating with the graphene. The high density and well-distributed Au NPs on the surface of graphene would induce more active sites for the catalytic redox reaction and bring about an efficient electrical network through their direct integrating with graphene, which would greatly increase the electrocatalytic activity.

Moreover, surface modification of Pt with Au was also found to dramatically improve NPG's activity toward glucose oxidation, especially in neutral and alkaline solutions. Yan *et al.* [97] investigated NPG samples decorated with different amounts of Pt and found that NPG-Pt (64 min) demonstrated the highest activity and stability. They also constructed and run the DGFCs using NPG-64 as the anode and commercial Pt/C as the cathode. In an alkaline solution of 2M NaOH + 0.5 M glucose, the maximum power density can achieve ~4.4 mW cm^{-2} at 60 °C, which is more than 20 times higher than that in neutral solution.

Table 2.4. Au-based electrocatalysts in DGFCs-performance characteristics.

Electrocatalysts	Maximum Power Density (mW cm-2)	Membrane	Experimental conditions	Ref.
Anode: NPG[a] **Cathode:** Pt/C (commercial)	4.4	Nafion 115	2 M NaOH, 0.5 M glucose (2 mL min^{-1}), air (120 mL min^{-1}), 60 ◦C	[97]
Anode: Pt-Au/C **Cathode:** activated charcoal	0.72	Membraneless	1 M KOH, 0.2 M glucose, 60 ◦C	[99]
Anode: Au_{film}/GC[b] **Cathode:** 3D-Pt_{porous}/C (commercial)	0.30	Membraneless	PBS, 400mM glucose, oxygen fed directly to the cathode, room temperature	[237]
Anode: silver modified-Au_{film}/C **Cathode:** silver modified-Au_{film}/C	0.22	Membraneless	0.3 M NaOH, 10mM glucose, air, , room temperature	[110]

a: Nanoporous Gold
b: Glassy carbon

A batch direct glucose fuel cell was constructed by Basu *et al.* [99]. The anode was submerged in bottom of the fuel–electrolyte solution inside a chamber and the cathode just touched the solution on the top of the chamber. Whereas one side of the cathode was touching the fuel–electrolyte solution, the other side of cathode was open to atmosphere. The distance between anode and cathode was 0.8 cm. The batch cell operated with anode of PtAu/C and cathode of activated charcoal produced OCV of 0.9 V in 0.2 M glucose and in 1 M KOH. The OCV obtained using commercial PtRu/C as anode is same as that of prepared PtAu/C. The peak power density obtained is 0.72 mW cm^{-2} (voltage: 0.35 V, current density: 2.05 mA cm^{-2}) at 30°C operating temperature.

4.4.3. Pd-based electrocatalysts

The electrooxidation of glucose on smooth Pd in alkaline medium had been studied for the first time in 1991 by Becerik *et al* using electrochemical and polarimetric techniques [240]. They proved that palladium electrodes in alkaline solution for the electro-oxidation of glucose exhibit a pronounced catalytic activity and generally the kinetics of the fuel oxidation is different to that on a platinum electrode.

On the basis of their experimental work the authors proposed a possible mechanism of glucose electrooxidation on Pd-based electrocatalysts:

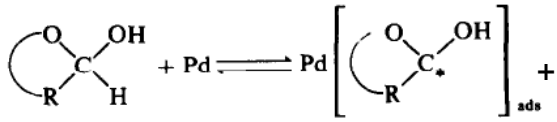

$+ H_{ads}$ (at <-0.7 mV vs reference) (24)

$$H_{ads} \rightarrow H_{aq}^{+} + e^{-} \quad (25)$$

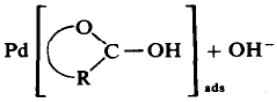

products (at >-0.7 mV vs reference) (26)

Scheme 2: Mechanism of glucose oxidation on Au electrocatalyst.

The authors during cyclic voltammetry, observed a small peak in the range of positive potentials, just before finishing the forward scanning. According to them this

was probably due to either a surface reaction of Pd(OH) or PdO with the solution phase glucose or a further oxidation of an adsorbed species in more anodic potentials.

However, the mechanism of the glucose oxidation in alkaline solution appears to be very complex, thus its elucidation requires a combination of electrochemical and separation methods as well as further investigation.

In literature the works that investigate Pd-based electrocatalysts for glucose electrooxidation are a few. As in case of Pt-based and Au-based electrocatalysts, nanoporous structure is preferred also for Pd-based electrocatalysts, since their three-dimensional (3D) network textures which present both considerable surface areas and high stability of the catalysts particles, show high electrocatalytic activity for some specific electrochemical reactions and for glucose also [241-243]. The electrocatalysis of the oxidation of glucose on a nanoporous Pd-modified TiO_2 electrode, prepared by the hydrothermal process, was investigated in 0.1 M NaOH solution for different glucose concentrations (with 30mM glucose to exhibit the highest activity) by Yi *et al.* [244].

Comparable to the single crystals Au(111) electrocatalyst, Pd/TiO_2 showed an attractive enhancement of electrocatalytic activity and lower onset potential. It was shown by An *et al.* [100] that alkaline direct glucose fuel cells with a relatively cheap membrane and catalysts can result in a maximum power density as high as 38 mW cm^{-2} at 60 ^{o}C. The high performance was attributed mainly to the increased kinetics of both the glucose oxidation reaction and the oxygen reduction reaction rendered by the alkaline medium with the anion-exchange membrane. The cathode was home-made by HYPERMEC™ catalyst (Acta) and the anode a home-made Pd-Ni electrocatalyst supported on carbon, with nickel being in the form of foam.

Although the fuel cell system developed in the above-mentioned work is promising in terms of its higher performance with cheaper electrolyte and catalyst materials than all other reported glucose fuel cells, some fundamental issues, such as the mechanism and the product of glucose oxidation on the present non-platinum catalyst in alkaline media, merit extensive research. Despite the fact that Pd-based

electrocatalysts present better activity in alkaline environment than Au and Pt-based, there are still no a lot of works in literature.

4.4.4. Raney-type electrocatalysts

Implantable glucose fuel cells use glucose and oxygen that are available in body fluids for producing from them electricity as it has been referred in 4.4.1 sub-section. Thus glucose and oxygen co-exist and cannot be fed separately in a direct glucose fuel cell. Consequently, are preferred electrocatalysts that are porous in order to be permeable to oxygen and to oxidize glucose' selectively (taking into consideration that only anode is exposed to body fluids). It is worth noticing that the general tissue implantability and in vivo operation of such an abiotically catalysed glucose fuel cell has already been demonstrated in a dog [245] yielding a stable power density of 1.6 μW cm^{-2} over a period of 5 months. Since a cardiac pacemaker nowadays only demanded 8 μW [246] and exhibited an external surface of more than 15 cm^2, it would be feasible to supply such an implant with a glucose fuel cell coated onto its external surface. If implemented as a thin layer coating onto implant surfaces such a fuel cell would not even consume additional space.

The research team of Kerzenmacher in 2010 [247, 248] presented a novel fabrication route yielding Raney-platinum film electrodes intended as glucose oxidation anodes for potentially implantable fuel cells. Gebhardt *et al.* [195] were the first that they proposed alternative electrode fabrication concept that obviates the need for hydrogel binders. They fabricated Raney-platinum film anodes by extraction of the non-noble component from annealed platinum–nickel bi-layers or homogenous alloy foils fabricated from a fusible regulus. Compared to conventional anodes, these anodes exhibited improved glucose oxidation performance as well as excellent resistance against oxidative and hydrolytic attack. However, the use of nickel as non-noble, extractable component is likely to be problematic in the context of implantable electrodes due to its allergenic and carcinogenic properties [249]. Kerzenmacher *et al.* [248] replaced the carcinogenic nickel by zinc as alloying partner. The experimental results showed that zinc release upon anode operation can be expected to have no

significant effect on physiological normal levels, which promises good biocompatibility. Moreover, they conducted experiments in artificial issue tissue with the novel electrocatalysts to perform long stability and tolerance.

In sequence, they examined Raney-platinum electrocatalysts as cathodes [247]. At the same time they examined their activity towards oxygen reduction in presence of glucose. The main advantage of the novel cathodes over previous approaches is their excellent resistance against hydrolytic and oxidative attack. They also proved that the formation of a mixed potential between glucose and oxygen at platinum electrodes can be minimized by the construction of very thin electrodes has thus been verified.

In 2011, an improved abiotically catalyzed glucose fuel cell, intended as energy harvesting tissue implantable power supply for medical implants was fabricated by Kerzenmacher *et al.* [250]. The exhibited power density was 4.4 μw cm^{-2}. Due to the fact that glucose and oxygen cannot be fed in an implantable direct glucose fuel cell separately in times many varying designs of direct glucose fuel cells have been proposed (see sub-section 4.3).

In a favorable embodiment of such a fuel cell a glucose permeable cathode, fabricated from hydrogel-dispersed activated carbon, is situated in front of the anode [177]. The prime advantage of this concept is that reactant access to the fuel cell from one side is sufficient, enabling its integration directly onto the surface of medical implants [251] at minimized geometric footprint. A drawback of previous glucose-permeable electrodes (cathodes) has been their limited stability against hydrolytic and oxidative attack, as they were fabricated from catalyst particles embedded in a poly(vinyl alcohol)–poly(acrylic acid) hydrogel matrix [184, 252].

Furthermore, the low electrical conductivity of hydrogel-catalyst compounds mandates the use of mesh-like current collectors embedded within the electrodes, leading to relatively thick structures in the range of several hundred μm.

Recently, modified Raney-type metal electrocatalysts have re-appeared and they seem to be good candidates as anode for glucose implantable fuel cells (Table 2.5). Kloke *et al.* [253] presented a novel type of abiotically catalysed implantable glucose

fuel cell with anode and cathode placed side by side, using a Raney-platinum glucose oxidation anode with high tolerance towards oxygen. The exhibited power density was 2.2 μW cm^{-2} (Table 2.5).

Table 2.5. Raney-type electrocatalysts for implantable glucose fuel cells.

Electrocatalysts	Maximum Power Density (μW cm-2)	Membrane	Experimental conditions	Ref.
Anode: Pt-Raney **Cathode:** Pt_{porous}	4.4±0.2	136-μm thick porous membrane (Supor-450, 0.45_mpore size, Pall, East Hills, New York, USA)	3mM glucose, 2mLmin^{-1}, 7% oxygen saturation	[250]
Anode: Pt-Raney type **Cathode:** SWCNT	3.4	Nafion	Cerebrospinal fluid, application in human brain	[254]
Anode: Pt-Raney **Cathode:** Pt-Raney	2.2	Membrane filter	PBS, 3mmol L^{-1} glucose, 37◦C, 7% O_2 saturation	[253]
Anode: PtNi (Raney type)/silicon wafer **Cathode:** Pt / porous substrate	1.5 (4 hours)	Carbon paper	5.0 mmol L^{-1}glucose, dissolved oxygen (7% saturation), 0.01 M phosphate buffer saline (pH 7.4), 37 ◦C	[229]

The peak power output of a micro-fabricated fuel cell by Oncescu *et al.* [229] was approximately 2 μW cm^{-2} and had a sustainable power density of 1.5 μW cm^{-2} at 10 μA cm^{-2}. The anode was Pt-Ni (Raney type) supported on silicon wafer and the cathode was porous Pt supported on conductive carbon paper. The carbon paper support allows for the fabrication of thinner and more stable electrodes which results in better glucose diffusivity through the cathode as indicated by the higher power density.

The most recent interesting application of direct glucose fuel cells was demonstrated by Rapoport *et al.* [254] in MIT University. They developed an implantable fuel cell that generated power through glucose oxidation, producing 3.4μW cm^{-2} steady-state power and up to 180μW cm^{-2} peak power. The

anode was nanostructured Raney-platinum and the cathode self-assembled single walled nanotubes.

4.4.5. Other electrocatalysts

Other alternative to metals is the use of molecular catalysts which mimic the enzymatic catalysis. The engineering of molecular electrocatalysts represents also a promising route in the design of glucose fuel cells since it can potentially approach the efficiency and durability of a metal-based electrode, and the selectivity of the enzymatic reaction. While molecular catalysts such as cobalt porphyrins or copper complexes are already well described for the reduction of oxygen at the cathode, only a few molecular catalysts have shown interesting catalytic properties toward the oxidation of glucose.

Rhodium porphyrins recently appeared to show interesting overpotentials as highly efficient catalysts for the oxidation of glucose, taking advantage of its well-known properties for the homogeneous oxidative catalysis of alcohols in the presence of oxygen [255].

Elouarzaki *et al.* [255] studied a deuteroporphyrin dimethylester (DPDE) rhodium(III) ((DPDE)RhIII) complex, immobilized within a MWCNT/Nafion electrode and its integration into a molecular catalysis-based glucose fuel cell. The exhibiting power density was 0.18 mW cm^{-2} (Table 2.6) at 0.22 V and an open circuit voltage (OCV) of 0.64 V.

Non-Pt metal of long lifetime and operational stability has to be considered, involving electrocatalytic activity towards the oxidation of glucose. Among the choices, nickel (Ni) has been widely studied [211]. Towards this direction, Zhao *et al.* [256] reported an alkaline glucose fuel cell based on nickel (Ni) electrodes without the catalyst poisoning found in Pt systems. Output current increased and power density (0.015 mW cm^{-2}) up to six times the initial value over extensive operation time, but long time operation is necessary.

Table 2.6. Other studied electrocatalysts for glucose oxidation reaction.

Electrocatalysts	Maximum Power Density (mW cm-2)	Membrane	Experimental conditions	Ref.
Anode: c-PAN12-Ag after silver metalization **Cathode:** Ag (AC65)	0.4	Membraneless	Air breathing, 0.8 M glucose, 1M KOH	[257]
Anode: MWCNT/(DPDE)Rh^{III} **Cathode:** MWCNT/PcCo	0.18	Nafion 115	0.5 M glucose, 0.5 M KOH ,room temperature	[255]
Anode: silver plated electrospun fibrous **Cathode:** E-TEK, Somerset	0.043	Membraneless	0.8 M glucose, 1M KOH, room temperature	[258]
Anode: Ni foam **Cathode:** Ni foam	0.015	Anion exchange membrane (Fumasep FAB)	in glucose solution, O_2: 10mL min^{-1} room temperature,	[256]

Investigation as an effort to develop low cost glucose-fueled fuel cell for portable devices has also be done by Schechner *et al.* [258]. They produced high surface-to-volume ratio membranes which were used to fabricate micrometer-size polycaprolactone (PCL) fibrous electrocatalytic anode membranes for the oxidation of glucose in an alkaline fuel cell. The membranes were coated with silver which served as anodes in the examined glucose fuel cell. The cell produced an open circuit voltage of 0.337 V and a peak power density of 0.043 mW cm^{-2} (Table 2.6).

In order to increase the surface area, the electrical conductivity, the suitable porosity for reactant flux and stability during the glucose fuel cell operation Prilutsky *et al.* [257] fabricated by the electrospinning process electrocatalysts made of carbonized polyacrylonitryle (cPAN) nanofibers, with and without embedded multiwall carbon nanotubes (MWCNTs). The evaluation of the as-prepared anodes in air-breathing glucose fuel cell [257]. The anode was c-PAN-Ag and the cathode was silver. Maxima values of open circuit voltage and PPD of silvered carbon electrodes were measured to be about 0.9 V and 0.400 mW cm^{-2}. Thus, carbonized nanofibers

with embedded MWCNTs may form a good basis for glucose fuel cell anodes, but better metallization and cell-configuration allowing proper mixing are required.

4.5. Direct glucose fuel cells applications & future prospects

In *in vitro* experiments under near-physiological conditions several groups demonstrated tissue implantable abiotically catalyzed glucose fuel cells delivering between 2.5 and 8 μWcm^{-2} for periods up to 100 days. *Flow-through* type fuel cells with *hydrophobic cathode membrane*, intended for operation in the blood stream, exhibited *in vitro* performance of up to 50 μWcm^{-2}, but successful *in vivo* operation has not been demonstrated [159].

Several studies revealed a detrimental influence of amino acids and other endogenous substances on electrode performance, indicating silver cathodes and Raney-type anodes fabricated from platinum–nickel alloys as promising candidates for stable *in vivo* performance.

However, a systematic approach comparing the fuel cell performance under physiological *in vitro* conditions, including amino acids and other endogenous substances present in body fluids, has to our knowledge not yet been reported. First *in vivo* experiments with fuel cells implanted subcutaneously in dogs yielded performances in the range of 2 μWcm^{-2} for periods up to 150 days. Although no negative tissue response to the implanted fuel cells has been observed, dedicated cytotoxicity and biocompatibility investigations have not been reported.

Whereas these results are encouraging with respect to the application of abiotically catalyzed glucose fuel cells as power supply for low-power medical implants, the majority of publications are imprecise with respect to materials and fabrication of the devices. The performance of different embodiments can therefore hardly be compared, and further effort will be necessary to redevelop the technology and establish an understanding of construction details governing long-term performance and *in vivo* stability.

Based on the so far demonstrated performance an *in vivo* power output of approximately 50 µW can be expected from abiotically catalyzed glucose fuel cells, assuming a reasonably sized device with 25 cm^2 surface area. Potential applications are thus limited to low power medical implants, such as cardiac pacemakers and implantable sensors. In the context of low power medical implants abiotically catalyzed glucose fuel cells compare well to other energy harvesting approaches.

Enzymatically catalyzed glucose fuel cells have exhibited performances of up to 430 μWcm^{-2} under physiological conditions [259]. Although this is an order of magnitude higher than the highest performance reported for abiotically catalyzed glucose fuel cells [159], the lifetime of their enzymatic catalysts has not yet been demonstrated beyond the order of a month [260]. At present, enzymatic fuel cells appear therefore to be limited to short-term applications.

For *vibrational energy harvesting* systems, subject to the simulated motions of the left ventricular wall of a goat, power outputs between 36 and 58 µW have been demonstrated. These variable capacitance-type electrostatic (VCES) generators weigh between 0.76 and 1.2 kg, and were therefore too large to be implanted in the thoracic cavity of a goat [261, 262]. A much smaller *vibrational energy harvesting* generator intended for biomedical applications has been described recently. For a device of 11mm by 11mm in size the authors projected a power output of 80 µW at an operating frequency of 30 Hz [263].

With regard to size the power output of this device is in the range of abiotically catalyzed glucose fuel cells. In contrast, the performance of implantable fuel cells is independent of continuous body motion which makes them superior compared to vibrational systems.

Considerably higher performances have been reported for *thermoelectric generators*. With the aim of supplying a cardiac pacemaker a thermopile system has recently been developed, that delivers 1100 μWcm^{-2} at a temperature difference of 2K [264]. However, the performance of encapsulated thermoelectric generators under the

relatively low-temperature gradients within the human body has not yet been demonstrated.

An important topic of future research will be the application of novel materials and fabrication techniques. Nano-patterned catalysts, carbon nanotubes, and electrically conductive polymers have already found application in biosensors and conventional fuel cells. They are exemplary for a number of promising new technologies that have not yet been explored in the context of implantable abiotically catalyzed glucose fuel cells. A further, largely unexplored field is the development of abiotic catalysts that are selective for glucose oxidation. Such catalysts would render reactant separation obsolete and therefore offer a high degree of freedom in cell construction.

References

[1] L.J.M.J. Blomen, N. Mugerwa, Fuel Cell Systems, Springer, 1993.

[2] F.T. Bacon, Electrochim. Acta 14 (1969) 569-585.

[3] T.A. Zawodzinski, C. Derouin, S. Radzinski, R.J. Sherman, V.T. Smith, T.E. Springer, S. Gottesfeld, Water Uptake by and Transport Through NafionB® 117 Membranes, 1993, pp. 1041-1047.

[4] P. Aircraft, Whitney, Design and development of H_2-O_2 Fuel Cell Power Plants for Apollo Command Module, NASA/Houston, 1962.

[5] J.M. Andújar, F. Segura, Renew. Sust. Energ. Rev. 13 (2009) 2309-2322.

[6] M. Wakizoe, O.A. Velev, S. Srinivasan, Electrochim. Acta 40 (1995) 335-344.

[7] A.B. Stambouli, Renew. Sust. Energ. Rev. 15 (2011) 4507-4520.

[8] J.H. Lee, S.T. Baek, H.J. Jung, H.H. Kang, J.M. Chung, I.Y. Suh, Development of a 250kW power conditioning system for Molten Carbonate Fuel Cell power generation system, Proceeding of International Conference on Electrical Machines and Systems, ICEMS 2007, 2007, pp. 354-358.

[9] A. Khaligh, A.M. Rahimi, L. Young-Joo, J. Cao, A. Emadi, S.D. Andrews, C. Robinson, C. Finnerty, Vehicular Technology, IEEE Transactions on 56 (2007) 3709-3721.

[10] F. Segura, E. Durán, J.M. Andújar, J. Power Sources 193 (2009) 276-284.

[11] M.J. Vasallo, J.M. Andujar, C. Garcia, J.J. Brey, Industrial Electronics, IEEE Transactions on 57 (2002) 1964-1975.

[12] S.S. Williamson, A. Emadi, M. Shahidehpour, Distributed fuel cell generation in restructured power systems, Power Engineering Society General Meeting, 2004. IEEE, 2004, pp. 2079-2084 Vol.2072.

[13] P.A. Lehman, C.E. Chamberlin, J.I. Zoellick, R.A. Engel, A photovoltaic/fuel cell power system for a remote telecommunications station, Photovoltaic Specialists Conference, 2000. Conference Record of the Twenty-Eighth IEEE, 2000, pp. 1552-1555.

[14] R.J. Spiegel, J.L. Preston, Waste Manage. 23 (2003) 709-717.

[15] H.A. Gasteiger, S.S. Kocha, B. Sompalli, F.T. Wagner, Appl. Catal. B-Environ. 56 (2005) 9-35.

[16] X. Yu, S. Ye, J. Power Sources 172 (2007) 133-144.

[17] A. Brouzgou, S.Q. Song, P. Tsiakaras, Applied Catalysis B: Environmental 127 (2012) 371-388.

[18] Y.-H. Cho, B. Choi, Y.-H. Cho, H.-S. Park, Y.-E. Sung, Electrochem. Commun. 9 (2007) 378-381.

[19] E. Antolini, S.C. Zignani, S.F. Santos, E.R. Gonzalez, Electrochim. Acta 56 (2011) 2299-2305.

[20] M. Cavarroc, A. Ennadjaoui, M. Mougenot, P. Brault, R. Escalier, Y. Tessier, J. Durand, S. Roualdès, T. Sauvage, C. Coutanceau, Electrochem. Commun. 11 (2009) 859-861.

[21] D. Gruber, N. Ponath, J. Müller, F. Lindstaedt, J. Power Sources 150 (2005) 67-72.

[22] R. Zeis, A. Mathur, G. Fritz, J. Lee, J. Erlebacher, J. Power Sources 165 (2007) 65-72.

[23] L. Xiong, A. Manthiram, Electrochim. Acta 50 (2005) 3200-3204.

[24] T. Yamanaka, T. Takeguchi, G. Wang, E.N. Muhamad, W. Ueda, J. Power Sources 195 (2010) 6398-6404.

[25] P.P. Lopes, E.A. Ticianelli, H. Varela, J. Power Sources 196 (2011) 84-89.

[26] M. Carmo, V.A. Paganin, J.M. Rosolen, E.R. Gonzalez, J. Power Sources 142 (2005) 169-176.

[27] T. Ioroi, N. Fujiwara, Z. Siroma, K. Yasuda, Y. Miyazaki, Electrochem. Commun. 4 (2002) 442-446.

[28] R. O'Hayre, S.J. Lee, S.W. Cha, F.B. Prinz, J. Power Sources 109 (2002) 483-493.

[29] A.D. Taylor, M. Michel, R.C. Sekol, J.M. Kizuka, N.A. Kotov, L.T. Thompson, Adv. Funct. Mater. 18 (2008) 3003-3009.

[30] C.H. Wan, Q.H. Zhuang, Int. J. Hydrogen Energy 32 (2007) 4402-4411.

[31] T. Ioroi, Z. Siroma, N. Fujiwara, S.I. Yamazaki, K. Yasuda, Electrochem. Commun. 7 (2005) 183-188.

[32] W.C. Chang, M.T. Nguyen, J. Power Sources 196 (2011) 5811-5816.

[33] C.H. Wan, M.T. Lin, Q.H. Zhuang, C.H. Lin, Surf. Coat. Technol. 201 (2006) 214-222.

[34] F. Alcaide, G. Álvarez, P.L. Cabot, O. Miguel, A. Querejeta, Int. J. Hydrogen Energy 35 (2010) 11634-11641.

[35] J.H. Kim, B. Fang, M. Kim, J.S. Yu, Catal. Today 146 (2009) 25-30.

[36] N. Cunningham, E. Irissou, M. LefΓ¨vre, M.C. Denis, D. Guay, J.P. Dodelet, Electrochem. Solid-State Lett. 6 (2003) A125-A128.

[37] S.S. Pethaiah, G.P. Kalaignan, G. Sasikumar, M. Ulaganathan, Solid State Ionics 190 (2011) 88-92.

[38] S. Chen, Z. Wei, H. Li, L. Li, Chem. Commun. 46 (2010) 8782-8784.

[39] A.C. Garcia, V.A. Paganin, E.A. Ticianelli, Electrochim. Acta 53 (2008) 4309-4315.

[40] D.C. Papageorgopoulos, M. Keijzer, J.B.J. Veldhuis, F.A. de Bruijn, J. Electrochem. Soc. 149 (2002) A1400-A1404.

[41] D.K. Ross, Vacuum 80 (2006) 1084-1089.

[42] A.N. Fatsikostas, D.I. Kondarides, X.E. Verykios, Catal. Today 75 (2002) 145-155.

[43] S.H. Ahn, O.J. Kwon, S.-K. Kim, I. Choi, J.J. Kim, Int. J. Hydrogen. Energ. 35 (2010) 13309-13316.

[44] J.-S. Choi, W.S. Chung, H.Y. Ha, T.-H. Lim, I.-H. Oh, S.-A. Hong, H.-I. Lee, J. Power Sources 156 (2006) 466-471.

[45] H. Liu, C. Song, L. Zhang, J. Zhang, H. Wang, D.P. Wilkinson, J. Power Sources 155 (2006) 95-110.

[46] F. Colmati, E. Antolini, E.R. Gonzalez, Electrochim. Acta 50 (2005) 5496-5503.

[47] J. Qi, L. Jiang, Q. Tang, S. Zhu, S. Wang, B. Yi, G. Sun, Carbon 50 (2012) 2824-2831.

[48] A.S. Aricò, V. Baglio, E. Modica, A. Di Blasi, V. Antonucci, Electrochem. Commun. 6 (2004) 164-169.

[49] X. Xue, J. Ge, C. Liu, W. Xing, T. Lu, Electrochem. Commun. 8 (2006) 1280-1286.

[50] E. Yoo, T. Okada, T. Kizuka, J. Nakamura, J. Power Sources 180 (2008) 221-226.

[51] A. Caillard, C. Coutanceau, P. Brault, J. Mathias, J.M. Léger, J. Power Sources 162 (2006) 66-73.

[52] M. Carmo, M. Brandalise, A.O. Neto, E.V. Spinacé, A.D. Taylor, M. Linardi, J.o.G. Rocha Poço, Int. J. Hydrogen. Energ. 36 (2011) 14659-14667.

[53] A. Murthy, E. Lee, A. Manthiram, Appl. Catal. B-Environ. 121-122 (2012) 154-161.

[54] H. Du, B. Li, F. Kang, R. Fu, Y. Zeng, Carbon 45 (2007) 429-435.

[55] E. You, R. Guzmán-Blas, E. Nicolau, M. Aulice Scibioh, C.F. Karanikas, J.J. Watkins, C.R. Cabrera, Electrochim. Acta 75 (2012) 191-200.

[56] G. Wang, G. Sun, Q. Wang, S. Wang, H. Sun, Q. Xin, Int. J. Hydrogen. Energ. 35 (2010) 11245-11253.

[57] X. Xue, T. Lu, C. Liu, W. Xu, Y. Su, Y. Lv, W. Xing, Electrochim. Acta 50 (2005) 3470-3478.

[58] Z. Cui, C. Liu, J. Liao, W. Xing, Electrochim. Acta 53 (2008) 7807-7811.

[59] Q. Wang, G.Q. Sun, L. Cao, L.H. Jiang, G.X. Wang, S.L. Wang, S.H. Yang, Q. Xin, J. Power Sources 177 (2008) 142-147.

[60] Z. Mingyuan, S. Gongquan, L. Huanqiao, C. Lei, X. Qin, Chinese J. Catal. 29 (2008) 765-770.

[61] H. Li, G. Sun, L. Cao, L. Jiang, Q. Xin, Electrochim. Acta 52 (2007) 6622-6629.

[62] L. Jiang, G. Sun, S. Sun, J. Liu, S. Tang, H. Li, B. Zhou, Q. Xin, Electrochim. Acta 50 (2005) 5384-5389.

[63] P.E. Tsiakaras, J. Power Sources 171 (2007) 107-112.

[64] X. Xue, J. Ge, T. Tian, C. Liu, W. Xing, T. Lu, J. Power Sources 172 (2007) 560-569.

[65] R.F.B. De Souza, L.S. Parreira, D.C. Rascio, J.C.M. Silva, E. Teixeira-Neto, M.L. Calegaro, E.V. Spinacé, A.O. Neto, M.C. Santos, J. Power Sources 195 (2010) 1589-1593.

[66] A.O. Neto, L.A. Farias, R.R. Dias, M. Brandalise, M. Linardi, E.V. Spinacé, Electrochem. Commun. 10 (2008) 1315-1317.

[67] D.F. Silva, A.N. Geraldes, A.O. Neto, E.S. Pino, M. Linardi, E.V. Spinacé, W.A.A. Macedo, J.D. Ardisson, Materials Science and Engineering: B 175 (2010) 261-265.

[68] R.F.B. De Souza, L.S. Parreira, J.C.M. Silva, F.C. Simões, M.L. Calegaro, M.J. Giz, G.A. Camara, A.O. Neto, M.C. Santos, Int. J. Hydrogen. Energ. 36 (2011) 11519-11527.

[69] M. Zhu, G. Sun, Q. Xin, Electrochim. Acta 54 (2009) 1511-1518.

[70] J. Tayal, B. Rawat, S. Basu, Int. J. Hydrogen. Energ. 36 (2011) 14884-14897.

[71] E. Lee, A. Murthy, A. Manthiram, Electrochim. Acta 56 (2011) 1611-1618.

[72] K. Fatih, V. Neburchilov, V. Alzate, R. Neagu, H. Wang, J. Power Sources 195 (2010) 7168-7175.

[73] A.S. Aricò, P. Creti, P.L. Antonucci, V. Antonucci, Electrochem. Solid St. 1 (1998) 66-68.

[74] J. Perez, V.A. Paganin, E. Antolini, J. Electroanal. Chem. 654 (2011) 108-115.

[75] J. Ribeiro, D.M. dos Anjos, K.B. Kokoh, C. Coutanceau, J.M. Léger, P. Olivi, A.R. de Andrade, G. Tremiliosi-Filho, Electrochim. Acta 52 (2007) 6997-7006.

[76] T.S. Almeida, L.M. Palma, P.H. Leonello, C. Morais, K.B. Kokoh, A.R. De Andrade, J. Power Sources 215 (2012) 53-62.

[77] S.C. Zignani, V. Baglio, J.J. Linares, G. Monforte, E.R. Gonzalez, A.S. Aricò, Electrochim. Acta 70 (2012) 255-265.

[78] E. Ribadeneira, B.A. Hoyos, J. Power Sources 180 (2008) 238-242.

[79] D.R. Lycke, E.d.L. Gyenge, Electrochim. Acta 52 (2007) 4287-4298.

[80] J. Tayal, B. Rawat, S. Basu, Int. J. Hydrogen Energy 37 (2012) 4597-4605.

[81] F.C. Simões, D.M. Dos Anjos, F. Vigier, J.M. Léger, F. Hahn, C. Coutanceau, E.R. Gonzalez, G. Tremiliosi-Filho, A.R. De Andrade, P. Olivi, K.B. Kokoh, J. Power Sources 167 (2007) 1-10.

[82] J. Prabhuram, T.S. Zhao, Z.K. Tang, R. Chen, Z.X. Liang, J. Phys. Chem. B 110 (2006) 5245-5252.

[83] M.Y. Wang, J.H. Chen, Z. Fan, H. Tang, G.H. Deng, D.L. He, Y.F. Kuang, Carbon 42 (2004) 3251-3272.

[84] S. Tang, G. Sun, J. Qi, S. Sun, J. Guo, Q. Xin, G.M. Haarberg, Chinese J. Catal. 31 (2010) 12-17.

[85] G. Girishkumar, K. Vinodgopal, P.V. Kamat, J. Phys. Chem. B 108 (2004) 19960-19966.

[86] S. Calabrese Barton, J. Gallaway, P. Atanassov, Chemical Reviews 104 (2004) 4867-4886.

[87] H. Liu, B.E. Logan, Environmental Science & Technology 38 (2004) 4040-4046.

[88] M. Guerra-Balcázar, D. Morales-Acosta, F. Castaneda, J. Ledesma-García, L.G. Arriaga, Electrochemistry Communications 12 (2010) 864-867.

[89] W.S. Cheng, Product analyses to study the mechanism of the electrochemical oxidation of glucose
The Univeristy of Hong Kong, Hong Kong, 2004.

[90] V.S. Bagotzky, Y.B. Vassilyer, Electrochim. Acta (1964) 1329.

[91] N. Fujiwara, S.-i. Yamazaki, Z. Siroma, T. Ioroi, H. Senoh, K. Yasuda, Electrochem. Commun. 11 (2009) 390-392.

[92] A. Brouzgou, A. Podias, P. Tsiakaras, J. Appl. Electrochem. 43 (2013) 119-136.

[93] C. Hui-Fang, Y. Jian-Shan, L. Xiao, Z. Wei-De, S. Fwu-Shan, Nanotechnology 17 (2006) 2334.

[94] Y.S. Li, T.S. Zhao, Z.X. Liang, J. Power Sources 187 (2009) 387-392.

[95] L. An, T.S. Zhao, S.Y. Shen, Q.X. Wu, R. Chen, Int. J. Hydrogen Energy 35 (2010) 4329-4335.

[96] Y.S. Li, T.S. Zhao, W.W. Yang, Int. J. Hydrogen Energy 35 (2010) 5656-5665.

[97] X. Yan, X. Ge, S. Cui, Nanoscale Research Letters 6 (2011) 313.

[98] F. Xie, Z. Huang, C. Chen, Q. Xie, Y. Huang, C. Qin, Y. Liu, Z. Su, S. Yao, Electrochemistry Communications 18 (2012) 108-111.

[99] D. Basu, S. Basu, Electrochim. Acta 56 (2011) 6106-6113.

[100] L. An, T.S. Zhao, S.Y. Shen, Q.X. Wu, R. Chen, J. Power Sources 196 (2011) 186-190.

[101] M. Guerra-Balcázar, F.M. Cuevas-Muñiz, L. Álvarez-Contreras, L.G. Arriaga, J. Ledesma-García, Journal of Power Sources 197 (2012) 121-124.

[102] L. Li, K. Scott, E.H. Yu, Journal of Power Sources 221 (2013) 1-5.

[103] Q. Shen, L. Jiang, H. Zhang, Q. Min, W. Hou, J.-J. Zhu, The Journal of Physical Chemistry C 112 (2008) 16385-16392.

[104] W. Huang, M. Wang, J. Zheng, Z. Li, The Journal of Physical Chemistry C 113 (2009) 1800-1805.

[105] H. Yin, C. Zhou, C. Xu, P. Liu, X. Xu, Y. Ding, The Journal of Physical Chemistry C 112 (2008) 9673-9678.

[106] J.P. Spets, Y. Kiros, M.A. Kuosa, J. Rantanen, M.J. Lampinen, K. Saari, Electrochimica Acta 55 (2010) 7706-7709.

[107] D. Basu, S. Basu, Electrochim. Acta 55 (2010) 5775-5779.

[108] D. Basu, S. Basu, International Journal of Hydrogen Energy 36 (2011) 14923-14929.

[109] Z. Liu, L. Huang, L. Zhang, H. Ma, Y. Ding, Electrochimica Acta 54 (2009) 7286-7293.

[110] C. Jin, I. Taniguchi, Mater. Lett. 61 (2007) 2365-2367.

[111] F.M. Cuevas-Muñiz, M. Guerra-Balcázar, F. Castaneda, J. Ledesma-García, L.G. Arriaga, Journal of Power Sources 196 (2011) 5853-5857.

[112] D. Basu, S. Basu, International Journal of Hydrogen Energy 37 (2012) 4678-4684.

[113] Y. Kuang, B. Wu, D. Hu, X. Zhang, J. Chen, Journal of Solid State Electrochemistry 16 (2012) 759-766.

[114] G. Merle, M. Wessling, K. Nijmeijer, J. Membr. Sci. 377 (2011) 1-35.

[115] R.C.T. Slade, J.P. Kizewski, S.D. Poynton, R. Zeng, J.R. Varcoe, Alkaline Fuel Cells-Chapter 3, in: R.A. Meyers (Ed.), Encyclopedia of Sustainability Science and Technology, 2013.

[116] M. Mamlouk, K. Scott, J.A. Horsfall, C. Williams, Int. J. Hydrogen Energy 36 (2011) 7191-7198.

[117] M. Mamlouk, X. Wang, K. Scott, J.A. Horsfall, C. Williams, Characterization and application of anion exchange polymer membranes with non-platinum group metals for fuel cells, 2011, pp. 152-160.

[118] B. Gurau, E.S. Smotkin, J. Power Sources 112 (2002) 339-352.

[119] G. Andreadis, V. Stergiopoulos, S. Song, P. Tsiakaras, Appl. Catal. B-Environ. 100 (2010) 157-164.

[120] S.S. Mahapatra, A. Dutta, J. Datta, Electrochim. Acta 55 (2010) 9097-9104.

[121] Y. Wang, L. Li, L. Hu, L. Zhuang, J. Lu, B. Xu, Electrochem. Commun. 5 (2003) 662-666.

[122] A.S. Aricò, V. Baglio, V. Antonucci, Electrocatalysis of Direct Methanol Fuel Cells, Wiley-VCH Verlag GmbH & Co. KGaA, 2009, pp. 1-78.

[123] A. Verma, S. Basu, Journal of Power Sources 174 (2007) 180-185.

[124] A.S. Aricò, P. Cretì, P.L. Antonucci, V. Antonucci, Comparison of Ethanol and Methanol Oxidation in a Liquid: Feed Solid Polymer Electrolyte Fuel Cell at High Temperature, 1998, pp. 66-68.

[125] J. Lobato, P. Cañizares, M.A. Rodrigo, J.J. Linares, Fuel Cells 9 (2009) 597-604.

[126] L. Jiang, G. Sun, S. Sun, J. Liu, S. Tang, H. Li, B. Zhou, Q. Xin, Electrochimica Acta 50 (2005) 5384-5389.

[127] M. Zhu, G. Sun, H. Li, L. Cao, Q. Xin, Chinese Journal of Catalysis 29 (2008) 765-770.

[128] F.L.S. Purgato, S. Pronier, P. Olivi, A.R. de Andrade, J.M. Léger, G. Tremiliosi-Filho, K.B. Kokoh, J. Power Sources 198 (2012) 95-99.

[129] P.E. Tsiakaras, J. Power Sources 171 (2007) 107-112.

[130] J. Tayal, B. Rawat, S. Basu, Int. J. Hydrogen Energy 36 (2011) 14884-14897.

[131] Z. Liu, X.Y. Ling, X. Su, J.Y. Lee, L.M. Gan, J. Power Sources 149 (2005) 1-7.

[132] X. Xue, J. Ge, T. Tian, C. Liu, W. Xing, T. Lu, J. Power Sources 172 (2007) 560-569.

[133] R.F.B. De Souza, L.S. Parreira, D.C. Rascio, J.C.M. Silva, E. Teixeira-Neto, M.L. Calegaro, E.V. Spinace, A.O. Neto, M.C. Santos, J. Power Sources 195 (2010) 1589-1593.

[134] A.O. Neto, L.A. Farias, R.R. Dias, M. Brandalise, M. Linardi, E.V. Spinacé, Electrochem. Commun. 10 (2008) 1315-1317.

[135] D.F. Silva, A.N. Geraldes, A.O. Neto, E.S. Pino, M. Linardi, E.V. Spinacé, W.A.A. Macedo, J.D. Ardisson, Mater. Sci. Eng., B 175 (2010) 261-265.

[136] R.F.B. De Souza, L.S. Parreira, J.C.M. Silva, F.C. Simões, M.L. Calegaro, M.J. Giz, G.A. Camara, A.O. Neto, M.C. Santos, Int. J. Hydrogen Energy 36 (2011) 11519-11527.

[137] E. Lee, A. Murthy, A. Manthiram, Electrochim. Acta 56 (2011) 1611-1618.

[138] E. Ribadeneira, B.A. Hoyos, J. Power Sources 180 (2008) 238-242.

[139] J.B. Xu, T.S. Zhao, S.Y. Shen, Y.S. Li, International Journal of Hydrogen Energy 35 (2010) 6490-6500.

[140] J. Datta, A. Dutta, M. Biswas, Electrochemistry Communications 20 (2012) 56-59.

[141] A.M. Bartrom, J.L. Haan, Journal of Power Sources 214 (2012) 68-74.

[142] C. Bianchini, V. Bambagioni, J. Filippi, A. Marchionni, F. Vizza, P. Bert, A. Tampucci, Electrochemistry Communications 11 (2009) 1077-1080.

[143] S.Y. Shen, T.S. Zhao, J.B. Xu, Y.S. Li, Journal of Power Sources 195 (2010) 1001-1006.

[144] V. Bambagioni, C. Bianchini, A. Marchionni, J. Filippi, F. Vizza, J. Teddy, P. Serp, M. Zhiani, Journal of Power Sources 190 (2009) 241-251.

[145] S. Shen, T.S. Zhao, J. Xu, Y. Li, Energy & Environmental Science 4 (2011) 1428-1433.

[146] L. An, T.S. Zhao, J.B. Xu, International Journal of Hydrogen Energy 36 (2011) 13089-13095.

[147] L. An, T.S. Zhao, Int. J. Hydrogen Energy 36 (2011) 9994-9999.

[148] L. An, T.S. Zhao, R. Chen, Q.X. Wu, Journal of Power Sources 196 (2011) 6219-6222.

[149] J.B. Xu, T.S. Zhao, Y.S. Li, W.W. Yang, Int. J. Hydrogen Energy 35 (2010) 9693-9700.

[150] S. Roundy, J. Intell. Mater. Syst. Struct. 16 (2005) 809-823.

[151] G. Gürge, M. Kirstein, R. Erbel, Herz 26 (2001) 64-68.

[152] C. Watkins, B. Shen, R. Venkatasubramanian, Low-grade-heat energy harvesting using superlattice thermoelectrics for applications in implantable medical devices and sensors, Thermoelectrics, 2005. ICT 2005. 24th International Conference on, 2005, pp. 265-267.

[153] S. Kerzenmacher, J. Ducrée, R. Zengerle, F. von Stetten, J. Power Sources 182 (2008) 1-17.

[154] J.O.M. Bockris, B.J. Piersma, E. Gileadi, Electrochim. Acta 9 (1964) 1329-1332.

[155] S.K. Wolfson Jr, S.L. Gofberg, P. Prusiner, L. Nanis, Transactions - American Society for Artificial Internal Organs 14 (1968) 198-203.

[156] A. Kozawa, V.E. Zilionis, R.J. Brodd, Oxygen and Hydrogen Peroxide Reduction at a Ferric Phthalocyanineβ€Catalyzed Graphite Electrode, 1970, pp. 1470-1474.

[157] G.G. Arzoumanidis, J.J. O'Connell, The Journal of Physical Chemistry 73 (1969) 3508-3510.

[158] R.F. Drake, B.K. Kusserow, S. Messinger, S. Matsuda, Transactions - American Society for Artificial Internal Organs 16 (1970) 199-205.

[159] P. Malachesky, G. Holleck, F. McGovern, R. Devarakonda, Parametric studies of implantable fuel cell (1972) 727-732.

[160] K.a. Koehler, Method of using solid organic fuels in a fuel cell, in: USA Patent 3, 950A (Ed.), 1966.

[161] B.W.R. H. Warner, Digest of the Seventh International Conference on Medical and Biological Engineering, Stockholm, Sweden, 1967, p. 250.

[162] C.K. Colton, R.F. Drake, Transactions - American Society for Artificial Internal Organs 15 (1969) 187-199.

[163] M.L.B. Rao, R.F. Drake, J. Electrochem. Soc. 116 (1969) 334-337.

[164] S.J. Yao, A.J. Appleby, A. Geisel, H.R. Cash, S.K. Wolfson, Nature (London) 224 (1969) 921-922.

[165] A. Kozawa, V.E. Zilionis, R.J. Brodd, J. Electrochem. Soc. 117 (1970) 1474-1478.

[166] A. Kozawa, V.E. Zilionis, R.J. Brodd, J. Electrochem. Soc. 117 (1970) 1470-1474.

[167] S.K. Wolfson Jr, S.J. Yao, A. Geisel, H.R. Cash Jr, Transactions - American Society for Artificial Internal Organs 16 (1970) 193-198.

[168] A.J. Appleby, D.Y.C. Ng, H. Weinstein, J. Appl. Electrochem. 1 (1971) 79-90.

[169] Implantable fuel cells using blood as oxygen and amino acid fuel source whose oxidation is catalysed by a redox-system., in: G.P.D. 2127206A (Ed.), Germany, 1972.

[170] S.J.Y. S.K. Wolfson, Proceedings of the Seventh Intersociety Energy Conversion Engineering Conference

1972, pp. 733-739.

[171] G.R. J.R. Rao, E. Weidlich, F. von Sturm, Physical Medical Biology 17 (1972) 738.

[172] G.H. J. Giner, P.A. Malachesky, PCCP 77 (1973) 782-783.

[173] J.F.H. J.H. Fishman, Journal of Electrochemical Society 120 (1973) 115.

[174] G.R. J.R. Rao, F. von Sturm, E. Weidlich, PCCP 77 (1973) 787-790.

[175] Implantable fuel cell, in: US Patent 3, 922A (Ed.), 1974.

[176] B.Y.C. Wan, A.C.C. Tseung, MED.BIOL.ENGINEERING 12 (1974) 14-28.

[177] J.R. Rao, G. Richter, F. von Sturm, E. Weidlich, M. Wenzel, Bio-Medical Engineering 9 (1974) 98-103.

[178] J.R. Rao, G. Richter, Naturwissenschaften 61 (1974) 200-206.

[179] S. Affrossman, J.M. Courtney, T. Gilchrist, I. Martin, MED.BIOL.ENGINEERING 13 (1975) 539-543.

[180] Implantable fuel cell, in: US Patent 3, 397 (Ed.), 1975.

[181] P.J. Sharrock, J.M. Courtney, T. Gilchrist, S. Affrossman, Anal. Lett. 9 (1976) 1085-1090.

[182] E. Weidlich, G. Richter, F. von Sturm, J.R. Rao, Biomaterials Medical Devices and Artificial Organs 4 (1976) 277-306.

[183] Pacemaker with biofuel cell, in: US Patent 3, 135 (Ed.), 1976.

[184] J.R. Rao, G.J. Richter, F. Von Sturm, E. Weidlich, Bioelectrochem. Bioenerget. 3 (1976) 139-150.

[185] Method for the manufacture of an electrode for electrochemical cells. , in: US Patent 4, 934 (Ed.), 1978.

[186] J.R. Rao, G.J. Richter, G. Luft, P. von Sturm, Artif. Cells Blood Substit. Biotechnol. 6 (1978) 127-149.

[187] J. Giner, L. MarinÄiÄ‡, J.S. Soeldner, C.K. Colton, J. Electrochem. Soc. 128 (1981) 2106-2114.

[188] J.R. Rao, G. Milazzo, M. Blank (Eds.), Bioelectrochemistry. I. Biological Redox Reactions, New York, 1983.

[189] P. Woias, Y. Manoli, T. Nann, F. Von Stetten, MST News 4 (2005) 42-45.

[190] S.K. F. von Stetten, A. Lorenz, V. Chokkalingam, N. Miyakawa, R. Zengerle, J. Ducrée, 19th IEEE International Conference on Micro Electro Mechanical Systems MEMS Istanbul, Turkey, 2006, pp. 934-937.

[191] S. Kerzenmacher, R. Sumbharaju, J. DucrÃ©e, R. Zengerle, F. Von Stetten, A surface mount able glucose fuel cell for medical implants, TRANSDUCERS and EUROSENSORS '07 - 4th International Conference on Solid-State Sensors, Actuators and Microsystems, 2007, pp. 125-128.

[192] G. Milazzo, M. Blank, J.R. Rao, Bioelectrochemistry I, Springer US, 1983, pp. 283-335.

[193] S. Ernst, J. Heitbaum, C.H. Hamann, Berichte der Bunsengesellschaft für physikalische Chemie 84 (1980) 50-55.

[194] M.R. Stetten, D. Stetten Jr, The Journal of biological chemistry 187 (1950) 241-252.

[195] U. Gebhardt, J.R. Rao, G.J. Richter, J. Appl. Electrochem. 6 (1976) 127-134.

[196] K.B. Kokoh, J.M. LÃ©ger, B. Beden, C. Lamy, Electrochim. Acta 37 (1992) 1333-1342.

[197] H. Lerner, J. Giner, J.S. Soeldner, C.K. Colton, J. Electrochem. Soc. 126 (1979) 237-242.

[198] M.F.L. De Mele, H.A. Videla, A.J. ArvÃa, Bioelectrochem. Bioenerget. 9 (1982) 469-487.

[199] Y.B. Vassilyev, O.A. Khazova, N.N. Nikolaeva, J. Electroanal. Chem. 196 (1985) 105-125.

[200] Y.B. Vassilyev, O.A. Khazova, N.N. Nikolaeva, Journal of Electroanalytical Chemistry 196 (1985) 127-144.

[201] M.F.L. De Mele, H.A. Videla, A.J. ArvÃa, J. Electrochem. Soc. 129 (1982) 2207-2213.

[202] M.F.L. De Mele, H.A. Videla, A.J. ArvÃa, Bioelectrochem. Bioenerget. 10 (1983) 239-249.

[203] G.R. J.R. Rao, F. von Sturm, E. Weidlich, Physical Chemistry Chemical Physics (1973) 787-790.

[204] B.Y.C. Wan, A.C.C. Tseung, Medical and biological engineering 12 (1974) 14-28.

[205] W. Preidel, S. Saeger, I. Von Lucadou, W. Lager, Biomedical Instrumentation and Technology 25 (1991) 215-219.

[206] V. Parsonnet, CHEST Journal 61 (1972) 165-173.

[207] M.F.L. De Mele, H.A. Videla, A.J. Arvía, Journal of The Electrochemical Society 129 (1982) 2207-2213.

[208] T.P. Tougas, M.J. Debenedetto, J.M. Demott, Electroanalysis 5 (1993) 669-675.

[209] R.R. Adzic, M.W. Hsiao, E.B. Yeager, J. Electroanal. Chem. Interf. Electrochem. 260 (1989) 475-485.

[210] A. Stitz, W. Buchberger, Electroanalysis 6 (1994) 251-258.

[211] A. Stitz, W. Buchberger, Fresenius J. Anal. Chem. 339 (1991) 55-57.

[212] Y.B. Vassilyev, O.A. Khazova, N.N. Nikolaeva, J. Electroanal. Chem. 196 (1985) 127-144.

[213] R. Parsons, T. VanderNoot, J. Electroanal. Chem. Interf. Electrochem. 257 (1988) 9-45.

[214] L.H.E. Yei, B. Beden, C. Lamy, J. Electroanal. Chem. Interf. Electrochem. 246 (1988) 349-362.

[215] K.D. Popović, N.M. Marković, A.V. Tripković, R.R. Adziić, J. Electroanal. Chem. Interf. Electrochem. 313 (1991) 181-199.

[216] H.-W. Lei, B. Wu, C.-S. Cha, H. Kita, Journal of Electroanalytical Chemistry 382 (1995) 103-110.

[217] B. Beden, F. Largeaud, K.B. Kokoh, C. Lamy, Electrochim. Acta 41 (1996) 701-709.

[218] A.E. Bolzan, T. Iwasita, W. Vielstich, J. Electrochem. Soc. 134 (1987) 3052-3058.

[219] S. Ernst, J. Heitbaum, C.H. Hamann, J. Electroanal. Chem. Interf. Electrochem. 100 (1979) 173-183.

[220] C.A. Apblett, D. Ingersoll, S. Sarangapani, M. Kelly, P. Atanassov, J. Electrochem. Soc. 157 (2009) B86-B89.

[221] C. Jin, I. Taniguchi, Mater. Lett. 61 (2007) 2365-2367.

[222] C.P. Wilde, M. Zhang, J. Chem. Soc., Faraday Trans. 89 (1993) 385-389.

[223] H.W. Lei, B. Wu, C.S. Cha, H. Kita, J. Electroanal. Chem. 382 (1995) 103-110.

[224] J.P. Spets, M.A. Kuosa, Y. Kiros, T. Anttila, J. Rantanen, M.J. Lampinen, K. Saari, J. Power Sources 195 (2010) 475-479.

[225] J. Ryu, H.-S. Kim, H.T. Hahn, D. Lashmore, Biosensors Bioelectron. 25 (2010) 1603-1608.

[226] Y. Sun, H. Buck, T.E. Mallouk, Anal. Chem. 73 (2001) 1599-1604.

[227] M. Guerra-Balcázar, F.M. Cuevas-Muñiz, L. Álvarez-Contreras, L.G. Arriaga, J. Ledesma-García, J. Power Sources 197 (2012) 121-124.

[228] F.v. Stetten, S. Kerzenmacher, A. Lorenz, V. Chokkalingam, N. Miyakawa, R. Zengerle, J. Ducree, A One-Compartment, Direct Glucose Fuel Cell for Powering Long-Term Medical Implants, Micro Electro Mechanical Systems, 2006. MEMS 2006 Istanbul. 19th IEEE International Conference on, 2006, pp. 934-937.

[229] A. Kloke, C. KГ¶hler, R. Zengerle, S. Kerzenmacher, The Journal of Physical Chemistry C 116 (2012) 19689-19698.

[230] Y. Vassilyev, O.A. Khazova, N.N. Nikolaeva, J. Electroanal. Chem. Interf. Electrochem. 196 (1985) 127-144.

[231] Y. Ding, M. Chen, J. Erlebacher, J. Am. Chem. Soc. 126 (2004) 6876-6877.

[232] H. Martín, P. Carro, A. Hernández Creus, J. Morales, G. Fernández, P. Esparza, S. González, R.C. Salvarezza, A.J. Arvia, The Journal of Physical Chemistry B 104 (2000) 8229-8237.

[233] D. Kramer, R.N. Viswanath, J. Weissmöller, Nano Lett. 4 (2004) 793-796.

[234] S.B. Aoun, G.S. Bang, T. Koga, Y. Nonaka, T. Sotomura, I. Taniguchi, Electrochem. Commun. 5 (2003) 317-320.

[235] F. Jia, C. Yu, K. Deng, L. Zhang, The Journal of Physical Chemistry C 111 (2007) 8424-8431.

[236] M. Pasta, R. Ruffo, E. Falletta, C.M. Mari, C.D. Pina, Gold Bulletin 43 (2010) 57-64.

[237] F. Xie, Z. Huang, C. Chen, Q. Xie, Y. Huang, C. Qin, Y. Liu, Z. Su, S. Yao, Electrochem. Commun. 18 (2012) 108-111.

[238] I. Ivanov, T.R. VidakoviΔ‡, K. Sundmacher, Electrochem. Commun. 10 (2008) 1307-1310.

[239] Y. Hu, J. Jin, P. Wu, H. Zhang, C. Cai, Electrochim. Acta 56 (2010) 491-500.

[240] I. Becerik, F. Kadirgan, Electrochim. Acta 37 (1992) 2651-2657.

[241] Q. Yi, A. Chen, W. Huang, J. Zhang, X. Liu, G. Xu, Z. Zhou, Electrochem. Commun. 9 (2007) 1513-1518.

[242] Q. Yi, L. Li, W. Yu, Z. Zhou, G. Xu, J. Mol. Catal. A: Chem. 295 (2008) 34-38.

[243] K. Koczkur, Q. Yi, A. Chen, Adv. Mater. 19 (2007) 2648-2652.

[244] Q. Yi, F. Niu, W. Yu, Thin Solid Films 519 (2011) 3155-3161.

[245] R.F. Drake, B.K. Kusserow, Messinge.S, S. Matsuda, Transactions American Society for Artificial Internal Organs 16 (1970) 199-&.

[246] L.S.Y. Wong, S. Hossain, A. Ta, J. Edvinsson, D.H. Rivas, H. Naas, Solid-State Circuits, IEEE Journal of 39 (2004) 2446-2456.

[247] S. Kerzenmacher, U. Kräling, M. Schroeder, R. Brämer, R. Zengerle, F. von Stetten, J. Power Sources 195 (2010) 6524-6531.

[248] S. Kerzenmacher, M. Schroeder, R. Brämer, R. Zengerle, F. Von Stetten, J. Power Sources 195 (2010) 6516-6523.

[249] Clin. Toxicol. 37 (1999) 239-258.

[250] S. Kerzenmacher, U. KrГ¤ling, T. Metz, R. Zengerle, F. von Stetten, J. Power Sources 196 (2011) 1264-1272.

[251] S. Kerzenmacher, R. Sumbharaju, J. Ducree, R. Zengerle, F. Von Stetten, A Surface Mountable Glucose Fuel Cell for Medical Implants, Solid-State Sensors, Actuators and Microsystems Conference, 2007. TRANSDUCERS 2007. International, 2007, pp. 125-128.

[252] S. Kerzenmacher, J. Ducrée, R. Zengerle, F. von Stetten, J. Power Sources 182 (2008) 66-75.

[253] A. Kloke, B. Biller, U. Kräling, S. Kerzenmacher, R. Zengerle, F. von Stetten, Fuel Cells 11 (2011) 316-326.

[254] B.I. Rapoport, J.T. Kedzierski, R. Sarpeshkar, PLoS ONE 7 (2012).

[255] K. Elouarzaki, A. Le Goff, M. Holzinger, J. Thery, S. Cosnier, J. Am. Chem. Soc. 134 (2012) 14078-14085.

[256] C.X. Zhao, K. Wang, H. Yan, G. Xu, J. Electrochem. Soc. 158 (2011) B1055-B1059.

[257] S. Prilutsky, P. Schechner, E. Bubis, V. Makarov, E. Zussman, Y. Cohen, Electrochim. Acta 55 (2010) 3694-3702.

[258] P. Schechner, E. Kroll, E. Bubis, S. Chervinsky, E. Zussman, J. Electrochem. Soc. 154 (2007) B942-B948.

[259] N. Mano, F. Mao, A. Heller, J. Am. Chem. Soc. 125 (2003) 6588-6594.

[260] R.A. Bullen, T.C. Arnot, J.B. Lakeman, F.C. Walsh, Biosensors Bioelectron. 21 (2006) 2015-2045.

[261] R. Tashiro, N. Kabei, K. Katayama, E. Tsuboi, K. Tsuchiya, J. Artificial Organs 5 (2002) 0239-0245.

[262] R. Tashiro, N. Kabei, K. Katayama, Y. Ishizuka, F. Tsuboi, K. Tsuchiya, JSME International Journal Series C 43 (2000) 916-922.

[263] P. Miao, P.D. Mitcheson, A.S. Holmes, E.M. Yeatman, T.C. Green, B.H. Stark, Microsystem Technologies 12 (2006) 1079-1083.
[264] R. Venkatasubramanian, C. Watkins, C. Caylor, G. Bulman, PowerMEMS 2006 (2006) 1-4.

CHAPTER III

Experimental Techniques*

Abstract

In Chapter III the experimental techniques and their main principles that were used for the physicochemical and electrochemical characterization of the studied electrocatalysts are described. Additionally, before the experimental techniques the electrocatalysts' preparation method is referred analytically. The electrocatalysts were prepared via a modified microwave assisted polyol method. Their physicochemical characterization was conducted by the techniques of Transmitting Electrode Microscopy (TEM), X-Ray Diffraction (XRD) and Thermogravimetry (TG). Their electrochemical characterization towards glucose electrooxidation was conducted by the Cyclic Voltammetry, Chronoamperometry and Rotating Disk methods.

* Y. Wang, Ch. He, A. Brouzgou, Y. Liang, R. Fu, D. Wu, P. Tsiakaras and S. Song, ***A facile soft-template synthesis of ordered mesoporous carbon/tungsten carbide composites with high surface area for methanol electrooxidation***, J. Power Sources 200 (2012) 8-13.

* S. Song, Ch. He, J. Liu, Y. Wang, A. Brouzgou and P. Tsiakaras, ***Two-step sequence for synthesis of efficient PtSn@Rh/C catalyst for oxidizing ethanol and intermediate products,*** Appl. Catal. B: Environm. 119-120 (2012) 227-233.

CONTENTS

CHAPTER III..... i

1. Preparation Method of Electrocatalysts: modified microwave assisted polyol method. 101

2. Physicochemical Characterization 103

2.1. Transmission Electron Microscopy 103

2.1.1. Historical background 104

2.1.2. Principles of operation 105

2.2. Scanning Electron Microscopy / Energy Dispersive X-Ray Spectroscopy (SEM/EDS) 107

2.2.1. Historical background 108

2.2.2. Principles of operation 108

2.3. X-Ray Diffraction Technique 111

2.3.1. Historical background 111

2.3.2. Principles of operation 113

2.4. Thermogravimetric analysis 115

2.4.1. Principles of operation 115

2.4.2. Instrumental apparatus 117

3. Electrochemical Methods for Catalyst Activity Evaluation 118

3.1. Introduction 118

3.2. Cyclic Voltammetry 120

3.2.1. Basic principles 120

3.2.2. Instrumental apparatus 124

3.2.3. Electro-kinetic analysis 126

3.3. Chronoamperometry 129

3.4. Rotating disk electrode technique (RDE) 130

3.4.1. Basic principles 130

3.4.2. Instrumental apparatus 131

References 134

List of Figures

Figure 3.1. Pulse microwave assisted polyol process. 103

Figure 3.2. Interactions between electrons and material [6]. 104

Figure 3.3. Schematic diagram of inner atomic electron shells. 109

Figure 3.4. EDS spectrum, showing K peaks of Na, Al and Si. 111

Figure 3.5. (a) A typical TGA of single walled carbon nanotubes, (b) Graph illustrating the ambiguity in determining T_{onset}. 116

Figure 3.6. Instrument of thermogravimetric analysis [11]. 118

Figure 3.7. A typical cyclic voltammogram for a reversible reaction. 121

Figure 3.8. A typical electrode reaction. 122

Figure 3.9. Fermi levels in a metal. 123

Figure 3.10. Fermi level when voltage is applied. 123

Figure 3.11. Illustration of the basic circuitry of a potentiostat [12]. 124

Figure 3.12. Schematic representation of the composition of the solution phase in the vicinity of the electrode surface [13]. 125

Figure 3.13. Methodology for extracting kinetic parameters from CV measurements [14]. 129

Figure 3.14. Rotating disk electrode equipment. Reprinted from Ref. [15]. 131

Figure 3.15. Scheme of the flow on working electrode surface. Reprinted from Ref. [15]. 132

Figure 3.16. Linear sweep voltammetric measurement with RDE. Reprinted from Ref. [15]. 133

1. Preparation Method of Electrocatalysts: modified microwave assisted polyol method.

Microwaves are electromagnetic waves with frequencies in the range of 0.3 to 300 GHz. The commonly used frequency for microwave heating is 2.45 GHz. The principle of microwave heating is related to the polar characteristics of molecules. During the microwave heating, polar molecules such as water molecules try to orientate with the electric field. When dipolar molecules try to re-orientate with the rapidly changing alternating electric field, the heat is generated by rotation, friction and collision of molecules. One of the advantages of the microwave heating is rapid volumetric heating, which results in the higher reaction rate and selectivity, reduction in the reaction time often by orders of magnitude and higher yield of the product compared to the conventional heating methods. As a result, the microwave heating opens up the possibility of realizing fast preparation of materials in a very short time, leading to relatively low cost, energy saving and high efficiency for materials production. The microwave energy is found to be more efficient in the selective heating in many processes. These processes are environmentally friendly, requiring less energy than the conventional methods [1].

Since the first reports of the microwave-assisted organic synthesis in 1986, the microwave heating has received considerable attention as a promising heating method for both organic and inorganic synthesis [1]. The use of microwave heating as an alternative heat source is becoming more and more popular in chemistry and materials science. The microwave heating has received considerable attention as a new promising method for the rapid preparation of inorganic nanostructures in the liquid solvents.

A variety of nanomaterials such as metals, metal oxides, metal sulphides, selenides, tellurides, carbonates organic/inorganic composites have been prepared by the microwave heating method [2, 3]. Nanostructures with various morphologies including spheres, polygonal plates, sheets, rods, wires, tubes and dendrites were prepared within a few minutes under microwave heating [1]. Morphologies and sizes

of metal nanostructures could be controlled by changing various experimental parameters, such as the concentration of metal salt and the chain length of the surfactant, the solvent and the reaction temperature. The heating rate and efficiency of the microwaves strongly depends on the properties of the reaction mixture. When good microwave absorbing solvents are used the results is a very fast heating. Among the typical solvents commonly used in microwave heating, water alcohols and ethylene glycol are ideal solvents and they are commonly used for the preparation of inorganic nanostructures. Ethylene glycol also has a reductive ability.

The microwave-assisted polyol method has been developed for the preparation of inorganic nanostructures such as metals, metal oxides and sulphides. Liu *et al.* [4] reported the synthesis of spherical metal nanoparticles by the microwave-polyol method.

In summary, the heating mechanism of the microwaves is different from the conventional heating. The remarkable advantages of the microwave heating are rapid volumetric heating, higher reaction rate and selectivity, shorter reaction time and higher yield of the product compared to the convention heating methods. As a result, the microwave heating makes the fast preparation of nanomaterials possible, leading to relative low cost, energy saving and high efficiency for materials production, thus advancing rapidly towards their practical applications [5]. Therefore, the use of microwave heating becomes more popular in scientific world.

In the present work the electrocatalysts' preparation procedure was the following:

A certain amount of $PdCl_2$/ethyl glycol (EG) or/and second metal salt/EG solution were well mixed with EG in ultrasonic bath, and then carbon powder was added into the solution according to the pre-calculated metal loading. After stirring, 2.0 mol L^{-1} NaOH/EG was added into the solution to adjust the pH value of the above mixture to be more than 12. After further stirring for another 1h, the slurry was pulse microwave-heated for several times in a 10s-on/10s-off pulse form and then re-acidified with hydrochloric acid. The pulse-microwave procedure was adopted in order to avoid the agglomeration of the metal particles at high temperatures. This is due to the fact that

continuous microwave can easily cause a quite rapid heating rate for carbon materials. In this process, EG acts not only as dispersant and reducing agent, but also as the microwave additive due to the fact that the dielectric constant (41.4 at 25 °C) and dielectric loss for ethylene glycol are high, and consequently rapid heating takes place under the microwave radiation. The support, carbon (Vulcan XC-72R, Cabot Corp.) is also a microwave-sensitive material, which is believed to play an important role in the acceleration of the metal reduction. Hydrochloric acid was added into the above dispersion system as the sedimentation promoter to accelerate the adsorption of the suspended Pt nanoparticles onto the carbon support (Figure 3.1). The obtained black solid sample was washed by hot deionized water and dried in a vacuum oven at 80°C for 12 h.

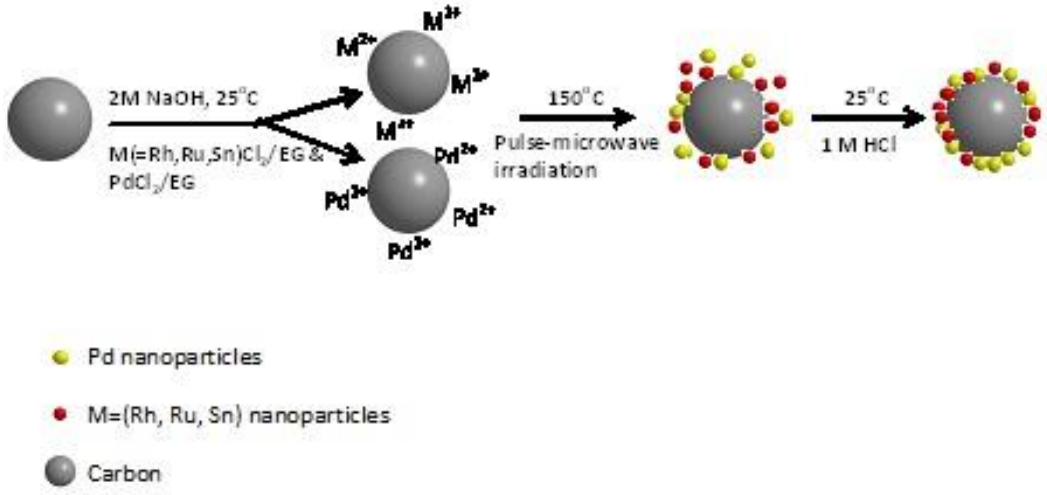

Figure 3.1. Pulse microwave assisted polyol process.

2. Physicochemical Characterization

2.1. Transmission Electron Microscopy

When electrons are accelerated up to high energy levels (few hundreds keV) and focused on a material, they can scatter or backscatter elastically or inelastically, or produce many interactions, source of different signals such as X-rays, Auger electrons or light (Figure 3.2). Some of them are used in transmission electron microscopy (TEM) [6].

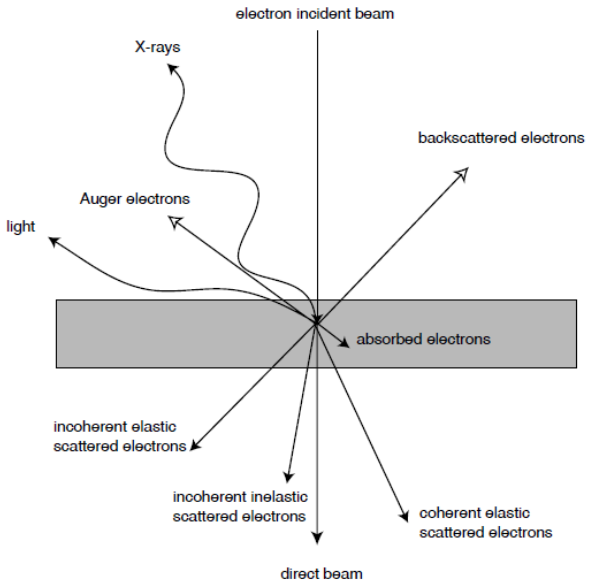

Figure 3.2. Interactions between electrons and material [6].

2.1.1. Historical background

The *resolution* ρ of a microscope is defined as the distance between two details in a just small distance from one another. It can be calculated using the Abbe theory of images formation for optic systems. For incoherent light or electron beam:

$$\rho = 0.61\lambda / \sin\alpha \qquad (1)$$

where λ is the wavelength of the light and α the maximum angle between incident and deflected beam in the limit of the lens aberrations. For optical microscopy, the resolution is therefore limited by the wavelength of light (410-660 nm). The X or γ rays have lower wavelength, but unfortunately, high-performance lenses necessary to focus the beam to form an image do not exist yet (however, X-rays can reveal structural information of materials by diffraction techniques). In 1923, De Broglie showed that all particles have an associated wavelength linked to their momentum: where m and v are the relativist mass and velocity respectively and h the Plank's constant. In 1927, Hans Bush showed that a magnetic coil can focus an electron beam in the same way that a glass lens for light. Five years later, a first image with a TEM was obtained by Ernst Ruska and Max Knoll [7].

In a TEM, the electrons are accelerated at high voltage (100-1000 kV) to a velocity approaching the speed of light (0.6-0.9 c); they must therefore be considered as

relativistic particles. The associated wavelength is five orders of magnitude smaller than the light wavelength (0.04-0.008 Å). Nevertheless, the magnetic lens aberrations limit the convergence angle of the electron beam to 0.5° (instead of 70° for the glass lens used in optics), and reduce the TEM resolution to the Å order. This resolution enables material imaging and structure determination at the atomic level. In the 1950s, Raymond Castaing developed an electron probe and X-ray detector for the chemical analyses. A modified version of his technique, the energy dispersive spectrometry EDS is nowadays usually added to the TEM.

2.1.2. Principles of operation

Theoretically, the maximum resolution, d, that one can obtain with a light microscope has been limited by the wavelength of the photons that are being used to probe the sample, λ and the numerical aperture of the system:

$$d = \lambda / 2n\sin\alpha \quad (2)$$

Early twentieth century scientists' theorised ways of getting around the limitations of the relatively large wavelength of visible light (wavelengths of 400–700 nanometres) by using electrons. Like all matter, electrons have both wave and particle properties (as theorized by Louis-Victor de Broglie), and their wave-like properties mean that a beam of electrons can be made to behave like a beam of electromagnetic radiation. The wavelength of electrons is related to their kinetic energy via the de Broglie equation. An additional correction must be made to account for relativistic effects, as in TEM an electron's velocity approaches the speed of light:

$$\lambda \approx h / \sqrt{2m_0 E(1 + E / 2m_0 c^2)} \quad (3)$$

where, h is Planck's constant, m_0 is the rest mass of an electron and E is the energy of the accelerated electron. Electrons are usually generated in an electron microscope by a process known as thermionic emission from a filament, usually tungsten, in the same manner as a light bulb, or alternatively by field electron emission.[18] The electrons are then accelerated by an electric potential (measured in volts) and focused by electrostatic and electromagnetic lenses onto the sample. The transmitted beam

contains information about electron density, phase and periodicity; this beam is used to form an image.

A TEM analysis system is consisted of the three following main parts:

i) **Source formation:** from the top down, the TEM consists of an emission source, which may be a tungsten filament, or a lanthanum hexaboride (LaB_6) source. For tungsten, this will be of the form of either a hairpin-style filament, or a small spike-shaped filament. LaB_6 sources utilize small single crystals. By connecting this gun to a high voltage source (typically ~100–300 kV) the gun will, given sufficient current, begin to emit electrons either by thermionic or field electron emission into the vacuum. This extraction is usually aided by the use of a Wehnelt cylinder. Once extracted, the upper lenses of the TEM allow for the formation of the electron probe to the desired size and location for later interaction with the sample. Manipulation of the electron beam is performed using two physical effects. The interaction of electrons with a magnetic field will cause electrons to move according to the right hand rule, thus allowing for electromagnets to manipulate the electron beam. The use of magnetic fields allows for the formation of a magnetic lens of variable focusing power, the lens shape originating due to the distribution of magnetic flux. Additionally, electrostatic fields can cause the electrons to be deflected through a constant angle. Coupling of two deflections in opposing directions with a small intermediate gap allows for the formation of a shift in the beam path, this being used in TEM for beam shifting, subsequently this is extremely important to STEM. From these two effects, as well as the use of an electron imaging system, sufficient control over the beam path is possible for TEM operation. The optical configuration of a TEM can be rapidly changed, unlike that for an optical microscope, as lenses in the beam path can be enabled, have their strength changed, or be disabled entirely simply via rapid electrical switching, the speed of which is limited by effects such as the magnetic hysteresis of the lenses.

ii) **Optics:** The lenses of a TEM allow for beam convergence, with the angle of convergence as a variable parameter, giving the TEM the ability to change magnification simply by modifying the amount of current that flows through the coil,

quadrupole or hexapole lenses. The quadrupole lens is an arrangement of electromagnetic coils at the vertices of the square, enabling the generation of a lensing magnetic fields, the hexapole configuration simply enhances the lens symmetry by using six, rather than four coils. Typically a TEM consists of three stages of lensing. The stages are the condensor lenses, the objective lenses, and the projector lenses. The condensor lenses are responsible for primary beam formation, whilst the objective lenses focus the beam that comes through the sample itself (in STEM scanning mode, there are also objective lenses above the sample to make the incident electron beam convergent). The projector lenses are used to expand the beam onto the phosphor screen or other imaging device, such as film. The magnification of the TEM is due to the ratio of the distances between the specimen and the objective lens' image plane. Additional quad or hexapole lenses allow for the correction of asymmetrical beam distortions, known as astigmatism. It is noted that TEM optical configurations differ significantly with implementation, with manufacturers using custom lens configurations, such as in spherical aberration corrected instruments, or TEMs utilizing energy filtering to correct electron chromatic aberration.

iii) **Display:** Imaging systems in a TEM consist of a phosphor screen, which may be made of fine (10–100 μm) particulate zinc sulphide, for direct observation by the operator. Optionally, an image recording system such as film based or doped YAG screen coupled CCDs. Typically these devices can be removed or inserted into the beam path by the operator as required.

2.2. Scanning Electron Microscopy / Energy Dispersive X-Ray Spectroscopy (SEM/EDS)

Surface analyses, chemical analysis and imaging on a variety of materials are performed using a Scanning Electron Microscope (SEM). The Scanning Electron Microscope is equipped with an Energy Dispersive Spectrometer (EDS). SEM/EDS provides chemical analysis of the field of view or spot analyses of minute particles. This micro-chemical analysis is also a non-destructive test.

2.2.1. *Historical background*

A method for analyzing small individual fluid inclusions was developed by Ayora and Fontarnau (1990), using a scanning electron microscope (SEM) with an attached X-ray energy dispersive system (EDS) to analyze frozen fluid inclusions in quartz crystals. Garcia-Veigas *et al.* (1995) and Fanlo and Ayora (1998) later successfully analyzed the major element chemical composition of fluid inclusions in halite crystals by this technique. The pioneering work of Ayora and colleagues at the University of Barcelona has provided the framework for the development of new methods, described in this paper, for the analysis of frozen fluid inclusions using an environmental scanning electron microscope (ESEM) with an attached EDS. The ESEM (Electroscan model 2020) is an advanced type of SEM that allows the sample to remain in a low-vacuum environment, for example, within an ambient atmosphere of 0.2 to 5.0 Torr nitrogen gas. This is accomplished by passing the electron beam through several pressure limiting apertures. These apertures create a pressure gradient between the sample chamber and the electron beam filament, which allows the filament to operate in a high vacuum while the sample chamber is maintained at a low vacuum. Such an environment greatly facilitates the examination of delicate hydrated samples [8].

2.2.2. *Principles of operation*

EDS makes use of the X-ray spectrum emitted by a solid sample bombarded with a focused beam of electrons to obtain a localized chemical analysis. All elements from atomic number 4 (Be) to 92 (U) can be detected in principle, though not all instruments are equipped for 'light' elements ($Z < 10$). Qualitative analysis involves the identification of the lines in the spectrum and is fairly straightforward owing to the simplicity of X-ray spectra. Quantitative analysis (determination of the concentrations of the elements present) entails measuring line intensities for each element in the sample and for the same elements in calibration Standards of known composition.

By scanning the beam in a television-like raster and displaying the intensity of a selected X-ray line, element distribution images or 'maps' can be produced. Also,

images produced by electrons collected from the sample reveal surface topography or mean atomic number differences according to the mode selected. The scanning electron microscope (SEM), which is closely related to the electron probe, was primarily designed for producing electron images, but can also be used for element mapping, and even point analysis if an X-ray spectrometer is added. There is thus a considerable overlap in the functions of these instruments.

According to the Rutherford-Bohr model of the atom, there is electrons orbit around the positive nucleus. In the normal state the number of orbital electrons equals the number of protons in the nucleus (given by the atomic number, Z). Only certain orbital states with specific energies exist and these are defined by quantum numbers (see standard texts). With increasing Z, orbits are occupied on the basis of minimum energy, those nearest the nucleus, and therefore the most tightly bound, being filled first. Orbital energy is determined mainly by the principal quantum number (n). The shell closest to the nucleus (n = 1) is known as the K shell; the next is the L3 shell (n = 2), then the M shell (n = 3), etc. The L shell is split into three subshells designated L1, L2 and L3, which have different quantum configurations and slightly different energies (whereas the K shell is unitary). Similarly, the M shell has five subshells. This model of the inner structure of the atom is illustrated in Figure 3.3.

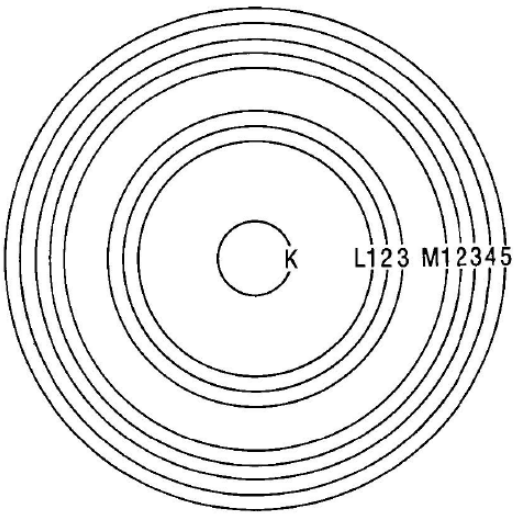

Figure 3.3. Schematic diagram of inner atomic electron shells.

The populations of the inner shells are governed by the Pauli exclusion principle, which states that only one electron may possess a given set of quantum numbers. The maximum population of a shell is thus equal to the number of possible states possessing the relevant principal quantum number. In the case of the K shell this is 2, for the L shell 8, and for the M shell 18. Thus for $Z \geq 2$ the K shell is full, and for $Z \geq 10$ the L shell is full. Electrons occupying outer orbits are usually not directly involved in the production of Xray spectra, which are therefore largely unaffected by chemical bonding etc [8].

'Characteristic' X-rays result from electron transitions between inner orbits, which are normally full. An electron must first be removed in order to create a vacancy into which another can 'fall' from an orbit further out. In electron probe analysis vacancies are produced by electron bombardment, which also applies to X-ray analysis in the TEM. X-ray lines are identified by a capital Roman letter indicating the shell containing the inner vacancy (K, L or M), a Greek letter specifying the group to which the line belongs in order of decreasing importance α, β, etc.), and a number denoting the intensity of the line within the group in descending order (1, 2, etc.). Thus the most intense K line is Kα**1** (The less intense Kα**2** line is usually not resolved, and the combined line is designated Kα**1,2** or just Kα). The most intense L line is Lα**1.** Because of the splitting of the L shell into three subshells, the L spectrum is more complicated than the K spectrum and contains at least 12 lines, though many of these are weak.
Energies are measured in electron volts (eV), 1 eV being the energy corresponding to a change of 1 V in the potential of an electron (= 1.602×10^{-19} J). This unit is applicable to both Xrays and electrons. X-ray energies of interest in electron probe analysis are mostly in the range 1-10 keV.

The ED spectrum is displayed in digitized form with the x-axis representing X-ray energy (usually in channels 10 or 20 eV wide) and the y-axis representing the number of counts per channel (Figure 3.4).

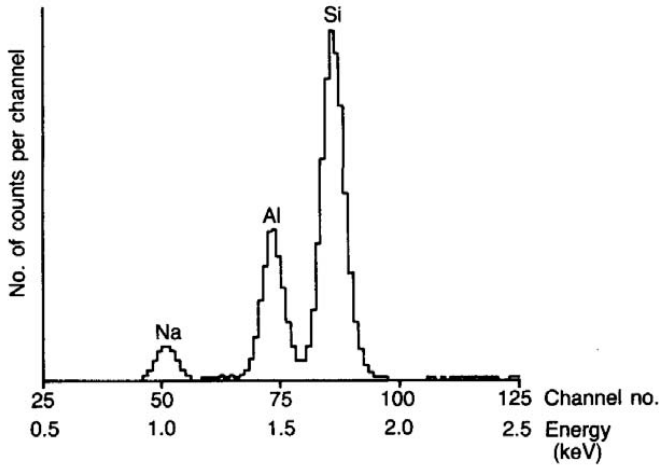

Figure 3.4. EDS spectrum, showing K peaks of Na, Al and Si.

In the present work The SEM-EDS was performed on scanning electron microscope (JEOL JSM-6330F) to determine the chemical composition of the samples.

2.3. X-Ray Diffraction Technique

X-ray powder diffraction (XRD) is one of the most powerful techniques for qualitative and quantitative analysis of crystalline compounds. This provides information that cannot be obtained with any other way. The information that can be obtained includes types and nature of present crystalline phases, structural make-up of phases, degree of crystallinity, amount of amorphous content, microstrain & size and orientation of crystallites.

2.3.1. Historical background

Several workers have reported that individual Laue spots obtained by x-ray diffraction from crystals do not appear uniform in contrast, but contain a structure that maps variations in the lattice planes causing the spots. As early as 1931 Berg (1931) had performed experiments on rock salt with monochromatic x-rays from a tube some distance away, in which the point-to-point variation of the reflecting power over the specimen was recorded on a photographic plate placed close to the crystal. The striated images that were produced were attributed to plastic deformation that the crystals had undergone. Barrett (1931) at about the same time concluded that the elastic strains produced by piezoelectric oscillations could alter the reflecting power of

quartz crystals, this he demonstrated by photographing the Laue spots in a fashion similar to Berg.

So although it was realized at this time that x-rays could be used as a tool for exploring the inhomogeneous strain produced in materials as well as natural imperfections, there followed a period of about ten years during which there were few advances in the technique. In particular little attempt was made to extend these original investigations to metallurgical specimens, until Barrett (1945) reported results from single crystals of silicon ferrite. With fine grain emulsion plates, the enlarged x-ray micrographs he obtained showed black lines corresponding to regions of high reflecting power on the specimen and white areas that represented non-reflecting portions of the crystal (regions that did not satisfy the Bragg relation n l = 2d sinq) [9].

It was Ramachandran (1944) who first used the term "topograph" to describe the appearance of Laue spots that he obtained from polished cleavage planes of diamond using a white X-ray beam from a tungsten target. The Laue spots were identified as a topographic map of the crystal plate exhibiting variations in structure. With a source-specimen distance of 30 cm and the photographic plate kept 2.5 cm from the crystal, using a pinhole source 0.3 mm in diameter Ramachandran achieved a resolution of 25 mm (calculated from the values given in the original paper). He realized the practical interest that such a technique might provide in detecting lattice perfection, as complementary to luminescence studies in general. The term became established in the literature when Wooster & Wooster (1945) obtained "topographs" from diamond surfaces using characteristic copper radiation rather than the bulk stone results of Ramachandran. The specimen and photographic plate were rocked through an angular range sufficient for all parts of the crystal to reflect the wide beam of filtered x-rays diverging from a pinhole.

Using polychromatic x-rays in transmission Guinier and Tennevin (1949) studied both orientation and extinction contrast in aluminum. These different contrast mechanisms are discussed more fully in section 2.4. Tuomi et al. (1974) used a similar geometry when performing the first synchrotron radiation topography experiments on silicon samples.

Improvement in resolution to that obtained by Ramachandran and Wooster was achieved by Bond and Andrus (1952) who examined structural imperfections in natural quartz surfaces using a double crystal technique. Consisting of a parallel double crystal spectrometer arrangement, this particular characteristic radiation (Cu) method provides very good sensitivity to lattice disorientation.

A micro focus x-ray tube introduced by Schulz (1954) having an apparent focal spot size of 30 mm x 3 mm enabled him to adjust the source-specimen distance (D) to the specimen-photographic plate (d) ratio to unity (see section 2.11). In this configuration (d/D ~ 1) the geometry gained sensitivity to orientation contrast as well as extinction (nowadays called diffraction) contrast. The method employed continuous radiation in a reflection mode while retaining topographic resolution (spatial resolution μ source size), a simple way of mapping disorientation textures of large single crystals.

Lang (1957a) examined crystal sections with slit collimated penetrating characteristic radiation (Ag Ka); these so-called section topographs are illustrated schematically in Figure 2.2. Linear and planar defects could be mapped with this technique by translating the specimen known distances and taking a series of section topographs. Lang (1957 b) used similar techniques to study low-angle boundaries in metal single crystals grown from the melt [9].

2.3.2. Principles of operation

When a material (sample) is irradiated with a parallel beam of monochromatic X-rays, the atomic lattice of the sample acts as a three dimensional diffraction grating causing the X-ray beam to be diffracted to specific angles. The diffraction pattern, that includes position (angles) and intensities of the diffracted beam, provides much information about the sample, which is discussed below:

- Angles are used to calculate the interplanar atomic spacings (d-spacings). Because every crystalline material will give a characteristic

diffraction pattern and can act as a unique 'fingerprint', the position (d) and intensity (I) information are used to identify the type of material by comparing them with patterns for over 80,000 data entries in the International Powder Diffraction File (PDF) database, complied by the Joint Committee for Powder Diffraction Standards (JCPDS). By this method, identification of any crystalline compounds, even in a complex sample, can be made.

- The position (d) of diffracted peaks also provides information about how the atoms are arranged within the crystalline compound (unit cell size or lattice parameter). The intensity information is used to assess the type and nature of atoms. Determination of lattice parameter helps understand extent of solid solution (complete or partial substitution of one element for another, as in some alloys) in a sample.
- Width of the diffracted peaks is used to determine crystallite size and micro-strain in the sample.
- The 'd' and 'I' from a phase can also be used to quantitatively estimate the amount of that phase in a multi-component mixture.

Quantitative analysis: As mentioned earlier, XRD can be used not only for qualitative identification but also for quantitative estimation of various crystalline phases. This is one of the important advantages of X-ray diffraction technique. Several methods have been proposed and successfully used to quantify crystalline phases in mixtures. They include external standard methods, the reference-intensity-ratio (RIR) method, chemical methods and the whole pattern fitting Rietveld method. Of the available methods, the Rietveld method is probably the most accurate and reliable method. It is a whole-pattern fitting least squares refinement technique and has been successfully used for quantification and characterization of inorganic and organic compounds It has also been used for crystal structure refinement, to determine size and strain of crystallites.

In the present work the X-ray Diffraction (XRD) measurements were carried out by the aid of a D/Max-IIIA (Rigaku Co., Japan) employing Cu K_α (λ = 0.15406 nm) as the radiation source. The samples were scanned over the range $10° \leq 2\theta \leq 86°$. The peak at

68° (Pd 220) was used for the calculation of crystallites size using the Scherrer formula and Bragg equation:

$$d=n\lambda/2\sin\theta \quad (4)$$

2.4. Thermogravimetric analysis

Thermogravimetric analysis (TGA) is an analytical technique used to determine a material's thermal stability and its fraction of volatile components by monitoring the weight change that occurs as a specimen is heated. The measurement is normally carried out in air or in an inert atmosphere, such as Helium or Argon, and the weight is recorded as a function of increasing temperature. Sometimes, the measurement is performed in a lean oxygen atmosphere (1 to 5% O_2 in N_2 or He) to slow down oxidation. In addition to weight changes, some instruments also record the temperature difference between the specimen and one or more reference pans (differential thermal analysis, or DTA) or the heat flow into the specimen pan compared to that of the reference pan (differential scanning calorimetry, or DSC). The latter can be used to monitor the energy released or absorbed via chemical reactions during the heating process. In the particular case of carbon nanotubes, the weight change in an air atmosphere is typically a superposition of the weight loss due to oxidation of carbon into gaseous carbon dioxide and the weight gain due to oxidation of residual metal catalyst into solid oxides.

2.4.1. Principles of operation

In most cases, TGA analysis is performed in an oxidative atmosphere (air or oxygen and inert gas mixtures) with a linear temperature ramp. The maximum temperature is selected so that the specimen weight is stable at the end of the experiment, implying that all chemical reactions are completed (i.e., all of the carbon is burnt off leaving behind metal oxides). This approach provides two important numerical pieces of information: ash content (residual mass, Mres) and oxidation temperature (To) (Figure 3.5). While the definition of ash content is unambiguous, oxidation temperature can be

336.93 °C

defined in many ways, including the temperature of the maximum in the weight loss rate (dm/dT_{max}) and the weight loss onset temperature (T_{onset}).

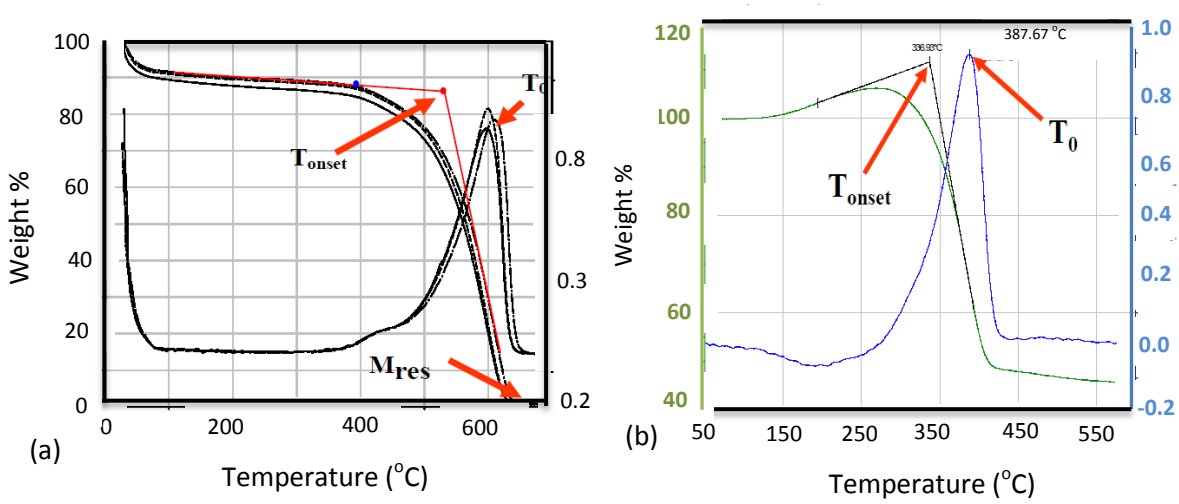

Figure 3.5. (a) A typical TGA of single walled carbon nanotubes, (b) Graph illustrating the ambiguity in determining T_{onset}.

The former refers to the temperature of the maximum rate of oxidation, while the latter refers to the temperature when oxidation just begins. The use of the former definition, $To=dm/dT_{max}$, is preferred for two reasons. First, due to the gradual initiation of transition (sometimes up to 100°C, Figure 3.5) it may be difficult to determine T_{onset} precisely. Gradual onset is believed to be due to nanotubes being contaminated with amorphous carbon and other types of carbonaceous impurities that oxidize at temperatures lower than that of nanotubes. In these cases, T_{onset} describes the properties of the impurities rather than the nanotubes. Second, weight loss due to carbon oxidation is often superimposed on the weight increase due to catalyst oxidation at low temperatures. In some cases this leads to an upward swing of the TGA curve prior to the bulk of the weight loss, which makes the definition of Tonset even more difficult and ambiguous. However, determining dm/dT_{max} is relatively straightforward. Therefore, oxidation temperature is herein defined as $To = dm/dT_{max}$ [10].

TGA measurement of "as-produced" nanotube material in air usually produces only one peak in the dm/dT curve, as "fluffy" raw nanotubes oxidize rapidly in an oxygen-rich environment. However, analysis of purified nanotube material in air may

produce more than one peak. These additional peaks are likely due to the fact that purified material contains a fraction of nanotubes with damage and/or with functional groups (i.e., the material is oxidized at lower temperatures) or because purified material is more compacted after drying. The position of each peak is also strongly affected by the amount and morphology of the metal catalyst particles and other carbon based impurities, as well as their distribution within a specimen. A lean oxygen environment can be used to better separate these peaks. In addition, these peaks have also been attributed to various components in the nanotube material (amorphous carbon, nanotubes, graphitic particles), and it may be possible to quantify these components by deconvolution of peaks.

Oxidation temperature, T_o, is basically a measure of the thermal stability of nanotubes in air and depends on a number of parameters. For example, smaller diameter nanotubes are believed to oxidize at lower temperature due to a higher curvature strain. Defects and derivatization moiety in nanotube walls can also lower the thermal stability. Active metal particles present in the nanotube specimens may catalyze carbon oxidation, so the amount of metal impurity in the sample can have a considerable influence on the thermal stability. It is impossible to distinguish these contributions, but, nevertheless, thermal stability is a good measure of the overall quality of a given nanotube sample. Higher oxidation temperature is always associated with purer, less defective samples [10].

2.4.2. *Instrumental apparatus*

Thermogravimetric analysis relies on a high degree of precision in three measurements: mass change, temperature, and temperature change. Therefore, the basic instrumental requirements for TGA are a precision balance with a pan loaded with the sample and a programmable furnace. The furnace can be programmed either for a constant heating rate or for heating to acquire a constant mass loss with time.

Though a constant heating rate is more common, a constant mass loss rate can illuminate specific reaction kinetics. Regardless of the furnace programming, the sample is placed in a small, electrically heated furnace equipped with

a thermocouple to monitor accurate measurements of the temperature by comparing its voltage output with that of the voltage-versus-temperature table stored in the computer's memory. A reference sample may be placed on another balance in a separate chamber. The atmosphere in the sample chamber may be purged with an inert gas to prevent oxidation or other undesired reactions. A different process using a quartz crystal microbalance has been devised for measuring smaller samples on the order of a microgram (*vs.* milligram with conventional TGA). Figure 3.6 provides schematic diagrams of a typical TGA instrument [10].

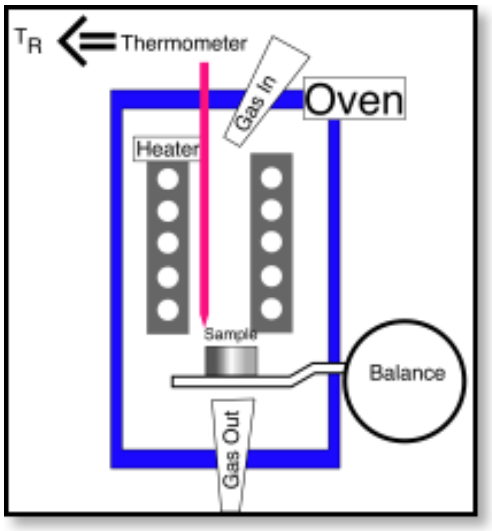

Figure 3.6. Instrument of thermogravimetric analysis [11].

In the present work for the determination of metal content in the catalysts, thermogravimetric (TG) experiments were carried out with a Netzsch TG-209 analyzer in air with a flow rate of 50 ml min^{-1} and a temperature ramp of 10 ^{o}C min^{-1}. The SEM-EDS were performed on scanning electron microscope (JEOL JSM-6330F) to determine the chemical composition of the samples.

3. Electrochemical Methods for Catalyst Activity Evaluation

3.1. Introduction

Electrochemical methods are deemed to play important roles in characterizing and evaluating the electrocatalysts before their use in a fuel cell. The most popular electrochemical characterization methods include potential step, potential sweep,

potential cycling, rotating disk electrode, rotating ring-disk electrode and impedance spectroscopy. Some techniques derived from these methods are also used for fuel cell characterization.

An electrochemical reaction involves at least the following steps: transport of the reactants to the surface of the electrode, adsorption of the reactants onto the surface of the electrode, charge transfer through either oxidation or reduction on the surface of the electrode and transport of the product(s) from the surface of the electrode. The purpose of the electrochemical characterizations is to determine the details of these steps [12].

The electrochemical characterizations are carried out in various electrochemical cells. There are typically three types of cells: conventional 3-electrode cells, half-cells, and single cells. In those cells, the entity (e.g., catalyst, electrode) to be characterized forms the working electrode, the potential of which or the current passing through which is controlled or monitored. What happens on the working electrode is the sole interest of the investigation. The working electrode and another electrode, called the counter electrode, form a circuit, and the current flowing through this circuit will cause some reaction on the counter electrode as well. However, the investigation has no interest in what happens on the counter electrode, except that the reaction occurring on it should not interfere with the working electrode.

In order to minimize the impact of the solution (or electrolyte) resistance on the potential of the working electrode, a reference electrode is often used to form another circuit with the working electrode. Ideally, this electrode is non-polarizable
and maintains a stable potential. There is high input impedance in the voltage measurement equipment, which makes the current flowing in this circuit very small. Therefore, the impact of the uncompensated electrolyte resistance on the potential of the working electrode is minimized [12].

In the following sub-sections a brief introduction to techniques, principles, and instrumentation of the electrocatalysts' electrochemical characterization is done. All electrochemical techniques involve the use of electricity as either an input or an output signal. The function of an electrochemical instrument is to generate an input electrical

signal and to measure the corresponding output electrical signal. The input signals can be a pre-programmed function of time, while the output signals often change with time. The signals are typically voltage, current, and charge. Charge is the integration of current with time. The input electrical signal causes the electrochemical reactions at the working and the counter electrodes. The rate of the reactions is controlled by the amplitude of the input signal and is represented by the amplitude of the output signal [12]. More details will be given in the discussion below of different types of electrochemical techniques.

3.2. Cyclic Voltammetry

3.2.1. Basic principles

Electron transfer plays a fundamental role in governing the pathway of chemical reactions. Yet the speed and size of the electron mean that tracing its movement is difficult using tradition methods such as spectroscopy and synthetic chemistry. Consequently our knowledge of the driving force for many reactions remains elusive. Electrochemical methods offer the potential to investigate these processes directly by the detection of the electrons involved.

Cyclic voltammetry refers to cycling the potential between a low and high potential value and recording the current in the potential cycling region. The resulting potential versus current plot is called a voltammogram. The sweeping of the potential is carried out linearly, and the sweeping rate can be controlled in a wide range. Most studies are carried out with a potential scanning rate between 1 and 1000 mV s^{-1}. Before the scanning starts, the working electrode is usually held at a potential that does not cause any electrochemical reactions. After the start of the scanning, the potential goes higher (or lower), and when it becomes high (or low) enough to cause the oxidation (or reduction) of an electrochemically active species, an anodic (or cathodic) current appears. The anodic (or cathodic) current increases as the potential increases (or decreases) because the reaction kinetics becomes faster.

When the potential reaches the standard potential E°, the concentrations, of the oxidized and the reduced forms of the electrochemically active species, become equal

on the surface of the electrode. The highest anodic (or cathodic) current is reached when the potential reaches a value at which all the reduced (or oxidized) form of the electrochemically active species at the electrode surface is consumed. The highest current is achieved at this moment because the mass transport rate of the electrochemically active species reaches a maximum rate, driven by the (largest) concentration gradient between the bulk concentration of the electrochemically active species and the surface concentration of this species. When the potential goes higher (or lower) beyond this point, the current starts to decline because the double-layer thickness increases, resulting in a less steep concentration gradient of the electrochemically active species. Therefore, an anodic (or a cathodic) peak develops. When the potential reaches the set high (or low) limit, it reverses direction and scans towards the set low (or high) limit (Figure 3.7).

During this reversed potential scan the oxidized (or reduced) form of the electrochemically active species reacts and develops a cathodic (or anodic) peak. The cathodic (anodic) peak is located at a slightly lower (higher) potential than the anodic (cathodic) peak. The cathodic and anodic peaks are of equal height (or, more accurately, equal area), unless there are complications caused by some side chemical or electrochemical processes (Figure 3.7).

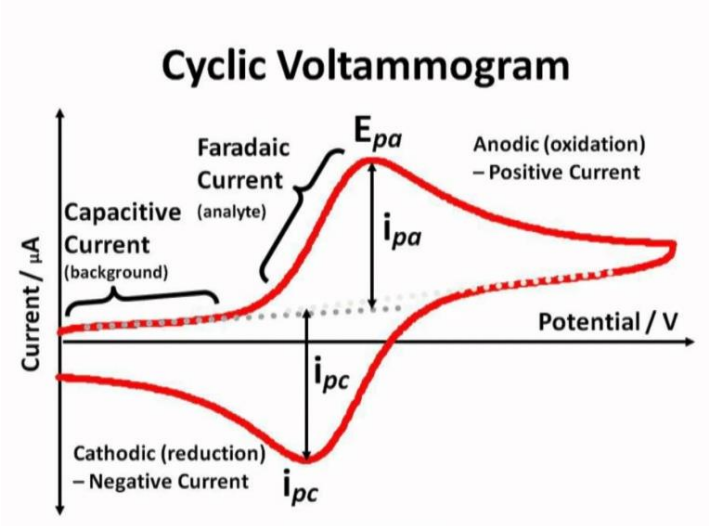

Figure 3.7. A typical cyclic voltammogram for a reversible reaction.

For a reversible electrochemical reaction the CV recorded has certain well defined characteristics.

1. The voltage separation between the current peaks.
2. The positions of peak voltage do not alter as a function of voltage scan rate.
3. The ratio of the peak currents is equal to one (ideal).
4. The peak currents are proportional to the square root of the scan rate.

A typical electrode reaction involves the transfer of charge between an electrode and a species in solution. The electrode reaction usually referred to as electrolysis, typically involves a series of steps (Figure 3.8):

- Reactant (O) moves to the interface: this is termed mass transport.
- Electron transfer can then occur via quantum mechanical tunneling between the electrode and reactant close to the electrode (typical tunneling distances are less than 2 nm).
- The product (R) moves away from the electrode to allow fresh reactant to the surface.

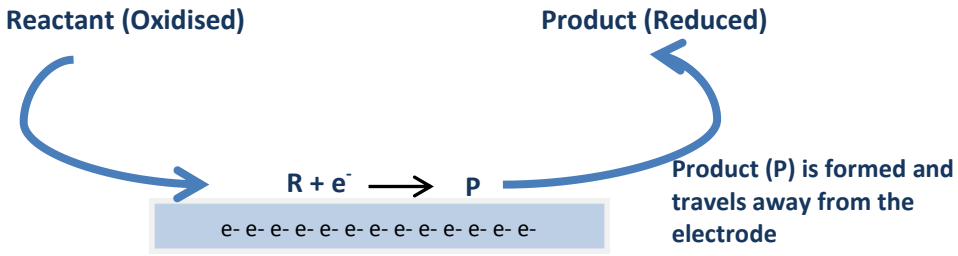

Figure 3.8. A typical electrode reaction.

The above electrode steps can also be complicated by:

- The applied voltage on the electrode.
- The reactivity of the species.
- The nature of the electrode surface.
- The structure of the interfacial region over which the electron transfer occurs.

The key to driving an electrode reaction is the application of a voltage (V). If the units of volts be considered:

V = Joule/Coulomb

it can be seen that a volt is simply the energy (J) required to move a charge (C). Application of a voltage to an electrode therefore supplies electrical energy. Since electrons possess charge an applied voltage can alter the 'energy' of the electrons within a metal electrode. The behaviour of electrons in a metal can be partly understood by considering the Fermi-level (E_F). Metals are comprised of closely packed atoms which have strong overlap between one another. A piece of metal therefore does not possess individual well defined electron energy levels that would be found in a single atom of the same material. Instead a continuum of levels is created with the available electrons filling the states from the bottom upwards. The Fermi-level corresponds to the energy at which the 'top' electrons sit Figure 3.9.

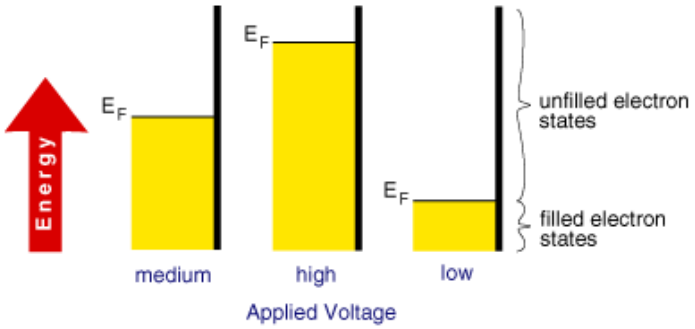

Figure 3.9. Fermi levels in a metal.

This level is not fixed and can be moved by supplying electrical energy. Electrochemists are therefore able to alter the energy of the Fermi-level by applying a voltage to an electrode, as it is depicted in Figure 3.10.

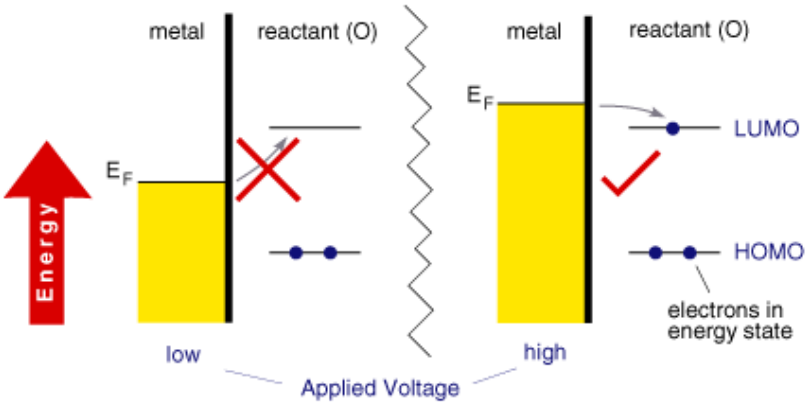

Figure 3.10. Fermi level when voltage is applied.

On the left hand side the Fermi-level has a lower value than the lowest unoccupied orbital (LUMO) of (O). It is therefore thermodynamically unfavourable for an electron to jump from the electrode to the molecule. However on the right hand side, the Fermi-level is above the LUMO of (O), where it is thermodynamically favourable for the electron transfer to occur, i.e. the reduction of O.

3.2.2. *Instrumental apparatus*

The instrument used to perform cyclic voltammetry and potential step experiments is a potentiostat, which controls the voltage and measures the current. The potentiostat maintains the potential of the working electrode at a desired value with respect to the potential of the reference electrode. The current flows between the working and the counter electrodes in response to the potential of the working electrode (Figure 3.11).

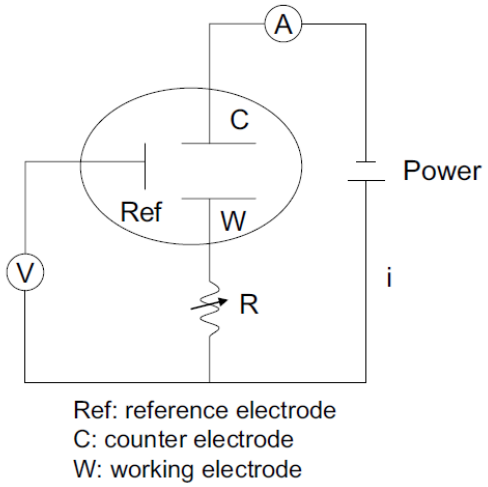

Figure 3.11. Illustration of the basic circuitry of a potentiostat [12].

A resistance in the electric circuit is used to adjust and maintain the potential of the working electrode. For example, in order to keep the potential of the working electrode constant during a potential step measurement that involves changing current, the resistance (R) of the resistors will be varied so that the voltage drop (iR) on the resistor is the same (Figure 3.11).

A potentiostat measures the voltage difference between the reference and the working electrodes. A potentiostat has extremely high input impedance so that the

input current is nearly zero, which enables the reference electrode to keep a constant potential. The current passing through the working and the counter electrodes is determined by measuring the voltage drop through a known resistor according to Ohm's law. When the electronic circuit is slightly modified so that the current is controlled and the corresponding potential of the working electrode is measured, it becomes a galvanostat [12].

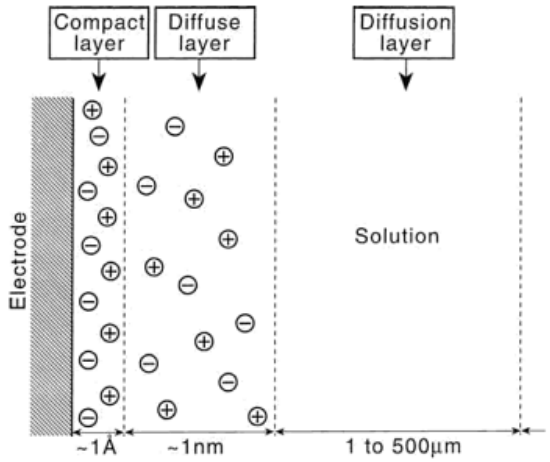

Figure 3.12. Schematic representation of the composition of the solution phase in the vicinity of the electrode surface [13].

With sufficient supporting electrolyte, the electrical double layer at the working electrode occupies a distance of about 1 nm from the electrode surface (Figure 3.12). The depicted layer has been shown to be consisted of a compact or "inner Helmholtz" layer and the diffuse or "Guy-Chapman" layer. The extent to which the diffuse layer extends into the solution phase depends on the concentration of the electrolyte and the double layer in some cases affect the kinetics of electrochemical processes. Experiments with low concentrations or no added supporting electrolyte can be desirable but since the double layer becomes more diffuse, they require careful data analysis. Furthermore the IR drop is extended into the diffusion layer. Under most experimental conditions, the size of the diffusion layer is several orders of magnitude larger than that of the diffuse layer (Figure 3.12).

3.2.3. *Electro-kinetic analysis*

If the electrochemical reactions are thermodynamically reversible, the positions (voltage) of the cathodic or anodic peaks do not change with the potential scan rate (v) and the peak height is proportional to the square root of the potential scan rate, $v^{1/2}$, according to the following equation:

$$i_p = (2.69 \times 10^5) n^{3/2} A D^{1/2} v^{1/2} C \quad (5)$$

where i_p is the peak current (in amperes), n is the number of electrons per reactant molecule, A is the electrode area (cm^2), n is the potential scan rate ($V\ s^{-1}$), D is the diffusion coefficient ($cm^2\ s^{-1}$), and C is the bulk concentration of the reactant ($mol\ cm^{-3}$).

If the reactions are not completely reversible, the anodic peak potential becomes more positive and the cathodic peak potential becomes more negative. The separation of the two peaks becomes larger than in the reversible case. Reversibility is often a relative term because it is related to the potential scan rate. A reaction that is reversible at low scan rates may become quasi-reversible (or even irreversible) at high scan rates. If quasi-reversible reaction happens, the peak current will become smaller than that expressed by equation 5 and the curve of i_p versus $v^{1/2}$ starts to bend down.

Special case results when a monolayer or an ultra-thin layer of an electrochemically active species is confined to the electrode surface and the thickness of this layer is less than that of the diffusion layer within the experiment time scale. Mass transport resistance becomes negligible. Both the anodic and the cathodic peaks become symmetrical, and they look like mirror images of each other. Integrating the current with time under the entire anodic (or cathodic) peak area gives the total charge of the oxidation (or reduction) process. From this charge the total amount of the electrochemically active species confined to the electrode surface can be calculated according to Faraday's law. If the potential is swept in only one direction, it is called linear sweep voltammetry. In such an experiment, the investigator is not interested in what happens during the reversed potential scan.

Charge transfer across an interface makes a chemical reaction, an electrochemical reaction. The addition of electrons to an oxidized reactant is termed reduction and oxidation is a process involving the removal of electrons:

$$\text{Oxidized species (A)} + ze^- \longleftrightarrow \text{Reduced Species (B)}$$

More precisely, the overall conversion of reactant A into product B must occur in a minimum of three steps:

$$A_{solution} \xrightarrow{mass\ transfer} A_{electrode}$$

$$A_{electrode} \xrightarrow{electron\ tranfer} B_{electrode}$$

$$B_{electrode} \xrightarrow{mass\ tranfer} B_{solution}$$

Both processes (A to B and B to A) involve charge transfer. During polarization, measured currents produced by oxidation or reduction of electro-active species will be limited by one of the following rate determining steps:

1. The transfer of electrons at the electrode/electrolyte interface (charge transfer controlled current).
2. The movement of reactants or products at distances close to the electrode (mass transport controlled current).
3. A combination of the both above-mentioned occasions (mixed control current).

The rate of conversion of reactant in the bulk solution into product in the bulk solution must always be determined by the slowest of these three steps. The rate of charge transfer between an electrode material and the electro-active species is related to how fast the substrate material can accept or give up electrons. This kinetic behaviour of an electrode will depend on its surface "activity". When dealing with the movement of charge, a simple way to improve the rate of reaction is to increase the potential difference (the applied energy) [11]. Then, catalytic activities accelerate without the required addition of extra energy.

It must be pointed out that electron transfer and mass transfer may usually are treated as independent processes, however they are not. According to the electrode kinetics the rate of reaction can be influenced by the cell potential difference.

However, the rate of transport to the surface can also effect or even dominate the overall reaction rate:

Assuming that the electron-transfer reaction has poor kinetics, the surface concentrations are controlled by the Butler-Volmer equation:

$$I = Ai_o \left\{ \exp[\frac{\alpha_\alpha nF}{RT}(E - E_{eq})] - \exp[-\frac{\alpha_c nF}{RT}(E - E_{eq})] \right\} \quad (6)$$

where I: measured current (A), A: electrode surface area (cm^2), i_o: exchange current density (mA cm^{-2}), E: electrode potential (V), E_{eq}: equilibrium potential, T: absolute temperature (K), n: number of electrons involved in the electrode reaction, F: Faraday constant (96485 C mol^{-1}), R: universal gas constant (8.314 J mol^{-1} K^{-1}), α_α: so-called anodic charge transfer coefficient (dimensionless), α_c: so-called cathodic charge transfer coefficient (dimensionless) and $E - E_{eq}$=η (V): activation overpotential.

The Butler-Volmer equation is one of the most fundamental relationships in electrochemical kinetics. It describes how the electrical current on an electrode depends on the electrode potential, considering that both a cathodic and an anodic reaction occur on the same electrode. At values of positive or negative overpotential typically greater than ±10 mV one term from the Butler-Volmer equation is usually more significant than the other and the lower contributing term can be ignored. The resulting forms are known as the cathodic and anodic Tafel equations:

$$\log i = \log i_o \frac{a_A nF}{2.3RT}\eta \quad (7)$$

$$\log i = \log i_o - \frac{a_C nF}{2.3RT}\eta \quad (7')$$

Alternatively, the Tafel equation can be presented in the following format:

$$\eta = a + b\log i \quad (8)$$

where 'a' and 'b' relate to a y-axis intercept and the measured slope, respectively of a current density (logarithmic scale) *vs.* overpotential plot. From Tafel plot (logI *vs.* η)

two significant kinetic parameters can be derived: i) the exchange current density (i_o)-value that give relative rates of reaction at equilibrium being calculated from the intercept at y-axis and ii) charge transfer coefficient (a_A or a_C)-that gives valuable information regarding the mechanism of a reaction and indications as to the identity of a rate-determining step of the overall reaction scheme.

In Figure 3.13 is given an example of the way that Tafel plots are derived from cyclic voltammograms.

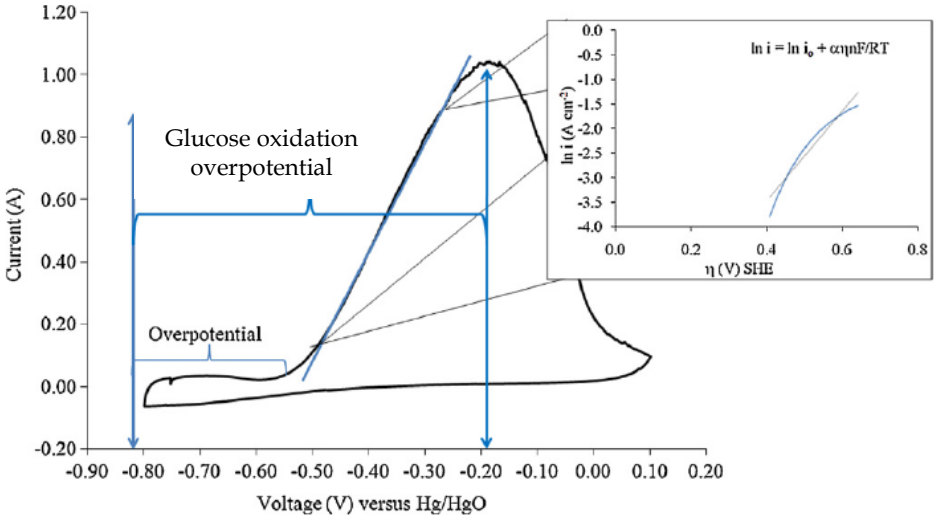

Figure 3.13. Methodology for extracting kinetic parameters from CV measurements [14].

It is important to appreciate that mechanistic details of a reaction can only be extracted via a Tafel analysis if any interfacial charge transfer process controls the electrochemical reaction rate.

3.3. Chronoamperometry

Electroanalytical chemistry, involves the analysis of chemical species through the use of electrochemical methods. Generally, we monitor alterations in the concentration of a chemical species by measuring changes in current in response to an applied voltage with respect to time. According to Faraday's law, the charge is directly proportional to the amount of species undergoing a loss (oxidation) or gain (reduction) of electrons.

$$Q=nFe \quad (7)$$

,where Q is the total charge generated (coulombs), n is the number of moles of a species undergoing oxidation or reduction, F is Faraday's constant (96,487 C/mol) e is the number of electrons per molecule lost or gained.
Current is the change in charge as a function of time:

$$I = dQ / dt \quad (8)$$

Thus, the current response with respect to time (voltammogram) gives information about changes in the concentration of the species of interest.

Chronoamperometry is a square wave pulsed voltammetric technique. Limited information about the identity of the electrolyzed species can be obtained from the ration of the peak oxidation current versus the peak reduction current. However, as with all pulsed techniques, Chronoamperometry generates high charging currents, which in this case, decay exponentially with time. To measure the faradaic current (the current that is proportional to the concentration of analyte), current in the last 70-8-% of each scan is integrated (when charging current has dissipated). In chronoamperometry, it takes approximately one second to complete a scan in the delayed pulse mode.

In the present work chronoamperometric measurements are conducted for measuring the tolerance of the electrocatalysts to the glucose electrooxidation reaction. Moreover, at long time the poisoning rate can be calculated.

3.4. Rotating disk electrode technique (RDE)

3.4.1. Basic principles

Hydrodynamic devices use convection to enhance the rate of mass transport to the electrode and can offer advantages over techniques which operate in stagnant solution. The addition of convection to the cell usually results in increased current and sensitivity in comparison to voltammetric measurements performed in stagnant solution. Also the introduction of convection (usually in a manner that is predictable) helps to remove the small random contribution from natural convection which can complicate measurements performed in stagnant solution. Finally, it is possible to vary

the rate of reaction at the electrode surface by altering the convection rate in the solution and this can be usefully exploited in mechanistic analysis and electroanalytical applications. There are two main approaches of introducing convection into the electrochemical cell. First the electrode can be held in a fixed position and solution is flowed over the surface by an applied force (usually a pressure). Second the electrode can be designed to move which acts to mix the solution via convection. The introduced (forced) convection is generally made to be considerably stronger than any natural convection processes and therefore the influence of natural convection becomes insignificant on the electrochemical reaction. To allow quantitative analysis it is vital that the forced convection introduced to the cell is predictable. The cell and experimental conditions are therefore designed so that the solution flow within the cell becomes laminar. In the present work for examining the current response time of electrocatalyst the RDE technique was used. That had the advantage of following the immediate response of the electrocatalyst when glucose concentration increases.

3.4.2. Instrumental apparatus

In Figure 3.14 is depicted the rotating disk electrode equipment. In this arrangement solution is brought to the surface by a Teflon disc which rotates in solution. The working electrode (glassy carbon) is embedded in the top face of the Teflon shield.

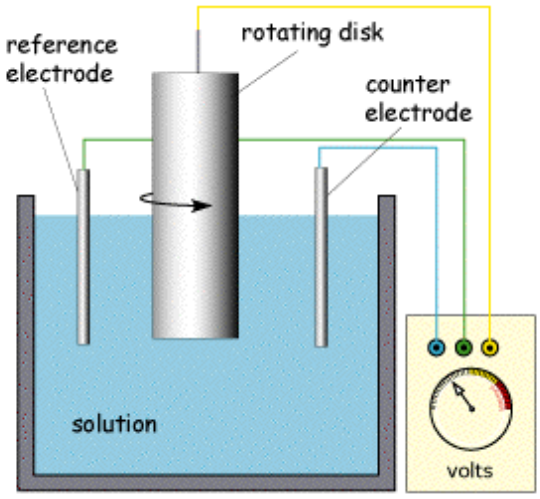

Figure 3.14. Rotating disk electrode equipment. Reprinted from Ref. [15].

When operated at rotation speeds of around 60 Hz (cycles per second) the flow profile to the electrode is laminar and so can be predicted mathematically. The Figure 3.15 below shows the type of flow profile that is developed when a circular object is rotated in solution and how this brings fresh reactant to the surface.

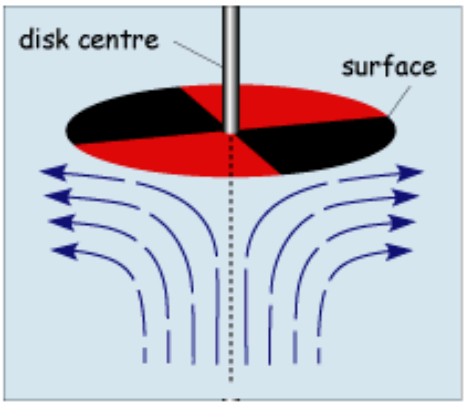

Figure 3.15. Scheme of the flow on working electrode surface. Reprinted from Ref. [15].

The act of rotation drags material to the electrode surface where it can react. Providing the rotation speed is kept within the limits that laminar flow is maintained then the mass transport equation is given by Eq. 8:

$$\frac{\partial[C]}{\partial t} = D_C \frac{\partial^2[C]}{\partial x^2} - v_x \frac{\partial[C]}{\partial x} \tag{8}$$

where the x dimension is the distance normal to the electrode surface. It is apparent that the mass transport equation is now dominated by both diffusion and convection and both these terms effect the concentration of reagent close to the electrode surface. Therefore to predict the current for this type of electrode we must solve this subject to the reactions occurring at the electrode.

A typical voltammetric measurement used with the rotating disc and other hydrodynamic systems is linear sweep voltammetry. The Figure 3.16 below shows a set of current voltage curves recorded for a reversible on electron transfer reaction and different rotation speeds. The scan rate used was 1 mV s^{-1} (compared to perhaps 20 mV s^{-1} for conventional cyclic voltammetry) and as can be seen the total current flowing depends upon the rotation speed used.

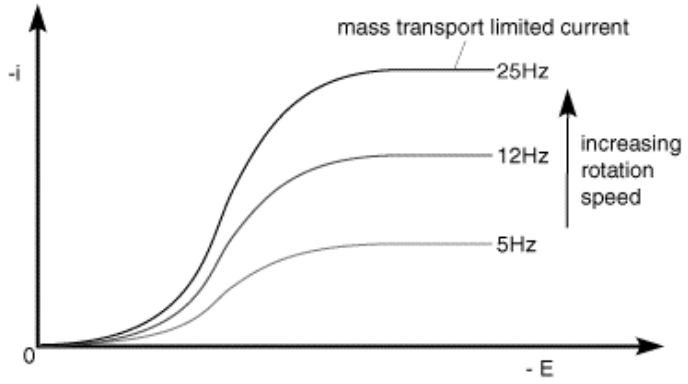

Figure 3.16. Linear sweep voltammetric measurement with RDE. Reprinted from Ref. [15].

This can be understood by returning to the concept of the 'diffusion layer' thickness controlling the flux of material to the surface. As the rotation speed is increased the distance that material can diffuse from the surface before being removed by convection is decreased. This results in a higher flux of material to the surface at higher rotation speeds. The mass transport limited current arises from the fact that the system reaches a steady state and so the current reaches a plateau once the equilibrium at the surface is driven to the products side.

References

[1] S.M. El-Refaei, M.I. Awad, B.E. El-Anadouli, M.M. Saleh, Electrochim. Acta 92 (2013) 460-467.

[2] S. Song, Y. Wang, P.K. Shen, J. Power Sources 170 (2007) 46-49.

[3] S. Song, W. Zhou, Z. Liang, R. Cai, G. Sun, Q. Xin, V. Stergiopoulos, P. Tsiakaras, Appl. Catal., B 55 (2005) 65-72.

[4] W. Yu, W. Tu, H. Liu, Langmuir 15 (1998) 6-9.

[5] X. Huang, Nanotechnology Research, NOVA Science Publisher, New York, 2008.

[6] P.B. Hirsch, in: U. Valdre (Ed.), Electron Microscopy in Material Science, Academic Press, 1971, pp. 3-11.

[7] E. Ruska, Biosci. Rep. 7 (1987) 607-629.

[8] M.N. Timofeeff, T.K. Lowenstein, W.H. Blackburn, Chem. Geol. 164 (2000) 171-181.

[9] C. Suryanarayana, M.G. Norton, X-Ray diffraction-A practical approach, New York, 1998.

[10] S. Vyazovkin, Characterization of Materials, John Wiley & Sons, Inc., 2002.

[11] T.A.G.-C.i.s. spaces (2008) http://webpages.scu.edu/ftp/adalsteinsson/GroupSite/Methods/DSCinfo/page30/page30.html.

[12] J. Zhang, Z. Qi, PEM Fuel Cell Electrocatalysts and Catalyst Layers, Springer London, 2008, pp. 547-607.

[13] Z. Qi, in: J. Zhang (Ed.), PEM Fuel Cell Electrocatalysts and Catalyst Layers, Springer London, 2008, pp. 547-607.

[14] B.K. Boggs, G.G. Botte, Electrochim. Acta 55 (2010) 5287-5293.

[15] U.o.C. Department of Chemical Engineering and Biotechnology, I.p.b. webmaster@ceb.cam.ac.uk, (2013) http://www.ceb.cam.ac.uk/pages/hydrodynamic-voltammetry.html

CHAPTER IV

Pd_xAu_y binary catalysts for glucose electrooxidation*

Abstract

Carbon supported Pd_xAu_y binary catalysts for glucose electrooxidation and detection was prepared by a modified pulse microwave assisted polyol method. The phyisco-chemical properties were obtained by X-ray diffraction (XRD), transmission electron microscopy (TEM) and scanning electron microscopy with (SEM-EDS). The electrochemical activity was investigated through cyclic voltammetry and chronoamperometry. Based on the experimental results, it can be concluded that the combination of Pd and Au to get Pd_xAu_y binary catalysts can take advantage of the high activity and low overpotential of Pd to glucose electrooxidation and poison tolerance of Au. More precisely, when the Pd/Au molar ratio was 30:70 ($Pd_{30}Au_{70}$/C), a desirable comprehensive performance, considering from current density, overpotential, and poison tolerance ability, was obtained. It was also found that $Pd_{30}Au_{70}$/C exhibited a very sensitive and linear amperometric response for glucose molecules, promising for the development of electrochemical glucose sensor and direct glucose fuel cells.

*L. Yan, A. Brouzgou, Y. Meng, M. Xiao, P. Tsiakaras, S. Song,
***Glucose Electrooxidation in Alkaline Medium: Efficient and Poison-Tolerant PdAu/C Catalysts for Fuel Cell and Sensor applications**, submitted to Applied Catalysis B: Environmental (2013).

CONTENTS

CHAPTER IV ..... **i**

1. Introduction **135**

2. Experimental **136**

2.1. Catalyst preparation 136

2.2. Physico-chemical characterization 136

2.3. Electrochemical analysis 137

3. Results and discussion **138**

3.1. Physico-chemical characterization 138

3.2. Electrochemical characterization 143

Conclusions **148**

References **149**

List of Tables

Table 4.1. Physico-chemical properties of the as-prepared Pd/C, Au/C and PdxAuy/C catalysts.....139

List of Figures

Figure 4.1. XRD patterns for Pd/C and Au/C (A) and PdxAuy/C binary catalysts (B) and their corresponding detailed Pd or Au (220) peaks scanned at 1°C min^{-1} (C).....138

Figure 4.2. TEM images of Pd/C (A), Au/C (B), Pd70Au30/C (C) and Pd30Au70/C (D) and their corresponding particle size distribution (A', B', C' and D').....140

Figure 4.3. Thermogravimetric curves of Pd/C, Au/C and PdxAuy/C samples.....141

Figure 4.4. SEM-EDS of the as prepared PdxAuy/C binary catalysts. The number in SEM is randomly and automatically given by the SEM instrument.....142

Figure 4.5.Cyclic voltammetric curves of Pd/C (A) and Au/C (B) in 0.1 mol L^{-1} NaOH aqueous solution in the absence or presence of 20 mmol L^{-1} glucose at 50 mV s^{-1} and at 36.5°C.....143

Figure 4.6. Comparative results of glucose electrooxidation at Pd/C and Au/C. Electrolyte: 0.1 mol L^{-1} NaOH+ 20 mmol L^{-1} glucose; Scan rate: 50 mV s^{-1}, Temperature: 36.5°C.....145

Figure 4.7. Cyclic voltammetric curves of Pd/C, Au/C and Pd_xAu_y/C mono and binary catalysts in 0.1 mol L^{-1} NaOH aqueous solution in the absence (A) or presence of 20 mmol L^{-1} glucose (B) at 50 mV s^{-1} and at 36.5°C.....145

Figure 4.8. Cyclic voltammograms for $Pd_{30}Au_{70}$/C catalyst in 0.1 mol L_{-1} NaOH aqueous solution containing different concentrations of glucose at 50 mV s^{-1} and at 36.5°C. Inset: current density vs. higher glucose concentration.....146

Figure 4.9. Current-time record of $Pd_{30}Au_{70}$/C catalyst fixed onto rotating disk electrode (1600 rpm) by successively injection 1 mM glucose into 0.1 M NaOH solution at a regular interval time of 60 s. Applied potential: -0.2 V. Inset: the relationship between the current density and the added glucose solution.....147

1. Introduction

Glucose electrooxidation has been the hot research topic in electrochemistry due to the importance of reliable and fast *in vivo* or *in vitro* monitoring of blood sugar for the treatment and control of diabetes through an electrochemical glucose sensor, as well as the interest for implantable glucose fuel cells intended for artificial hearts and heart pacer [1-5]. However, their research and development is far away from satisfaction and real applications for lack of highly efficient and stable electrocatalysts for glucose electrooxidation. Desirable electrocatalysts, reflected in terms of high current and low overpotential for glucose oxidation and good poison tolerance, is the solution to achieve fast response for glucose detection and high performance for direct glucose fuel cells. At present, Pt [6-8], Au [9-15], Pd [16-18] and their based binary or ternary catalysts such as Pt-Pd [5,19-20], PtBi [21], PtRu [21], PtPb [22-23], PtAu [19, 21, 24-26], Au-Ag [27], PtAuPd [5] etc, and multi-wall carbon nanotubes [28] have been found to exhibit electrocatalytic activity towards glucose oxidation. Among them, Pt is the first and most widely investigated material for glucose electrooxidation. However, it is not a very suitable catalyst due to its high chemisorbability and its poor selectivity of different substances presented in physiological solutions [9]. A number of investigations have also been devoted to Au, after it was found to be more active and poison tolerant than Pt towards the reaction of glucose electrooxidation in neutral and alkaline solutions [29].

However, the potential for glucose oxidation on Au is still too high for glucose detection [30]. Alloyed electrocatalysts are often adopted to obtain better performance than pure metals, through exploiting the specific properties of each component. It has been recognized that the activity of Pt to glucose electrooxidation in alkaline media can be enhanced by alloying Pd, Au, Bi, Ru etc [5, 19-26]. However, novel efficient and stable electrocatalysts for glucose electrooxidation are still urgently needed.

Palladium has been known to exhibit superior activity for electrooxidation of alcohols and polyalcohols in alkaline solutions [31]. Furthermore, the abundance of Pd

on the earth is at least 50 times more than that of Pt's. The combination of Pd and Au has shown good catalytic activity to glucose selective oxidation [32]. However, for the electrochemical oxidation of glucose on PdAu/C, to our best knowledge, there is no systematic investigation. In the present investigation, a series of Pd_xAu_y/C with different Pd/Au molar ratio were prepared by the modified pulse microwave assisted polyol synthesis method in a very short time (2 min). Their corresponding physico-chemical characteristics were obtained by *X-ray diffraction* (XRD), *Transmission Electron Microscopy* (TEM), and *Scanning Electron Microscopy-Energy Dispersive Spectroscopy* (SEM-EDS). Their electrocatalytic activity to glucose electrooxidation was evaluated by the electrochemical methods of *Cyclic Voltammetry* (CV) and *Chronoamperometry* (CA) in alkaline environment.

2. Experimental

2.1. Catalyst preparation

Vulcan XC 72R carbon black (Cabot Corp.) supported Pd_xAu_y/C binary catalysts with 20 wt.% noble metal were prepared by the modified microwave assisted polyol method [33-34]. A certain amount of $PdCl_2$/ethyl glycol (EG) or/and $HAuCl_4$/EG solution were well mixed with EG in ultrasonic bath, and then carbon powder was added into the solution according to the pre-calculated metal loading. After stirring, 2.0 mol L^{-1} NaOH/EG was added into the solution to adjust the pH value of the above mixture to be more than 12. After further stirring for another 1h, the slurry was microwave-heated for several times in a 10s-on/10s-off pulse form and then re-acidified. The obtained black solid sample was washed by hot deionized water and dried in a vacuum oven at 80°C for 12 h.

2.2. Physico-chemical characterization

The XRD patterns were recorded on a D-MAX 2200 VPC diffractometer using Cu Kα radiation (30 kV, 30 mA). Transmission electron microscope (TEM) investigations

were carried out on a JEOL TEM-2010 (HR) to determine the size and surface morphology of the particles. Before the measurements, the catalysts were uniformly dispersed in ethanol solution using ultrasonic water bath and then dried onto carbon coated copper grid.

For the determination of metal content in the catalysts, thermogravimetric (TG) experiments were carried out with a Netzsch TG-209 analyzer in air with a flow rate of 50 ml min^{-1} and a temperature "ramp" of 10°C min^{-1}. The SEM-EDS was performed on scanning electron microscope (JEOL JSM-6330F) to determine the chemical composition of the samples.

2.3. Electrochemical analysis

Three-electrode electrolytic cell was used to perform the electrochemical evaluation on an AUT84480 instrument in a thermostatic water bath. Platinum foil (1.0 cm ×1.0 cm) and Hg/HgO electrode (0.1 mol L^{-1} NaOH) were used as the counter and reference electrodes respectively. The thin catalyst film was covered onto the surface of the glassy carbon disk electrode (d=0.5 cm), which was used as the working electrode.

The catalyst slurry was obtained by dispersing 5.0 mg of the as-prepared catalyst powder in 1.8 mL ethanol and 0.2 mL Nafion solution (Dupont company, USA). The above obtained catalyst ink was then quantitatively (10 µL) transferred onto the surface of the glassy carbon electrode and dried in an infrared lamp.

The cyclic voltammetry (CV) and chronoamperometry (CA) techniques were adopted to evaluate and compare the electrocatalytic performance of the catalysts for glucose electrooxidation in alkaline medium.

Before experiments, the solution was saturated with high-purity N_2 gas for 30 min to remove the dissolved oxygen in the electrolyte. It should be noted that the potential is referred to Hg/HgO (0.1 mol L^{-1} NaOH) reference electrode without specification.

3. Results and discussion

3.1. Physico-chemical characterization

XRD patterns for all the as-prepared Pd/C, Au/C, and Pd_xAu_y/C samples are displayed in Figure 4.1. All the catalysts give a broad peak at about 25º assigned to graphitic carbon (002). Moreover, all the samples present a typical fcc pattern. By comparing Figure 4.1 A and B, one can distinguish that for single metal, the corresponding diffraction angles of Au/C are a little higher than those of Pd/C (Figure 4.1A).

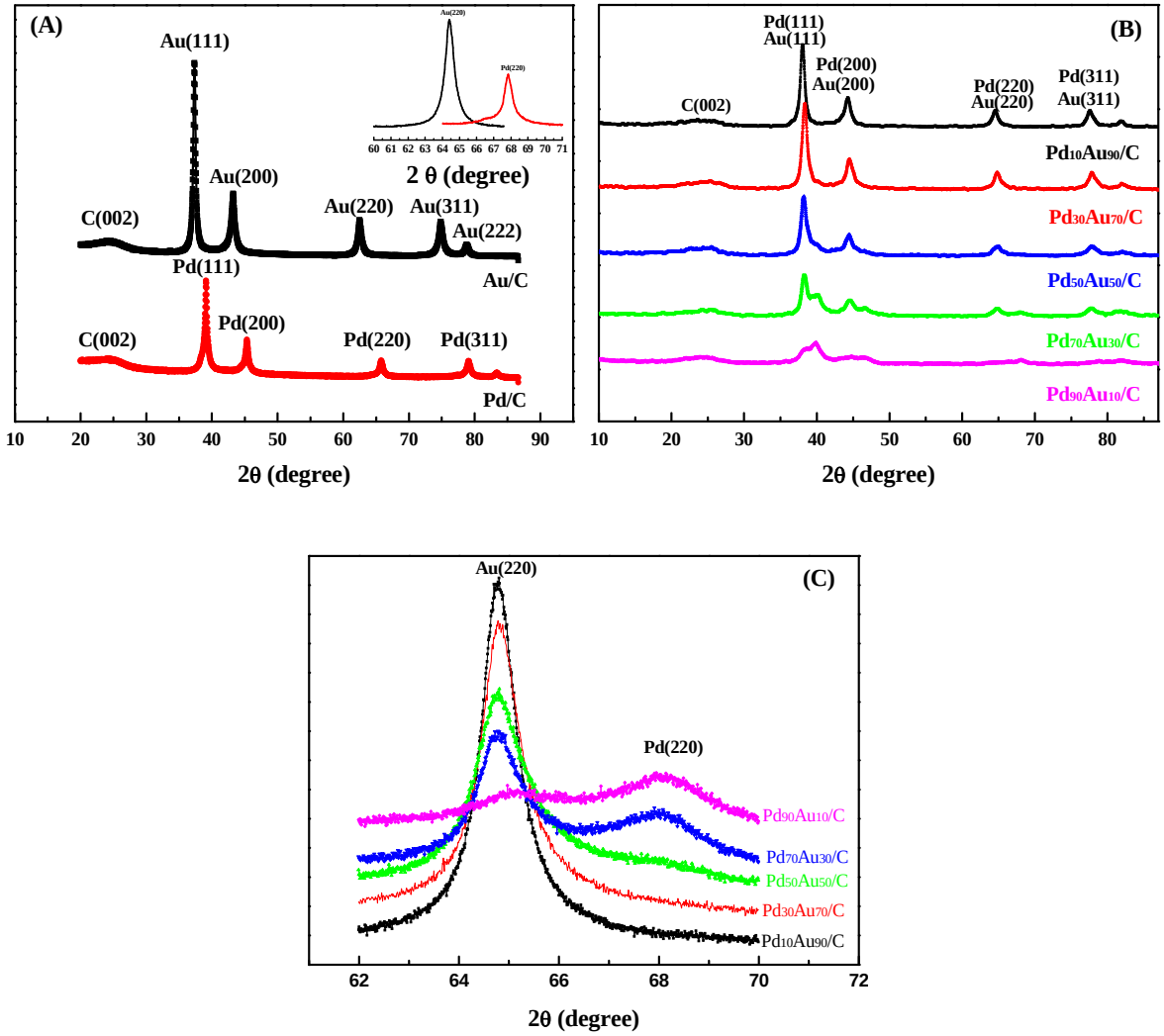

Figure 4.1. XRD patterns for Pd/C and Au/C (A) and PdxAuy/C binary catalysts (B) and their corresponding detailed Pd or Au (220) peaks scanned at 1ºC min^{-1} (C).

Nevertheless, for binary Pd_xAu_y/C catalysts, the diffraction peaks for Pd and Au are overlapped and cannot be obviously differentiated (Figure 4.1B). However, in a fine scanning from 62 to 70° at a rate of 1° min^{-1}, the diffraction peaks for Au (311) and Pd (311) can be distinguished. This could indicate that in Pd_xAu_y/C binary catalysts there are some interactions between Pd and Au. However, PdAu alloy was not formed due to the low temperature of catalysts preparation process (<160°C).

Table 4.1 lists the particle sizes calculated from the Pd (220) or/and Au (220) diffraction lines, using the Scherrer formula [35]. It can be clearly seen from Table 4.1 that the particle size of mono metallic catalysts is bigger than that of binary ones. A further decrease in the particle size of the catalysts could give higher activity, and this part of work is under investigation.

Table 4.1. Physico-chemical properties of the as-prepared Pd/C, Au/C and PdxAuy/C catalysts.

Samples	Mean particle size /nm		Pd/Au atomic ratio		Metal content (wt.%) (TG)
	XRD	TEM	EDS	Feeding ratio	
Pd/C	12.6	8.1	-	-	19.2
$Pd_{90}Au_{10}/C$	9.7	-	88.4/11.6	90/10	21.3
$Pd_{70}Au_{30}/C$	8.1	4.9	77.0/23.0	70/30	22.1
$Pd_{50}Au_{50}/C$	7.3	-	53.3/46.7	50/50	19.7
$Pd_{30}Au_{70}/C$	7.1	4.8	24.5/75.5	30/70	18.5
$Pd_{10}Au_{90}/C$	6.6	-	7.6/92.4	10/90	19.5
Au/C	16.2	14.0	-	-	20.8

Figure 4.2 depicts the typical TEM images for Pd/C, Au/C, $Pd_{70}Au_{30}/C$ and $Pd_{30}Au_{70}/C$ and their corresponding metal particles size distribution. Obviously, Pd/C has a smaller particle size and better dispersion than Au/C. For the binary catalysts, the metal particle size becomes smaller than that of the single metal. These results agree with those of the XRD spectra, although the calculated particle size from XRD is bigger than the mean statistical value calculated from the TEM micrographs.

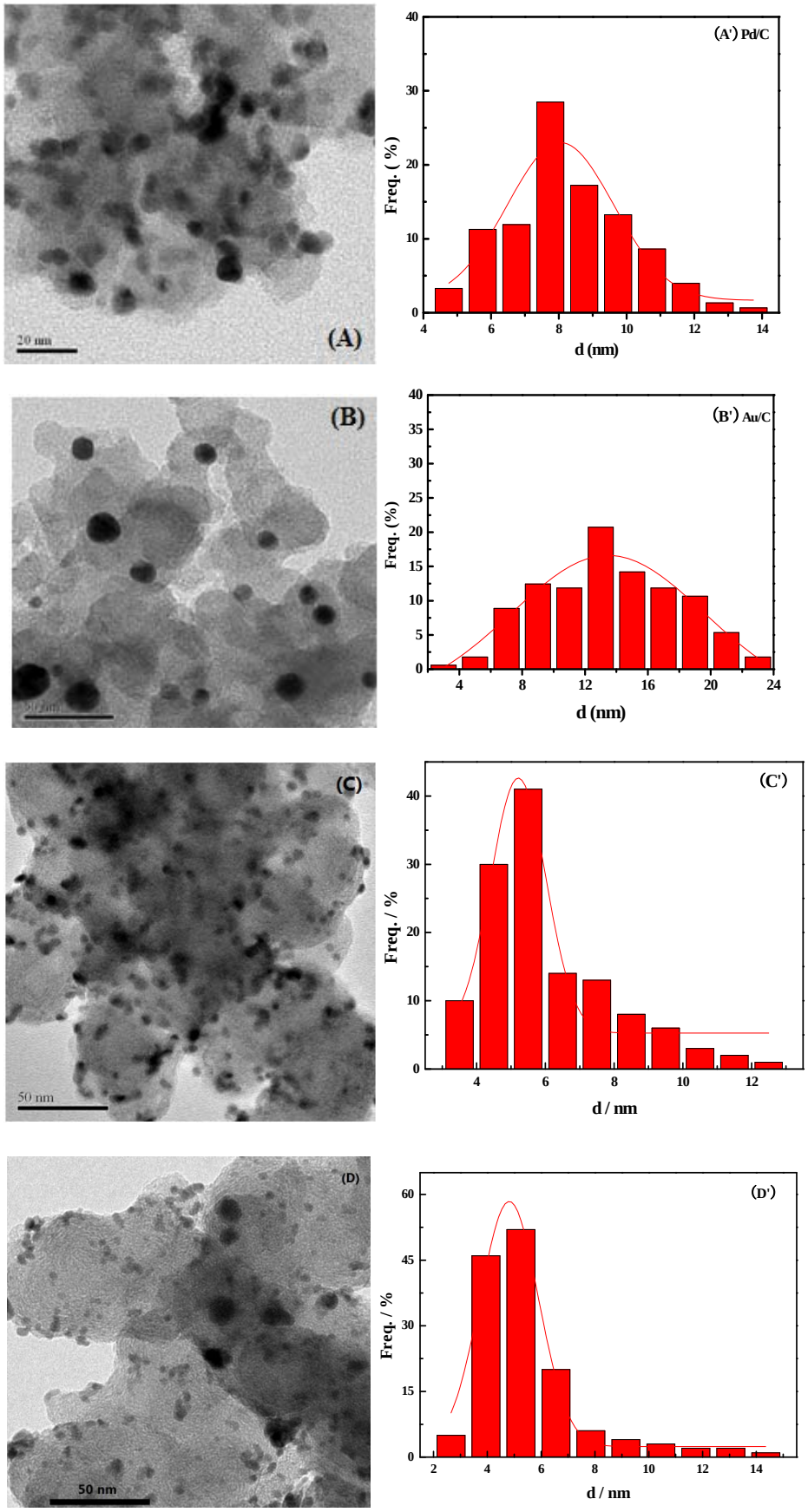

Figure 4.2. TEM images of Pd/C (A), Au/C (B), Pd70Au30/C (C) and Pd30Au70/C (D) and their corresponding particle size distribution (A', B', C' and D').

The metal content in the catalysts is a very important parameter for comparing their activity. So, the metal content in Pd/C and Au/C was determined by TG to check, in which extend the metal precursors can be reduced. As shown in Figure 4.3, below 200°C, the weight loss for the above two samples can be attributed to the water vapor and the residual EG desorption.

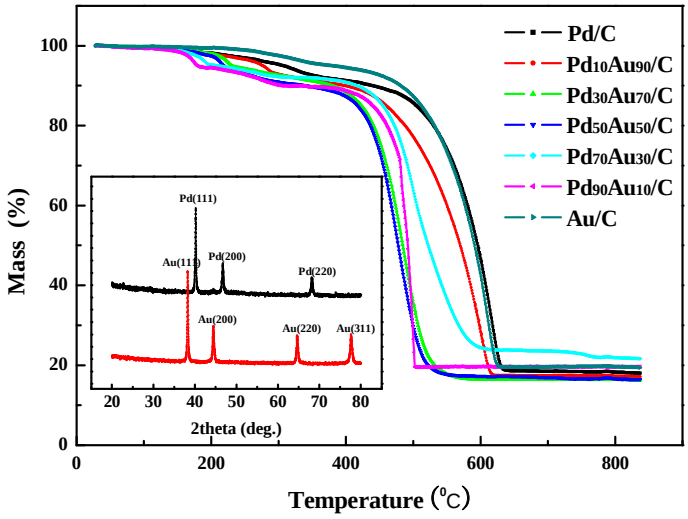

Figure 4.3. Thermogravimetric curves of Pd/C, Au/C and PdxAuy/C samples.

Therefore, the metal loading in the electrocatalysts can be calculated from their TG curves after subtracting the weight of the adsorbed water (the results are summarized in Table 4.1). Setting the weight of the anhydrous material to 100 wt.%, the metal loading in all the catalysts is 20.0±1.5 wt.%, which is basically in accordance with the feeding weight ratio (20.0 wt.%) for catalysts preparation. This indicates that the pulse-microwave assisted polyol synthesis method adopted in the present work is an effective and fast one for both Pd and Au catalysts.

The Pd/Au molar ratio in the Pd_xAu_y/C binary catalysts was determined from SEM-EDS (Figure 4.4) and summarized in Table 4.1. According to the results, the final Pd/Au molar ratio is close to the feeding ratio in the precursor solutions.

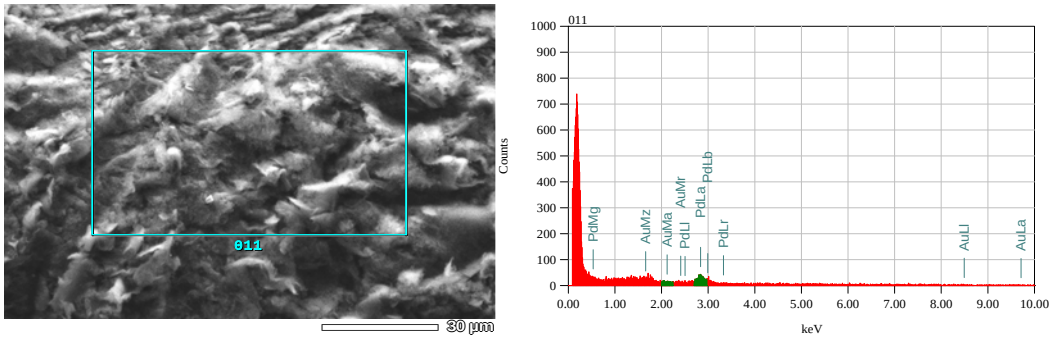

(A) $Pd_{90}Au_{10}/C$

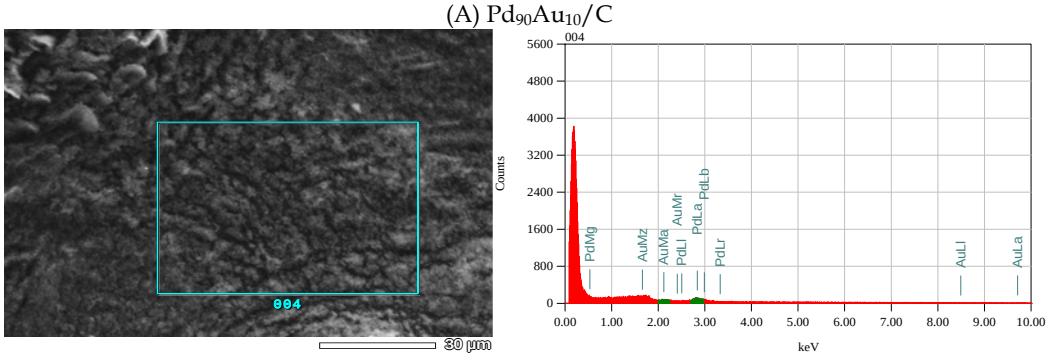

(B) $Pd_{70}Au_{30}/C$

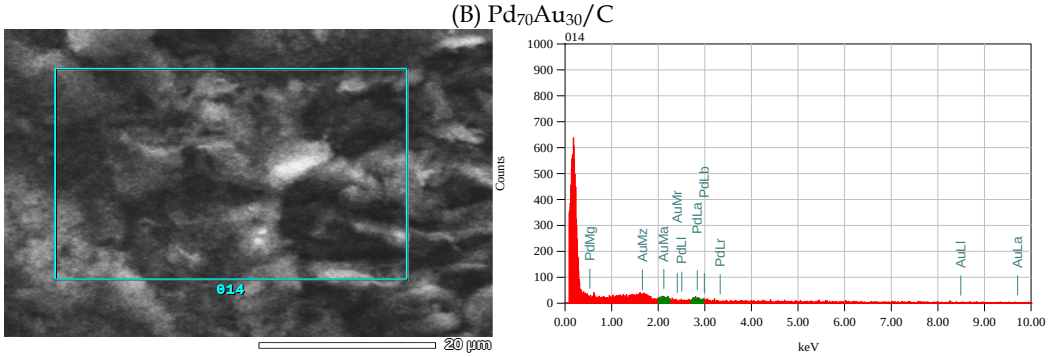

(C) $Pd_{50}Au_{50}/C$

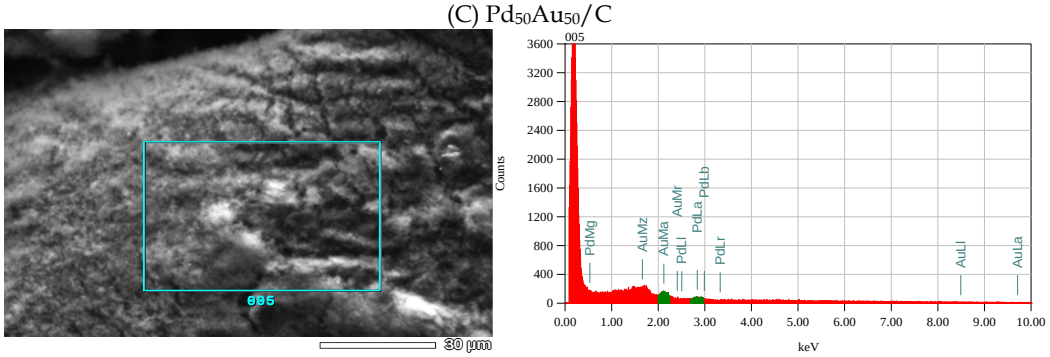

(D) $Pd_{30}Au_{70}/C$

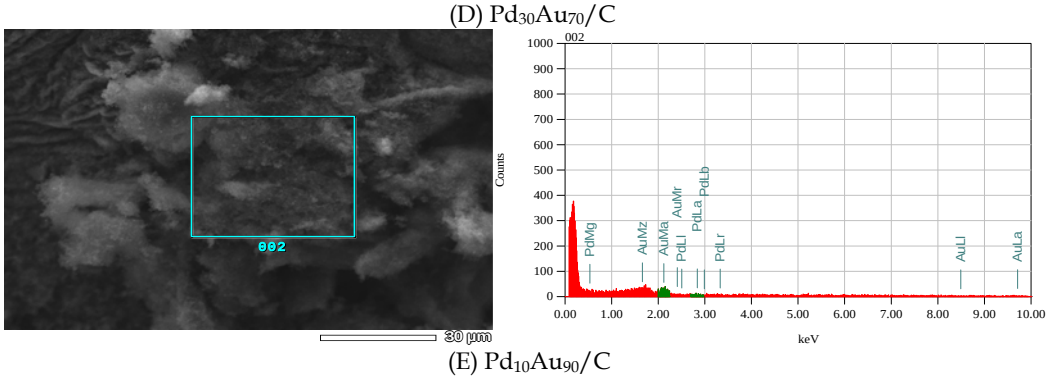

(E) $Pd_{10}Au_{90}/C$

Figure 4.4. SEM-EDS of the as prepared PdxAuy/C binary catalysts. The number in SEM is randomly and automatically given by the SEM instrument.

3.2. Electrochemical characterization

The electrocatalytic activities of the as-prepared catalysts towards glucose electrooxidation were evaluated through potentiodynamic voltammetric curves. The polarization curves for Pd/C and Au/C mono-metallic catalysts in 0.1 mol L^{-1} NaOH solution in absence or presence of 20 mmol L^{-1} glucose are given in Figure 4.5. For Pd/C catalyst (Figure 4.5 A), the disappearance of hydrogen desorption peak in the presence of glucose indicates the adsorption of glucose at Pd hinders the adsorption of hydrogen.

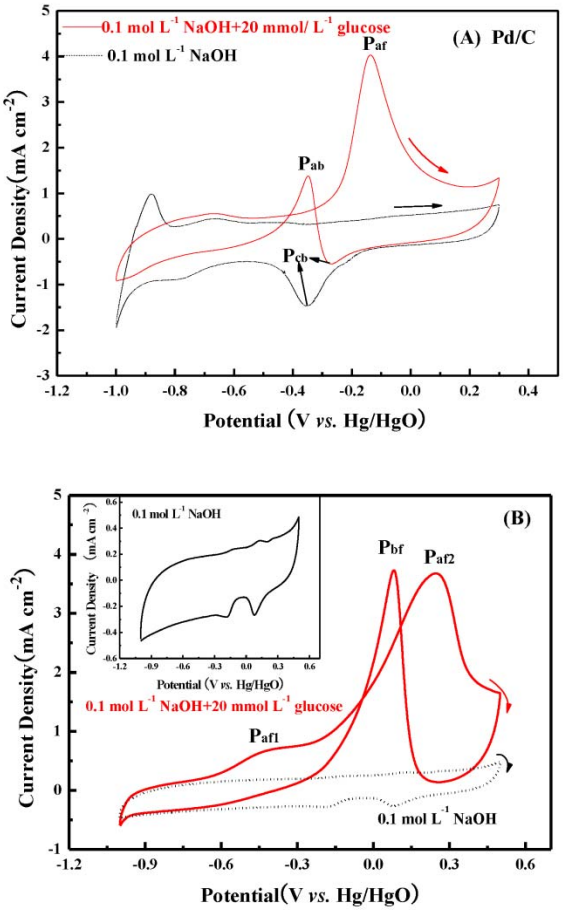

Figure 4.5. Cyclic voltammetric curves of Pd/C (A) and Au/C (B) in 0.1 mol L^{-1} NaOH aqueous solution in the absence or presence of 20 mmol L^{-1} glucose at 50 mV s^{-1} and at 36.5°C.

An obvious maximum (peak anodic forward-P_{af}) can be discerned in the forward direction, which corresponds to the direct glucose oxidation after the poisoning intermediates on the electrocatalytic surface are moved by the OH_{ad} radicals, which

have been formed by the partial discharge of OH_{ad} under the upper potential region [36-37]. After the maximum point (peak current density) current density decreases sharply due to the formation of palladium oxides (PdO) at this potential. In the backwards direction, the reduction peak (peak cathodic backward-P_{cb}) is attributed to the reduction of PdO and the oxidation peak (peak anodic backward-P_{ab}) is formed through the direct glucose oxidation over Pd reduced from PdO.

Further comparison of polarization curve of glucose electrooxidation over Pd/C with the potentiodynamic curve of Pd/C in the blank solution shows that the reduction peak of PdO is obviously decreased in presence of glucose. This suggests that during the electrooxidation of glucose part of Pd/C has been poisoned. For Au/C catalyst (Figure 4.5 B), in the forward direction, the observed first oxidation peak (P_{af1}) is probably due to the formation of $Au(OH)^{1-\lambda}$ and the adsorption of glucose [12, 38]. The other two significant oxidation peaks (P_{af2} in forward direction and P_{bf} in the backward direction) are probably appeared due to the electrooxidation of glucose over gold hydroxide. Furthermore, the narrow peaks current density of P_{af2} and P_{bf} give an indicator that Au/C is tolerant to the intermediate products of glucose oxidation. By comparing the CV curves on Au/C in 0.1 mol L^{-1} NaOH in the absence or presence of glucose, it can be distinguished that glucose electrooxidation starts at much lower potentials than the noticeable oxidation of gold begins.

The polarization curves of glucose electrooxidation on Pd/C and Au/C are compared in Figure 4.6. As it is clearly shown, from the point of view of current density, Pd/C gives a little higher activity than Au/C in the forward potential scanning, while in the backward direction Au/C exhibits superior performance. On the other hand, in terms of overpotential, Pd/C has an obvious advantage over Au/C. Taking also into consideration the above discussions of poison sensitivity of Pd/C and at the same time the good poison tolerance of Au/C during glucose electrooxidation, the combination of Pd and Au is expecting to be the solution for active and poison tolerant catalysts.

In background solution (0.1 mol L^{-1} NaOH), the potentiodynamic curves of Pd/C, Au/C and Pd_xAu_y/C are shown in Fig. 6A. The red-colored peak (P_{R1}) is attributed to

the reduction of gold oxide species, while the black-colored peak (P_{R2}) is attributed to the reduction of palladium oxide species. Clearly, along with the Au content increment in the catalysts, the peak area of P_{R1} is increased while that of P_{R2} is decreased. The electrocatalytic activities were obtained in 0.1 mol L^{-1} NaOH aqueous solution containing 20 mmol L^{-1} glucose.

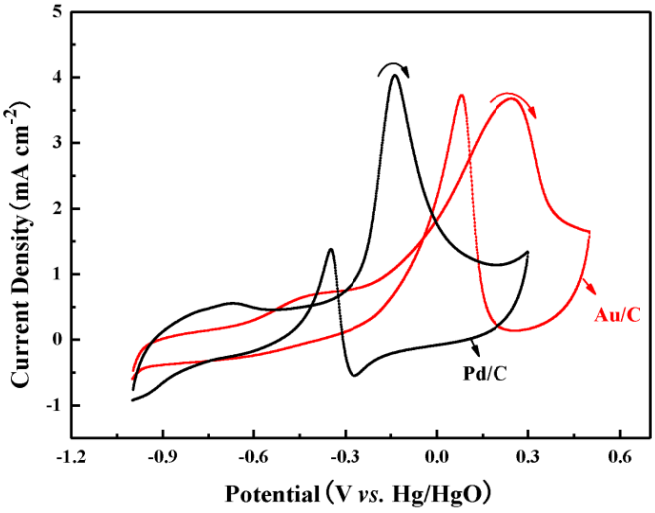

Figure 4.6. Comparative results of glucose electrooxidation at Pd/C and Au/C. Electrolyte: 0.1 mol L^{-1} NaOH+ 20 mmol L^{-1} glucose; Scan rate: 50 mV s^{-1}, Temperature: 36.5°C.

As shown in Figure 4.7 B, the samples with high Pd content (Pd/C, $Pd_{90}Au_{10}$/C, $Pd_{70}Au_{30}$/C, and $Pd_{50}Au_{50}$/C) exhibit two visible oxidation peaks in the forward sweep and an oxidation and a reduction peak in the backward sweep.

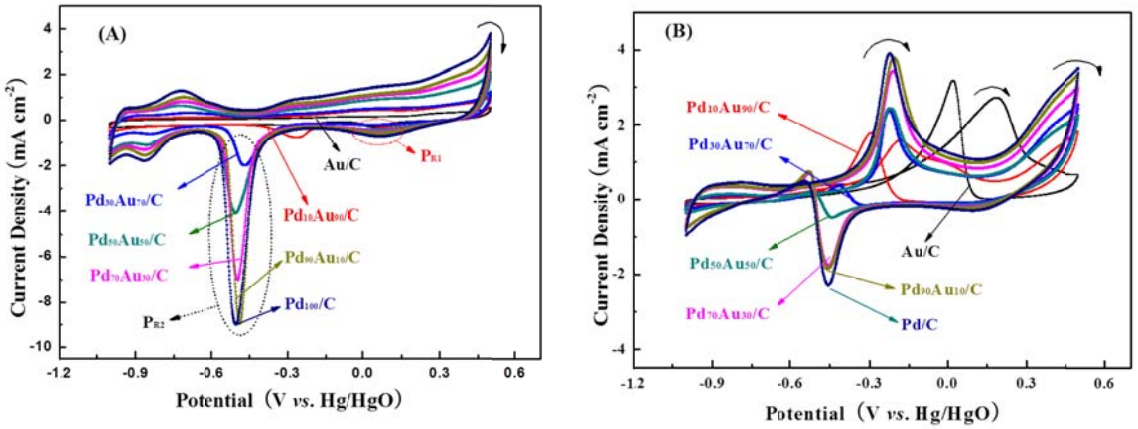

Figure 4.7. Cyclic voltammetric curves of Pd/C, Au/C and Pd_xAu_y/C mono and binary catalysts in 0.1 mol L^{-1} NaOH aqueous solution in the absence (A) or presence of 20 mmol L^{-1} glucose (B) at 50 mV s^{-1} and at 36.5°C.

While for the samples with low Pd content (Au/C, $Pd_{30}Au_{70}$/C, and $Pd_{10}Au_{90}$/C), the reduction peak in the backward sweep disappears. With the Pd content decrement, the first oxidation peak current in the forward sweep is decreased.

Furthermore, one can distinguish that the introduction of Au into Pd/C catalyst almost does not change the onset potential of glucose oxidation. Moreover, as the Au content increases, the oxidation peak current in the backward sweep increases and the corresponding peak potentials are obviously more positive. This indicates the introduction of Au increase the poison tolerance of Pd to the intermediate products of glucose oxidation. Considering the activity and poison-tolerance together, $Pd_{30}Au_{70}$/C is chosen for further investigation. Figure 4.8 shows the cyclic voltammetry curves over $Pd_{30}Au_{70}$/C in different concentrations of glucose at a constant concentration of NaOH (0.1 mol L^{-1}). From Figure 4.8A, it is obvious that as the glucose concentration increases the response current density linearly increases and reaches about 3.0 mA cm^{-2} for 50 mmol L^{-1} of glucose.

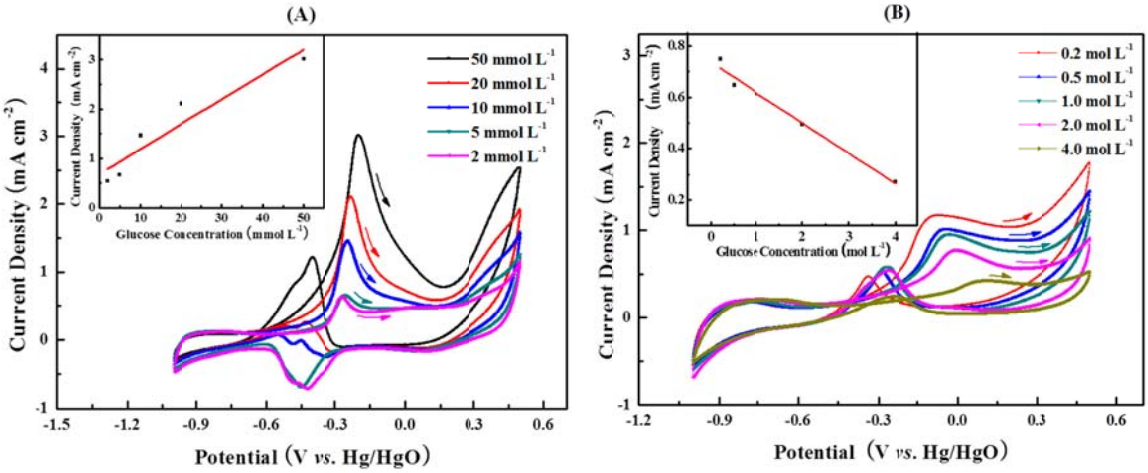

Figure 4.8. Cyclic voltammograms for $Pd_{30}Au_{70}$/C catalyst in 0.1 mol L_{-1} NaOH aqueous solution containing different concentrations of glucose at 50 mV s^{-1} and at 36.5°C. Inset: current density vs. higher glucose concentration.

This performance enhancement could be attributed to the fact that as glucose concentration increases, a greater amount of the reactants is involved in the reaction. On the other hand, further increase of glucose concentration causes a linear decrease of the corresponding current density, as shown in Figure 4.8 B. This behavior could be due to the

following reasons: i) the given electrode surface cannot provide sufficient active sites for the electrocatalytic process, which leads to the ineffectiveness of higher concentration of glucose; ii) higher concentration of glucose gives rise to higher viscosity of the solution, and thus more difficult mass transfer; and iii) the byproducts may also cover the electrode surface to decrease its catalytic activity. This tendency agrees well with results already reported in literature [13]. For the application of chemical sensor, electrocatalysts are generally evaluated by monitoring the current response along with time at a fixed potential after addition of the analyte and possible interfering agents [39-40]. In order to detect the actual signals corresponding to the successive increment in glucose concentration at $Pd_{30}Au_{70}/C$, a chronoamperometric test was carried out on a rotating disk electrode (1600 rpm) at -0.2 V (*vs.* Hg/HgO), which is positive enough to oxidize the glucose molecules as clearly seen from CV results (Figure 4.9).

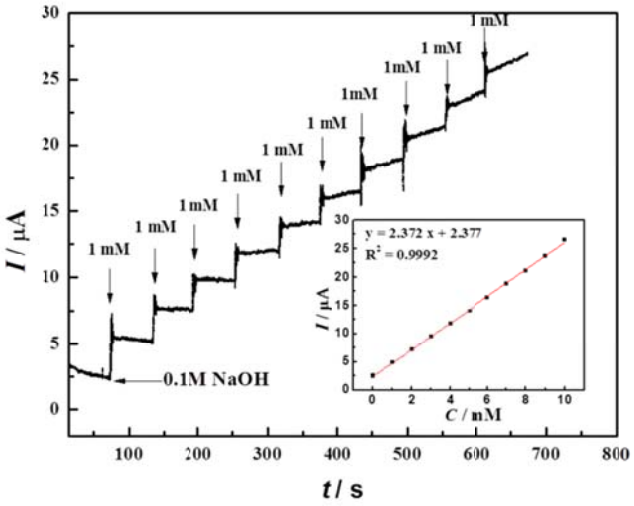

Figure 4.9. Current-time record of $Pd_{30}Au_{70}/C$ catalyst fixed onto rotating disk electrode (1600 rpm) by successively injection 1 mM glucose into 0.1 M NaOH solution at a regular interval time of 60 s. Applied potential: -0.2 V. Inset: the relationship between the current density and the added glucose solution.

As it is shown in Figure 4.9, once 1 mM glucose is successively injected into 0.1 mol L^{-1} NaOH solution, the current sharply increases and then decreases to relatively constant value. The current response time is very short (*ca.* 3 s). The corresponding calibration plot for current versus glucose concentration is linear in the investigated rang with a slope of 2.372 μA mM^{-1}. On one hand, in all the investigated glucose concentration range, obvious current signals are observed. On the other hand, along

with the subsequent addition of more glucose, the total current response decreases, especially in the last two additions, as it can also be seen from the calibration plot. This indicates the electrode is poisoned by the intermediate products of glucose oxidation to some extent.

Conclusions

Pd_xAu_y/C binary catalysts were synthesized by the modified pulse microwave assisted polyol method and investigated for glucose electrooxidation and detection. The composition of Pd_xAu_y/C catalysts could be controlled and adjusted by changing the corresponding composition ratio in the precursor solutions. Pd/C mono-metalic catalyst exhibits high activity towards glucose electrooxidation but not good poison tolerance. The introduction of Au is vital to relieve poisoning of Pd, and the optimum $Pd_{30}Au_{70}/C$ exhibits the desirable both activity to glucose oxidation and tolerance to the intermediate species produced from glucose oxidation. Pd_xAu_y binary catalysts are expecting to have potential applications for electrochemical glucose sensors or direct glucose fuel cells.

References

[1] M.L.B. Rao, R.F. Drake, J. Electrochem. Soc. 116 (1969) 334-337.

[2] U. Gebhardt, J.R. Rao, G.J. Richter, J. Appl. Electrochem. 6 (1976) 127-134.

[3] N. Mano, F. Mao, A. Heller, J. Am. Chem. Soc. 124 (2002) 12962-12963.

[4] A. Heller, Phys. Chem. Chem. Phys. 6 (2004) 209-216.

[5] D. Basu, S. Basu, Int. J. Hydrogen Energy 97 (2012) 4678-4684.

[6] Y.B. Vassilyev, O.A. Khazova, N.N. Nikolaeva, J. Electroanal. Chem. 196 (1985) 105-125.

[7] S. Park, T.D. Chung, H.C. Kim, Anal. Chem. 75 (2003) 3046-3049.

[8] K.B. Kokoh, J.M. Léger, B. Beden, H. Huser, C. Lamy, Electrochim. Acta 37 (1992) 1909-1918.

[9] Y.B. Vassilyev, O.A. Khazova, N.N. Nikolaeva, J. Electroanal. Chem. 196 (1985) 127-144.

[10] L. Li, K. Scott, E.H. Yu, J. Power Sources 221 (2013) 1-5.

[11] M. Pasta, L. Hu, F.L. Mantia, Y. Cui, Electrochem. Commun. 19 (2012) 81-84.

[12] M.W. Hsiao. R.R. Adžic, E.B. Yeager, J. Electrochem. Soc. 143 (1996) 759-767.

[13] S.P. Tung, T.K. Huang, C.Y. Lee, H.T. Chiu, RSC Adv. 2 (2012) 1068-1073.

[14] Q. Li, S. Cui, X. Yan, J. Solid State Electrochem. 16 (2012) 1099-1104.

[15] Z. Liu, L. Huang, L. Zhang, H. Ma, Y. Ding, Electrochim. Acta 54 (2009) 7286-7293.

[16] Q. Wang, X. Cui, J. Chen, X. Zheng, C. Liu, T. Xue, H. Wang, Z. Jin, L. Qiao, W. Zheng, RSC Adv. 2 (2012) 6245-6249.

[17] L.M. Lu, H.B. Li, F. Qu, X.B. Zhang, G.L. Shen, R.Q. Yu, Biosens. Bioelectron. 26 (2011) 3500-3504.

[18] Y. Kuang, B.H. Wu, D. Hu, X. Zhang, J. chen, J. Solid State Electrochem. 16 (2012) 759-766.

[19] C. Zhu, S. Guo, S. Dong, Adv. Mater. 24 (2012) 2326-2331.

[20] İ. Becerik, Turk. J. Chem. 23 (1999) 57-66.

[21] D. Basu, S. Basu, Electrochim. Acta 56 (2011) 6106-6113.

[22] H.F. Cui, J.S. Ye, X. Liu, W.D. Zhang, F.S. Sheu, Nanotechnology 17 (2006) 2334-2339.

[23] Y. Sun, H. Buck, T.E. Mallouk, Anal. Chem. 73 (2001) 1599-1604.

[24] A. Habrioux, E. Sibert, K. Servat, W. Vogel, K.B. Kokoh, N. Alonso-Vante, J. Phys. Chem. B 111 (2007) 10329-10333.

[25] Y. Yamauchi, A. Tonegawa, M. Komatsu, H. Wang, L. Wang, Y. Nemoto, N. Suzuki, K. Kuroda, J. Am. Chem. Soc. 134 (2012) 5100-5109.

[26] X. Yan, X. Ge, S. Cui, Nanoscale Res. Lett. 6 (2011) 313-319.

[27] Z. Liu, L. Huang, L. Zhang, Ho. Ma, Y. Ding, Electrochim. Acta 54 (2009) 7286-7293.

[28] J.S. Ye, Y. Wen, W.D Zhang, L.M. Gan, G.Q. Xu, F.S. Sheu, Electrochem. Commun. 6 (2004) 66-70.

[29] V.S. Bagotzky, Y.B. Vassilyev, Fuel cells, Their Electrochemical Kinetics, Consult. Bureau, New York, 1966, p. 77.

[30] S.B. Aoun, G.S. Bang, T. Koga, Y. Nonaka, T. Sotomura, I. Taniguchi, Electrochem. Commun. 5 (2003) 317-320.

[31] C. Bianchini, P.K. Shen, Chem. Rev. 109 (2009) 4183-4206.

[32] S. Hermans, A. Deffernez, M. Devillers, Appl. Catal. A: Gen. 395 (2011) 19-27.

[33] S.Q. Song, Y. Wang, P.K. Shen, J. Power Sources 170 (2007) 46-49.

[34] S.Q. Song, J.C. Liu, J.Y. Shi, H. Liu, V. Maragou, Y. Wang, P. Tsiakaras, Appl. Catal. B: Environ. 103 (2011) 287-293.

[35] V. Radmilovic, H.A. Gasteiger, P.N. Ross, J. Catal. 154 (1995) 98-106.

[36] A. Nirmala Grace, K. Pandian, J. Phys. Chem. Solids 68 (2007) 2278-2285.

[37] S.B. Aoun, Z. Dursun, T. Koga, G.S. Bang, T. Sotomura, I. Taniguchi, J. Electroanal. Chem. 567 (2004) 175-183.

[38] S.Z. Cui, The electrocatalytic oxidation of D-glucose based on nanoporous gold film, Shandong University Master's Thesis, 2010.

[39] J. Wang, G. Rivas, M. Chicharrro, J. Electroanal. Chem. 439 (1997) 55-61.

[40] M.S. Gelej, G. Rivas, Electroanal. 10 (1998) 771-775.

CHAPTER V

Pd_xRh_y/C binary catalysts for glucose electrooxidation*

Abstract

In the present work carbon Vulcan XC-72R supported PdxRh (x=1, 2, 3) nanoparticles have been prepared by a modified pulse microwave assisted polyol method and have been studied for glucose electrooxidation in alkaline media. The PdxRh/C electrocatalysts have been characterized by X-ray diffraction (XRD), Transmission Electron Microscopy (TEM), Cyclic Voltammetry (CV) and Chronoamperometric measurements (CA). The effects of the concentration of electrolyte and glucose as well as of temperature on the activity of glucose electrooxidation have been investigated. According to the CV results, the electro-catalytic activity towards glucose electrooxidation of the investigated catalysts has the following order: PdRh/C>Pd/C>Pd_2Rh/C>Pd_3Rh/C. It was found that increasing electrolyte's concentration until 1.0 M KOH the current density increases, while higher (> 1.0 M KOH) OH^- concentrations prevent the adsorption of glucose on the electrode. Moreover, increasing glucose's concentration from 0.02 M to 0.5 M the current increases for 0.1, 0.3, 0.5, 1.0 and 2.0 M KOH. Additionally, the increment of temperature enhances glucose electrooxidation until 36.5°C, while for temperatures > 36.5°C the catalytic activity decreases. Finally, electro-kinetic analysis of the PdRh/C show that further investigation is necessary.

*A. Brouzgou, L. Yan, S. Song, P. Tsiakaras, ***Glucose Electrooxidation on PdxRh/C Electrocatalysts in Alkaline Medium***, In Press, accepted for publication to Applied Catalysis B: Environmental (2014).

CONTENTS

CHAPTER V i

1. Introduction 151

2. Experimental 153

2.1. Materials 153

2.2. Catalyst preparation 153

2.3. Physicochemical Characterization 154

2.4. Electrochemical Characterization 154

3. Results & Discussion 155

3.1. Characterization of Pd_xRh/C 155

3.2. Electrochemical Characterization 157

3.2.1. Glucose Electrooxidation 157

3.2.2. Effect of concentration of electrolyte and glucose 159

3.2.3. Effect of varying potential sweep rate 162

3.2.4. Effect of temperature 164

3.2.5. Chronoamperometric measurements 165

Conclusions 166

References 168

List of Tables

Table 5.1. Structural parameters of the as prepared catalysts.....156

Table 5.2. Electrocatalytic kinetic parameters on different electrodes in 0.5 mol L^{-1} KOH, at 25 ^{o}C, 20 mV s^{-1}.....159

List of Figures

Figure 5.1. XRD results of the as-prepared carbon supported Pd_xRh/C electrocatalysts. 155

Figure 5.2. TEM images of (A) PdRh/C, (B) Pd_2Rh/C, (C) Pd_3Rh/C and (D) Pd/C..156

Figure 5.3. Cyclic voltammograms of the PdxRh/C electrocatalysts in: (A) 0.5 mol L^{-1} KOH solution and (B) 0.5 mol L^{-1} KOH containing 0.5 mol L^{-1} glucose (scan rate: 20 mV s^{-1}, room temperature). 158

Figure 5.4. Cyclic voltammograms of the PdRh/C electrocatalyst in: (A) 0.1, (B) 0.3, (C) 0.5 and (D) 1 mol L^{-1} KOH containing y (=0.02, 0.05, 0.2, and 0.5 mol L^{-1}) glucose (scan rate: 20 mV s^{-1}, room temperature). Fig. 5.4 (E): Peak current desnsity in terms of KOH's and glucose's concentration.....160

Figure 5.5. (A) Cyclic voltammograms of PdRh/C electrocatalyst in 0.5 mol L^{-1} KOH containing (=0.02, 0.05, 0.2, and 0.5 mol L^{-1}) glucose (scan rate: 5 mV s^{-1}, room temperature), (B) Tafel plots derived from Fig. 5.5 (A). 161

Figure 5.6. (A) Cyclic voltammograms of the PdRh/C electrocatalyst in 0.5 mol L^{-1} KOH containing 0.5 mol L^{-1} glucose at different scan rates in room temperature, (B) Anodic peak current density vs. square root of scan rate, extracted from Fig.5.6 (A), (C)Peak potential vs. ln(v) extracted from Fig. 5.6 (A).....163

Figure 5.7. (A) Cyclic voltammograms of PdRh/C at different temperature values (T=25, 36.5, 48 and 60^{o}C), in 0.5 mol L^{-1} KOH containing 0.5 mol L^{-1} glucose, 5 mV s^{-1}, (B) Arrhenius plots for the Pd_xRh/C and Pd/C electrocatalysts derived from cyclic voltammograms at 5 mV s^{-1}. 164

Figure 5.8. Chronoamperometric curves at -0.13 V (vs. Hg/HgO) for 1300 sec, in a 0.5 mol L^{-1} KOH with 0.5 mol L^{-1} glucose solution.....166

1. Introduction

Glucose is the most abundant carbohydrate in nature easily produced by photosynthesis in plants such as sugar cane or corn and by a large amount of waste biomass generated by agricultural activities [1, 2]. The theoretical energy of glucose is 4430 Wh kg^{-1} and its complete oxidation to carbon dioxide can produce 24 electrons for each glucose molecule through the following chemical reactions:

Anode reaction: $C_6H_{12}O_6 + 24OH^- \rightarrow 6CO_2 + 18H_2O + 24e^-$ (1)

Cathode reaction: $6O_2 + 12H_2O + 24e^- \rightarrow 24OH^-$ (2)

Overall reaction: $C_6H_{12}O_6 + 6O_2 \rightarrow 6CO_2 + 6H_2O$ (3)

A potential approach to obtain energy from glucose is to be used as fuel of a fuel cell, where glucose can be directly oxidized generating electricity, similarly to direct methanol (DMFCs) [3, 4] and direct ethanol fuel cells (DEFCs) [5, 6].

The electrooxidation of glucose has mainly two purposes: i) in vivo applications (as human implantable devices that will power microelectromechanical (MEMS) devices [7, 8] and ii) the development of glucose electrochemical sensors for diabetes check. Glucose could be virtually withdrawn without limit from the flow of blood providing a long-term or even permanent power supply for such devices as pacemakers, glucose sensors for diabetics or small valves for bladder control. Consequently, many attempts have been mainly focused on the development of enzymatic and microbial glucose fuel cells. More precisely, in the past few decades most researches had been turned to the immobilization methods for enzymatic catalysts in an effort to increase the lifetime of enzymes and therefore of glucose fuel cells [9-15]. Enzymatic catalysts for glucose/O_2 fuel cells have excellent selectivity and can produce power densities of several mW cm^{-2}. However, they have very short lifetime, typically less than thirty days, due to the fragile nature of the enzymes and poor immobilization techniques. This makes them generally unsuitable for long-term

implantable applications despite having been successfully tested in-vivo. Thus, recently, there has been an increase interest in non-enzymatic glucose fuel cells where platinum [16-21] and gold alloys [16, 20-23] are mainly used as anodes electrocatalysts and usually activated carbon as cathode electrocatalyst [24-26].

The reported results prove that such fuel cells present much better stability having been successfully tested in-vivo [27]. However, the poor anode selectivity towards glucose oxidation in the presence of oxygen is still the biggest challenge for direct in-vivo glucose fuel cells. Recently, Kerzenmacher *et al.* [7, 8, 28] proposed novel DGFC structures with Raney platinum or Raney platinum doped with zinc electrodes as anode and thin layer platinum as cathode, and they examined their compatibility with a body tissue environment. The Raney-platinum fuel cells exhibited a power density of up to (4.4 ± 0.2) μW cm^{-2} with 7.0% oxygen saturation, despite the limited oxygen supply. This high performance was attributed to the increased oxygen tolerance of the Raney-platinum film anodes.

At present, Pt [17, 29], Au [22, 30] and their bi-metallic catalysts, Pt-Bi [25], Pt-Pd [31], Pt-Ru [24], Pt-Au [21, 26], Ag-Au [32-34] and their tri-metallic catalysts [35] have been studied for glucose electrooxidation. There are also some researches [36-39] that have examined Pd-based electrocatalysts for glucose electrooxidation. It has been proved [40] that Pd presents better activity than Pt and Au towards alcohols electrooxidation in alkaline media, reducing at the same time the high cost of the electrodes, if it is considered that last year the cost of platinum was double of that of palladium [41]. However, the cost of rhodium was almost the same with platinum's one [41]. For this reason also electrocatalysts with very low rhodium amount are also studied and investigated in the present manuscript.

In the present investigation, we report for first time the study of glucose electrooxidation over 20%wt Pd_xRh/C (x=1, 2, 3) electrocatalysts. Since in literature there is no similar work, this constitutes a novelty and a first step for further investigation of modified PdRh/C electrocatalysts. The home-made electrocatalysts were physicochemically characterized by X-ray diffraction (XRD) and transmission

electron microscope (TEM) techniques. Cyclic voltammetry (CV) and Chronoamperometry (CA) techniques were used to evaluate their electrocatalytic activity and their stability to glucose electrooxidation. The results are compared with those of a home-made Pd carbon supported (Pd/C) (20 wt.% metal).

2. Experimental

2.1. Materials

Carbon powder Vulcan XC-72R (Cabot Corporation) was used as support. $PdCl_2$ and $RhCl_3$ were the platinum and rhodium precursors, respectively. All aqueous solutions were prepared by ultrapure water (18.2 MΩ cm Millipore–MilliQ) during catalyst preparation. Ethanol (>99% purity) (Sigma Aldrich) and Nafion® (5 wt%, IonPower, GmbH) were used for catalyst ink preparation. D-glucose (99.5% pure, assay) and KOH (>85% assay, flakes purified), fuel and electrolyte, respectively were provided by Sigma Aldrich.

2.2. Catalyst preparation

The 20 wt. % Pd_xRh/C ($x=1,2,3$ denotes the molar ratio for Pd) electrocatalysts were fast and easily prepared by a pulse-microwave assisted polyol synthesis method [42]. The primary steps of this synthesis process are given as follows: In a beaker, the starting precursors ($PdCl_2$ and $RhCl_4$) were well mixed with ethylene glycol (EG) in an ultrasonic bath, and then XC-72 R carbon black (Cabot Corp.) was added into the mixture. After the pH value of the system was adjusted to be 13 by the drop-wise addition of 1.0 mol L^{-1} NaOH/EG, a well-dispersed slurry was obtained with ultrasonic stirring for 30 min. Thereafter, the slurry was microwave-heated in the pulse form with every 10 s for several times. In order to promote the adsorption of the suspended metal nanoparticles onto the support, hydrochloric acid was adopted as the sedimentation promoter and the solution was re-acidified with a pH value of about 3-4.

The resulting black solid sample was filtered, washed and dried at 80 °C for 10 h in a vacuum oven. For the sake of comparison, 20 wt.% Pd/C was also prepared and examined in the same way.

2.3. Physicochemical Characterization

The X-ray Diffraction (XRD) measurements were carried out by the aid of a D/Max-IIIA (Rigaku Co., Japan) employing Cu K_α (λ = 0.15406 nm) as the radiation source. The samples were scanned over the range $10° \leq 2\theta \leq 86°$. The peak at 68° (Pd 220) was used for the calculation of crystallites size. Catalysts were also investigated by transmission electron microscopy (TEM) using a Philips CM12 microscope (resolution 0.2nm), provided with high resolution camera, at an accelerating voltage of 120 kV.

2.4. Electrochemical Characterization

Three-electrode cell assembly connected to electrochemical station (AMEL 5000) was used for the CV and CA measurements. Hg/HgO (in 1.0 mol L^{-1} KOH) and platinum wire electrodes were adopted as reference and counter electrodes, respectively. The working electrode was a glassy carbon electrode (d=3.0 mm). The catalyst slurry was prepared with the aid of magnetic stirrer, dispersing 5.0 mg of the as-prepared electrocatalyst powder in 1.8 mL ethanol and 0.2 mL Nafion® ionomer for 40 min [43]. The catalyst ink was then quantitatively (10 µL) transferred onto the surface of the glassy carbon disk electrode by using a micropipette and dried under infrared lamp to obtain a catalyst thin film. Initially, in order to find out the most active electrocatalyst towards glucose electrooxidation, CV measurements were carried out in aqueous solution containing 0.5 mol L^{-1} KOH in absence and in presence of 0.5 mol L^{-1} glucose. Before each measurement the solution was deareated for 30 min with high-purity nitrogen gas to remove the dissolved oxygen from the aqueous solution. The potential window ranged from −0.8 to 1.2 V (*vs.* Hg/HgO) at a sweeping rate of 20 mV s^{-1}. Additionally, the effects of glucose's (0.02, 0.05, 0.2 and 0.5 mol L^{-1}) and the electrolyte's concentration (0.1, 0.3, 0.5,

1.0 and 2.0 mol L^{-1} KOH) were separately investigated over the PdRh/C electrocatalyst which presented the best performance among the examined electrocatalysts. Moreover, the influence of temperature and scan rate in 0.5 mol L^{-1} KOH containing 0.5 mol L^{-1} glucose aqueous solution was studied. It should be noted that the potential is referred to Hg/HgO (1 mol L^{-1} NaOH) reference electrode without specification.

3. Results & Discussion

3.1. Characterization of Pd_xRh/C

XRD patterns of the as-prepared electrocatalysts are shown in Figure 5.1. As it is observed there are no noticeable peaks for phase-separated structures such as Rh metals, which is probably due to the formation of Pd_xRh/C alloys, reported also in literature [44]. The first peak at 25° is associated with the Vulcan XC-72 support material for all the four samples. There are five observed characteristic diffraction peaks at *ca.* 38°, 45°, 65°, 79° and 83° belonging to the face-centered cubic (fcc) phase of Pd (111), (200), (220), (311) and (222), respectively. The Pd (111) plane has the largest intensity among those planes, which becomes more intense as the palladium ratio increases (Pd_3Rh/C) [45]. Moreover as the palladium ratio increases the peak position slightly shifts to more positive angles (PdRh/C=38.826°, Pd_2Rh/C=38.96°, Pd_3Rh/C=38.81°) indicating that part of the Rh has been alloyed with Pd [46].

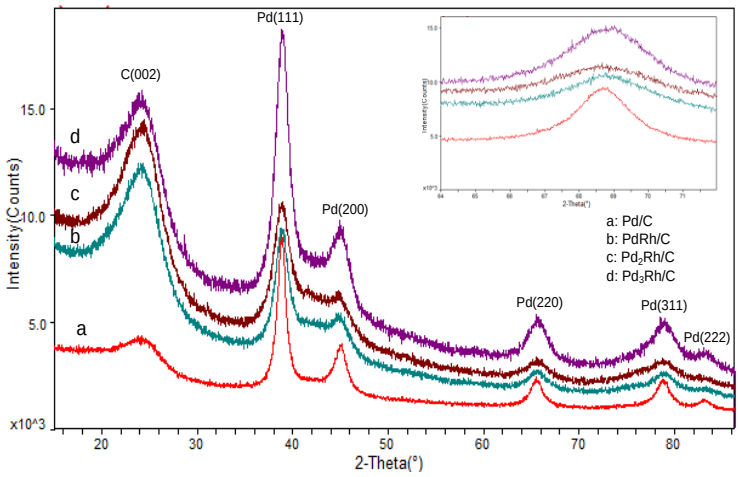

Figure 5.1. XRD results of the as-prepared carbon supported Pd_xRh/C electrocatalysts.

In Table 5.1, the crystallites size and the corresponding lattice parameters calculated from the Pd (220) diffraction line using the Scherrer formula and Bragg equations are summarized [47, 48]. It can be clearly seen that the lattice parameter decreases in the following order: $Pd_3Rh/C > Pd_2Rh/C > Pd/C > PdRh/C$.

Table 5.1. Structural parameters of the as prepared catalysts.

Catalysts	Crystalline Size (nm)	Lattice parameter (nm)	Particle Size (nm)
Pd/C	8.2	0.38645	5<d<10
PdRh/C	7.0	0.38593	5<d<10
Pd_2Rh/C	22	0.38796	5<d<12
Pd_3Rh/C	14	0.38961	5<d<10

The surface morphology of the prepared Pd_xRh/C electrocatalysts was examined by TEM. TEM images in Figure 5.2 (A, B, C & D) show a successful loading dispersion of PdRh/C and Pd_3Rh/C, Pd/C nanoparticles onto the surface of carbon substrate.

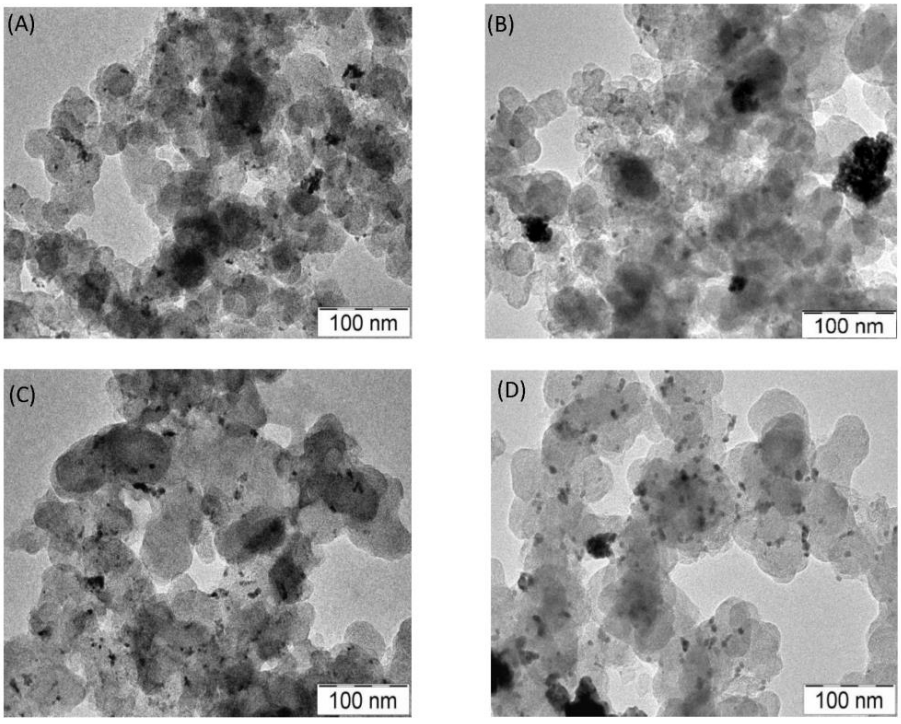

Figure 5.2. TEM images of (A) PdRh/C, (B) Pd_2Rh/C, (C) Pd_3Rh/C and (D) Pd/C.

3.2. Electrochemical Characterization

3.2.1. Glucose Electrooxidation

In Figure 5.3 (A & B) the voltammetric curves of Pd/C, PdRh/C, Pd_2Rh/C and Pd_3Rh/C electrocatalysts in 0.5 mol L^{-1} KOH (Figure 5.3 (A)) and in 0.5 mol L^{-1} KOH + 0.5 mol L^{-1} glucose (Figure 5.3 (B)) are depicted. In the case of Pd-based electrocatalysts the electrochemical active surface area (EASA) is calculated by determining the coulombic charge (Q) for the reduction of palladium oxide (peak IV in Figure 5.3 (A)) [49]. The values of the EASA, reported in Table 5.2, are estimated using the following equation:

$$EASA = Q/S*I \quad (4)$$

where '*S*' is the proportionality constant used to relate charge with area and '*l*' is the catalyst loading in '*gr*'. A charge value of 405 μC cm^{-2} is assumed for the reduction of PdO monolayer [50]. The calculated electrochemical active surface areas have the following order $EASA_{PdRh/C}$ (26 m^2 g^{-1}) > $EASA_{Pd2Rh/C}$ (14.8 m^2 g^{-1}) > $EASA_{Pd3Rh/C}$ (12.8 m^2 g^{-1}) > $EASA_{Pd/C}$ (10.3 m^2 g^{-1}) .

In Figure 5.3 (A) during the positive-going sweep, three oxidation peaks can be observed which correspond to different electrochemical processes occurring on the surface of the Pd electrode [51]. Peak I in the potential range between −0.6 V and −0.4 V is due to the oxidation of the absorbed hydrogen [52-54]. Peak III, which emerges above −0.25 V, could be attributed to the formation of palladium (II) oxide layer on the surface of the catalyst. Although the mechanism of this oxidation process remains unclear, it has been widely accepted that OH^- ions are firstly chemisorbed in the initial stage of the oxide formation, and then at higher potentials they are transformed into higher valence oxides, as described by [54-56]. The adsorption of OH^- starts at the far negative potential from the onset potential of the Pd oxidation (peak II). As it can be observed peak II is more intense for the Pd/C sample. Finally, peak IV can be attributed to the reduction of the Pd(II) oxide during the cathodic sweep [54, 55].

In Figure 5.3 (B) are depicted the cyclic voltammograms of the Pd_xRh/C and Pd/C electrocatalysts in 0.5 mol L^{-1} solution containing 0.5 mol L^{-1} glucose. As it can be seen, the electrocatalytic activity towards glucose electrooxidation has the following order: PdRh/C > Pd/C > Pd_2Rh/C > Pd_3Rh/C. In the case of lower Rh content, its effect on Pd's activity towards glucose electrooxidation is decreased. Moreover the onset potential for PdRh/C is much lower than that of the other electrocatalysts. As far as Pd/C electrocatalyst is concerned, despite the fact that it presents high activity, the onset potential of glucose oxidation shifts to higher potential (more positive) values and the peak potential also occurs at higher potential value.

During the forward scan one peak is formed for all the examined electrocatalysts, which can be attributed to the formation of palladium oxides [57] and glucose electrosorption of glucose to form an adsorbed intermediate. The decrease in current at potentials more positive with respect to the peak could be due to the formation of thick palladium oxide which competes for surface adsorption sites with glucose and in turn inhibits the electrooxidation of glucose as well [58].

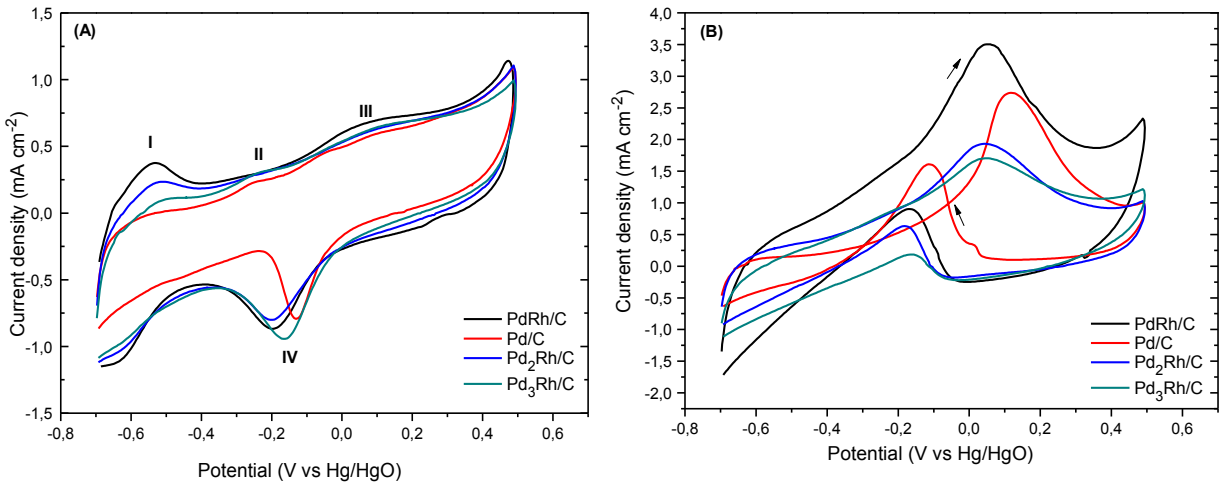

Figure 5.3. Cyclic voltammograms of the PdxRh/C electrocatalysts in: (A) 0.5 mol L^{-1} KOH solution and (B) 0.5 mol L^{-1} KOH containing 0.5 mol L^{-1} glucose (scan rate: 20 mV s^{-1}, room temperature).

During the reverse scan, oxidation of glucose happens, in the potential region in which the surface oxides are reduced. The reduction of the surface palladium oxides

occur at potential values more negative than -0.1 V (*vs* Hg/HgO) and enough surface active sites are available for the direct oxidation of glucose. Therefore, there is a sharp increase in anodic current with the peak at -0.10 V (*vs.* Hg/HgO) for the Pd/C and at -0.16 V (*vs.* Hg/HgO) for the rest electrocatalysts.

Table 5.2. Electrocatalytic kinetic parameters on different electrodes in 0.5 mol L^{-1} KOH, at 25 ^{o}C, 20 mV s^{-1}.

Catalysts (20 wt.%)	Pd loading (μg cm^{-2})	EASA (m^2 g^{-1})	Onset potential (V vs. Hg/HgO)	I_f (peak current density, mA cm^{-2})	I_b (peak current density, mA cm^{-2})
Pd/C	72	10.3	-0.19	2.73	1.60
PdRh/C	36	26.0	-0.55	3.50	0.90
Pd_2Rh/C	48.2	14.8	-0.34	1.93	0.63
Pd_3Rh/C	54	12.8	-0.34	1.70	0.18

By shifting the potential to more negative values, the electrosorption of glucose on the catalyst surface starts again, resulting in the accumulation of intermediates on the electrocatalyst surface leading again to the decrease of the anodic current as it is shown in Figure 5.3 (B).

3.2.2. Effect of concentration of electrolyte and glucose

The effect of different: i) KOH concentrations of 0.1, 0.3, 0.5, 1 and 2.0 mol L^{-1} and ii) glucose concentrations of 0.02, 0.05, 0.2 and 0.5 mol L^{-1}, for the reaction of glucose electrooxidation, are investigated over PdRh/C electrocatalyst, which presented the highest catalytic activity to glucose electrooxidation. The results are presented in Figure 5.4.

The oxidation current increases almost linearly as the KOH concentration increases from 0.1 to 1.0 mol L^{-1}. However, further increase in the concentration of KOH (> 1 M KOH) leads to a decrease of the peak current density. The same behavior was observed by Liang *et al.* [51]. From this behavior one might deduce that glucose

oxidation can be accelerated by the presence of OH^- anions, leading to an increase in the anodic peak.

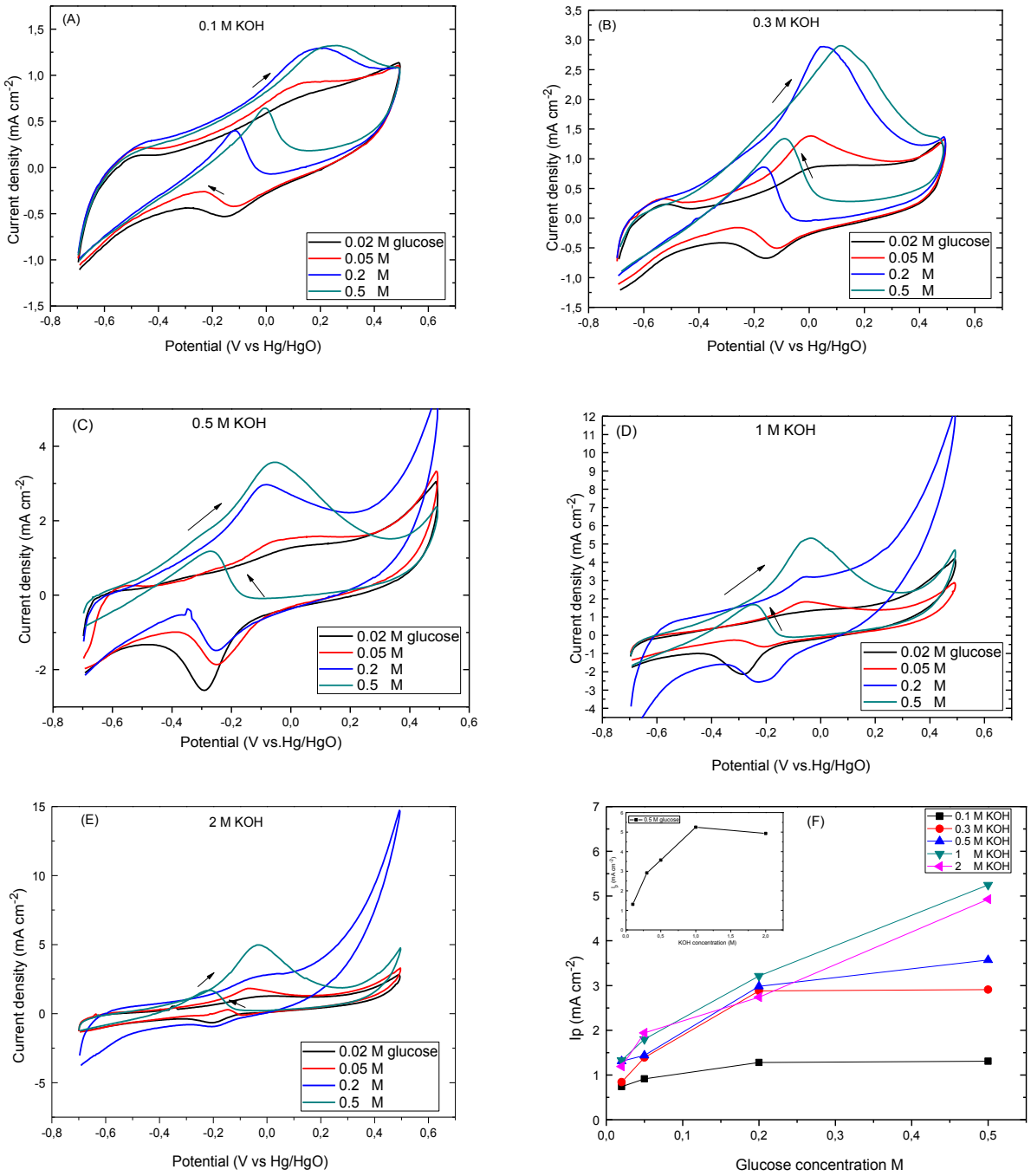

Figure 5.4. Cyclic voltammograms of the PdRh/C electrocatalyst in: (A) 0.1, (B) 0.3, (C) 0.5 and (D) 1 mol L^{-1} KOH containing y (=0.02, 0.05, 0.2, and 0.5 mol L^{-1}) glucose (scan rate: 20 mV s^{-1}, room temperature). Fig. 5.4 (E): Peak current desnsity in terms of KOH's and glucose's concentration.

However, at concentrations higher than 1.0 M KOH the adsorption of the OH^- anions on Pd prevents the adsorption of glucose on it [51]. Furthermore, the peak potential shifts to more negative values with the increase of KOH's concentration, while at all the examined electrolyte's concentration values, the peak potential shifts to more positive values with the increase of glucose's concentration. The maximum current density reaches 5.2 mA cm^{-2} for 1.0 mol L^{-1} KOH containing 0.5 mol L^{-1} glucose.

Tafel plots are obtained from the onset region of the polarization curves [59] from the limiting form of the ButlerVolmer:

$$logi=logi_o+(a_a nF/2.303RT)\eta \quad (5)$$

,where η is the overpotential, i_o is the exchange current density and a_a is the anodic transfer coefficient, n are the electrons involved in the reaction, F is the Faraday's constant, R is the universal gas constant and T the temperature.

In Figure 5.5(A) the voltammetric curves for glucose electrooxidation taken for 5 mV s^{-1} scan rate are depicted. In order to reduce the mass transfer effect as much as possible and to derive kinetic parameters the scan rate was low.

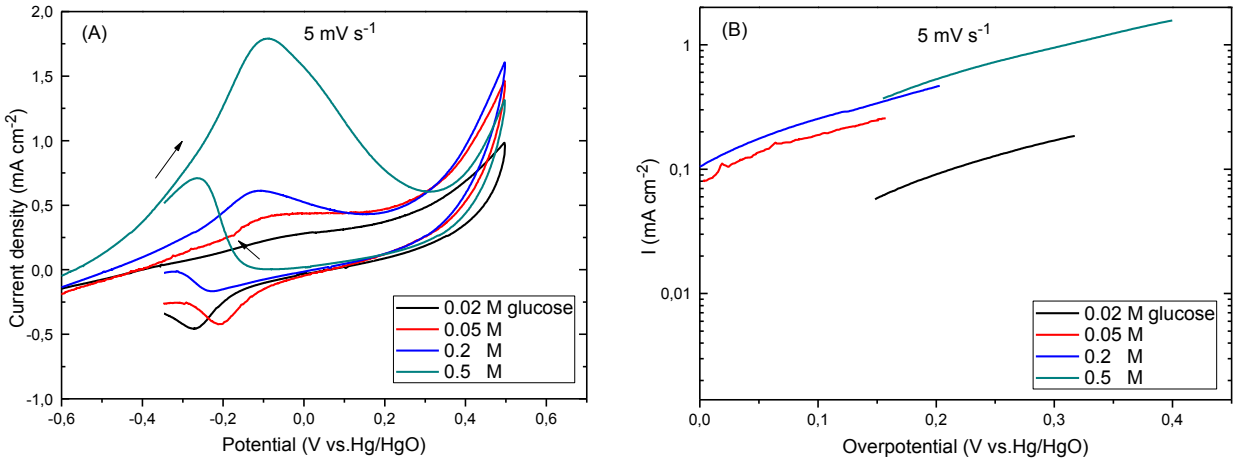

Figure 5.5. (A) Cyclic voltammograms of PdRh/C electrocatalyst in 0.5 mol L^{-1} KOH containing (=0.02, 0.05, 0.2, and 0.5 mol L^{-1}) glucose (scan rate: 5 mV s^{-1}, room temperature), (B) Tafel plots derived from Fig. 5.5 (A).

Figure 5.5Figure 5.5 (B) derives from Figure 5.5 (A) and the exchange current density is calculated according to Ref. [59]. From Figure 5.5 (B) the exchange current density values (i_o) are calculated: 0.02, 0.09, 0.12 and 0.17 mA cm^{-2}, for 0.02, 0.05, 0.2 and 0.5 mol L^{-1} glucose, respectively. The calculated values of the exchange current densities according to literature [60] are reasonable.

The *a* value was calculated 0.17<0.5 (for all the four cases), indicating according to the theory of analytical electrochemistry [61, 62] an irreversible diffusion control process. Comparing the result with other works in literature the calculated value is reasonable. Becerik. [63] studied glucose electrooxidation at platinum-palladium electrodes calculating *a*=0.4, while Hu *et al.* [64] studying the electrooxidation of glucose at palladium predicted *a*=0.5. From the low values of the exchange current density it is obvious that further research is necessary in order to obtain higher activity.

3.2.3. Effect of varying potential sweep rate

The effect of scan rate on the peak current density at PdRh/C in 0.5 mol L^{-1} KOH + 0.5 mol L^{-1} glucose is shown in Figure 5.6.

It is observed that the peak current density increases rapidly by increasing the potential scan rate from 5 to 200 mV s^{-1}. Moreover, the shift of the peak potential to higher values is possibly due to the IR drop generated at high current density values [65]. As it is observed in Figure 5.6 (B) the line does not cross through the origin which can be ascribed to the fact that the rate-determining step of glucose oxidation involves adsorption and diffusion. Similar results have been also reported from Hu *et al.* [64].

The linear relationship between the square root of the scan rate and the peak current density (Figure 5.6 (B)), proves that the control of the overall glucose oxidation reaction is controlled by the mass transport of the glucose from the bulk solution to the electrode surface [66]. In general, for an electrochemical oxidation reaction, the linear relationship between E_p and $\ln(v)$ can be represented by the following equation (Laviron's theory) [67-69]:

$$E_p = E^o + \frac{RT}{anF}\ln\frac{RTk_s}{anF} - \frac{RT}{anF}\ln v \qquad (6)$$

where α is the transfer coefficient, k_s is the electron transfer rate parameter, v is the scan rate and E^o is the standard potential. The plot of E_p *vs.* $\ln v$ should be linear.

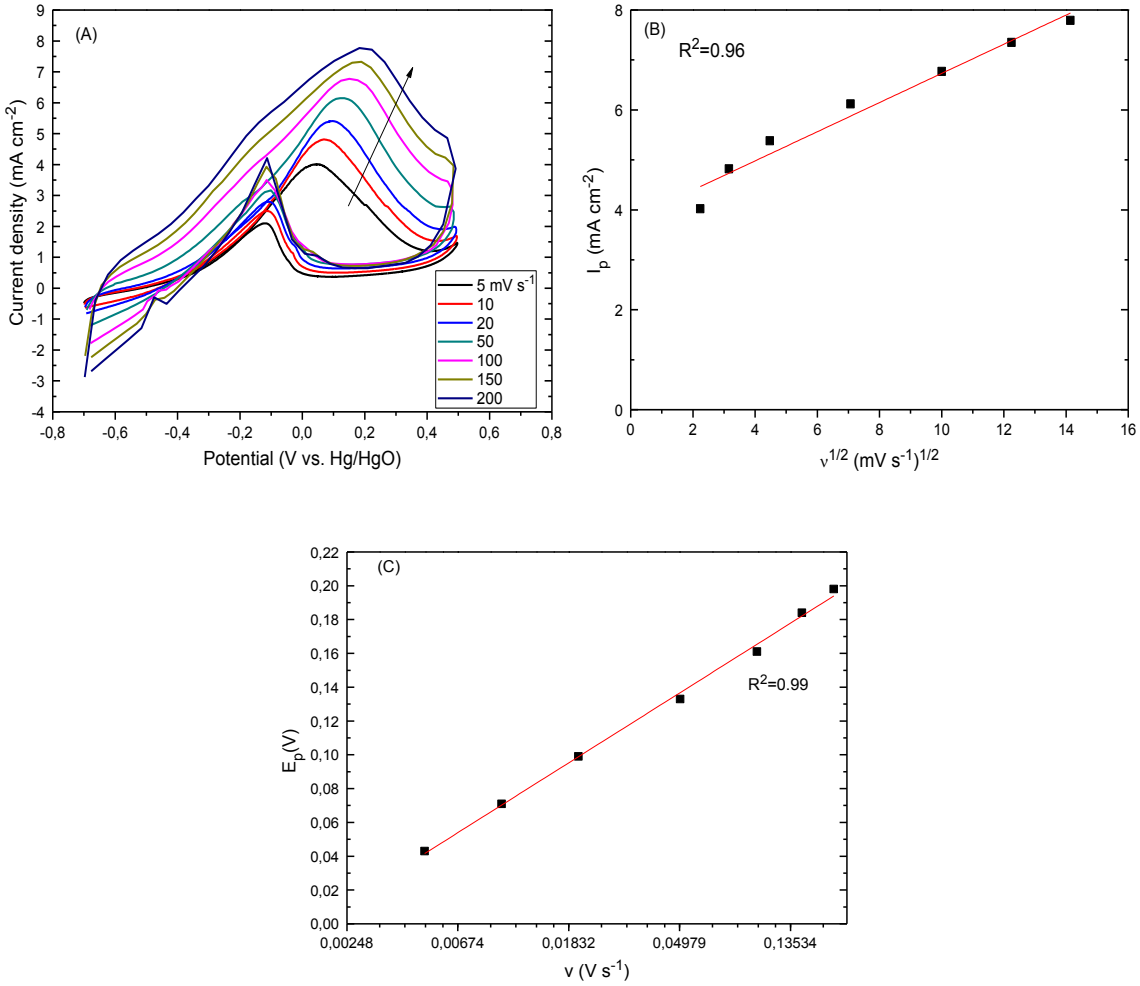

Figure 5.6. (A) Cyclic voltammograms of the PdRh/C electrocatalyst in 0.5 mol L^{-1} KOH containing 0.5 mol L^{-1} glucose at different scan rates in room temperature, (B) Anodic peak current density vs. square root of scan rate, extracted from Fig.5.6 (A), (C)Peak potential vs. ln(v) extracted from Fig. 5.6 (A).

From its slope the an product can be determined; from its intercept the k_s can be calculated if the values of E^o is known. The E^o can be also estimated from the intercept of E_p *vs.* v plot on the coordinate by extrapolating to $v = 0$ [70].

From Figure 5.6 (C) it can also be seen that the E_p (positive scan) rises with the increase of ν and shows the linear relationship between E_p and $\ln(\nu)$, indicating that the oxidation of glucose is an irreversible charge transfer process. The irreversibility of the reaction is also obvious from the cyclic voltammogram curves, since the reduction curve continues at positive current density values. In case of reversibility the reduction curve should be the mirror (negative current densities) of the first oxidation peak. According to Laviron's theory the electron transfer rate was calculated, k_s=1 s^{-1}.

3.2.4. Effect of temperature

The effect of temperature (T=25-60ºC) on the electrooxidation of glucose is also investigated. Figure 5.7 (A) shows the CVs over the PdRh/C electrode for glucose oxidation at different temperature values.

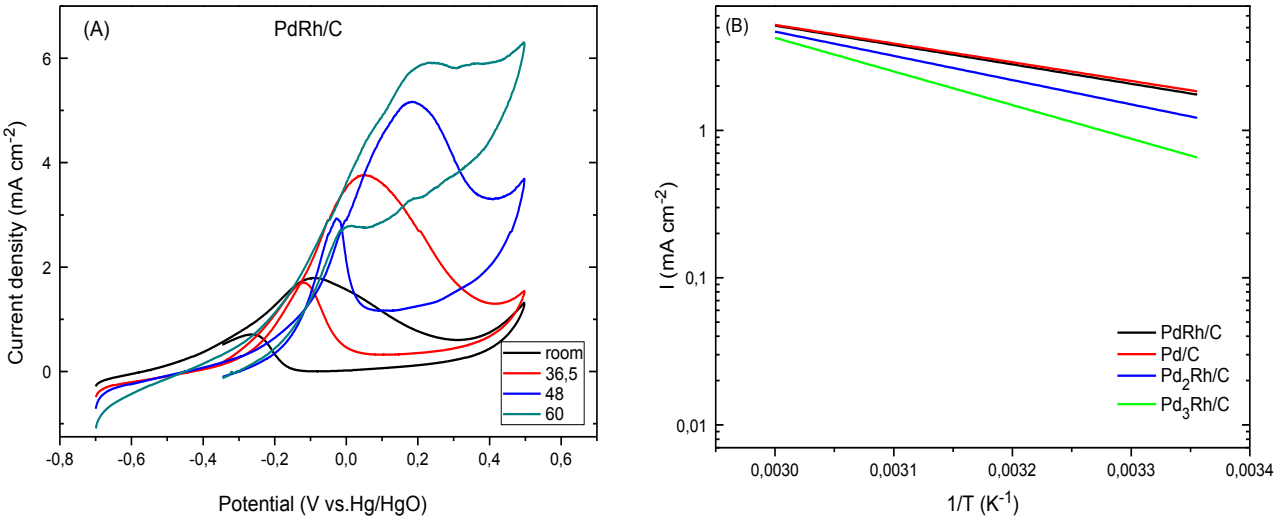

Figure 5.7. (A) Cyclic voltammograms of PdRh/C at different temperature values (T=25, 36.5, 48 and 60ºC), in 0.5 mol L^{-1} KOH containing 0.5 mol L^{-1} glucose, 5 mV s^{-1}, (B) Arrhenius plots for the Pd_xRh/C and Pd/C electrocatalysts derived from cyclic voltammograms at 5 mV s^{-1}.

The increase in temperature causes an evident increase in the anodic peak current density until 36.5ºC. This behavior is justified since it agrees with the results reported by Yei *et al.* [71] .

According to them glucose degraded rapidly above 40°C as evidenced by a rapid change of color to yellow-brown and caramel like smell. The same degradation phenomena were also observed during our experiments. As it is observed, in Figure 5.7 (A), increasing the temperature the baseline of the cyclic voltammograms curves shifts up to higher current densities. However, the net current density decreases for T > 36.5°C. The same behavior was observed for the rest electrocatalysts.

The activation energy E_a can be obtained from the currents measured at different temperatures using the following equation:

$$E_a = R(d(lnI) / d(1/T)) \quad (7)$$

The activation energy Ea was calculated at specific potential value (at 0.06, 0.24, 0.245 and 0.097V (vs.Hg/HgO), for PdRh/C, Pd_2Rh/C Pd_3Rh/C and Pd/C, respectively) from the cyclic voltammograms in 0.5 mol L^{-1} KOH containing 0.5 mol L^{-1} glucose at 5 mV s^{-1} [72].

The activation energy E_a was calculated to be 25.0, 24.3, 31.0 and 43.0 kJ mol^{-1} for the PdRh/C, Pd/C, Pd_2Rh/C and Pd_3Rh/C, respectively. Low activation energy means high intrinsic activity. Obviously, PdRh/C electrocatalyst exhibits the highest activity to glucose electrooxidation among the investigated samples. The estimated activation energy values almost coincide with those estimated by Hu *et al.* [64], implying that the formed $PdOH_{ads}$ exhibit a catalytic property for glucose electrooxidation similar to a radical reaction.

3.2.5. Chronoamperometric measurements

Chronoamperometric experiments were carried out to observe the stability and possible poisoning of the catalysts under short time continuous operation.

Figure 5.8 depicts the evaluation of activity of PdRh/C, Pd_2Rh/C, Pd_3Rh/C and Pd/C electrodes along with time at a constant applied potential of -0.13 V (*vs.* Hg/HgO) for 1300 s._ The long-term poisoning rate (d) is calculated by measuring the linear decay

of the current for a period of more than 500 s from Figure 5.8 by using the following equation [73]:

$$\delta = (100 / Io)(dI / dt)_{t>500s} \quad (8)$$

where $(dI / dt)_{t>500s}$, is the slope of the linear portion of current decay and I_o is the current at the start of polarization back extrapolated from the linear current decay.

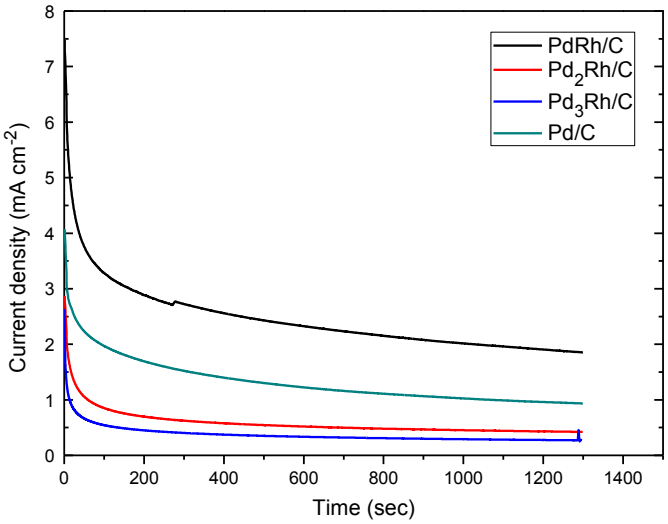

Figure 5.8. Chronoamperometric curves at -0.13 V (vs. Hg/HgO) for 1300 sec, in a 0.5 mol L^{-1} KOH with 0.5 mol L^{-1} glucose solution.

The poisoning rate is found to be 0.01, 0.0056, 0.018 and 0.0019 % s^{-1} for the PdRh/C, Pd_2Rh/C, Pd_3Rh/C and Pd/C, respectively. From the values, obviously, the poison rate at PdRh/C is the highest one, which means that it is more easily poisoned.

Conclusions

Novel Pd_xRh/C electrocatalysts for glucose electrooxidation were synthesized by a pulse microwave assisted polyol technique and characterized by the XRD, TEM, CV and CA techniques. From TEM characterizations the nanoparticles size was estimated at ~10 nm. Furthermore, according to the electrochemical results the addition of Rh can increase the activity of Pd towards glucose oxidation in alkaline medium. However, PdRh/C is poisoned easier than the other electrocatalysts. The study of the

effect of glucose and electrolyte's concentration shows that for 1 mol L^{-1} KOH containing 0.5 mol L^{-1} glucose the highest catalytic activity can be exhibited. For electrolyte's concentration higher than 1 mol L^{-1} KOH the electrocatalytic activity decreases due to the great number of hydroxide ions which may block the glucose's adsorption on the electrode's surface. Kinetic data were also extracted from studying the effect of sweep rate. The electron transfer rate for the PdRh/C was calculated k_s=1s^{-1}. Finally, it has been found that the increase of temperature until 36.5 °C enhances the electrocatalytic activity, while at higher temperature values the rapid degradation of glucose solution suppresses electrocatalysts' catalytic activity. Consequently, PdRh/C is a good candidate for glucose electrooxidation reaction and further investigation in a direct glucose fuel cell or sensor would be very promising.

References

[1] J.P.H. Van Wyk, Trends Biotechnol. 19 (2001) 172-177.

[2] K.C. Swades, R.L. Derek, Nat. Biotechnol. 21 (2003) 1229-1232.

[3] S. Song, W. Zhou, Z. Liang, R. Cai, G. Sun, Q. Xin, V. Stergiopoulos, P. Tsiakaras, Appl. Catal., B 55 (2005) 65-72.

[4] C. Feng, T. Takeuchi, M.A. Abdelkareem, T. Tsujiguchi, N. Nakagawa, J. Power Sources 242 (2013) 57-64.

[5] Y. Wang, S. Song, G. Andreadis, H. Liu, P. Tsiakaras, J. Power Sources 196 (2011) 4980-4986.

[6] G. Andreadis, V. Stergiopoulos, S. Song, P. Tsiakaras, Appl. Catal., B 100 (2010) 157-164.

[7] S. Kerzenmacher, M. Schroeder, R. Brämer, R. Zengerle, F. Von Stetten, J. Power Sources 195 (2010) 6516-6523.

[8] S. Kerzenmacher, U. Kräling, M. Schroeder, R. Brämer, R. Zengerle, F. von Stetten, J. Power Sources 195 (2010) 6524-6531.

[9] S.C. Barton, H.-H. Kim, G. Binyamin, Y. Zhang, A. Heller, J. Am. Chem. Soc. 123 (2001) 5802-5803.

[10] S.C. Barton, J. Gallaway, P. Atanassov, Chem. Rev. 104 (2004) 4867-4886.

[11] H.-H. Kim, Y. Zhang, A. Heller, Anal. Chem. 76 (2004) 2411-2414.

[12] S. Shleev, J. Tkac, A. Christenson, T. Ruzgas, A.I. Yaropolov, J.W. Whittaker, L. Gorton, Biosens. Bioelectron. 20 (2005) 2517-2554.

[13] R.A. Bullen, T.C. Arnot, J.B. Lakeman, F.C. Walsh, Biosensors Bioelectron. 21 (2006) 2015-2045.

[14] C. Kang, H. Shin, A. Heller, Bioelectrochem. 68 (2006) 22-26.

[15] F. Gao, Y. Yan, L. Su, L. Wang, L. Mao, Electrochem. Commun. 9 (2007) 989-996.

[16] F. Jia, C. Yu, K. Deng, L. Zhang, J. Phys. Chem. C 111 (2007) 8424-8431.

[17] Q. Shen, L. Jiang, H. Zhang, Q. Min, W. Hou, J.-J. Zhu, J. Phys. Chem. C 112 (2008) 16385-16392.

[18] A. Kloke, C. Kloke, R. Zengerle, S. Kerzenmacher, J. Phys. Chem. C 116 (2012) 19689-19698.

[19] C.A. Apblett, D. Ingersoll, S. Sarangapani, M. Kelly, P. Atanassov, Direct Glucose Fuel Cell: Noble Metal Catalyst Anode Polymer Electrolyte Membrane Fuel Cell with Glucose Fuel, 2010, pp. B86-B89.

[20] F. Xie, Z. Huang, C. Chen, Q. Xie, Y. Huang, C. Qin, Y. Liu, Z. Su, S. Yao, Electrochem. Commun. 18 (2012) 108-111.

[21] X. Yan, X. Ge, S. Cui, Nanoscale Research Letters 6 (2011) 313.

[22] W. Huang, M. Wang, J. Zheng, Z. Li, J. Phys. Chem. C 113 (2009) 1800-1805.

[23] M. Pasta, R. Ruffo, E. Falletta, C.M. Mari, C.D. Pina, Gold Bulletin 43 (2010) 57-64.

[24] D. Basu, S. Basu, Electrochim. Acta 55 (2010) 5775-5779.

[25] D. Basu, S. Basu, Electrochim. Acta 56 (2011) 6106-6113.

[26] D. Basu, S. Basu, Int. J. Hydrogen Energy 36 (2011) 14923-14929.

[27] V. Oncescu, D. Erickson, High volumetric power density, non-enzymatic, glucose fuel cells, Scientific Reports, 2013.

[28] S. Kerzenmacher, U. Kräling, T. Metz, R. Zengerle, F. von Stetten, J. Power Sources 196 (2011) 1264-1272.

[29] N. Fujiwara, S.-i. Yamazaki, Z. Siroma, T. Ioroi, H. Senoh, K. Yasuda, Electrochem. Commun. 11 (2009) 390-392.

[30] H. Yin, C. Zhou, C. Xu, P. Liu, X. Xu, Y. Ding, J. Phys. Chem. C 112 (2008) 9673-9678.

[31] J.P. Spets, Y. Kiros, M.A. Kuosa, J. Rantanen, M.J. Lampinen, K. Saari, Electrochim. Acta 55 (2010) 7706-7709.

[32] Z. Liu, L. Huang, L. Zhang, H. Ma, Y. Ding, Electrochim. Acta 54 (2009) 7286-7293.

[33] C. Jin, I. Taniguchi, Mater. Lett. 61 (2007) 2365-2367.

[34] F.M. Cuevas-Muñiz, M. Guerra-Balcázar, F. Castaneda, J. Ledesma-García, L.G. Arriaga, J. Power Sources 196 (2011) 5853-5857.

[35] D. Basu, S. Basu, Int. J. Hydrogen Energy 37 (2012) 4678-4684.

[36] Q. Yi, F. Niu, W. Yu, Thin Solid Films 519 (2011) 3155-3161.

[37] L. An, T.S. Zhao, S.Y. Shen, Q.X. Wu, R. Chen, J. Power Sources 196 (2011) 186-190.

[38] Q. Wang, X. Cui, J. Chen, X. Zheng, C. Liu, T. Xue, H. Wang, Z. Jin, L. Qiao, W. Zheng, RSC Advances 2 (2012) 6245-6249.

[39] L.-M. Lu, H.-B. Li, F. Qu, X.-B. Zhang, G.-L. Shen, R.-Q. Yu, Biosens. Bioelectron. 26 (2011) 3500-3504.

[40] A. Brouzgou, A. Podias, P. Tsiakaras, J. Appl. Electrochem. 43 (2013) 119-136.

[41] A. Brouzgou, S.Q. Song, P. Tsiakaras, Appl. Catal., B 127 (2012) 371-388.

[42] S. Song, Y. Wang, P.K. Shen, J. Power Sources 170 (2007) 46-49.

[43] C. He, S. Song, J. Liu, V. Maragou, P. Tsiakaras, J. Power Sources 195 (2010) 7409-7414.

[44] S. Lee, H.J. Kim, S.M. Choi, M.H. Seo, W.B. Kim, Appl. Catal., A 429-430 (2012) 39-47.

[45] X.G. Tang, Q.X. Liu, L.L. Jiang, A.L. Ding, Mater. Chem. Phys. 103 (2007) 329-333.

[46] W. He, H. Jiang, Y. Zhou, S. Yang, X. Xue, Z. Zou, X. Zhang, D.L. Akins, H. Yang, Carbon 50 (2012) 265-274.

[47] A. Pozio, M. De Francesco, A. Cemmi, F. Cardellini, L. Giorgi, J. Power Sources 105 (2002) 13-19.

[48] T. Lopes, E. Antolini, F. Colmati, E.R. Gonzalez, J. Power Sources 164 (2007) 111-114.

[49] R. Pattabiraman, Appl. Catal. A-Gen. 153 (1997) 9-20.

[50] M.H. Seo, S.M. Choi, H.J. Kim, W.B. Kim, Electrochem. Commun. 13 (2011) 182-185.

[51] Z.X. Liang, T.S. Zhao, J.B. Xu, L.D. Zhu, Electrochim. Acta 54 (2009) 2203-2208.

[52] T. Takamura, K.i. Minamiyama, J. Electrochem. Soc. 112 (1965) 333-335.

[53] J. Prabhuram, R. Manoharan, H.N. Vasan, J. Appl. Electrochem. 28 (1998) 935-941.

[54] M. Grdeń, A. Czerwiński, J. Solid State Electrochem. 12 (2008) 375-385.

[55] M.C. Jeong, C.H. Pyun, I.H. Yeo, J. Electrochem. Soc. 140 (1993) 1986-1989.

[56] L. Vračar, S. Burojević, N. Krstajić, Int. J. Hydrogen Energy 23 (1998) 1157-1164.

[57] I. Becerik, F. Kadirgan, Electrochim. Acta 37 (1992) 2651-2657.

[58] L. Meng, J. Jin, G. Yang, T. Lu, H. Zhang, C. Cai, Anal. Chem. 81 (2009) 7271-7280.

[59] B.K. Boggs, G.G. Botte, Electrochim. Acta 55 (2010) 5287-5293.

[60] T. Maiyalagan, K. Scott, J. Power Sources 195 (2010) 5246-5251.

[61] J. Wang, Analytical Electrochemistry, Canada, 2006.

[62] M. Shamsipur, M. Najafi, M.-R.M. Hosseini, Bioelectrochem. 77 (2010) 120-124.

[63] I. Becerik, Turk. J. Chem. 23 (1999) 57-66.

[64] C.-C. Hu, T.-C. Wen, Electrochim. Acta 39 (1994) 2763-2771.

[65] M.A. Abdel Rahim, R.M. Abdel Hameed, M.W. Khalil, J. Power Sources 134 (2004) 160-169.

[66] M. Noroozifar, M. Khorasani-Motlagh, R. Khaleghian-Moghadam, M.-S. Ekrami-Kakhki, M. Shahraki, J. Solid State Chem. 201 (2013) 41-47.

[67] E. Laviron, J. Electroanal. Chem. Interf. Electrochem. 101 (1979) 19-28.

[68] E. Laviron, L. Roullier, Journal of Electroanalytical Chemistry and Interfacial Electrochemistry 115 (1980) 65-74.

[69] H. Tang, J. Chen, S. Yao, L. Nie, Y. Kuang, Z. Huang, D. Wang, Z. Ren, Mater. Chem. Phys. 92 (2005) 548-553.

[70] P. Sharma, B. Sikarwar, G. Gupta, A. Nigam, B. Tripathi, P. Pandey, M. Boopathi, K. Ganesan, B. Singh, Appl Nanosci (2012) 1-10.

[71] L.H.E. Yei, B. Beden, C. Lamy, J. Electroanal. Chem. 246 (1988) 349-362.

[72] S.T. Nguyen, D.S. Ling Tan, J.-M. Lee, S.H. Chan, J.Y. Wang, X. Wang, Int. J. Hydrogen Energy 36 (2011) 9645-9652.

[73] Z.H. Teng, G. Wang, B. Wu, Y. Gao, J. Power Sources 164 (2007) 105-110.

CHAPTER VI

Pd_xSn_y/C binary catalysts for glucose Electrooxidation*

Abstract

PdSn (20 wt%) and Pd_3Sn_2 (20 wt%) nanoparticles supported on Vulcan XC-72 carbon powders were prepared by a modified microwave-assisted polyol method and studied for glucose electrooxidation in alkaline media. The as-prepared electro-catalysts were characterized by X-Ray Diffraction (XRD), Transmitting Electron Microscope (TEM), Cyclic Voltammetry (CV) and Chronoamperometry (CA). For comparison reasons, Pd/C (20 wt%) was also prepared. According to the CV results, the electrochemical active surface areas (EASA) were in the order of Pd_3Sn_2/C > PdSn/C > Pd/C (28.8, 22.8 and 10.3 $m^2\ g^{-1}$). For glucose electrooxidation, at room temperature Pd_3Sn_2/C exhibited the highest electrocatalytic activity, 3.64 mA cm^{-2}, which increased to 5.7 mA cm^{-2} when the temperature increased to 40°C. The effect of the concentration of both electrolyte and glucose on the activity was also studied and it was found that the increase of the amount of electrolyte and glucose enhances glucose electrooxidation. Additionally, from chronoamperometric results, the diffusion coefficients of glucose were calculated to be 7.8×10^{-9}, 1.52×10^{-9} and 1.79×10^{-9} $cm^2\ s^{-1}$ for Pd_3Sn_2/C, PdSn/C and Pd/C, respectively.

*A. Brouzgou, S. Song, P. Tsiakaras, ***Carbon-supported PdSn and Pd_3Sn_2 Anodes for Direct Glucose Alkaline Fuel Cells,*** in press corrected proof, International Journal of Hydrogen Energy (2013).

CONTENTS

CHAPTER VI..... 172

1. Introduction..... 175

2. Experimental..... 176

2.1. Electrocatalysts Preparation..... 176

2.2. Electrocatalysts Characterization..... 177

2.2.1. Physico-chemical Characterization..... 177

2.2.2. Electrochemical Characterization..... 177

3. Results and discussion..... 178

3.1. Physico-chemical Characterization..... 178

3.2. Electrochemical Characterization..... 180

3.2.1. Electrochemical active surface area (EASA)..... 180

3.2.2. Glucose electrooxidation reaction (GOR)..... 183

3.2.3. Effect of glucose's and electrolyte's concentration..... 184

3.2.4. Effect of the scan rate..... 187

3.2.5. The effect of temperature..... 188

3.2.6. Chronoamperometric measurements..... 190

Conclusions..... 191

References..... 192

List of Tables

Table 6.1. Structural parameters of the as-prepared catalysts. 179
Table 6.2. Electrocatalytic kinetic parameters on different electrodes in 0.5 M KOH, ... 182
Table 6.3. Cyclic voltammetry parameters on different electrodes in 0.5 M KOH + 0.5 glucose, at 25 ^{o}C, 20 mV s^{-1}. 184

List of Figures

Figure 6.1. XRD results of the as-prepared carbon supported Pd/C and PdxSny/C electrocatalysts. 179
Figure 6.2. TEM images of Pd_3Sn_2/C (A), PdSn/C (B) and Pd/C (C). 180
Figure 6.3. Cyclic voltammogram for Pd/C, PdSn/C and Pd_3Sn_2/C in 0.5 M KOH at 25 ^{o}C, 20 mV s^{-1}. 181
Figure 6.4. Cyclic voltammogram for Pd/C, PdSn/C and Pd3Sn2/C in 0.5 M KOH + 0.5 M Glucose at 25 ^{o}C, 20 mV s^{-1}. 183
Figure 6.5. Cyclic voltammograms of the Pd_3Sn_2/C electrocatalyst in: (A) 0.1, (B) 0.3, (C) 0.5 (D) 1 and 2 M KOH containing y (=0.02, 0.05, 0.2, and 0.5 M) glucose (scan rate: 20 mV s^{-1}, room temperature). Fig. 6.5 (F): Peak current density dependence of glucose's concentration. 185
Figure 6.6. Cyclic voltammograms of Pd_3Sn_2/C electrocatalyst in 0.5 mol L^{-1} KOH containing (=0.02, 0.05, 0.2, and 0.5 mol L^{-1}) glucose (scan rate: 5 mV s^{-1}, room temperature). Inset: Tafel plots. 186
Figure 6.7. (A) Cyclic voltammograms of the Pd_3Sn_2/C electrocatalyst in 0.5 M KOH containing 0.5 M glucose at different scan rates in room temperature. Inset: Dependence of anodic peak current during the forward sweep on the square roots of potential sweep rate, (B) E_p *vs.* ln(v). 187
Figure 6.8. Cyclic voltammograms at different temperature values (T=25, 30, 36.5 and 40^{o}C), in 0.5 mol L^{-1} KOH containing 0.5 mol L^{-1} glucose, 5 mV s^{-1} of: Pd_3Sn_2/C, PdSn/C and Pd/C . Arrhenius plots (second graph). 189
Figure 6.9. Chronoamperometric curves at -0.13 V (vs. Hg/HgO) for 1300 sec, in a 0.5 mol L^{-1} KOH with 0.5 mol L^{-1} glucose solution. 191

1. Introduction

Glucose has been started attracting much interest mostly due to its high energy content (4430 Wh kg^{-1}) and its importance as fuel in Direct Glucose Fuel Cells (DGFCs) and their applications as implantable human devices [1-3].

Its complete oxidation to carbon dioxide can produce 24 electrons per molecule of glucose through the following chemical equations:

Anode reaction: $C_6H_{12}O_6 + 24OH^- \rightarrow 6CO_2 + 18H_2O + 24e^-$ (1)

Cathode reaction: $6O_2 + 12H_2O + 24e^- \rightarrow 24OH^-$ (2)

Overall reaction: $C_6H_{12}O_6 + 6O_2 \rightarrow 6CO_2 + 6H_2O$ (3)

However further research is necessary since glucose is a very stable and difficult oxidized molecule and up to date glucose oxidation has gone through a process generating only two electrons [4], yielding gluconic acid according to the following chemical equations:

Anode reaction: $C_6H_{12}O_6 + 2OH^- \rightarrow C_6H_{12}O_7 + H_2O + 2e^-$ (4)

Cathode reaction: $0.5O_2 + H_2O + 2e^- \rightarrow 2OH^-$ (5)

Overall reaction: $C_6H_{12}O_6 + 0.5O_2 \rightarrow C_6H_{12}O_7$ (6)

According to literature alkaline membrane fuel cells tend to perform superior performance than proton conducting membrane fuel cells [5]. More precisely when the electrolyte is changed from acidic to alkaline the enhanced kinetics of the GOR and ORR in alkaline media compared with those in acid media [6]. Moreover, in an AEM-DGFC the direction of the electro-osmotic drag is from the cathode to the anode, which can reduce the rate of fuel crossover from the anode to cathode and thereby improve cell performance [7, 8]. In addition, the cost of AEMs is much lower than that of PEMs' (typically Nafion®).

In literature many attempts [9-13] have been done to develop efficient and stable electrocatalysts for glucose electro-oxidation mostly in alkaline media. Many of them have been focused on Pt [4, 14] and Au [15, 16] or on their bi-metallic catalysts, Pt-Bi [11], Pt-Pd [17], Pt-Ru [18], Pt-Au [9, 19], Ag-Au [20-22] and tri-metallic catalysts [23], while Pd-based electrocatalysts have not been yet studied towards glucose electrooxidation.

Pd-based electro-catalysts have been proved [5, 24] to perform much better activity than Pt-based ones in alkaline environment due to the quicker oxidation kinetics of various alcohols' electrooxidation. In acidic environment among the reported electrocatalysts, PtSn-based ones [25, 26] have been proved to be the most appropriate for ethanol electrooxidation which is a difficult oxidized molecule.

Consequently based on the two above-mentioned facts and taking into consideration at the same time that glucose as ethanol [27] is a hardly oxidizable molecule, we consider that Pd-based electrocatalysts can be good candidates for glucose electrooxidation. The two electrocatalysts were compared with Pd/C prepared in the same way. Physicochemical characterization of the catalysts was conducted using Transmitting Electron Microscopy (TEM) and X-ray diffraction (XRD). Their electrocatalytic activity towards glucose electrooxidation was examined by cyclic voltammetry (CV) and their stability and poisoning rate during time by chronoamperometric measurements. Moreover, the effect of temperature, glucose's and electrolyte's concentration was also investigated.

2. Experimental

2.1. Electrocatalysts Preparation

PdSn and Pd_3Sn_2 supported on Vulcan-XC 72 carbon electrocatalysts (the metal loading was 20 wt% for all the catalysts) were prepared by a modified pulse-microwave assisted polyol synthesis procedure. In a beaker, the starting precursors ($PdCl_2$ and $SnCl_2$ provided by Strem Chemicals) were well mixed with ethylene glycol (EG) in an

ultrasonic bath, and then XC-72 R carbon black (Cabot Corporation) was added into the above mixture. After the pH value of the system was adjusted to be 13 by the drop-wise addition of 1.0 M NaOH/EG, a well-dispersed slurry was obtained with ultrasonic stirring for 60 min. Thereafter, the slurry was microwave-heated in the pulse form 10sec on/10sec off for several times. In order to promote the adsorption of the suspended metal nanoparticles onto the carbon support, hydrochloric acid was adopted as the sedimentation promoter and the solution was re-acidified with a pH value of about 2-4. The resulting black solid sample was filtered, washed and dried at 80°C for 10 h in a vacuum oven. For the sake of comparison, 20 wt% Pd/C was also prepared in the same way and it was examined for glucose electrooxidation.

2.2. Electrocatalysts Characterization

2.2.1. *Physico-chemical Characterization*

The X-ray Diffraction (XRD) measurements were carried out by the aid of a D/Max-IIIA (Rigaku Co., Japan) employing Cu K_α (λ = 0.15406 nm) as the radiation source at 40 kV and 40 mA. The morphology of the as-prepared catalysts was obtained by Transmitting Electron Microscopy (TEM). For sample preparation, the catalysts were ultrasonically dispersed in ethanol solution to get uniform catalyst ink and fixed onto a copper grid. The TEM investigations were performed on a JEOL TEM-2010 (HR) operating at 200 kV.

2.2.2. *Electrochemical Characterization*

All the electrochemical measurements were conducted with AMEL 5000 electrochemical station in a three-electrode model cell 497 (AMEL) with a mercury/mercury oxide (Hg/HgO) and platinum wire as the reference electrode and counter electrode, respectively. The thin catalyst film was prepared onto the glassy carbon disk surface with a diameter of 0.3 cm. A mixture containing 5.0 mg

electrocatalyst, 1.8 mL ethanol and 0.2 mL Nafion solution (5 wt%, IonPower, GmbH) was ultrasonicated for 40 min to obtain a well-dispersed ink. The catalyst ink was then quantitatively (10 μL) transferred onto the surface of the glassy carbon electrode and dried under infrared lamp to obtain a catalyst thin film. The electrochemical tests were performed initially in 0.5 M KOH (Sigma Aldrich) aqueous solutions containing 0.5 M glucose (Sigma Aldrich), for the electrochemical activity evaluations. Then the effect of the concentration of the electrolyte (0.1, 0.3, 0.5, 1 and 2 M KOH) for varies glucose concentration (0.02, 0.05, 0.2 and 0.5 M glucose) was investigated. Moreover, the effect of temperature (25-40^{o}C) on glucose electrooxidation was also investigated. Before each experiment, the solution was bubbled with high-purity N_2 for 30 minutes in order to remove the dissolved oxygen. It should be noted that all the potential is referred to Hg/HgO reference electrode without specification.

3. Results and discussion

3.1. Physico-chemical Characterization

XRD patterns for the as-prepared electrocatalysts are shown in Figure 6.1. The first peak at 25^{o} is associated with the Vulcan XC-72 support material for all the four samples. There are four observed characteristic diffraction peaks at *ca* 38°, 45°, 65°, 79° and 83° belonging to the face-centered cubic (fcc) phase of Pd (111), (200), (220), (311) and (222), respectively.

The (1 1 1) plane has the largest intensity among those planes, which becomes more intense as the palladium ratio is increased (Pd_3Sn_2/C). The two peaks that appear at *ca* 33° and 50° are attributed to the Sn plane (101) and (211), respectively.

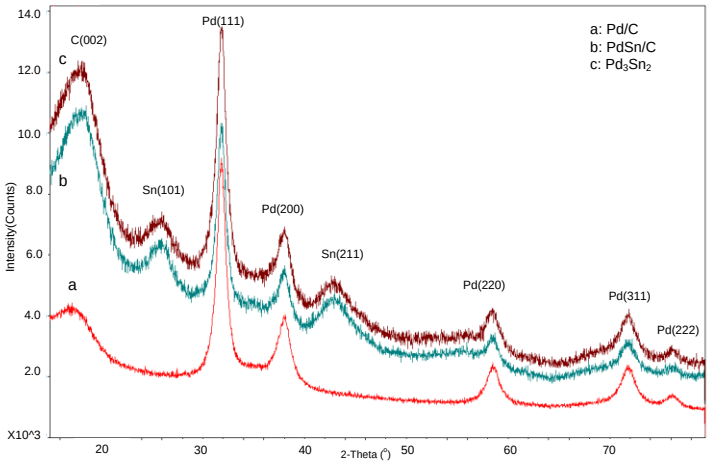

Figure 6.1. XRD results of the as-prepared carbon supported Pd/C and PdxSny/C electrocatalysts.

Table 6.1 lists the crystallites sizes and the corresponding lattice parameters calculated from the Pd (2 2 0) diffraction peak using the Scherrer formula and Bragg equations [28]. It can be clearly seen (Table 6.1) that the lattice parameter decreases in the order: Pd/C ≈ PdSn/C > Pd_3Sn_2/C.

Table 6.1. Structural parameters of the as-prepared catalysts.

Catalysts	Crystallite Size (nm)	Nanoparticles size (nm)	Lattice parameter (nm)
Pd/C	8.2	8.0<d<10.0	0.38645
PdSn/C	8.1	~8.0	0.38645
Pd_3Sn_2/C	7.8	~8.0	0.38636

Figure 6.2 depicts the typical TEM images for Pd/C, PdSn/C and Pd_3Sn_2/C. Obviously, Pd/C and Pd_3Sn_2/C have better dispersion than PdSn/C.

For the binary catalysts, the metal particle size becomes smaller than that of the single metal. These results agree with those of the XRD spectra, although the calculated particle size from XRD is a little bit bigger than the value calculated from the TEM micrographs.

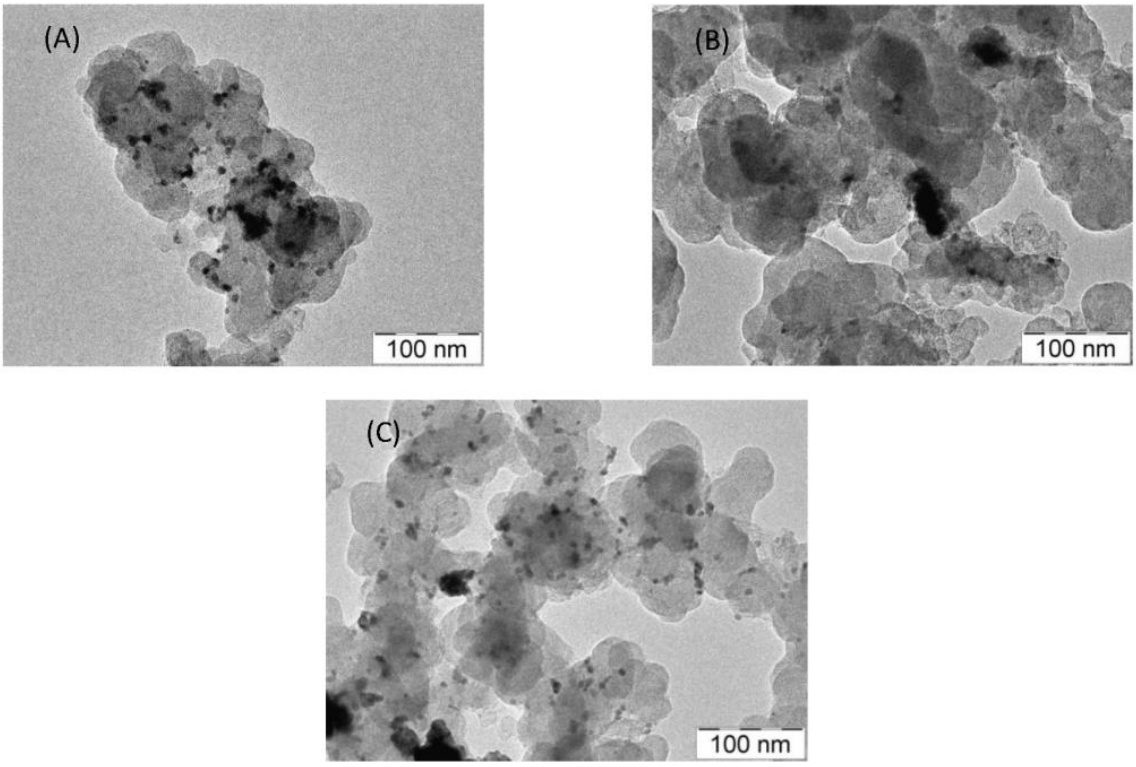

Figure 6.2. TEM images of Pd_3Sn_2/C (A), PdSn/C (B) and Pd/C (C).

3.2. Electrochemical Characterization

3.2.1. Electrochemical active surface area (EASA)

The CV technique was used to determine the catalytic activity towards glucose electrooxidation and the electrochemical active surface area of the examined electrocatalysts. The catalytic activity of an electrode material is known to depend upon its geometrical and its electronic properties. As described elsewhere [29], the EASAs of the electrodes have been measured by determining the coulombic charge (Q) for the reduction of palladium oxide (as it is indicated from the ellipse in Figure 6.3) of CV measurements in 0.5 M KOH, at 25 ^{o}C for 20 mV s^{-1} scan rate (Figure 6.3).

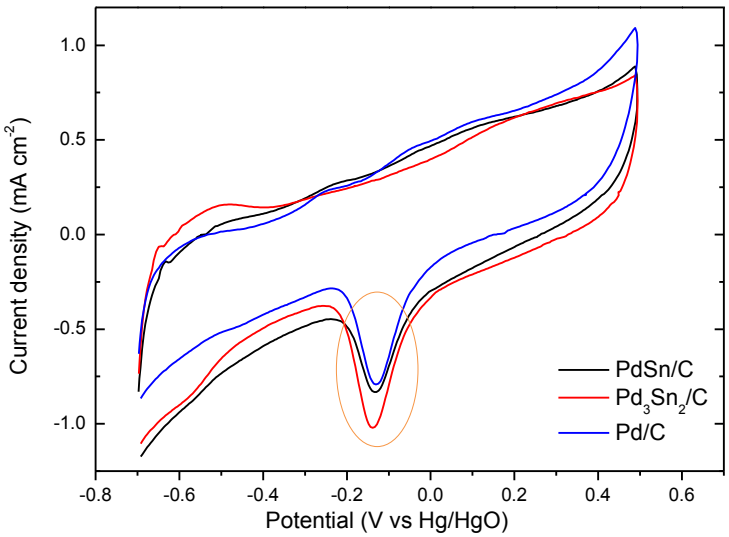

Figure 6.3. Cyclic voltammogram for Pd/C, PdSn/C and Pd_3Sn_2/C in 0.5 M KOH at 25 °C, 20 mV s^{-1}.

Calculated values of the EASA, as shown in Table 6.2, were estimated using the following equation:

$$EASA=Q/S*I \quad (7)$$

where '*S*' is the proportionality constant used to relate charge with area and '*l*' is the catalyst loading in '*g*'. A charge value of 405 µC cm^{-2} is assumed for the reduction of PdO monolayer [30].

As it can be clearly seen from the CV curves reported in Figure 6.3, Pd_3Sn_2/C shows stronger peaks characteristics of PdO reduction in the potential range between -0.2 and 0 V (*vs.* Hg/HgO) than the other electrocatalysts. This demonstrates that Pd_3Sn_2/C has a higher electrochemical active surface area compared to Pd/C, PdSn/C and Pd_3Sn_2/C, as it is also reported in Table 6.2.

Additionally, the percent Pd-utilization (=100 x observed EASA, m^2 g^{-1}/448 m^2 g^{-1}) was estimated by considering the surface area for 100% utilization of 1 g Pd as ~448 m^2 (=charge required to reduce 1 g Pd^{+2}, 1813.3 C/ 405 µC cm^{-2}) [31]. The Pd utilization is the highest for the Pd_3Sn_2, as it was expected (Table 6.2).

Table 6.2. Electrocatalytic kinetic parameters on different electrodes in 0.5 M KOH, at 25 °C, 20 mV s^{-1}.

Catalysts (20 wt%)	Pd loading (μg cm^{-2})	EASA (m^2 g^{-1})	Pd utilization %
Pd/C	72.0	10.3	2.29
PdSn/C	34.0	22.8	2.45
Pd_3Sn_2/C	41.0	28.8	3.60

Additionally, from Figure 6.3, it can be observed a typical electrochemical behavior of Pd-based electrocatalysts. The first peak from -0.6 to -0.4 V (*vs.* Hg/HgO) can be attributed to the oxidation of the adsorbed hydrogen [31-33].

The peak that is appeared from -0.3 to -0.1 V (*vs.* Hg/HgO) is ascribed to adsorbed OH^- which partially overlaps the hydrogen desorption peak, while the third peak which starts from -0.1 to 0.3 V (*vs.* Hg/HgO) can be attributed to the formation of the palladium (II) oxide layer on the surface of the catalyst. In general, the mechanism of glucose oxidation process on Pd-based electrocatalysts remains unclear. However, it has been widely accepted that OH^- ions are first chemisorbed in the initial stage of the oxide formation, and then they are transformed into higher valence oxides at higher potentials, as described by [34-36]:

$$Pd\text{-}H_{abs/ads} + OH^- \rightarrow Pd + H_2O + e^- \quad (8)$$

$$Pd + OH^- \rightleftarrows Pd\text{-}OH_{ads} + e^- \quad (9)$$

$$Pd\text{-}OH_{ads} + OH^- \rightleftarrows Pd\text{-}O + H_2O + e^- \quad (10)$$

$$Pd\text{-}OH_{ads} + Pd\text{-}OH_{ads} \rightleftarrows Pd\text{-}O + H_2O \quad (11)$$

During the backward scan the reduction of the Pd(II) oxides (according to eq.5) is responsible for the negative peak at ~-0.15 V (*vs.* Hg/HgO) [34, 36]:

$$Pd\text{-}O + H_2O + 2e^- \rightleftarrows Pd + 2OH^- \quad (12)$$

3.2.2. *Glucose electrooxidation reaction (GOR)*

The CV results for the GOR, depicted in Figure 6.4, clearly indicate that Pd_3Sn_2/C exhibits the highest electrocatalytic activity.

Its enhanced activity (compared with Pd/C and PSn/C) could be attributed to its small lattice parameter, its small crystallite size (7.8 nm) and to the higher utilization of Pd. According to Figure 6.4, during the forward scanning, the formation of palladium oxides (PdO) at ~0.1 V (*vs*.Hg/HgO) and glucose electrosorption of glucose forming an adsorbed intermediate, take place.

Moreover, the hydrogen desorption/sorption region (<−0.45 V) is suppressed in the presence of glucose in the solution. The observed decrease of current density at potentials more positive, with respect to the peak potential value, could be due to the formation of thick palladium oxide which competes for surface adsorption sites with glucose and in turn inhibits the electrooxidation of glucose [37].

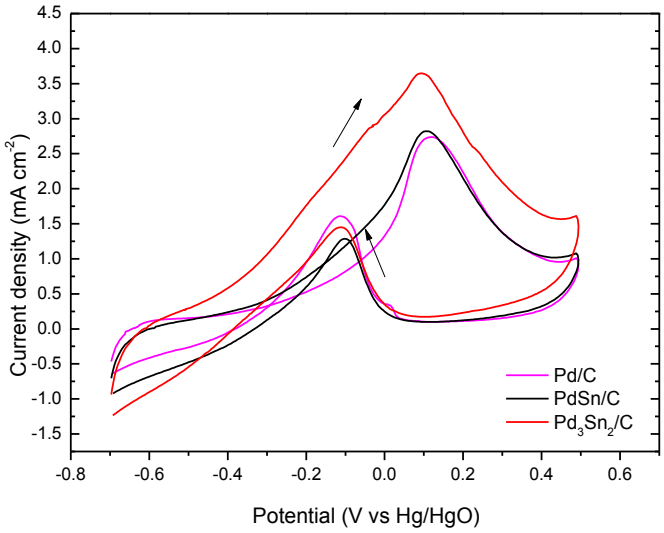

Figure 6.4. Cyclic voltammogram for Pd/C, PdSn/C and Pd3Sn2/C in 0.5 M KOH + 0.5 M Glucose at 25 ^{o}C, 20 mV s^{-1}.

The peak at ~ -0.1 V, during the backward scanning, can be attributed to the reduction of PdO that have been formed during the forward scanning [38]. From Figure 6.4 it can be seen that Pd/C has a little bit higher activity towards the reduction of palladium oxides compared to the other two electrocatalysts (see Table 6.3).

Furthermore, in Table 6.3 the cyclic voltammetry parameters are given. As it is observed the onset potential is more negative for the Pd_3Sn_2/C compared to the other two electrocatalysts.

Table 6.3. Cyclic voltammetry parameters on different electrodes in 0.5 M KOH + 0.5 glucose, at 25 ^{o}C, 20 mV s^{-1}.

Catalysts (20 wt.%)	Onset potential (mV vs. Hg/HgO)	Forward Scan		Backward Scan	
		j_p/mA cm^{-2}	E_p / mV	j_p/mA cm^{-2}	E_p / mV
Pd/C	-0.32	2.70	0.11	1.60	-0.10
PdSn/C	-0.38	2.80	0.10	1.40	-0.11
Pd_3Sn_2/C	-0.56	3.64	0.08	1.23	-0.09

3.2.3. *Effect of glucose's and electrolyte's concentration*

The cyclic voltammograms of the Pd_3Sn_2/C electrocatalyst which exhibited the highest activity to glucose electrooxidation, for different glucose's and electrolyte's concentration are depicted in Figure 6.5.

It is observed that the oxidation current increases as glucose and electrolyte's concentration increases. Moreover increasing electrolyte's concentration the peak potential shifts to more negative values and a linear relationship is observed between glucose's concentration and peak current density (Figure 6.5 (F)). The negative-shift in the peak potential suggests that the KOH concentration seems to have a favorable effect on the oxidation of glucose [39]. The increase in KOH's concentration may lead to a greater coverage of the reactive Pd-OH_{ads} which may facilitate glucose's oxidation.

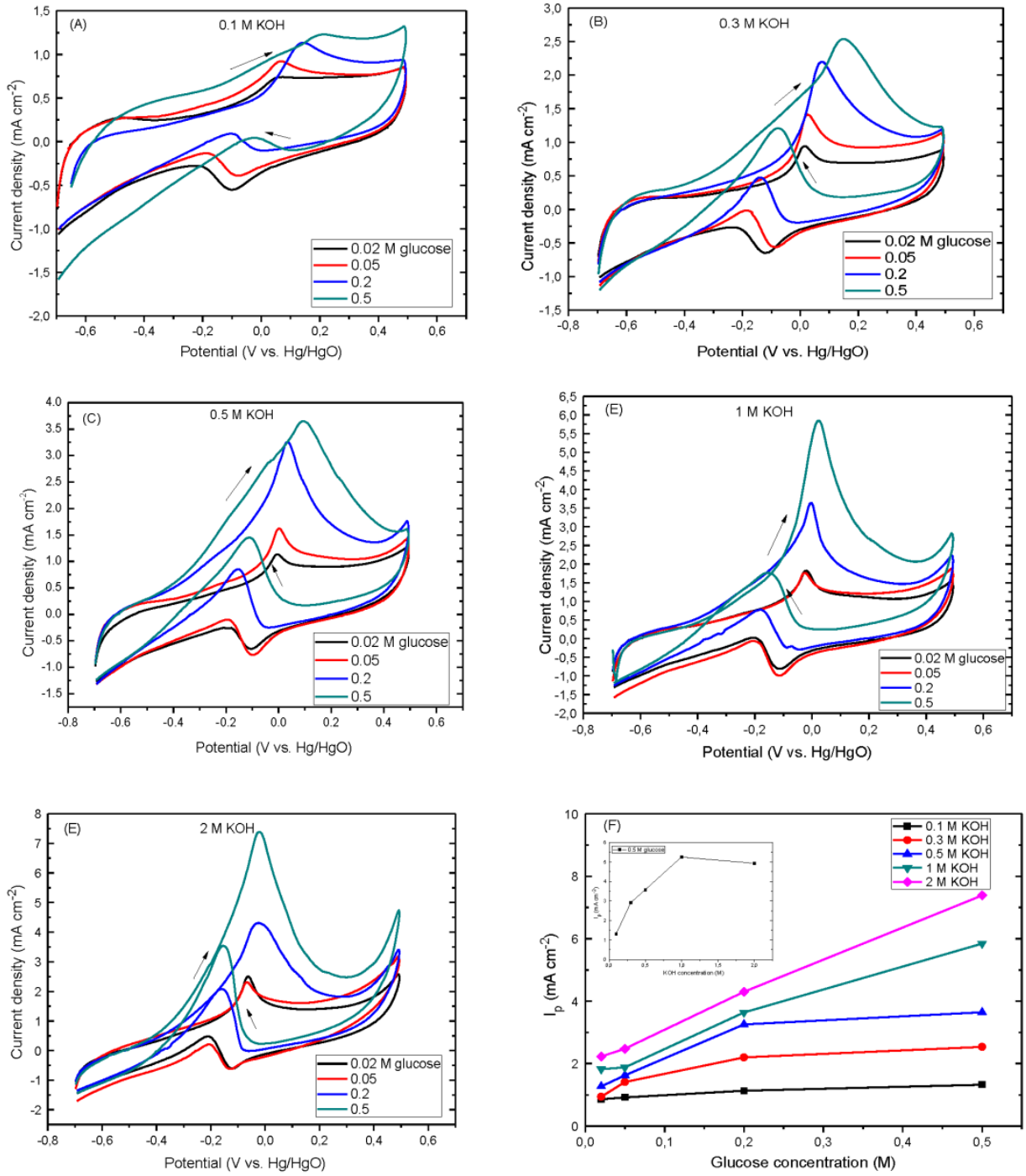

Figure 6.5. Cyclic voltammograms of the Pd_3Sn_2/C electrocatalyst in: (A) 0.1, (B) 0.3, (C) 0.5 (D) 1 and 2 M KOH containing y (=0.02, 0.05, 0.2, and 0.5 M) glucose (scan rate: 20 mV s^{-1}, room temperature). Fig. 6.5 (F): Peak current density dependence of glucose's concentration.

Tafel plots were obtained from the onset region of the polarization curves [40] from the limited form of the Butler-Volmer equation:

$$logi = logi_o + (a_a nF/2.303RT)\eta \quad (13)$$

where η is the overpotential, i_o is the exchange current density and a_a is the anodic transfer coefficient, F is the Faraday's constant, R is the universal gas constant and T the temperature.

From Tafel plot (logI *vs.* η) two significant kinetic parameters can be derived: i) the exchange current density (i_o)-value that give relative rates of reaction at equilibrium being calculated from the intercept at y-axis and ii) charge transfer coefficient (a_a)-that gives valuable information regarding the mechanism of a reaction and indications as to the identity of a rate-determining step of the overall reaction scheme.

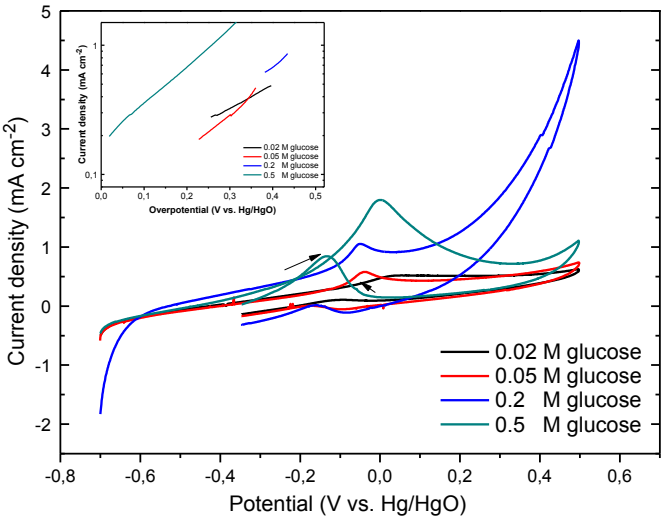

Figure 6.6. Cyclic voltammograms of Pd_3Sn_2/C electrocatalyst in 0.5 mol L^{-1} KOH containing (=0.02, 0.05, 0.2, and 0.5 mol L^{-1}) glucose (scan rate: 5 mV s^{-1}, room temperature). Inset: Tafel plots.

From Figure 6.6, the exchange current density was calculated 0.09, 0.042, 0.056 and 0.19 mA cm^{-2} and the charge transfer coefficient 0.10, 0.165, 0.16 and 0.17 for 0.02, 0.05, 0.2 and 0.5 M glucose, respectively, in 0.5 M KOH. Consequently, increasing glucose's

concentration the catalytic activity is enhanced. However, the exchange current density remains at low values indicating that further research is necessary.

3.2.4. Effect of the scan rate

The kinetics of glucose oxidation reaction was further investigated. Figure 6.7 (A) depicts the CVs of the Pd_3Sn_2/C in 0.5 M glucose + 0.5 M KOH solution. The scan rate was increased from 5 to 150 mV s^{-1}. The anodic peak current density (positive scan) is linearly proportional to the square root of the scan rate (R^2 = 0.9834), indicating that the electrode process was controlled via diffusion [41].

The peak current density values of the oxidation of the palladium intermediates and the reduction of them are enhanced with increasing the scan rate and the peak potential swifts to higher values. The shift of the peak potential to higher values is possibly due to the IR drop generated at higher current density values [42].

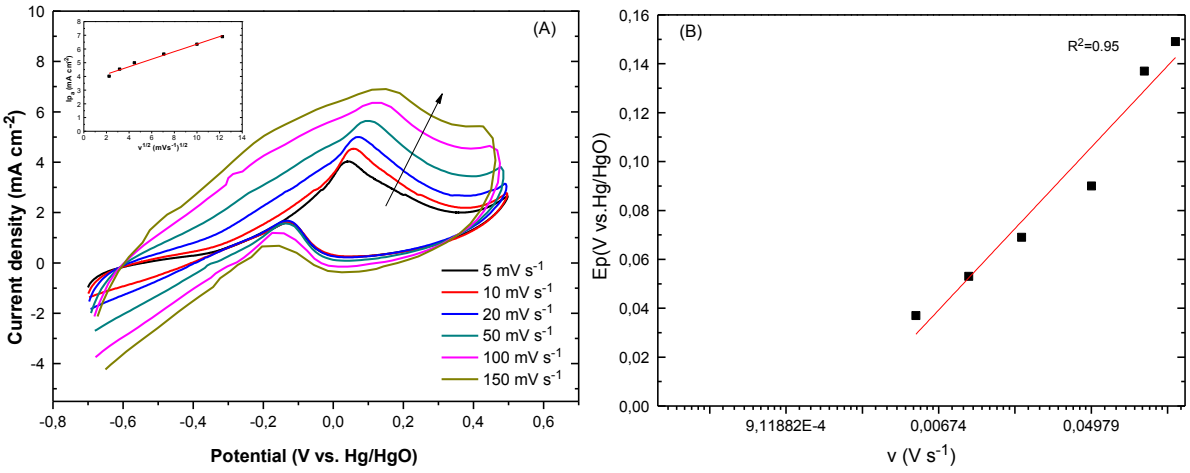

Figure 6.7. (A) Cyclic voltammograms of the Pd_3Sn_2/C electrocatalyst in 0.5 M KOH containing 0.5 M glucose at different scan rates in room temperature. Inset: Dependence of anodic peak current during the forward sweep on the square roots of potential sweep rate, (B) E_p *vs.* ln(v).

The linear relationship between the square root of the scan rate and the peak current density (Figure 6.7 (B)), proves that the control of the overall glucose oxidation reaction is controlled by the mass transport of the glucose from the bulk solution to the electrode surface [43]. In

general, for an electrochemical oxidation reaction, the linear relationship between E_p and $\ln(v)$ can be represented by the following equation (Laviron's theory) [44-46]:

$$E_p = E^o + \frac{RT}{anF}\ln\frac{RTk_s}{anF} - \frac{RT}{anF}\ln v \quad (14)$$

where α is the transfer coefficient, k_s is the electron transfer rate parameter, v is the scan rate and E^o is the standard potential. The plot of E_p *vs.* $\ln v$ should be linear. From its slope the an product can be determined; from its intercept the k_s can be calculated if the values of E^o is known. The E^o can be also estimated from the intercept of E_p *vs.* v plot on the coordinate by extrapolating to $v = 0$ [47]. The k_s was calculated 1 s^{-1}.

3.2.5. The effect of temperature

The effect of temperature on glucose's electrooxidation reaction was examined for T=30, 36.5 and 40°C. Yei *et al.* [48] proved that glucose degraded rapidly above 40°C as evidenced by rapid change of color to yellow-brown and caramel like smell.

As it is observed in Figure 6.8, increasing the temperature the current density is increased, while the peak potential shifts to positive values. The activation energy E_a can be obtained from the currents measured at different temperatures using the following equation:

$$E_a = R(d(\ln I)/d(1/T)) \quad (15)$$

In Figure 6.8 the Arrhenius plots are depicted from that were extracted from Figure 6.8 for the three examined electrocatalysts. The activation energy was calculated to be 45.2 kJ mol^{-1}, 52.3 and 50.3 (all close to 0.5eV), for the Pd_3Sn_2/C, PdSn/C and Pd/C electrocatalysts, respectively.

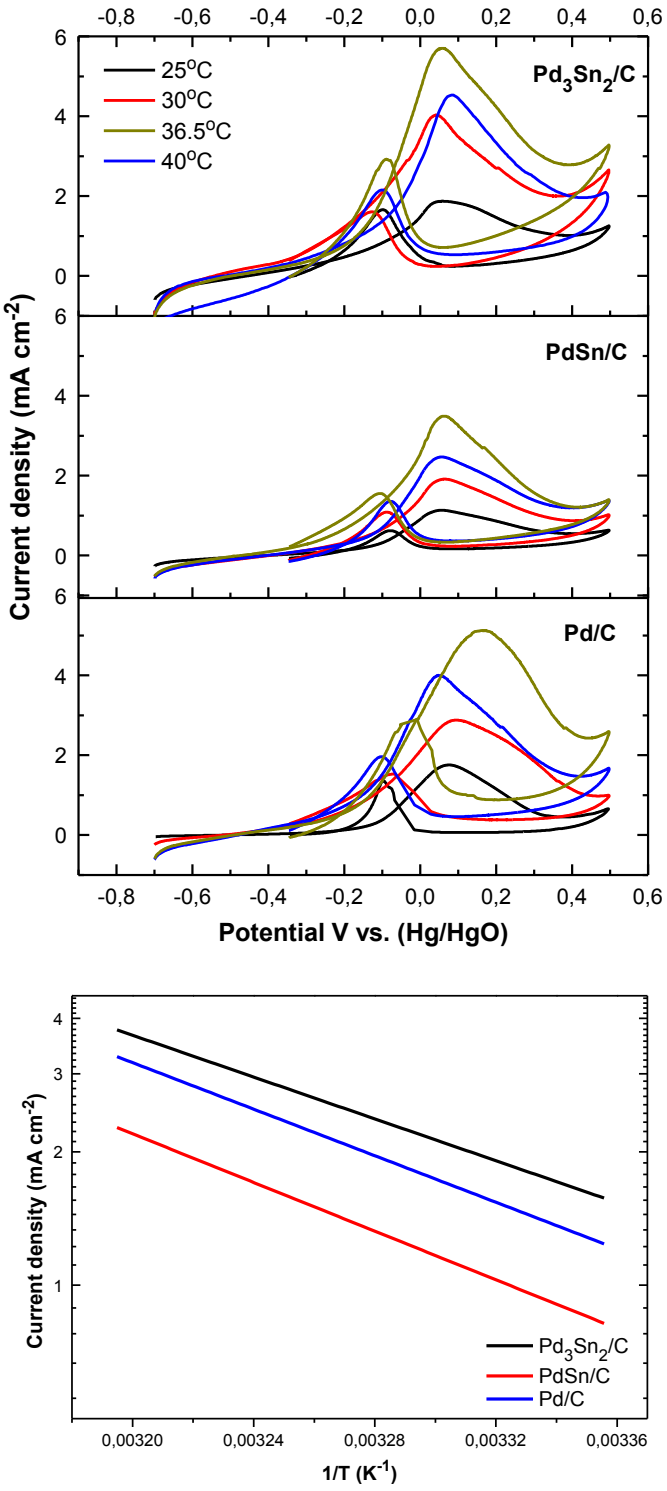

Figure 6.8. Cyclic voltammograms at different temperature values (T=25, 30, 36.5 and 40ºC), in 0.5 mol L^{-1} KOH containing 0.5 mol L^{-1} glucose, 5 mV s^{-1} of: Pd_3Sn_2/C, PdSn/C and Pd/C . Arrhenius plots (second graph).

3.2.6. *Chronoamperometric measurements*

Figure 6.9 shows the chronoamperometric plots for the examined electrocatalysts in 0.5 M KOH + 0.5 M glucose at 25 °C for 1300 sec at a fixed potential (-0.13 V (*vs.* Hg/HgO)). An initial rapid decrease in the current density with time is observed for all catalysts.

The current density stabilized more quickly for PdSn/C and Pd/C electrocatalysts than Pd_3Sn_2/C, however the current density of the Pd_3Sn_2/C stabilized over 2 mA cm^{-2} than that of Pd/C. From Figure 6.9 the poisoning rate (δ) can be calculated by measuring the linear decay of the current for a period of more than 500s using the following equation:

$$\delta = (100 / Io)(dI / dt)_{t>500s} \quad (16)$$

where $(dI / dt)t > 500s$, is the slope of the linear portion of current decay and I_o is the current at the start of polarization back extrapolated from the linear current decay.

The poisoning rate was calculated 0.014, 0.008 and 0.0019 % s^{-1} for the Pd_3Sn_2/C, PdSn/C and Pd/C, respectively. The poisoning rate is more intense for the Pd_3Sn_2/C. Moreover, chronoamperometry was employed for the investigation of diffusion coefficient of glucose. Under the diffusion controlled conditioned and according to the Cottrell equation [49] the current intensity is given by:

$$I = nFAD^{1/2}C / \pi^{1/2}t^{1/2} \quad (17)$$

where A is real surface area (0.07 cm^2), D is diffusion coefficient, C is the bulk concentration of glucose, F the Faraday constant (96485 C mol^{-1}).

The slope of the linear plot of I vs. $t^{-1/2}$ can be used for the estimation of glucose diffusion coefficient. Glucose diffusion coefficients were calculated to be: 7.8 $\times 10^{-9}$, 1.52 $\times 10^{-9}$ and 1.79 $\times 10^{-9}$ cm^2 s^{-1}, for the Pd_3Sn_2/C, PdSn/C and Pd/C, respectively. The results are reasonable based on CV's results.

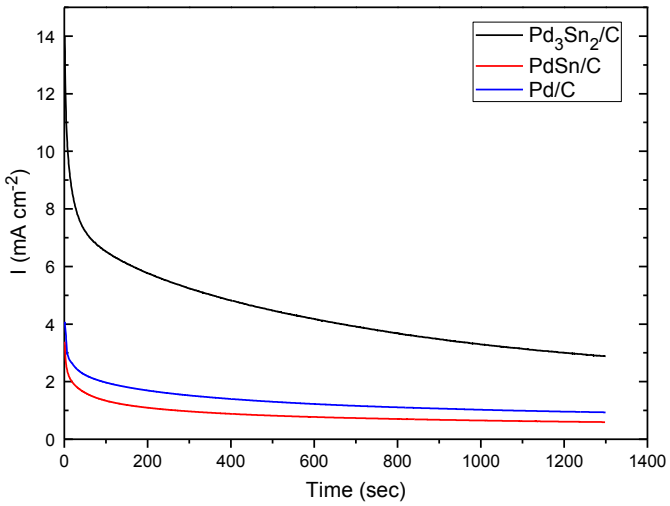

Figure 6.9. Chronoamperometric curves at -0.13 V (vs. Hg/HgO) for 1300 sec, in a 0.5 mol L^{-1} KOH with 0.5 mol L^{-1} glucose solution.

Conclusions

Pd_xSn_y/C binary catalysts were synthesized by a modified pulse microwave assisted polyol method and were investigated for the reaction of glucose electrooxidation. The results were compared with Pd/C which was synthesized with the same method. The optimum Pd_3Sn_2/C exhibited the desirable activity to glucose electrooxidation, but according to chronoamperometric results it was poisoned faster compared to the PdSn/C and Pd/C electrocatalysts. Moreover, from the chronoamperometric results glucose's diffusion coefficient was calculated for Pd_3Sn_2/C to be 7.8 ×10-9 cm^2 s^{-1}, in agreement with that reported in literature. Glucose electrooxidation reaction over Pd_3Sn_2/C was also studied for a range of values of temperature, glucose and electrolyte concentration. According to the cyclic voltammetry's results, as temperature increases from 25°C to 40°C, the current density increases from 1.87 to 5.7 mA cm^{-2}. Additionally, at a constant glucose's concentration, increasing electrolyte's concentration from 0.1 to 2 M KOH, current density increases from 1.3 to 7.4 mA cm^{-2}. Increment of the current density is also observed when glucose's concentration increases from 0.02 to 0.5 M, for all KOH's concentrations. The observed increment becomes more intense at high (1M and 2M KOH) electrolyte's concentration. Finally, studying the effect of scan rate indicated that the electrode process is diffusion limited and the electron transfer rate is 1 s^{-1}.

References

[1] S. Calabrese Barton, J. Gallaway, P. Atanassov, Chem. Rev. 104 (2004) 4867-4886.

[2] H. Liu, B.E. Logan, Environ Sci Techno 38 (2004) 4040-4046.

[3] M. Guerra-Balcázar, D. Morales-Acosta, F. Castaneda, J. Ledesma-García, L.G. Arriaga, Electrochem. Commun. 12 (2010) 864-867.

[4] N. Fujiwara, S.-i. Yamazaki, Z. Siroma, T. Ioroi, H. Senoh, K. Yasuda, Electrochem. Commun. 11 (2009) 390-392.

[5] A. Brouzgou, A. Podias, P. Tsiakaras, J. Appl. Electrochem. 43 (2013) 119-136.

[6] C. Hui-Fang, Y. Jian-Shan, L. Xiao, Z. Wei-De, S. Fwu-Shan, Nanotechnology 17 (2006) 2334.

[7] L. An, T.S. Zhao, S.Y. Shen, Q.X. Wu, R. Chen, Int. J. Hydrogen Energy 35 (2010) 4329-4335.

[8] Y.S. Li, T.S. Zhao, W.W. Yang, Int. J. Hydrogen Energy 35 (2010) 5656-5665.

[9] X. Yan, X. Ge, S. Cui, Nanoscale Research Letters 6 (2011) 313.

[10] F. Xie, Z. Huang, C. Chen, Q. Xie, Y. Huang, C. Qin, Y. Liu, Z. Su, S. Yao, Electrochem. Commun. 18 (2012) 108-111.

[11] D. Basu, S. Basu, Electrochim. Acta 56 (2011) 6106-6113.

[12] M. Guerra-Balcázar, F.M. Cuevas-Muñiz, L. Álvarez-Contreras, L.G. Arriaga, J. Ledesma-García, J. Power Sources 197 (2012) 121-124.

[13] L. Li, K. Scott, E.H. Yu, J. Power Sources 221 (2013) 1-5.

[14] Q. Shen, L. Jiang, H. Zhang, Q. Min, W. Hou, J.-J. Zhu, J. Phys. Chem. C 112 (2008) 16385-16392.

[15] W. Huang, M. Wang, J. Zheng, Z. Li, J. Phys. Chem. C 113 (2009) 1800-1805.

[16] H. Yin, C. Zhou, C. Xu, P. Liu, X. Xu, Y. Ding, J. Phys. Chem. C 112 (2008) 9673-9678.

[17] J.P. Spets, Y. Kiros, M.A. Kuosa, J. Rantanen, M.J. Lampinen, K. Saari, Electrochim. Acta 55 (2010) 7706-7709.

[18] D. Basu, S. Basu, Electrochim. Acta 55 (2010) 5775-5779.

[19] D. Basu, S. Basu, Int. J. Hydrogen Energy 36 (2011) 14923-14929.

[20] Z. Liu, L. Huang, L. Zhang, H. Ma, Y. Ding, Electrochim. Acta 54 (2009) 7286-7293.

[21] C. Jin, I. Taniguchi, Mater. Lett. 61 (2007) 2365-2367.

[22] F.M. Cuevas-Muñiz, M. Guerra-Balcázar, F. Castaneda, J. Ledesma-García, L.G. Arriaga, J. Power Sources 196 (2011) 5853-5857.

[23] D. Basu, S. Basu, Int. J. Hydrogen Energy 37 (2012) 4678-4684.

[24] Y. Kuang, B. Wu, D. Hu, X. Zhang, J. Chen, J. Solid State Electrochem. 16 (2012) 759-766.

[25] W.J. Zhou, S.Q. Song, W.Z. Li, Z.H. Zhou, G.Q. Sun, Q. Xin, S. Douvartzides, P. Tsiakaras, J. Power Sources 140 (2005) 50-58.

[26] Y. Wang, S. Song, G. Andreadis, H. Liu, P. Tsiakaras, J. Power Sources 196 (2011) 4980-4986.

[27] S. Vyazovkin, Characterization of Materials, John Wiley & Sons, Inc., 2002.

[28] A. Pozio, M. De Francesco, A. Cemmi, F. Cardellini, L. Giorgi, J. Power Sources 105 (2002) 13-19.

[29] R. Pattabiraman, Appl. Catal. A-Gen. 153 (1997) 9-20.

[30] M.H. Seo, S.M. Choi, H.J. Kim, W.B. Kim, Electrochem. Commun. 13 (2011) 182-185.

[31] T. Takamura, K.i. Minamiyama, J. Electrochem. Soc. 112 (1965) 333-335.

[32] J. Prabhuram, R. Manoharan, H.N. Vasan, J. Appl. Electrochem. 28 (1998) 935-941.

[33] M. Grdeń, A. Czerwiński, J. Solid State Electrochem. 12 (2008) 375-385.

[34] M.C. Jeong, C.H. Pyun, I.H. Yeo, J. Electrochem. Soc. 140 (1993) 1986-1989.

[35] L. Vračar, S. Burojević, N. Krstajić, Int. J. Hydrogen Energy 23 (1998) 1157-1164.

[36] M. Grdeń, A. Czerwiński, J. Solid State Electrochem. 12 (2008) 375-385.

[37] L. Meng, J. Jin, G. Yang, T. Lu, H. Zhang, C. Cai, Anal. Chem. 81 (2009) 7271-7280.

[38] I. Becerik, F. Kadirgan, Electrochim. Acta 37 (1992) 2651-2657.

[39] Z.X. Liang, T.S. Zhao, J.B. Xu, L.D. Zhu, Electrochim. Acta 54 (2009) 2203-2208.

[40] B.K. Boggs, G.G. Botte, Electrochim. Acta 55 (2010) 5287-5293.

[41] Y. Zhang, M. Zhang, Z. Cai, M. Chen, F. Cheng, Electrochim. Acta 68 (2012) 172-177.

[42] M.A. Abdel Rahim, R.M. Abdel Hameed, M.W. Khalil, J. Power Sources 134 (2004) 160-169.

[43] M. Noroozifar, M. Khorasani-Motlagh, R. Khaleghian-Moghadam, M.-S. Ekrami-Kakhki, M. Shahraki, J. Solid State Chem. 201 (2013) 41-47.

[44] E. Laviron, J. Electroanal. Chem. Interf. Electrochem. 101 (1979) 19-28.

[45] E. Laviron, L. Roullier, Journal of Electroanalytical Chemistry and Interfacial Electrochemistry 115 (1980) 65-74.

[46] H. Tang, J. Chen, S. Yao, L. Nie, Y. Kuang, Z. Huang, D. Wang, Z. Ren, Mater. Chem. Phys. 92 (2005) 548-553.

[47] P. Sharma, B. Sikarwar, G. Gupta, A. Nigam, B. Tripathi, P. Pandey, M. Boopathi, K. Ganesan, B. Singh, Appl Nanosci (2012) 1-10.

[48] L.H.E. Yei, B. Beden, C. Lamy, J. Electroanal. Chem. 246 (1988) 349-362.

[49] I. Danaee, M. Jafarian, F. Forouzandeh, F. Gobal, M.G. Mahjani, Int. J. Hydrogen Energy 33 (2008) 4367-4376.

CHAPTER VII

Pd_xRu_y /C binary catalysts for glucose Electrooxidation

Abstract

Pd_xRu_y/C (x:y=3:1, 2:1, 1:1, 1:2, and 1:3) electrocatalysts were prepared by a modified pulse microwave assisted polyol method and studied for glucose electrooxidation in alkaline media. The physicochemical characterization of electrocatalysts was conducted by X-ray diffraction (XRD) and Transmission Electron Microscopy (TEM), and the electrochemical characterization with Cyclic Voltammetry (CV) and Chronoamperometry techniques (CA). The effects of electrolyte's and glucose's concentrations as well as of temperature on the activity of glucose electrooxidation were also investigated. According to the CV results, the electro-catalytic activity towards glucose electrooxidation of the investigated catalysts has the following order: Pd_2Ru/C> Pd_3Ru/C > PdRu/C > $PdRu_2$/C > $PdRu_3$/C. (At least we should have the result that Ru can accelerate glucose electrooxidation at Pd, if not, for what reasons we should introduce Ru into Pd?) It was found that increasing electrolyte's concentration until 2.0 M KOH the current density increases and at the same time the increase of OH^- concentration decreases the poisonous effect. Moreover, increasing glucose's concentration from 0.02 M to 0.5 M the current increases for all the examined electrolyte's concentration values. According to chronoamperometric measurements, poisonous rate is more intense for Pd_2Ru/C and $PdRu_2$/C. Additionally, the increment of temperature enhances glucose electrooxidation until 40°C.

CONTENTS

CHAPTER VII ..... **i**

1. Introduction **192**

2. Experimental **193**

2.1. Catalysts' preparation 193

2.2. Physicochemical Characterization 194

2.3. Electrochemical Characterization 194

3. Results & Discussion **195**

3.1. Physicochemical Characterization 195

3.2. Electrochemical Characterization 197

3.2.1. Glucose electrooxidation *197*

3.2.2. Effect of glucose's and electrolyte's concentration *199*

3.2.4. Effect of temperature *200*

3.2.5. Chronoamperometric measurements *201*

Conclusions **202**

References **203**

List of Tables

Table 7.1. Structural parameters of the Pd_xRu_y/C electrocatalysts. 196

Table 7.2. Electrocatalytic kinetic parameters on different electrodes in 0.5 M KOH, at room temperature, 20 mV s^{-1}. 198

List of Figures

Figure 7.1. XRD patterns of (a) $PdRu_3/C$, (b) $PdRu_2/C$, (c) PdRu/C, (d) Pd_2Ru/C and (e) Pd_3Ru/C. 195

Figure 7.2. TEM images of the: PdRu/C (A), PdRu2/C (B), PdRu3/C (C), Pd2Ru/C (D) and Pd3Ru/C (E). 196

Figure 7.3. Cyclic voltammograms of the Pd_xRu_y/C electrocatalysts in 0.5 M KOH solution, 20 mV s^{-1}, room temperature. 197

Figure 7.4. Cyclic voltammograms of the Pd_xRu_y/C electrocatalysts in 0.5 M KOH containing 0.5 M glucose, 20 mV s^{-1}, room temperature. 198

Figure 7.5. Cyclic voltammograms of the Pd_2Ru/C electrocatalyst in: (A) 0.1, (B) 0.3, (C) 0.5 (D) 1 and (E) 2 M KOH containing y (=0.02, 0.05, 0.2, and 0.5 M) glucose (20 mV s^{-1}, room temperature). 199

Figure 7.6. (A, B, C, D & E) Cyclic voltammograms of Pd_xRu_y/C at different temperature values (T=25, 30, 36.5 and 40°C), in 0.5 mol L^{-1} KOH containing 0.5 mol L^{-1} glucose, 5 mV s^{-1}, (F) Arrhenius plots for the Pd_xRu_y/C electrocatalysts derived from cyclic voltammograms at 5 mV s^{-1}. 200

Figure 7.7. Chronoamperometric curves at -0.13 V (vs. Hg/HgO) for 1300 sec, in a 0.5 mol L^{-1} KOH with 0.5 mol L^{-1} glucose solution. 202

1. Introduction

The electrooxidation of glucose has been extensively and principally studied because of the interest in the development of glucose sensors [1]. An implantable, miniature, accurate and reliable sensor to monitor the glucose concentration in the body is desirable for the treatment of diabetes mellitus. An implantable glucose-oxygen fuel cell [2] has been proposed for artificial hearts using glucose and oxygen in the blood as the reactants. Two types of electroanalytic glucose sensors have been developed for this application: i) the enzyme electrode glucose sensor [3] and ii) electrocatalytic glucose sensor [4]. The oxidation of glucose at different kinds of electrode surfaces has been studied in order to develop this kind of sensor to monitor the glucose level in the human blood. Among them platinum [5-10] and gold [11-15] are the most widely studied electrodes for glucose electrooxidation because of their high activity for this reaction. Glucose oxidation reaction has been studied in acid [16], neutral [16, 17] and alkaline solutions. In acid solutions, the oxidation of glucose has been studied at the Pt electrode mostly in H_2SO_4 and $HClO_4$ solutions. While usually the neutral electrolyte is phosphate buffer and the alkaline electrolyte is sodium or potassium hydroxide. It has been proved that alkaline environment enhances the electrooxidation of liquid fuels [18]. However, platinum is not a suitable electrode for the sensor application in the blood and psychological condition due to itself poisoning in glucose oxidation and chemisorption of chloride ion and other blood components. Moreover, it lacks of long term stability, and it is rare and expensive metal [19]. On the other hand, gold shows bigger current than platinum electrodes for glucose oxidation in neutral and alkaline solutions, indicating that the mechanism of glucose oxidation is different at Au and Pt.

Besides Pt and Au, many other electrodes have also been studied for glucose electrooxidation reaction. Many also other electrodes, besides Pt and Au, have been studied for glucose electrooxidation reaction. The peak current of glucose electrooxidation iridium, rhodium, and copper is smaller than that at platinum in acid or neutral solutions [20, 21]. Also, iridium and rhodium show a poor reproducibility in neutral solutions [20].

However, no current has been found for cobalt, nickel and silver electrodes in neutral buffer solutions and for palladium electrodes in acid solutions [20, 21].

There are few reports [7, 22] concerning the study of glucose electrooxidation at carbon supported Pd-based/ electrocatalysts. Very recently we reported for first time the investigation of glucose electrooxidation on Pd-X/C (X=Au [23] and Rh [24]). Continuing our investigation for glucose electrooxidation on binary Pd-based electrocatalysts, in the present work we report for first time in literature, the study of glucose electrooxidation on Pd_xRu_y (20 wt%)/C (x:y=3:1, 2:1, 1:1, 1:2, and 1:3). More precisely, the effect of glucose's, electrolyte's concentration and temperature were studied, extracting important kinetic parameters for glucose's reaction.

2. Experimental

2.1. Catalysts' preparation

The Pd_xRu_y/C electrocatalysts were fast and easily prepared by a modified pulse-microwave assisted polyol synthesis method [25]. Initially, the starting precursors ($PdCl_2$/EG and $RhCl_3$/EG) were well mixed in a beaker with ethylene glycol (EG) by the aid of an ultrasonic bath, and then XC-72R carbon black was added into the mixture. After the pH value of the system was adjusted to be ~13 by the drop-wise addition of 1.0 mol L^{-1} NaOH/EG a well-dispersed slurry was obtained by ultrasonic stirring for 30 min. Thereafter, the slurry was microwave-heated for several times in a 10s-on/10s-off pulse form. In order to promote the adsorption of the suspended metal nanoparticles onto the support, hydrochloric acid was adopted as the sedimentation promoter and the solution was re-acidified to a pH value of about 3-4. The resulting black solid sample was filtered, washed with hot de-ionized water and dried at 80°C for 10 h in a vacuum oven. For the sake of comparison, 20 wt.% Pd/C was also prepared in the same way and examined under the same experimental conditions for the glucose electrooxidation.

2.2. Physicochemical Characterization

The X-ray Diffraction (XRD) measurements were carried out by the aid of a D/Max-IIIA (Rigaku Co., Japan) employing Cu K_α (λ = 0.15406 nm) as the radiation source. The samples were scanned over the range $10° \leq 2\theta \leq 86°$. The peak at 68° (Pd 220) was used for the calculation of crystallites size. Transmission electron microscopy (TEM) was used to determine the surface morphology and size of the particles. To prevent the agglomeration of carbon supports, the prepared catalyst was diluted in ethanol using ultrasonic water bath for some minutes and dried before TEM analysis. High dilution helps to separate the catalyst particles from each other.

2.3. Electrochemical Characterization

The as-prepared electrocatalysts were evaluated for glucose electrooxidation in a three-electrode cell assembly connected to electrochemical station (AMEL 5000). As reference electrode was used a mercury/mercury oxide (Hg/HgO) (in 1.0 mol L^{-1} KOH) and as a counter electrode was used a platinum wire one. The catalyst layer was prepared dispersing 5.0 mg of the as-prepared electrocatalyst powder in 1.8 mL ethanol and 0.2 mL Nafion® ionomer for 40 min [26]. The catalyst ink was then quantitatively (10 μL) transferred onto the surface of the glassy carbon disk electrode by using a micropipette and dried under infrared lamp to obtain a catalyst thin film. Initially, the as-prepared electrocatalysts were evaluated in 0.5 M KOH solution (blank measurements), in order to calculate the electrochemical active surface area. Then for comparison reasons the electrocatalysts were evaluated for glucose electrooxidation in 0.5 M KOH, containing 0.5 M glucose. Moreover, the effect of glucose's and electrolyte's concentration were studied over Pd_2Ru/C (which presented the highest activity to glucose electrooxidation), as well as the effect of temperature over all the studied electrocatalysts.

3. Results & Discussion

3.1. Physicochemical Characterization

XRD patterns of Pd_xRu_y/C are shown in Figure 7.1. Typical peaks of face-centered cubic (FCC) structure including (1 11), (2 0 0), (2 2 0), (3 1 1) and (2 2 2) lattices are marked on all the patterns. A peak of carbon black (0 0 2) is observed in the range of 20–30° of the diffraction spectra and a peak of Ru (1 0 1) between Pd (1 1 1) and Pd (2 0 0). Scherrer's equation was used to estimate the average size of the crystallites, from (2 2 0) peaks (inset of Figure 7.1):

$$d=k\lambda/\beta\cos\theta \quad (1)$$

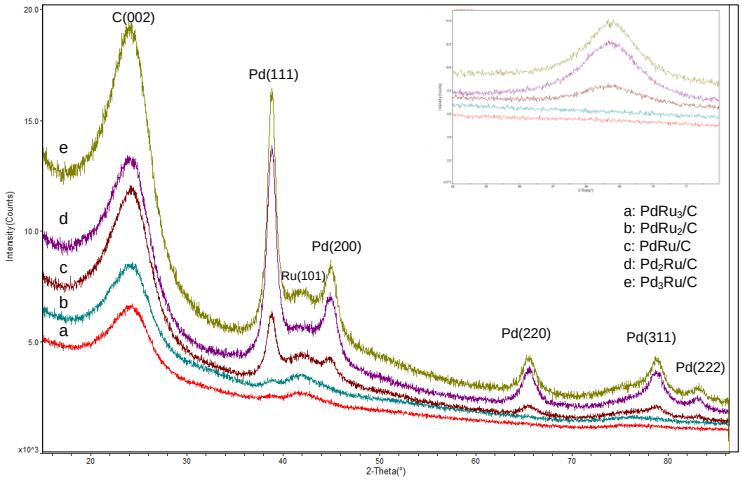

Figure 7.1. XRD patterns of (a) $PdRu_3/C$, (b) $PdRu_2/C$, (c) PdRu/C, (d) Pd_2Ru/C and (e) Pd_3Ru/C.

The lattice parameter and interatomic distance were also calculated based on the (2 2 0) diffraction peak. The results are summarized in Table 7.1. It is observed that with the increase of palladium content the interatomic distance decreases. Moreover with the increase of ruthenium content the (2 2 0) diffraction peak become increasingly indiscernible and it has been unsuitable for the calculation of particle size and lattice parameter. Consequently, the calculation of the particle size (Table 7.1) was based on TEM images, as it is shown in Figure 7.2

Table 7.1. Structural parameters of the Pd_xRu_y/C electrocatalysts.

Catalysts	Crystallite Size (nm)	Nanoparticles size (nm)	Lattice parameter (nm)
PdRu/C	9.38	~3.0	0.8860
Pd_2Ru/C	7.90	~4.0	0.8854
Pd_3Ru/C	10.0	~4.0	0.8853
$PdRu_2/C$	-	~20	-
$PdRu_3/C$	-	~30	-

From the TEM images it is obvious that many agglomerates have been formed in case of the $PdRu_2/C$ and $PdRu_3/C$ electrocatalysts.

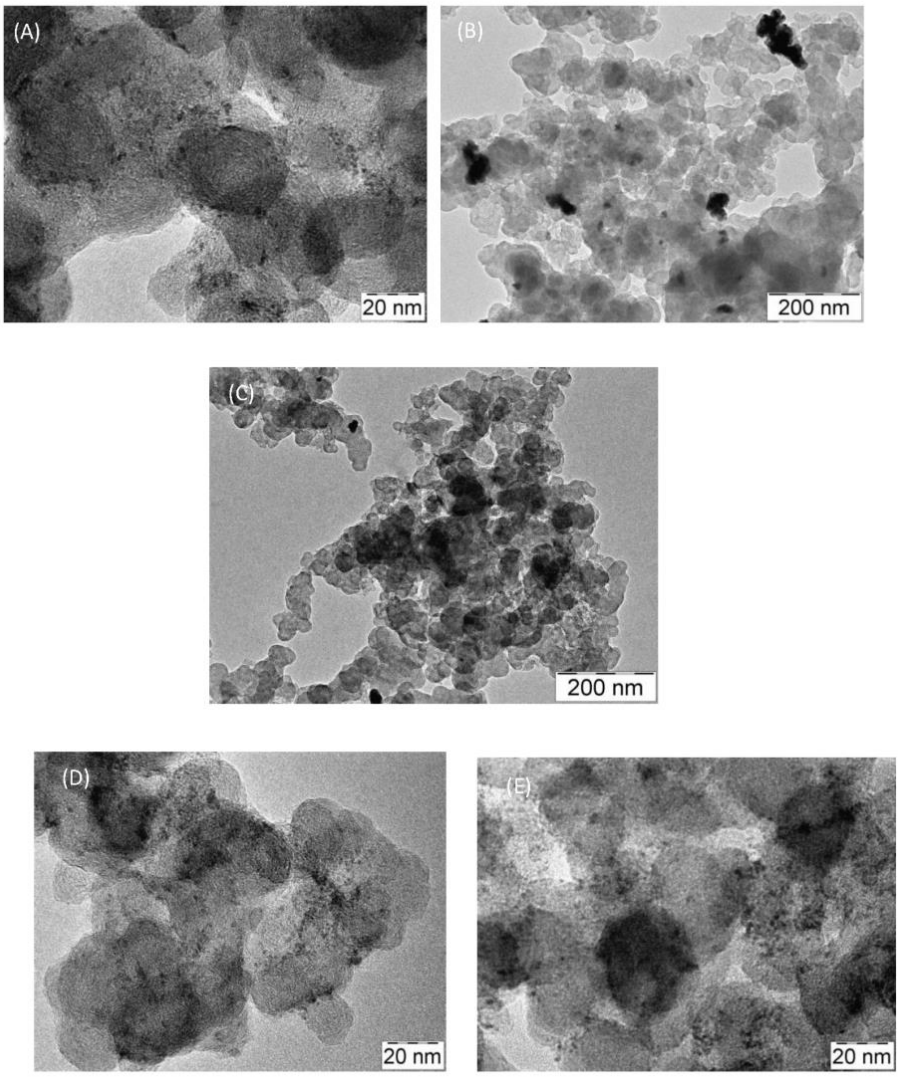

Figure 7.2. TEM images of the: PdRu/C (A), PdRu2/C (B), PdRu3/C (C), Pd2Ru/C (D) and Pd3Ru/C (E).

3.2. Electrochemical Characterization

3.2.1. Glucose electrooxidation

Initially, in order to evaluate the electrochemical active surface area of the as-prepared electrocatalysts cyclic voltammetry measurements were conducted in 0.5 M KOH (Figure 7.3), for 20 mV s^{-1}. In the case of Pd-based electrocatalysts the electrochemical active surface area (EASA) is calculated by determining the coulombic charge (Q) for the reduction of palladium oxide peak (Figure 7.3, at -0.14 V vs. Hg/HgO) [27]. The values of the EASA, reported in Table 7.2 are estimated using the following equation:

$$EASA=Q/S*I \quad (2)$$

where '*S*' is the proportionality constant used to relate charge with area and '*l*' is the catalyst loading in '*g*'. A charge value of 405 μC cm^{-2} is assumed for the reduction of PdO monolayer [28].

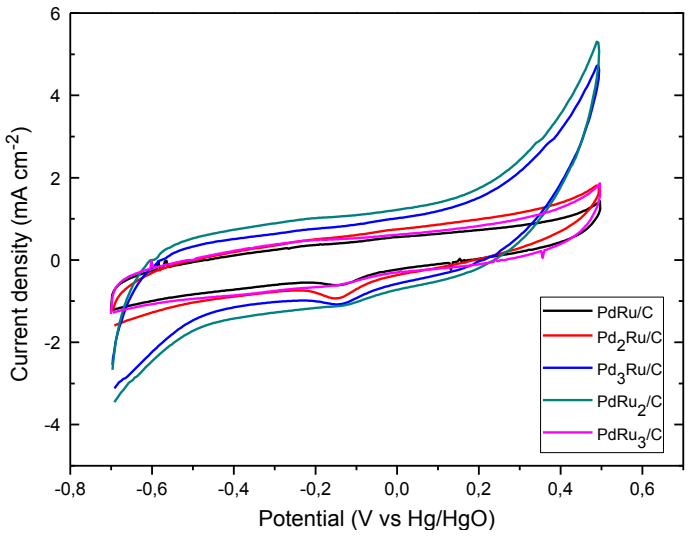

Figure 7.3. Cyclic voltammograms of the Pd_xRu_y/C electrocatalysts in 0.5 M KOH solution, 20 mV s^{-1}, room temperature.

The electrochemical active surface areas have the following order: Pd_2Ru/C (4.81 m^2 g^{-1}) > Pd_3Ru/C (3.67 m^2 g^{-1}) > PdRu/C (2.75 m^2 g^{-1}) > $PdRu_2$/C (1.65 m^2 g^{-1}) > $PdRu_3$/C (1.17 m^2 g^{-1}). Increasing ruthenium's content the electrochemical active

surface area decreases. While, increasing palladium's content, until the ratio Pd:Rh=2:1, the electrochemical active surface area increases.

Table 7.2. Electrocatalytic kinetic parameters on different electrodes in 0.5 M KOH, at room temperature, 20 mV s^{-1}.

Catalysts	EASA (m^2 g^{-1})	Onset potential (V *vs.* Hg/HgO)	I_{f1} (peak current density, mA cm^{-2})	I_{f2} (peak current density, mA cm^{-2})	I_b (peak current density, mA cm^{-2})
PdRu/C	4.7	-0.24	0.97	1.09	0.14
Pd_2Ru/C	6.5	-0.29	2.17	2.25	0.39
Pd_3Ru/C	4.4	-0.19	1.40	1.77	0.27
$PdRu_2$/C	4.3	-0.23	1.62	-	-0.44
$PdRu_3$/C	4.0	-0.20	1.10	1.32	0.14

In Figure 7.4 are depicted the cyclic voltammograms of the Pd_xRu_y/C electrocatalysts in 0.5 M KOH containing 0.5 M glucose.

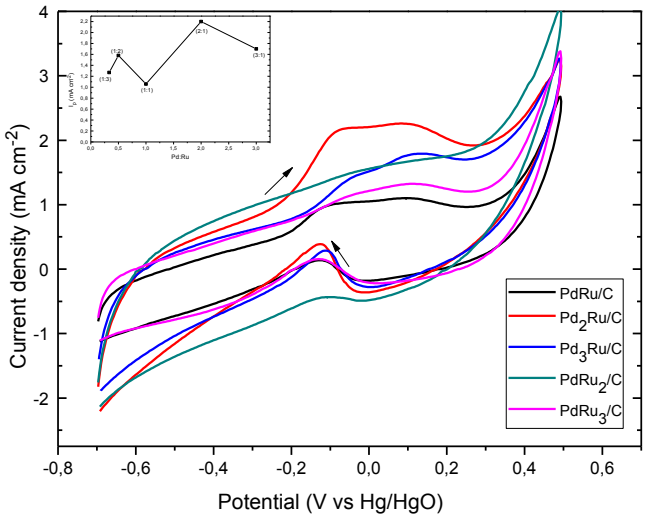

Figure 7.4. Cyclic voltammograms of the Pd_xRu_y/C electrocatalysts in 0.5 M KOH containing 0.5 M glucose, 20 mV s^{-1}, room temperature.

In contrast to the previous experiments, where during the forward scanning one peak was formed, for Pd_xAu_y/C [29], Pd_xRh_y/C [24] and Pd_xSn_y/C [30] electrocatalysts, in the case of Pd_xRu_y/C two anodic broad peaks (united in one) are formed (Figure 7.4). The observed two peaks during the forward scan can be attributed to the oxidation of glucose and resulting intermediates. During the cathodic potential scan, the oxidation of glucose is suppressed in the high potential range because of the presence of surface oxide [31]. With

the reduction of Pd-oxides (at -0.012 V *vs.* Hg/HgO) some more surface-active sites are available for the oxidation of glucose (at -0.012 V *vs.* Hg/HgO). More free surface-active sites were available for the Pd_2Ru/C as it can be seen from Figure 7.4. Furthermore, the onset potential is lower for the Pd_2Ru/C.

3.2.2. *Effect of glucose's and electrolyte's concentration*

The effect of glucose's and electrolyte's concentration was also studied (Figure 7.5).

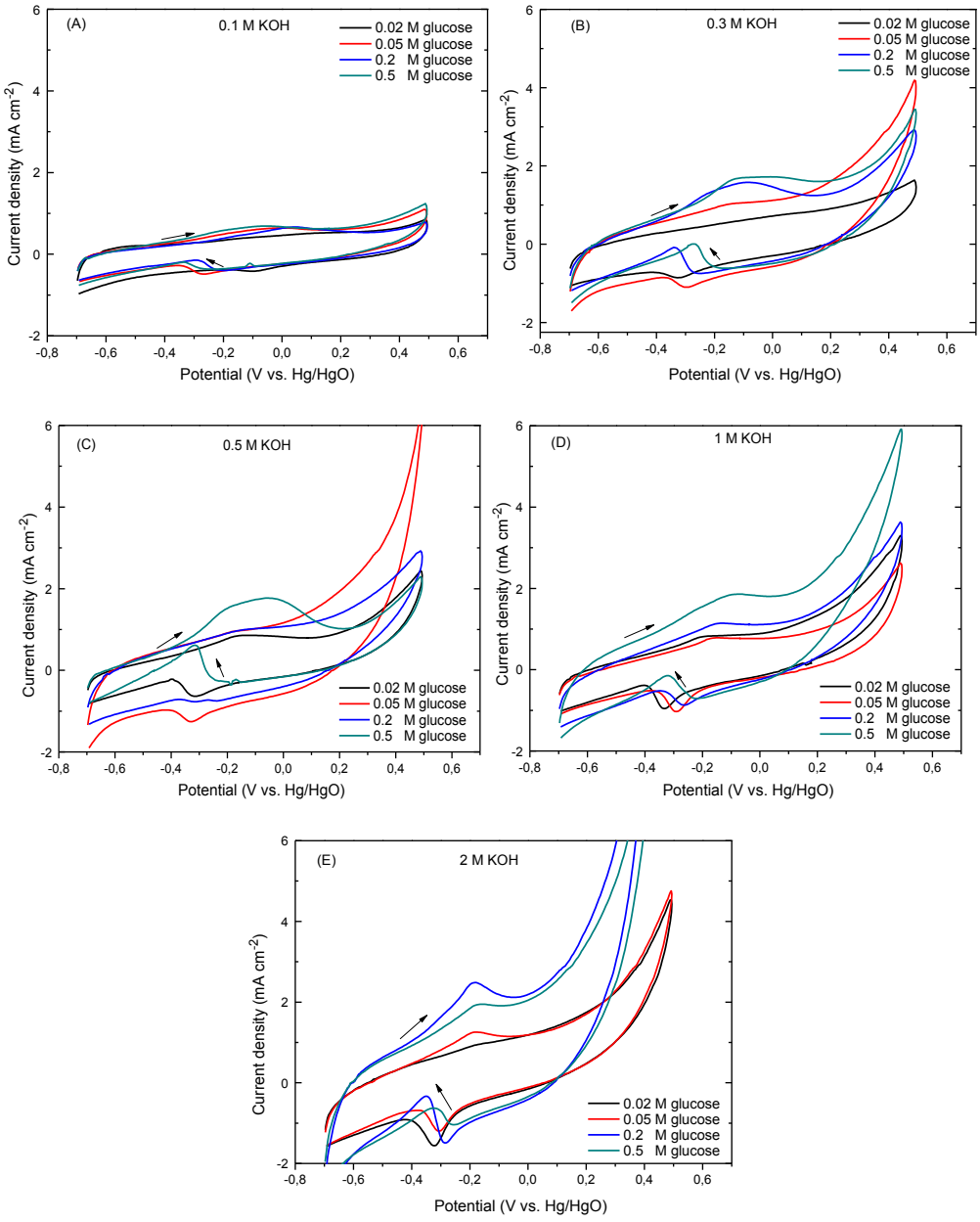

Figure 7.5. Cyclic voltammograms of the Pd_2Ru/C electrocatalyst in: (A) 0.1, (B) 0.3, (C) 0.5 (D) 1 and (E) 2 M KOH containing y (=0.02, 0.05, 0.2, and 0.5 M) glucose (20 mV s^{-1}, room temperature).

The cyclic voltammograms of the Pd_2Ru/C electrode in the glucose solution of the concentration ranging from 0.02 to 0.5 M are shown in Figure 7.5.

3.2.4. *Effect of temperature*

Glucose electrooxidation on Pd_xRu_y/C catalysts, cyclic voltammetric measurements were conducted in 0.5 M glucose in 0.5 M KOH solutions at 25, 30, 36.5 and 40 °C (Figure 7.6).

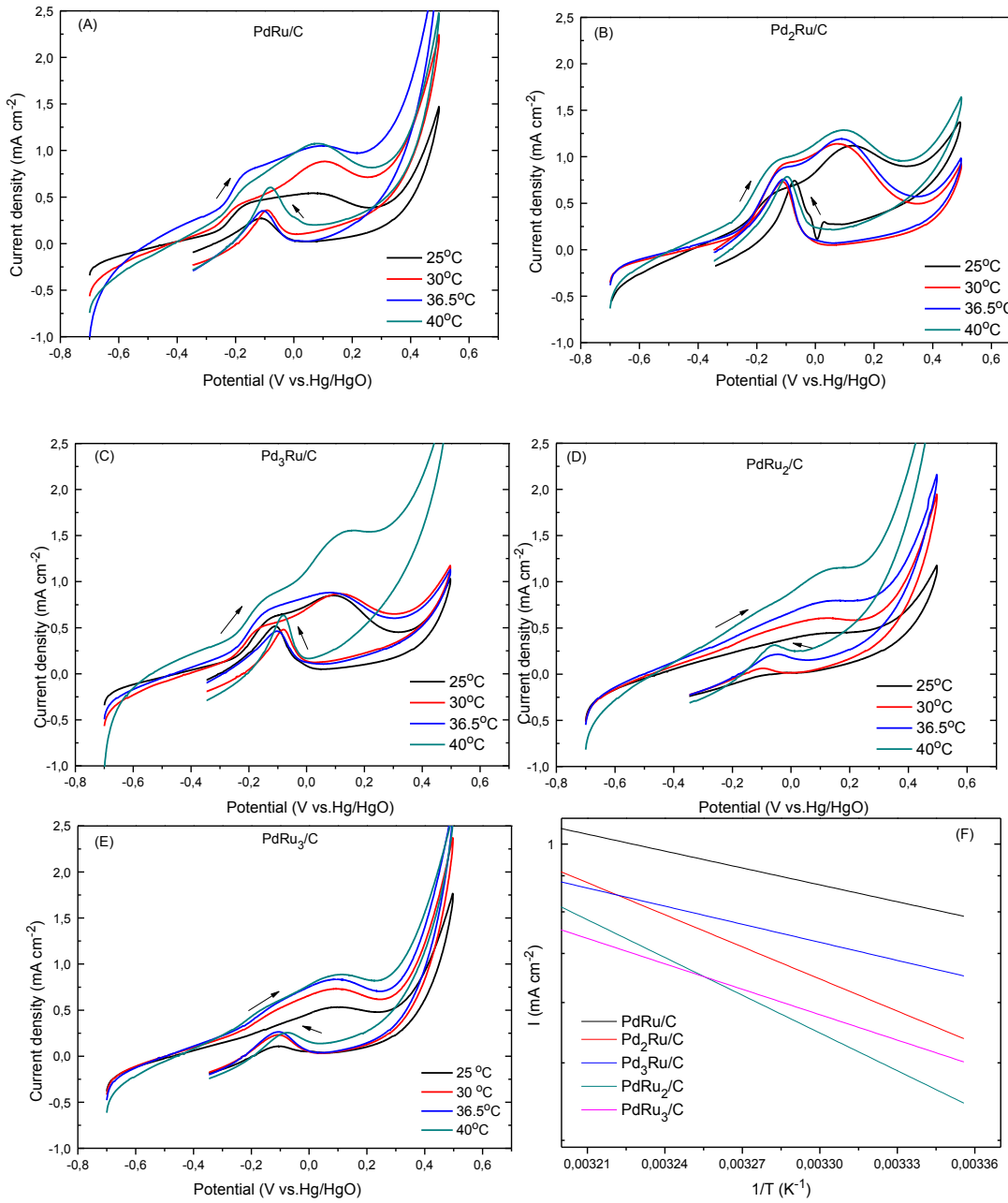

Figure 7.6. (A, B, C, D & E) Cyclic voltammograms of Pd_xRu_y/C at different temperature values (T=25, 30, 36.5 and 40°C), in 0.5 mol L^{-1} KOH containing 0.5 mol L^{-1} glucose, 5 mV s^{-1}, (F) Arrhenius plots for the Pd_xRu_y/C electrocatalysts derived from cyclic voltammograms at 5 mV s^{-1}.

As it is observed from Figure 7.6, increasing the temperature, electrocatalytic activity is enhanced and peak potentials shift to more positive values. Arrhenius plots of current density ($\log I$ *vs*.$1/T$) are given in Figure 7.6 (F), from which activation energies were estimated from these slopes of linear fitted. The activation energy of glucose electrooxidation on Pd_xRu_y/C calculated 17.3 (Pd_2Ru/C) < 18.6 (Pd_3Ru/C) < 26.13 ($PdRu_3/C$) < 33.0 (PdRu/C) < 38.8 ($PdRu_2/C$) kJ mol^{-1}. Lower activation energy means higher intrinsic activity. Thus, as it was expected from cyclic voltammetry's results (Figure 7.6) Pd_2Ru/C presented the lowest activation energy, while $PdRu_2/C$ the lowest one. However, despite the fact that the activation energies of the Pd_xRu_y/C electrocatalysts are lower than the other examined electrocatalysts the current density is very low, perhaps due to the quick poisoning (this is indicated by the broad peak towards forward scanning).

3.2.5. Chronoamperometric measurements

Chronoamperometric measurements were carried out to determine the performance, stability and poisoning rate of the examined Pd_xRu/C electrocatalysts in 0.5 M glucose in 0.5 M KOH solution at -0.13 V (*vs*.Hg/HgO). Figure 7.7 shows the CA results of different catalysts for glucose electro-oxidation in which steady-state current density is plotted against time at a constant potential. The current density decreases with time following a parabolic path and reaches the pseudo steady-state within 300 s. Pd_2Ru/C electrocatalyst presented the highest current density after 1300 s and $PdRu_3/C$ exhibited the lowest current density after 1300 s. However, Pd_3Ru/C and PdRu/C, as it is seen in Figure 7.7 have the same performance during the 1300 s.

The poisoning rate (d) is calculated by measuring the linear decay of the current for a period of more than 500 s from Fig. 8 by using the following equation [32]:

$$\delta = (100 / Io)(dI / dt)_{t>500s} \ (\% \ s^{-1}) \qquad (2)$$

where $(dI / dt)_{t>500s}$, is the slope of the linear portion of current decay and I_o is the current at the start of polarization back extrapolated from the linear current decay.

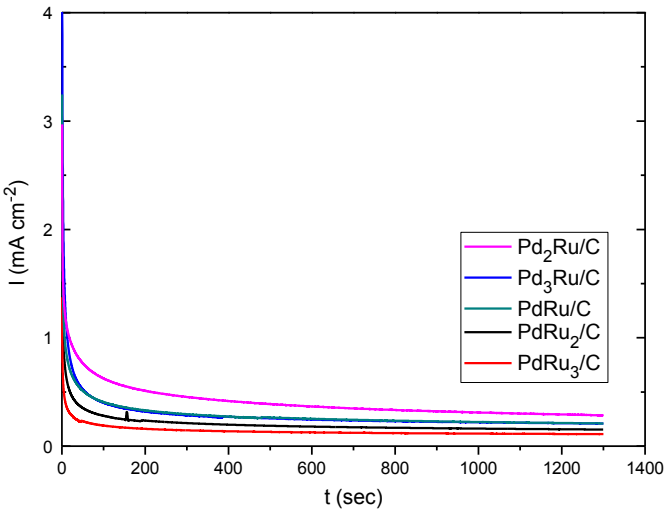

Figure 7.7. Chronoamperometric curves at -0.13 V (vs. Hg/HgO) for 1300 sec, in a 0.5 mol L^{-1} KOH with 0.5 mol L^{-1} glucose solution.

The poisoning rate is found to be with the following order: 0.0023 (Pd_2Ru/C) > 0.0024 ($PdRu_2/C$) > 0.0020 (Pd_3Ru/C) > 0.0019 (PdRu/C) > 0.0017 ($PdRu_3/C$) % s^{-1}. As it is obvious Pd_2Ru/C is more susceptible to glucose's electrooxidation reaction intermediates, while $PdRu_3/C$ is more tolerant to poisonous intermediates.

Conclusions

According to the measurements the increase of ruthenium's content in PdRu/C electrocatalyst suppresses current density, while on the other hand the addition of palladium (until Pd:Ru=2:1) enhances catalytic activity to glucose electrooxidation, with Pd_2Ru/C to exhibit the highest catalytic activity. According to cyclic voltammetry results, many intermediates are formed on Pd_xRu_y/C electrocatalysts, whose effect is reduced when electrolyte's concentration increases to 2 M KOH. Moreover, increasing temperature from 25°C to 40°C current density increases and activation energy of electrocatalysts was calculated: 17.3 (Pd_2Ru/C) < 18.6 (Pd_3Ru/C) < 26.13 ($PdRu_3/C$) < 33.0 (PdRu/C) < 38.8 ($PdRu_2/C$) kJ mol^{-1}. According to the present results Pd_xRu_y/C electrocatalysts are not suggested for glucose electrooxidation reaction. Due to the double peak that glucose oxidation presents, kinetic parameters, such as electron transfer rate could not be extracted, as were calculated for the PdRh/C and Pd_3Sn_2/C electrocatalysts.

References

[1] S.J. Updike, G.P. Hicks, Nature 214 (1967) 986-988.

[2] S.J. Yao, A.J. Appleby, S.K. Wolfson, Z. Phys. Chem. 82 (1972) 225-235.

[3] P.N. Bartlett, R.G. Whitaker, Biosensors 3 (1987) 359-379.

[4] U. Gebhardt, G. Luft, G.J. Richter, F. von Sturm, Bioelectrochem. Bioenerg. 5 (1978) 607-624.

[5] Q. Shen, L. Jiang, H. Zhang, Q. Min, W. Hou, J.-J. Zhu, J. Phys. Chem. C 112 (2008) 16385-16392.

[6] N. Fujiwara, S.-i. Yamazaki, Z. Siroma, T. Ioroi, H. Senoh, K. Yasuda, Electrochem. Commun. 11 (2009) 390-392.

[7] J.P. Spets, Y. Kiros, M.A. Kuosa, J. Rantanen, M.J. Lampinen, K. Saari, Electrochim. Acta 55 (2010) 7706-7709.

[8] D. Basu, S. Basu, Electrochim. Acta 55 (2010) 5775-5779.

[9] X. Yan, X. Ge, S. Cui, Nanoscale Research Letters 6 (2011) 313.

[10] D. Basu, S. Basu, Int. J. Hydrogen Energy 36 (2011) 14923-14929.

[11] W. Huang, M. Wang, J. Zheng, Z. Li, J. Phys. Chem. C 113 (2009) 1800-1805.

[12] H. Yin, C. Zhou, C. Xu, P. Liu, X. Xu, Y. Ding, J. Phys. Chem. C 112 (2008) 9673-9678.

[13] Z. Liu, L. Huang, L. Zhang, H. Ma, Y. Ding, Electrochim. Acta 54 (2009) 7286-7293.

[14] C. Jin, I. Taniguchi, Mater. Lett. 61 (2007) 2365-2367.

[15] F.M. Cuevas-Muñiz, M. Guerra-Balcázar, F. Castaneda, J. Ledesma-García, L.G. Arriaga, J. Power Sources 196 (2011) 5853-5857.

[16] K.B. Kokoh, J.M. Léger, B. Beden, C. Lamy, Electrochim. Acta 37 (1992) 1333-1342.

[17] A. Habrioux, E. Sibert, K. Servat, W. Vogel, K.B. Kokoh, N. Alonso-Vante, The Journal of Physical Chemistry B 111 (2007) 10329-10333.

[18] A. Brouzgou, A. Podias, P. Tsiakaras, J. Appl. Electrochem. 43 (2013) 119-136.

[19] A. Brouzgou, S.Q. Song, P. Tsiakaras, Appl. Catal., B 127 (2012) 371-388.

[20] Y.B. Vassilyev, O.A. Khazova, N.N. Nikolaeva, J. Electroanal. Chem. 196 (1985) 127-144.

[21] Y.B. Vassilyev, O.A. Khazova, N.N. Nikolaeva, J. Electroanal. Chem. 196 (1985) 105-125.

[22] A. Ahmadalinezhad, S. Chatterjee, A. Chen, Electrochim. Acta In press corrected proof (2013).

[23] Y. Longlong, A. Brouzgou, H. Liu, M. Yuezhong, P. Tsiakaras, M. Xiao, S. Song, submitted in Appl. Catal., B (2013).

[24] A. Brouzgou, Y. Longlong, S. Song, P. Tsiakaras, Applied Catalysis B: Environmental 147 (2014) 481-489.

[25] S. Song, Y. Wang, P.K. Shen, J. Power Sources 170 (2007) 46-49.

[26] C. He, S. Song, J. Liu, V. Maragou, P. Tsiakaras, J. Power Sources 195 (2010) 7409-7414.

[27] R. Pattabiraman, Applied Catalysis A: General 153 (1997) 9-20.

[28] M.H. Seo, S.M. Choi, H.J. Kim, W.B. Kim, Electrochem. Commun. 13 (2011) 182-185.

[29] L. Yan, A. Brouzgou, H. Liu, Y. Meng, P. Tsiakaras, M. Xiao, S. Song, Appl. Catal., B In press corrected proof (2013).

[30] A. Brouzgou, S. Song, P. Tsiakaras, submitted in Appl. Catal., B (2014).

[31] F. Xiao, F. Zhao, D. Mei, Z. Mo, B. Zeng, Biosens. Bioelectron. 24 (2009) 3481-3486.

CHAPTER VIII

Glucose electrooxidation in alkaline media for fuel cell applications: A comparative study of PdM/C (M=Au, Sn, Rh) based electrocatalysts

Abstract

In this Chapter a comparative review of the present work's examined electrocatalysts is done. The results of physicochemical and electrochemical evaluations towards glucose electrooxidation (as anode for direct alkaline glucose fuel cells) are reported and compared. Among the examined electrocatalysts $Pd_{30}Au_{70}/C$, Pd_3Sn_2/C, PdRh/C and Pd/C exhibited good electrocatalytic activity towards glucose electrooxidation. The Pd_3Sn_2/C one presented the highest electrocatalytic activity at low temperature values ($T<30^oC$), while PdRh/C exhibited the highest electrocatalytic activity at high temperature values ($T>30^oC$). However, $Pd_{30}Au_{70}/C$ was the one which showed high poisonous tolerance to the formed intermediates.

CONTENTS

CHAPTER VIII i

1. Introduction 205

2. Physicochemical Evaluation 206

3. Electrochemical Evaluation 208

References 216

List of Tables

Table 8.1. Physico-chemical properties of the as-prepared electrocatalysts. 207

Table 8.2. Electrochemical active surface area calculated from cyclic voltammetry measurement in 0.5 M KOH, 20 mV s^{-1}. 208

Table 8.3. Forward and backward anodic peak current density. 211

Table 8.4. Kinetic parameters derive from Tafel equation. 212

List of Figures

Figure 8.1. XRD patterns (only the Pd planes are indicated). 207

Figure 8.2. Comparison of cyclic voltammetry results of the best Pd-binary electrocatalysts, in 0.5 M KOH with 0.5 M glucose, 20 mV s^{-1}, room temperature, (*$Pd_{30}Au_{70}$/C: 20 mmol L^{-1}, 36.5^{o}C, 50mV s^{-1}). 209

Figure 8.3. Peak current density *vs.* metal loading. In all cases Pd+M loading equals to 72 μgcm^{-2}. 210

Figure 8.4. *E*lectrochemical active surface area and lattice parameter dependency on peak current density 211

Figure 8.5. Comparison of electrocatalytic activity (peak current density) of the examined electrocatalysts at different temperature values: 0.5 M KOH, 0.5 M glucose, 5 mV s^{-1}, room temperature. 212

Figure 8.6. Arrhenius plots. 213

Figure 8.7. Comparison of examined electrocatalysts at different glucose's and electrolyte's concentration, 20 mV s^{-1}, room temperature (A-E), comparison of electrocatalysts at 0.5 M glucose. 214

Figure 8.8. Comparison of chronoamperometric measurements of the examined electrocatalysts, ,in 0.5 M KOH with 0.5 M glucose, 5 mV s^{-1}, room temperature. 215

1. Introduction

The aim of the present Chapter is from one side to compare the investigated electrocatalysts in terms of glucose electrooxidation under different temperature values, electrolyte's as well glucose's concentration and sweep rate values and from the other side to summarize the results of the present PhD thesis.

The preparation method of the electrocatalysts plays a great role to their electrocatalytic activity. As previously mentioned, the method that was used in the present work was a modified microwave assisted polyol method. The initial (for the electrocatalysts' preparation) total metal content was 20 wt.% supported on carbon (Vulcan XC-72R). The main advantages of the specific electrocatalysts' preparation method are the following: i) the metals are homogenously dispersed on carbon, ii) nanoparticles are formed that means more electro-active area, iii) it is a cheap and quick method, iv) there is no loss of the initial metal loading [1].

X-Ray diffraction, Transmission Electron Microscopy and Scanning Electron Microscopy-Energy Dispersive X-Ray Spectroscopy techniques were used for the physicochemical characterization of the as-prepared electrocatalysts. According to the obtained results, nanoparticles were formed, homogenously dispersed on carbon. However, some agglomerates were observed, fact that may affect at a small percentage the electrocatalytic activity. From the XRD results it was deduced, that in the case of Pd_xRh_y/C alloys were formed, while for the other examined electrocatalysts there are noticeable peaks for phase-separated structures of Sn or Au. The metal content is a very important parameter for comparing the electrocatalytic activity. Thus in order to confirm that the selected preparation method do not affect the metal loading thermogravimetric measurements were carried out. In all cases, the metal loading was maintained at 20.0±1.5 wt.%, which is basically in agreement with the feeding weight ratio (20.0 wt.%), initially chosen for the electrocatalysts preparation. This indicates that the pulse-microwave assisted polyol synthesis method, adopted in the present work, is fast and effective. The SEM-EDS was

performed on scanning electron microscope (JEOL JSM-6330F) to determine the chemical composition of the samples.

The binary Pt_xAu_y/C is the most studied electrocatalyst for glucose electrooxidation [2-7]. However Pd, which has lower cost compared to platinum, presents higher activity in alkaline media. For this reason, in the present work, Pd_xAu_y/C electrocatalysts were initially prepared and characterized as materials that could eventually be used for direct glucose fuel cells application in alkaline media. It should be noted that the Pd_xAu_y/C electrocatalysts were also examined as glucose sensors. Then Pd_xSn_y/C and Pd_xRh_y/C were studied as anode materials for the reaction of glucose electrooxidation in a range of temperature, glucose and electrolyte concentration values. The results were compared with those of pure Pd/C. Moreover, detailed kinetic parameters for the reaction of glucose electrooxidation were obtained at different sweep rates of cyclic voltammetry measurements.

It is believed that the comparison of the electrooxidation characteristics of the above mentioned materials it will be helpful for future anode materials selection for the electrooxidation of glucose at low temperature working alkaline fuel cells.

2. Physicochemical Evaluation

The crystallite sizes as well as the metal phases of the as-prepared electrocatalysts were evaluated with XRD measurements. The XRD patterns were recorded on a D-MAX 2200 VPC diffractometer using Cu Kα radiation (30 kV, 30 mA) (Figure 8.1). For all examined samples, the first peak at 25° is associated with the Vulcan XC-72 carbon. Then, there are four observed characteristic diffraction peaks at *ca.* 38°, 45°, 65°, 79° and 83° belonging to the face-centered cubic (fcc) phase of Pd (111), (200), (220), (311) and (222), respectively. It is observed that all the peaks for the $Pd_{30}Au_{70}/C$ are more intense compared to the other ones. That may explain the small particle size that is estimated from the TEM images.

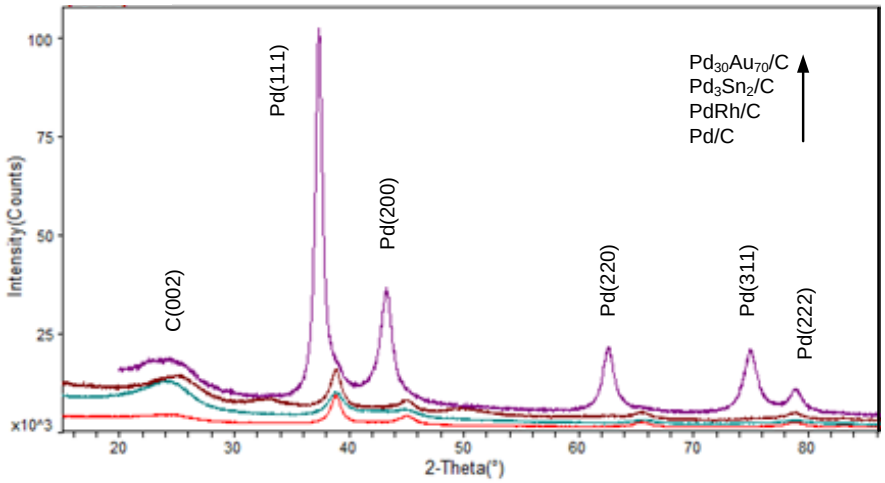

Figure 8.1. XRD patterns (only the Pd planes are indicated).

In Table 8.1 the mean particle size of all the examined electrocatalysts is reported, according to the XRD and TEM results.

Table 8.1. Physico-chemical properties of the as-prepared electrocatalysts.

Samples	Crystallite size /nm (XRD)	Mean particle size /nm (TEM)	Lattice parameter / nm
Pd/C	8.2	~8.0	0.3865
Pd_3Sn_2/C	7.8	~8.0	0.3863
$Pd_{30}Au_{70}$/C	7.1	~4.8	0.1005
PdRh/C	7.0	5.0<d<10.0	0.3859

As one can conclude from the above results the particle size of mono metallic catalysts is bigger than that of binary ones. While the $Pd_{30}Au_{70}$/C electrocatalyst has the smallest nanoparticles' mean particle size compared to the others. In the same table, the lattice parameters are also reported. It is characteristic that for the binary electrocatalysts the lattice parameter is decreased due to the substitution of Pd by Sn or Rh or Au [8]. For the $Pd_{30}Au_{70}$/C electrocatalyst the lattice parameter is decreased a lot. That may happen due to the substitution of Pd with Au. A further decrease in the particle size of the catalysts could give higher activity, and this part of work is under investigation, as it has already been referred in Chapter III.

In the following sub-section the results from the electrochemical evaluation of the as-examined electrocatalysts are compared independently of the experimental conditions; since $Pd_{30}Au_{70}/C$ electrocatalyst, was examined near human body conditions (due to its good poisonous-tolerance), while the rest three were investigated as anodes for direct glucose alkaline fuel cells.

3. Electrochemical Evaluation

In Table 8.2 the electrochemical active surface areas are reported for the as-prepared electrocatalysts.

Table 8.2. Electrochemical active surface area calculated from cyclic voltammetry measurement in 0.5 M KOH, 20 mV s^{-1}.

Samples	Electrochemical active surface area (EASA, $m^2\ g^{-1}$)
Pd/C	10.3
PdRh/C	26.0
Pd_3Sn_2/C	28.8

The estimated electrochemical active surface areas have the following order:

Pd_3Sn_2/C >PdRh/C>Pd/C

In Figure 8.2 a comparison is made among the Pd-binary electrocatalysts that exhibited the best electrocatalytic activity. As it is observed Pd_3Sn_2/C and PdRh/C exhibited similar activity, 3.8 mA cm^{-2}, while for the Pd/C and $Pd_{30}Au_{70}/C$ the current density, evaluated almost 2.8 mA cm^{-2}. However, the peak potential (Figure 8.2) for the $Pd_{30}Au_{70}/C$ electrocatalyst is lower from the other three electrocatalysts.

Moreover, despite the fact that Pd_3Sn_2/C presents high current density towards glucose electrooxidation, its poisonous tolerance is very poor ($I_{backward}$), while Pd/C has the best performance towards poisonous intermediates (high $I_{backward}$).

For the four electrocatalysts the disappearance of hydrogen desorption peak in the presence of glucose indicates the adsorption of glucose on their surface preventing the adsorption of hydrogen. The highest current density is exhibited by the Pd_3Sn_2/C (3.6

mA cm^{-2} at 0.094 V), presenting at the same time the lowest onset potential, -0.55 V. The peak current densities for the rest electrocatalysts are: 3.5 (at 0.04V), 2.3 (-0.23V) and 2.7 (0.12 V) mA cm^{-2}, having onset potential -0.47 V, -0.40 V and -0.29 V, for the PdRh/C, $Pd_{30}Au_{70}$/C and Pd/C respectively.

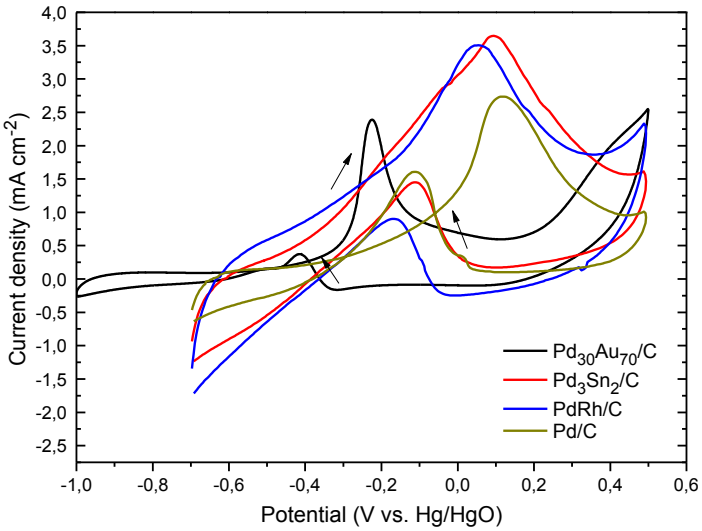

Figure 8.2. Comparison of cyclic voltammetry results of the best Pd-binary electrocatalysts, in 0.5 M KOH with 0.5 M glucose, 20 mV s^{-1}, room temperature, (*$Pd_{30}Au_{70}$/C: 20 mmol L^{-1}, 36.5°C, 50mV s^{-1}).

The lowest onset potential is observed for the Pd_3Sn_2/C, suggesting that the electrocatalytic activity towards glucose electrooxidation occurs more favorably over it , then over PdRh/C followed by $Pd_{30}Au_{70}$/C and finally over Pd/C electrocatalyst. The peak current densities in backward scan are: 1.58 (Pd/C) > 1.45 (Pd_3Sn_2/C) > 0.89 (PdRh/C) > 0.37 mA cm^{-2} (Table 8.3). High peak backward current density means good poisonous tolerance. Thus, according to Figure 8.2 and Figure 8.3, the introduction of Sn (Pd_3Sn_2/C) increases the poison tolerance of Pd to the intermediate products.

Despite the fact that PdRh/C and Pd_3Sn_2/C exhibit the highest activity of the examined electrocatalysts, more intermediates are involved in the glucose electrooxidation reaction, factor that is obvious from the broad peak that they form during the forward scanning [9].

In Figure 8.3 peak current density versus metal loading is reported. The increase of Au loading seems to affect positively the electrocatalyst's poisonous tolerance, while Sn loading seems not having impact on poisonous effect.

As it can be seen the backward peak current density remains the same as the Sn loading increases. On the other hand the addition of Rh, when metal loading exceeds 20 μgcm^{-2}, enhances poisonous tolerance.

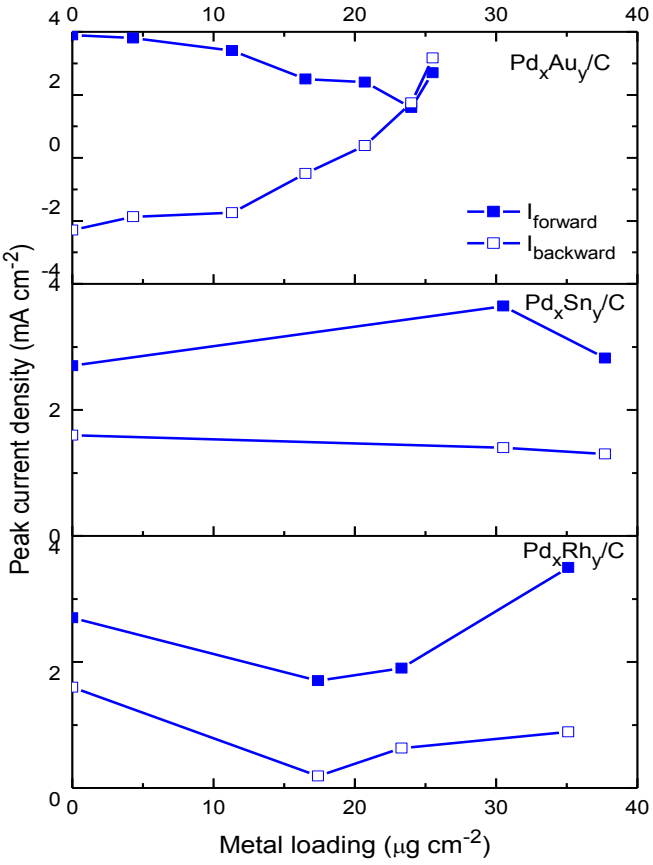

Figure 8.3. Peak current density *vs.* metal loading. In all cases Pd+M loading equals to 72 μgcm^{-2}.

The ratio of the forward anodic peak current density (I_f) to the reverse anodic peak current density (I_b), I_f/I_b, can be used to describe the catalyst's tolerance to carbonaceous species accumulation [10].

The results of the forward and backward scan peak current densities are listed in Table 8.3. Low I_f/I_b ratio indicates poor oxidation of glucose to carbon dioxide during the anodic scan and extensive accumulation of carbonaceous residues on the catalyst surface.

Table 8.3. Forward and backward anodic peak current density.

Catalysts	I_f/mA cm^{-2}	I_b/mA cm^{-2}	I_f/ I_b	Onset potential/ V *vs.* Hg/HgO
Pd/C	2.7	1.6	1.7	-0.29
$Pd_{30}Au_{70}$/C	2.3	0.4	6.2	-0.40
PdRh/C	3.5	0.9	3.9	-0.47
Pd_3Sn_2/C	3.6	1.4	2.5	-0.55

Figure 8.4 depicts the effect of the electrochemical active surface area and lattice parameter on the electrocatalytic activity. It is obvious that as the electrochemical active surface area increases, the electrocatalytic activity (peak current density) also increases, suggesting that more active sites are available for glucose electrooxidation.

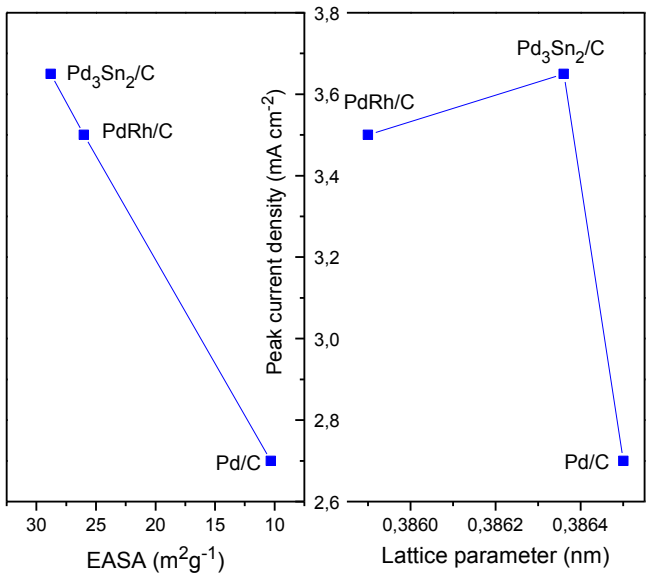

Figure 8.4. *E*lectrochemical active surface area and lattice parameter dependency on peak current density.

Furthermore, in Figure 8.4 is reported peak current density *vs.* lattice parameter, indicating the effect of metal's size that is doped in the Pd metal. It can be deduced that a little contraction of lattice parameter enhances catalytic activity attributed perhaps to the reduction of the interatomic distances, while further contraction has negatively impact on activity of electrocatalyst. Tafel equation can provide kinetic parameters, such as exchange current density (I_o) and charge transfer coefficient (α) [6]. In Table 8.4 the kinetic results for the Pd/C, PdRh/C and Pd_3Sn_2/C are reported. The calculated

transfer coefficient are <0.5, indicating that glucose electrooxidation reaction is an irreversible process.

Table 8.4. Kinetic parameters derive from Tafel equation.

Catalysts	I_o/mA cm^{-2}	α
Pd/C	0.05	0.09
PdRh/C	0.17	0.10
Pd_3Sn_2/C	0.18	0.13

From the estimated kinetic parameters (

Table **8.4**) Pd/C has very low exchange current density in comparison with PdRh/C and Pd_3Sn_2/C, maybe due to the adsorbed intermediates on the catalytic surface. Temperature has a great effect on the electrocatalytic oxidation of glucose. It was found (it has already been reported in the experimental section) that above 45^{o}C degrades and many other compounds are formed, such as lactic acid, glycolic acid, e.t.c. For this reason the maximum examined temperature was 40 ^{o}C. In

Figure **8.5** the peak current density values for the Pd_3Sn_2/C, PdRh/C and Pd/C at different temperature values are depicted.

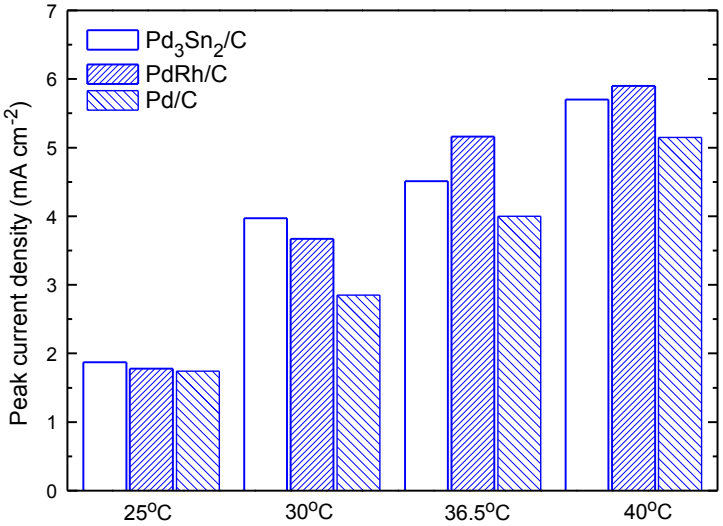

Figure 8.5. Comparison of electrocatalytic activity (peak current density) of the examined electrocatalysts at different temperature values: 0.5 M KOH, 0.5 M glucose, 5 mV s^{-1}, room temperature.

At room temperature Pd_3Sn_2/C and PdRh/C electrocatalysts present almost the same catalytic activity. At 30°C it seems that Pd_3Sn_2/C's activity exceeds the other electrocatalysts' activity, while at higher temperature values (36.5 and 40°C) the electrocatalytic activity of PdRh/C exceeds the one of Pd_3Sn_2/C. Increasing the temperature the catalytic activity of Pd_3Sn_2/C and PdRh/C increases intensely. That may happens because the increment of temperature may help for the increase of mobility of ions and consequently to the increase of molar conductivity.

The activation energy values are calculated from Arrhenius plots (Figure 8.6). Low activation energy means high intrinsic activity and faster charge transfer process. The apparent activation energy for the Pd_3Sn_2/C, PdRh/C and Pd/C was calculated, 52 kJ mol^{-1}, 59 kJ mol^{-1} and 54 kJ mol^{-1}, respectively. Thus, according to the results the addition of Rh does not enhance Pd's electrooxidation reaction, while on the other hand the addition of Sn into Pd/C reduces the activation energy and consequently promotes glucose electrooxidation.

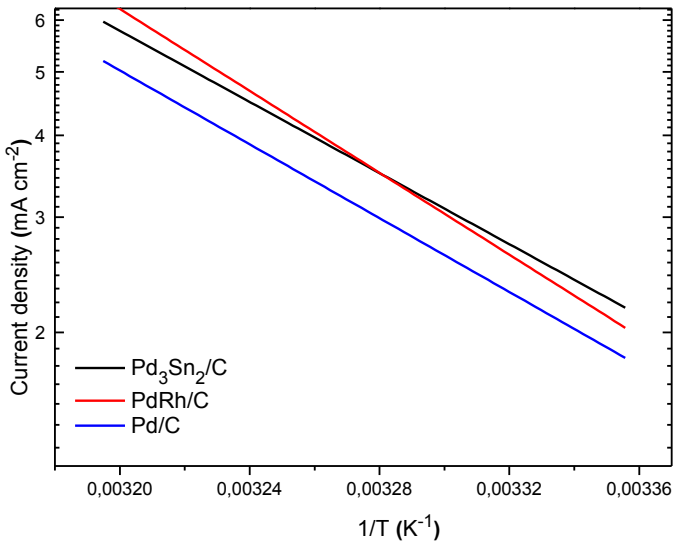

Figure 8.6. Arrhenius plots.

In Figure 8.7 the comparison of Pd_3Sn_2/C and PdRh/C is made as far as concerns glucose electrooxidation in different electrolyte's and glucose's concentration. As it can be seen for low electrolyte's concentration values, 0.1 and 0.3 M KOH, PdRh/C electrocatalyst exhibits higher current density than Pd_3Sn_2/C. While at higher electrolyte's concentration values Pd_3Sn_2/C presents the best electrocatalytic activity compared to PdRh/C. The decrease of the current density of the PdRh/C electrocatalyst,

increasing electrolyte's concentration as well as the better electrocatalytic activity of Pd_3Sn_2/C at high electrolyte's concentration values could be attributed to the fact that the last one has higher electrochemical active surface area, as it is reported in Table 8.2.

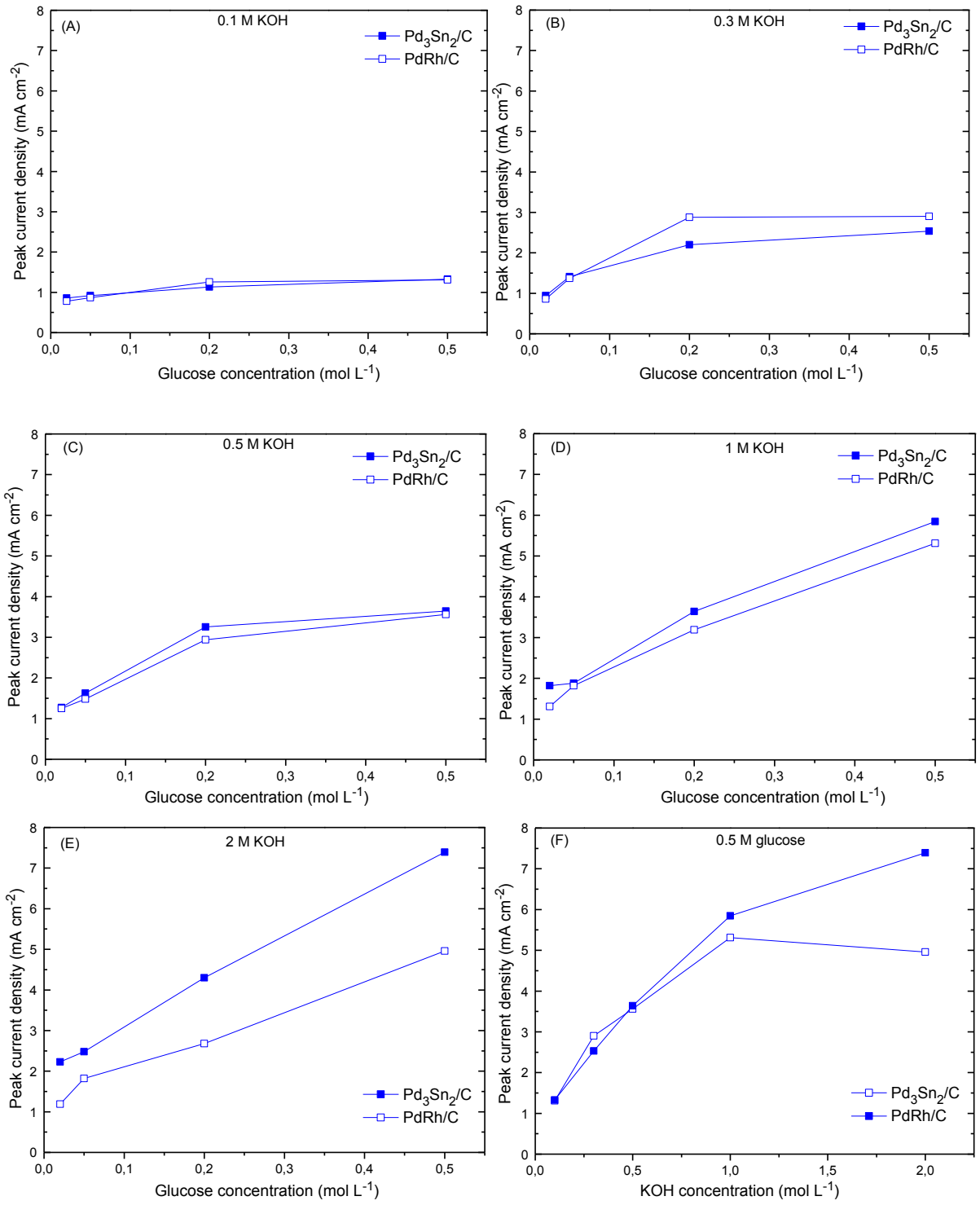

Figure 8.7. Comparison of examined electrocatalysts at different glucose's and electrolyte's concentration, 20 mV s^{-1}, room temperature (A-E), comparison of electrocatalysts at 0.5 M glucose.

The increase of electrolyte's concentration increases the active species and so more active surface area is necessary.

In Figure 8.8 the chronoamperometric curves of the examined electrocatalysts are depicted. The decay of the current density as it can be observed is more intense for the Pd_3Sn_2/C.

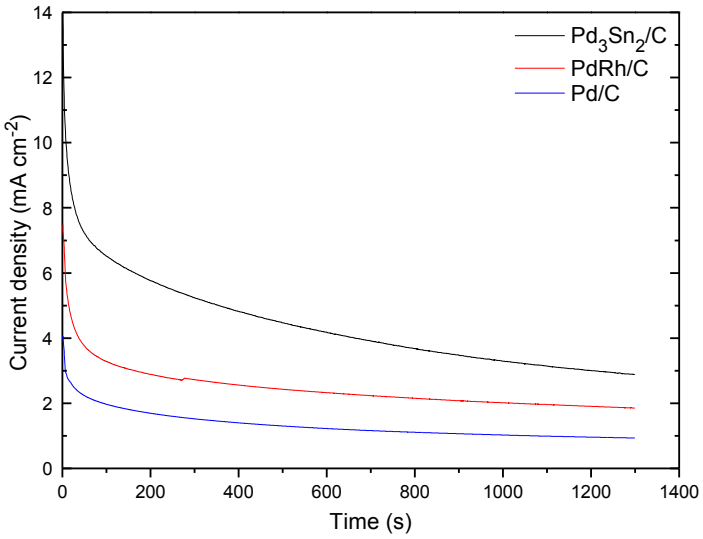

Figure 8.8. Comparison of chronoamperometric measurements of the examined electrocatalysts, ,in 0.5 M KOH with 0.5 M glucose, 5 mV s^{-1}, room temperature.

According to the chronoamperometric measurements the poisoning rate was calculated: 0.014, 0.010 and 0.002 % s^{-1}, for Pd_3Sn_2/C PdRh/C and Pd/C, respectively. This is more intense for the Pd_3Sn_2/C, however when the curve is stabilized the current density remains the highest for the Pd_3Sn_2/C. Developing a sensor low potential is very important. Reliable and fast determination of glucose is important in many areas: biotechnology, clinical diagnostics and food industry and thus the development of electrochemical glucose sensors and direct glucose fuel cells have attracted extensive attention.

References

[1] S. Song, Y. Wang, P.K. Shen, J. Power Sources 170 (2007) 46-49.

[2] A. Habrioux, E. Sibert, K. Servat, W. Vogel, K.B. Kokoh, N. Alonso-Vante, The Journal of Physical Chemistry B 111 (2007) 10329-10333.

[3] J. Zhang, H. Liu, Electrocatalysis of Direct Methanol Fuel Cells: From Fundamentals to Applications, Wiley, 2009.

[4] D. Basu, S. Basu, Electrochim. Acta 56 (2011) 6106-6113.

[5] X. Yan, X. Ge, S. Cui, Nanoscale Research Letters 6 (2011) 313.

[6] J. Liu, J. Ye, C. Xu, S.P. Jiang, Y. Tong, Electrochem. Commun. 9 (2007) 2334-2339.

[7] A.B. Stambouli, Renew. Sust. Energ. Rev. 15 (2011) 4507-4520.

[8] E. Antolini, J.R.C. Salgado, M.J. Giz, E.R. Gonzalez, Int. J. Hydrogen Energy 30 (2005) 1213-1220.

[9] Z. Liu, L. Huang, L. Zhang, H. Ma, Y. Ding, Electrochim. Acta 54 (2009) 7286-7293.

[10] Z. Ogumi, N. J. Dudney, S.R. Narayanan, Battery/Energy Technology (General) - 216th ECS meeting 35 ed., The Electrochemical Society, Pennington, New Jersey, 2010.

CHAPTER IX

Conclusions and Future Perspectives

This very last part summarizes the scientific results of research done in the framework of the present PhD dissertation. At the same time some outlooks for further continuation of this research are provided.

Glucose electrooxidation has been the research hot topic due to the importance of reliable and fast *in vivo* or *in vitro* monitoring of blood sugar for the treatment and control of diabetes through an electrochemical glucose sensor. Moreover the increased interest for implantable glucose fuel cells intends for artificial hearts and heart pacemakers. However, their research and development is far away from satisfaction and real applications due to lack of high efficient and stable electrocatalysts for glucose electrooxidation.

General, whatever the fuel that is used in a fuel cell, Pt considers the first and most widely investigated material for fuel (hydrogen, methanol, ethanol, methane) electrooxidation in acidic media. In alkaline media however Pd is more active and stable than Pt for hydrogen, direct methanol and ethanol fuel cells. The same, for glucose electrooxidation Pt is not a very suitable catalyst due to its high chemisorbability and its poor selectivity of different substances presented in physiological solutions. Concerning glucose electrooxidation a number of

investigations have also been devoted to Au, after it was found to be more active and poison tolerant than Pt in neutral and alkaline solutions.

Preparation method is a very important parameter for catalysts' preparation as it affects their properties (lattice parameter, diameter of nanoparticles, catalysts dispersion on the support). A modified microwave assisted polyol method was chosen because of the following remarkable advantages: i) rapid volumetric heating, ii) higher reaction rate and selectivity, iii) shorter reaction time and iv) higher yield of the product compared to the convention heating methods. As a result, the microwave heating makes the fast preparation of nanomaterials possible, leading to relative low cost, energy saving and high efficiency for materials production, thus advancing rapidly towards their practical applications. Therefore, the use of microwave heating is more popular in scientific world.

The metal content in the catalysts is a very important parameter for comparing their activity. Consequently, in order to assure that the chosen preparation method does not affect the initial metal loading (20 wt.% on carbon) thermogravimetric measurements were conducted for Pd/C and Au/C electrocatalysts. The loss weight was only ±1.5% proving that the pulse-microwave assisted polyol synthesis method adopted is an effective and fast one preparation method. Further physicochemical characterizations were carried out with the XRD, TEM and SEM-EDS measurements. When a second metal is adopted with palladium a further decrease in the particle size of the catalysts could give higher activity, and this part of work is under investigation. In general the mean particle size such as is extracted from XRD and TEM results of the prepared electrocatalysts is ~10 nm. For the electrochemical evaluation initially, Pd_xAu_y/C binary catalysts were investigated for glucose electrooxidation and detection. The composition of Pd_xAu_y/C catalysts could be controlled and adjusted by changing the corresponding composition ratio in the precursor solutions. Pd/C mono-metalic catalyst exhibited high activity towards glucose electrooxidation but not good poison tolerance. The introduction of Au is vital to relieve poisoning of Pd, and the optimum $Pd_{30}Au_{70}/C$ exhibited the desirable both activity to glucose oxidation and tolerance to the intermediate species produced from glucose oxidation. For this reason it was examined as glucose sensor, giving a good reliability. In general Pd_xAu_y binary

electrocatalysts are expecting to have potential applications for electrochemical glucose sensors. Then three Pd-based binary electrocatalysts, Pd_xRu_y/C, Pd_xRh_y/C and Pd_xSn_y/C were also examined for glucose electrooxidation prepared by a modified pulse microwave assisted polyol method.

As far as concerns Pd_xRh_y/C from XRD and TEM characterizations the nanoparticles' size was estimated at ~10 nm. Furthermore, according to the electrochemical results the addition of Rh can increase the activity of Pd towards glucose oxidation in alkaline medium with PdRh/C to exhibit the highest activity. However, it can be poisoned easier than the other Pd_xRh_y/C electrocatalysts. The study of the effect of glucose and electrolyte's concentration show that for 1 mol L^{-1} KOH containing 0.5 mol L^{-1} glucose the highest catalytic activity can be obtained. For electrolyte's concentration higher than 1 mol L^{-1} KOH the electrocatalytic activity decreases maybe due to the great number of hydroxide ions which may block the glucose's adsorption on the electrode's surface. Finally, it was found that the increase of temperature until 40^{o}C enhances the electrocatalytic activity, while at higher temperature values the rapid degradation of glucose solution suppresses electrocatalysts' catalytic activity.

The results for the Pd_xSn_y/C showed that the optimum Pd_3Sn_2/C exhibited the desirable activity to glucose electrooxidation, but according to chronoamperometric results it was poisoned faster compared to the PdSn/C and Pd/C electrocatalysts. Since Pd_3Sn_2/C presented the highest catalytic activity for glucose electrooxidation some more parameters such as diffusion coefficient were calculated. From the chronoamperometric results and as it was expected glucose's diffusion coefficient was calculated higher for the Pd_3Sn_2/C (7.8×10^{-9} cm^2 s^{-1}). Glucose electrooxidation reaction over Pd_3Sn_2/C was also studied for a range of values of temperature, glucose and electrolytes concentration values. According to the cyclic voltammetry's results, as temperature increases from 25^{o}C to 40^{o}C, current density increases from 1.87 to 5.7 mA cm^{-2}. Additionally, at a constant glucose's concentration, increasing electrolyte's concentration from 0.5 to 2 M KOH, current density increases. Increment of the current density is also observed when glucose's concentration increases from 0.02 to 0.5 M (for a constant electrolyte's concentration value). This increment is more intense almost linear

at the maximum concentration of electrolyte (2 M KOH). Finally, studying the effect of scan rate indicated that the electrode process is diffusion limited.

The study of Pd_xRu_y/C showed that the increase of ruthenium's content in PdRu/C electrocatalyst suppresses current density, while on the other hand the addition of palladium (until Pd:Ru=2:1) enhances catalytic activity to glucose electrooxidation, with Pd_2Ru/C to exhibit the highest catalytic activity. According to cyclic voltammetry results, many intermediates are formed on Pd_xRu_y/C electrocatalysts, whose effect is reduced when electrolyte's concentration increases to 2 M KOH. In comparison with Pd/C, $Pd_{30}Au_{70}/C$, Pd_3Sn_2/C and PdRh/C, the Pd_xRu_y/C electrocatalysts are not suggested for glucose electrooxidation reaction, due to the formation of many intermediates and their easier poisoning.

The results of the present study have been published in literature for first time, providing some more data about glucose electrooxidation reaction in alkaline media over Pd-based electrocatalysts. The recognition of some efficient anode electrocatalysts which constitutes the first step of design and development of a fuel cell has been accomplished. However, the following issues must be taken into account in the future: i) optimization of the preparation method for forming nanoparticles with lower diameter, ii) recognition of the most efficient cathode electrocatalysts for a direct glucose alkaline fuel cell, iii) study of more Pd-based anode electrocatalysts (e.g. Pd-Ni, Pd-Ir) and iv) development of a single direct glucose alkaline fuel cell (using anion solid membrane provided by Tokuyama company) using the most efficient electrocatalysts.